



HAL
open science

Synthesis of State Observer and Nonlinear Output Feedback Controller Design of AC Machines

* A.A.R Al Tahir

► **To cite this version:**

* A.A.R Al Tahir. Synthesis of State Observer and Nonlinear Output Feedback Controller Design of AC Machines . Engineering Sciences [physics]. universite de caen normandie, 2016. English. NNT : . tel-01465299

HAL Id: tel-01465299

<https://hal.science/tel-01465299>

Submitted on 11 Feb 2017

HAL is a multi-disciplinary open access archive for the deposit and dissemination of scientific research documents, whether they are published or not. The documents may come from teaching and research institutions in France or abroad, or from public or private research centers.

L'archive ouverte pluridisciplinaire **HAL**, est destinée au dépôt et à la diffusion de documents scientifiques de niveau recherche, publiés ou non, émanant des établissements d'enseignement et de recherche français ou étrangers, des laboratoires publics ou privés.



Normandie Université

THESE

**Pour obtenir le diplôme de doctorat
Spécialité (Génie Electrique)**

**Normandie Université
U.F.R de Sciences
ECOLE DOCTORALE SIMEM**

Synthèse d'Observateur d'État et Commande Non-Linéaire à Retour de Sortie des Machines AC

**Présentée et soutenue par
Ali Abdul Razzaq AL TAHIR**

**Thèse soutenue publiquement le (16 décembre 2016)
devant le jury composé de**

Mr / Mohamed Benbouzid	Professeur des Universités/ Université de Bretagne Occidentale, France	Rapporteur
Mr / Maxime Wack	Maître de Conférences HDR Emérite / Université de Technologie de Belfort-Montbéliard, France	Rapporteur
Mr / Fayçal Ikhouane	Professeur des universités / Universitat Politècnica de Catalunya, Spain	Examinateur
Mr / Salah Laghrouche	Maître de Conférences HDR/ Université de Technologie de Belfort-Montbéliard, France	Examinateur
Mr / F. Giri	Professeur des universités/ Normandie Université, France	Directeur de thèse
Mr / Tarek Ahmed - Ali	Professeur des universités / Normandie Université, France	Directeur de thèse

Laboratoire : Groupe de recherche en informatique, image, automatique et instrumentation de Caen (GREYC)



Acknowledgements

First of all, I will give my thanks forever to my God, who makes me able to complete this work. This thesis is submitted to the School of Doctorate ‘‘SIMEN ‘‘ at University of Caen Lower Normandy in partial fulfillment of the requirements for the Ph.D. degree in Electrical Engineering. The dissertation has been followed by two supervisors: Professor F. Giri from CNRS – 6072, *GREYC* laboratory, UFR Science 2 and Tarek. A. Ali from School National Superior Engineer of Caen and Research Center (*ENSICAEN*) at University of Caen Lower Normandy. I would like to express my special thanks to them for their support and enduring patience, advice, guidance and their response to my work during my PhD research. Without them, this project would not have been possible. Also, I would like to express my special thanks to members of jury for their responses.

I greatly appreciate the Iraqi government, ministry of higher education and scientific research in Iraq. Thanks also to all staff of the Iraqi Cultural Attaché and Campus France for administrative assistance, which are fully sponsored to carry - out my PhD study at university of Caen lower Normandy. During the project period of three years, I had many valuable discussions with the colleagues at *GREYC* laboratory for providing the research facilities that make it possible for me to conduct this work. I would like to thank all of them for scientific assistance. My thanks also to the laboratory staff of *GREYC*, who helped me to build the implementation test for this project.

Finally, I must express my profound gratitude to my father, my mother, who never lived to see the fruit of their dedicates, to my sisters, and siblings for supporting me, continuous encouragement and patience, even when the road was bumpy throughout my years of study and through the process of researching and writing this thesis. This accomplishment would not have been possible without them. I am really thankful to them. Words cannot explain how I am grateful to my wife beside me throughout my study.

Ali

PhD AL TAHIR Ali Abdul Razzaq,

2016

List of Publications and Communications

Here are the list of the publications and the communications on the results of this work:

International Conferences

1. A. A.R. AL-Tahir, A. El Magri, T. Ahmed-Ali, A. El Fadili, F. Giri, (2015). Sampled - Data High-Gain Nonlinear Observer Design for Synchronous PMSM. *1'st IFAC Conference on Modelling, Identification and Control of Nonlinear Systems*, Saint Petersburg, Russia, Papers Online Science Direct, *ELSEVIER*, 48 (11): 327 - 332. [doi:10.1016/j.ifacol.2015.09.206](https://doi.org/10.1016/j.ifacol.2015.09.206).
- 2- A. A.R. AL-Tahir, R. Lajouad, F.Z. Chaoui, R. Tami, F.Z. Chaoui, T. Ahmed-Ali, F. Giri, (2016). A Novel Observer Design for Sensorless Sampled Output Measurement: Application of Variable Speed Doubly Fed Induction Generator. *12'th IFAC International workshop on Adaptation and Learning in Control and Signal Processing*, University of Technology, Eindhoven, Netherlands, Papers Online Science Direct, *ELSEVIER*, 49 (13): 235 - 240. doi.org/10.1016/j.ifacol.2016.07.957.
- 3- M. Kissaoui, A. A.R. AL - Tahir, A. Abouloifa, F.Z. Chaoui Y. Abouelmahjoub, F. Giri, (2016). Output-Feedback Nonlinear Adaptive Control of Three-phase AC/DC Converter for On-line UPS Systems. *12'th IFAC International workshop on Adaptation and Learning in Control and Signal Processing*, University of Technology, Eindhoven, Netherlands, Papers Online Science Direct, *ELSEVIER*, 49 (13): 324 - 329. doi.org/10.1016/j.ifacol.2016.07.987

Articles accepted in the international journal

- 1- A. A.R. AL-Tahir, (2016). Sensorless Online Measurements: Application to Variable Speed Drive Systems. *Submitted to International Journal for computation and mathematics in electrical and electronic engineering*, early accepted for publication.

Articles under revision in the international journals

- 2- A. A.R. AL-Tahir, (2016). Reduced order nonlinear state observer design having inter-sampled output behaviour. *Submitted to Journal of Dynamic Systems, Measurements and Control*, (under revision).

Communication Posters

- 4- [Al Tahir,2015] Poster presentation entitled of “ Sampled Data Nonlinear Observer Design for Permanent Magnet Synchronous Machines”, Journee’s du GREYC 2015, 4 - 5 June, 2015, organized by University of Caen Basse Normandy, and ENSICAEN, Campus 2, Amphi S3 – 057 et Salle S3 – 037.

Communication Oral

- 5- Workshop entitled “Sampled – Data - High Gain Observer Design for Globally Exponential Convergence Dealing with PMSM”, *presented to association OPTIC*, University of Caen Basse Normandy, UCBN 2014.
- 6- Oral presentation entitled “High - Gain Observer Synthesis based on Sampled Output Measurements”. The doctoral school day DSD organized by the *SIMEM*'s student representatives together with *OPTIC* association, University of Caen Basse Normandy, UCBN, 10 / 06 / 2016.

Table of contents

	page
Acknowledgements	i
List of publications and communications	ii
List of figures	ix
List of tables	xii
List of abbreviations and symbols	xiii
1. Introduction	2
1.1 State of the art	2
1.1.1 Development of synchronous machine drives	2
1.1.2 Continuous – time nonlinear state observer design	2
1.1.3 Sampled – data nonlinear state observer design	3
1.1.3.1 Emulation design process	6
1.1.3.2 Direct discrete-time design process	6
1.1.3.3 Sampled-data design process	6
1.1.4 Electrical power system control techniques	7
1.1.5 Wind power generation systems	8
1.2 Contribution of the thesis	10
1.3 Objectives and motivations of the thesis	10
1.4 On-line observer design techniques for some of AC machines	11
1.4.1 Sampled – data observer design for PMSM drives	13
1.4.2 DFIG running with non-standard sampled observer	14
1.5 Adaptive output feedback control of VSC for UPS system	15
1.6 Outline of thesis	16
1.7 Appendices	18
2. Mathematical Models and Control Fundamentals for On-line Stabilization	19

2.1	Fundamentals of permanent - magnets electric machine	20
2.1.1	Rotor position sensor elimination	21
2.1.2	PM synchronous machines versus induction machines	22
2.2	Permanent magnet synchronous machine modeling	22
2.2.1	Modeling of PMSM in abc – representations	23
2.2.2	Model of PMSMs in rotating ($d - q$) reference frame	25
2.2.3	Model of PMSMs in ($\alpha - \beta$) representation	27
2.3	Modeling of wind generation power systems	28
2.3.1	Wind turbine mathematical model	29
2.3.2	Doubly fed induction generator model	30
2.4	Wind speed types and operating regions of WPGSs	31
2.4.1	Cut - in wind speed	32
2.4.2	Rated wind speed	32
2.4.3	Cut - out wind speed	32
2.5	Wind turbine concepts	33
2.5.1	Fixed speed wind turbines	33
2.5.2	Partial VSWT with rotor resistance	33
2.5.3	VSWT with partial-scale converter	34
2.5.4	VSWT with full-scale power converter	35
2.6	Observability study for sensorless control design	36
2.7	Backstepping control design techniques	42
2.7.1	Continuous - time backstepping design technique	43
2.8	Introduction for a class of system studied	48
2.9	Fundamental properties for stability convergence analysis	50
2.9.1	Input – to – state stability concept	50
2.9.2	Fundamentals of ISS small - gain condition	51
3.	Sampled – Data Nonlinear Observer Design for Sensorless Synchronous PMSM	54
3.1	Introduction	55
3.1.1	Review of related research	55
3.1.2	Purposes and contributions	55

3.2	Synchronous machine modeling and model transformation	56
3.2.1	Synchronous PMSM model	57
3.2.2	MIMO Model transformation of PMSM	59
3.2.3	Observability analysis of full order variable speed PMSM	61
3.3	Sampled-data observer design and convergence analysis	62
3.3.1	Sampled – data observer structure	63
3.3.2	Some technical hypotheses	63
3.3.3	Comparison with published results	64
3.3.4	Some definition and notation	65
3.3.5	Stability analysis of the proposed observer	66
3.3.6	Discussion the main result	71
3.3.7	Observer equation in the original coordinates	71
3.4	Simulation results and verifications	72
3.4.1	Implementation considerations	72
3.4.2	Observer dynamic tracking performance	75
3.4.3	Sensorless sampled output measurements	75
3.5	Conclusions	80
4.	A Novel Observer Design based on Sensorless Sampled Output Measurements: Application to Variable Speed DFIG based Wind Turbines	83
4.1	Introduction	84
4.1.1	Review of related research	84
4.1.2	Purposes and contributions	87
4.2	Representation of DFIG based wind turbine	88
4.2.1	Wind turbine modeling	88
4.2.2	Modeling assumptions	90
4.2.3	Full version of DFIG model	90
4.2.4	Power calculation in $(d - q)$ quantities	92
4.2.5	Observability analysis of full version DFIG model	94
4.2.6	Motivations of using reduced model DFIG	97
4.2.7	Reduced version of DFIG model	97
4.3	Position sensorless measurements	100

4.4	Reduced - order state observer design	101
4.4.1	Observer design assumptions	102
4.4.2	Some remarks and notations	103
4.5	Comparison with published results	104
4.6	Sampled - data observer design and convergence analysis	104
4.6.1	Stability analysis of the proposed observer	106
4.6.2	Discussion of the main result	113
4.7	Simulation results and verifications	114
4.7.1	Implementation considerations	114
4.7.2	Observer dynamic tracking performance	116
4.7.3	Sensorless sampled output measurements	117
4.7.4	Sensorless position measurements	118
4.8	Conclusions	122
5.	Output Feedback Nonlinear Adaptive Control Strategy of Three - Phase AC/DC Boost Power Converter for Online UPS Systems	124
5.1	Introduction	125
5.1.1	Review of related research	126
5.1.2	Purpose and contribution	127
5.2	Uninterruptable power supply topologies	128
5.3	Problem formulation	129
5.3.1	System topology and modeling	129
5.3.2	Main control objectives	132
5.3.3	Comparing with published results	134
5.4	Adaptive controller design	135
5.4.1	Observability analysis of on-line UPS system	135
5.4.2	Adaptive observer design	139
5.4.3	Stability convergence analysis	140
5.4.4	Inner control loop design - PFC achievement	142
5.4.5	Outer control loop design - DC output voltage regulation	145
5.4.6	Power factor calculation and estimation	146

5.5 Numerical simulation and verification	151
5.5.1 Implementation considerations	151
5.5.2 Tracking performance in presence of constant load	152
5.5.3 Control performance in presence of resistive load uncertainty	157
5.6 Conclusions	160
6. General Conclusions and Perspectives	162
6.1 General conclusions	162
6.2 Suggestions for future works	165
Appendices	166
A1. Clarke’s transformation	166
A2. Park ‘s transformation	166
A3. Pulse width modulation (PWM) generation	168
A4. Derivation of wind power equation	168
A5. Young’s inequality.....	169
Bibliography	173

List of Figures

Chapter One

1.1 A Simple block diagram for sampled - data design process	7
1.2 Basic feedback control system	8
1.3 Basic scheme for sensorless control of PMSM drives	9
1.4 General block diagram of the WPGS	10
1.5 The general scheme for sampled – output HGO observer design	13
1.6 Schematic diagram of the proposed adaptive output feedback controller.....	15
1.7 Logical sequence of the thesis chapters	18

Chapter Two

2.1 Transformation of abc - coordinates to fixed and rotating frame,	24
2.2 Variable speed wind turbine with partial - scale power converter	34
2.3 Stabilization of three-state nonlinear system	48

Chapter Three

3.1 Electrical equivalent circuit for PMSM expressed in $(\alpha - \beta)$ representation	58
3.2 Angles between stator and rotor electrical frames	58
3.3 Proposed observer combines benefits of HG structure and output predictor ...	64
3.4 PMSM model and sampled - output HGO structure	66
3.5 Computer flowchart of the proposed applied on variable speed PMSM	72
3.6 Single line diagram of case study including sampled – output HGO	74
3.7 Motor rotor speed profile in (rad /sec)	77
3.8 Motor external load torque profile in (N. m)	77
3.9 Estimated (Blue line) and real (Black dotted) rotor speed (rad /sec)	77
3.10 Estimation error for motor rotor speed in (rad /sec)	77
3.11 Estimated (Blue line) and real (Black dotted) load torque (N. m)	77
3.12 Estimation error for motor load torque (N. m)	77

3.13	Estimated (Blue line) and real (Black dotted) α – axis rotor flux (Wb)	78
3.14	Estimation error for α – axis rotor flux in (Wb)	78
3.15	Estimated (Blue line) and real (Black dotted) β – axis rotor flux (Wb)	78
3.16	Estimation error for β – axis rotor flux in (Wb)	78
3.17	Estimated (Blue line) and real (Black dotted) rotor position (rad)	78
3.18	Estimation error for motor rotor position in (rad /sec)	78
3.19	Measured, predicted and estimated α – axis stator current (A)	79
3.20	Measured, predicted and estimated β – axis stator current (A)	79
3.21	Current prediction error for α – axis (A)	79
3.22	Current prediction error for β – axis (A)	79
3.23	Evolution of sampling period, $\forall t \in [t_k, t_{k+1})$	79

Chapter Four

4.1	Turbine output power versus wind speed for varying pitch angles	89
4.2	Power coefficient of turbine versus tip speed ratio for varying pitch angles	89
4.3	Equivalent circuit models of the DFIG expressed in $(d - q)$ representation	94
4.4	Sector bound for saturation nonlinearity function	103
4.5	Structure of proposed HGO observer for DFIG system	106
4.6	Typical DFIG based wind turbine with sensorless HGO design	116
4.7	Wind velocity profile (m/sec)	118
4.8	DFIG Generator torque profile (N. m)	119
4.9	DFIG electromagnetic torque and its estimate (N. m)	119
4.10	DFIG Generator torque and its estimate (N. m)	119
4.11	DFIG rotational speed and its estimate (rad /sec)	119
4.12	Dynamic performance of the term $S_2(i)$	119
4.13	Stator and rotor side active power (Watt)	119
4.14	Stator and rotor side reactive power (VAR)	120
4.15	d - Axis stator current and its predictor	120
4.16	q - Axis stator current and its predictor	120
4.17	d - Axis rotor current and its predictor	120
4.18	q - Axis rotor current and its predictor	120
4.19	Evolution of sampling period, $\forall t \in [t_k, t_{k+1})$	120

4.20	Tracking performance of stator flux position θ_s and its estimate $\hat{\theta}_s$ (rad)	121
4.21	Tracking performance of rotor position θ_r and its estimate $\hat{\theta}_r$ (rad)	121

Chapter Five

5.1	Electrical power circuit of the three-phase AC/DC boost converter for on-line UPS system	129
5.2	Exact equivalent circuit of AC/DC boost converter in $(d - q)$ frame	133
5.3	Schematic diagram of nonlinear adaptive controller design strategy	137
5.4	Computer flowchart of the proposed approach	137
5.5	Structure of system/adaptive observer based HGO design	142
5.6	Structure of single-phase power factor estimation in UPS	149
5.7	Block diagram of UPFC tracking design and DC voltage regulator	152
5.8	Magnitude of grid voltage and its estimate (V) in presence of uncertain bounded grid phase voltage	155
5.9	Uncertain load resistance and its estimate (Ω) in presence of constant load	155
5.10	DC output voltage; its estimate and desired reference	156
5.11	Input phase currents in $(d - q)$ rotor frame	156
5.12	Inner control loop signals in $(d - q)$ rotor frame	156
5.13	Dynamic performance of tuning control signal	156
5.14	Power factor estimation of the three single - phase AC/DC converter	156
5.15	Dynamic performance for separate and total distortion factor	156
5.16	Dynamic performance for both active (W) and reactive power (VAr)	157
5.17	Resistive load and its estimate (Ω) in presence of load change	158
5.18	Grid phase voltage and its estimate	158
5.19	DC output voltage, it's estimate and desired reference	159
5.20	Power factor estimation of the three single- phase AC/DC converter	159
5.21	Dynamic performance for separate and total distortion factor	159
5.22	Dynamic performance for active (W) and reactive power (VAr) for case 2	159

Appendices

A.1	Combined stationary and rotating frames	169
A.2	Circuit diagram for pulse width modulation generator	170
A.3	Schematic diagram of a HAWT	171

List of Tables

Chapter 3

3.1 PMSM system nominal mechanical and electrical characteristics	76
3.2 Parameters of sampled output high - gain observer	76

Chapter 4

4.1 DFIG system nominal features	116
4.2 Numerical HGO observer design parameters	116

Chapter 5

5.1 State variables and unknown parameters for online UPS system	133
5.2 Three phase AC/DC boost converter for UPS system characteristics	154
5.3 Controller parameters	155

List of Abbreviations and Symbols

List of Abbreviations

A	technical assumption
AC	alternating current
AC/DC	AC to DC converter (rectifier)
BEMF	back electromotive force induced in stator windings
B.B	bus bar
CO	control objective
CTM	continuous time measurements
<i>D</i>	power electronic diode
DC	direct current
DC/AC	DC to AC converter (inverter)
DC/DC	DC to DC converter (chopper)
DFIG	doubly fed induction generator
DDWTG	direct drive wind turbine generator
<i>dSPACE</i>	digital signal processing and automatic control equipment
DSP	digital signal processing
<i>dim</i>	dimension of matrix
<i>det (.)</i>	determinant of matrix
DTM	discrete time measurements
EKF	extended <i>Kalman</i> filter
<i>exp(.)</i>	exponential function
FOC	field oriented control
FP	fixed pitch approach
iff	if and only if
G	Generator mode of operation
GAS	globally asymptotically stable
GEC	globally exponential convergence
GSC	grid side converter
<i>H</i>	hypothesis

HGO	high gain observer
HAWT	horizontal axis wind turbine
IPMSM	interior permanent magnet synchronous machine
IM	induction machine
<i>KCL</i>	<i>Kirchhoff</i> current law
<i>KVL</i>	<i>Kirchhoff</i> voltage law
KVA	kilo volt ampere
kW	kilo watt
kVAR	kilo volt ampere reactive
LPF	low pass filter
LFC	<i>Lyapunov</i> function candidate
LMI	linear matrix inequality
LTV	linear time varying
LKF	<i>Lyapunov Krasovskii</i> functional
LHS	left hand side
ISS	input – to – state stability
MIMO	multi input multi output system
MPP	maximum power point
MSC	machine side converter
NL	Non-linear
OS	overshoot
ODE	ordinary differential equation
OFC	output feedback controller
PM	permanent magnet
PMSM	permanent magnet synchronous machine
PI	proportional, integral regulator
PWM	pulse width modulation generation
PFC	power factor correction
PLL	phase – locked loop
PEC	persistence excitation condition
PE	power electronic
RMS	root mean square value
RHS	right hand side
RT	rate transition

SISO	single input single output
SMO	sliding – mode observer
SPDM	symmetric positive definite matrix
SPMSM	surface – mounted permanent magnet synchronous machine
SNDF	semi - negative definite function
SFC	state feedback controller
SDM	sampled – data measurements
SCADA	signal conditioning and data acquisition module
THD	total harmonic distorsion factor
UPS	uninterruptible emergency power supply
VSC	voltage source converter
VAWT	vertical axis wind turbine
VS	variable wind speed
WTG	wind turbine generator
WPGS	wind power generation system
WECS	wind energy conversion system
<i>w.r.t</i>	with respect to
ZOH	zero - order hold

List of Symbols

A	state transition matrix
A_w	swept area of the wind turbine blade measured in m^2
B	gain matrix corresponding to input control signals
C_e	correction error
C	output state vector
c_i	aerodynamic wind turbine coefficient depends on blades shape design, $i = 1:6$
C_{bus}	DC - bus capacitor in measured measured in F
C_f	grid filter capacitance side measured measured in F
C_p	power coefficient (unit less)
D	rotor diameter measured in m
d	The usual partial derivative
e_w	output state prediction error
e_i	i 'th error
f_s	main supply frequency measured in Hz

$f(\cdot)$	vector field function
f_v	combined rotor and load viscous friction
h_i	constant design parameter, $i = 1:6$
$i_{s\alpha}, i_{s\beta}$	stator currents projected on $(\alpha - \beta)$ representation measured in A
i_M	upper bound of generator current measured in A
i_c	capacitive current measured in A
i_R	rectified current output from MSC measured in A
\mathbb{I}_n	identity matrix size $(n \times n)$
$J_{\Phi(x)}$	<i>Jacobian</i> matrix of the PMSM system
J	combined rotor and load moment of inertia
K	gain matrix corresponding to measurements error
k	sampling sequence
L_s, L_a	self-inductance of stator or armature windings.
$L_f^k h(x)$	k 'th order <i>Lie - algebra</i> of the function $h(x)$ with respect to vector field function
m	is the air mass in kg
\mathcal{N}	set of nonnegative integers
n	full order state space model representation or dimension of the system under study
n_p	number of magnet pole - pairs
\mathcal{O}	observability matrix
ORC	observability rank condition
P_{nom}	nominal rated real power measured in Watt
P_m	mechanical output power measured in Watt
P_w	wind power measured in Watt
P_{wt}	wind turbine power measured in Watt
P	positive definite matrix
R_s, R_a	stator or armature resistance measured in (Ω)
R_o	load resistance measured in (Ω)
R	wind turbine rotor radius measured in m
\mathbb{R}	set of real numbers
r	strictly positive real number chosen sufficiently large enough
S_{nom}	nominal apparent power measured in KVA
S	symmetrical positive definite matrix
S_i, G_i	PWM input signals controlling converter IGBT's
T_m	external input mechanical torque measured in N. m

G_i	i 'th transistor switching device, $i = 1:6$
T_g	aerodynamic generator torque measured in N. m
T_{em}	electromagnetic torque produced by generator measured in N. m
T	stands for matrix transposed
T_2	square matrix, $\in \mathbb{R}^{2 \times 2}$
t	continuous - time index
t_k	sampling instant.
u_i	average values of u_1, u_2, u_3 over cutting period (duty ratios) measured in V
$V_{s\alpha}, V_{s\beta}$	$(\alpha - \beta)$ axis stator voltage components measured in V
V_{sd}, V_{sq}	$(d - q)$ axis stator voltage components measured in V
V_{dc}	DC - bus voltage measured in V
V_{dcref}	reference value of DC - bus voltage measured in V
V_w	wind velocity measured in (m/sec)
V, W	<i>Lyapunov</i> functions introduced in the observer and closed loop design
w	output state predictor between sampling instants
x	real state vector
x_0	arbitrarily initial condition chosen in state - space
x_i	i 'th real state variable
\hat{x}	state estimate
\tilde{x}	state observation error
\dot{x}	dynamics of state variable
x^*	reference state signal
y	output measured state vector
y_s	output of the system dynamics
z	state transformation under the form of, z benchmarck
ω_r	arbitrary angular rotor speed measured in <i>rad/sec</i>
ω_g	arbitrary generator rotor speed measured in <i>rad/sec</i>
ω_s	fixed synchronous speed measured in <i>rad/sec</i>
θ	high - gain design parameter measured in <i>rad</i>
θ_1, θ_2	parametric uncertainties
θ_e	electrical rotor position angle measured in <i>rad</i>
θ_m	mechanical rotor position angle measured in <i>rad</i>
θ_s	stator position angle measured in <i>rad</i>
$\phi_{r\alpha}, \phi_{r\beta}$	rotor flux expressed in $(\alpha - \beta)$ axis representation
$\Phi(x)$	transformation mapping (or, observability mapping)

ψ_{PM}	permanent magnet flux constant measured in Wb
$\lambda_{min}(P)$	minimum eigenvalues of matrix P
$\lambda_{max}(P)$	maximum eigenvalues of matrix P
λ_{TSR}	tip speed ratio (unit less)
τ_s	sampling time interval
τ_{MASP}	maximum allowable sampling time interval
α, β	orthogonal coordinates of stationary reference frame
d, q	orthogonal coordinates of rotating reference frame
μ	positive design parameter, $\mu > 0$
$(\mu_1 \ \mu_2 \ \mu_3)^T$	control inputs in finite discrete set bounded between $\{-1, 1\}$
ρ	air density in kg / m^3 at room temperature
ρ^*	upper bound constant scalar value
Δ	block diagonal matrix
∇	gradient vector
β_0	<i>positive Lipschitz</i> constant
L_{local}	<i>local Lipschitz</i> constant
L_{global}	<i>global Lipschitz</i> constant
σ	saturated function bounded between upper and lower level
ρ	leakage – coefficient (unitless)
$\ \cdot \ $	<i>Euclidean</i> norm of the vector
$ \cdot $	absolute value

Chapter One

General Introduction

Table of Contents	page
1.1 State of the art.....	2
1.1.1 Development of synchronous machine drives.....	2
1.1.2 Continuous – time nonlinear state observer design.....	2
1.1.3 Sampled – data nonlinear state observer design.....	3
1.1.3.1 Emulation design process.....	6
1.1.3.2 Direct discrete-time design process	6
1.1.3.3 Sampled-data design process.....	6
1.1.4 Electrical power system control techniques.....	7
1.1.5 Wind power generation systems	8
1.2 Contribution of the thesis.....	10
1.3 Objectives and motivations of the thesis.....	10
1.4 Online observer design techniques for some of AC machines.....	11
1.4.1 Sampled – data observer design for PMSM drive systems	13
1.4.2 DFIG running with non-standard sampled observer	14
1.5 Adaptive output feedback control of VSC for UPS system	15
1.6 Outline of thesis.....	16
1.7 Appendices	18

1.1 State of the art

Electricity generation is the process of generating electric power from other sources of primary energy. The fundamental principles of electricity generation were discovered during the 1830s by the British scientist, called Michael. The electro-mechanical energy transformation occupies a significant role in the processing of energy in a wide range of the world. Most of world energy resources are fossil fuel, nuclear fuel, potential energy, kinetic energy and renewable resources. Basically, wind power generation system converts the energy of moving air into useful electricity either for stand-alone system in rural locations or grid integration through power electronic components and optional three – phase coupling transformer. Brief review of related research will be presented in the next subsections of the present thesis.

1.1.1 Development of synchronous machine drives

As a matter of fact, synchronous machine is so called because the speed of the rotor in this AC machine is same as the speed of the rotating magnetic field. Basically, it is a fixed speed machine and therefore it's in synchronism with the supply frequency. Synchronous machines are widely represented and they are still in continuous growing. They include wide variety of structures and topologies. Among many features that made their success include a naturally outperform than other electric machines reside in, the ability to regulate reactive power, voltage regulation and great freedom in designing process and manufacturing for this type of AC machines [Klempner et al., 2004].

Recently, the synchronous machines are also used in variable speed motoring. The PMSM manufactures are developing various categories and structures of synchronous machines ranging from small scale up to large size. On the other hand, an efficient development has been considered in the field of power electronics technology. It has made the task of flexible rotor speed variation a realizable target. In effect, PMSMs are more efficient for applications demanded rotor speed reversion. Synchronous machine is much more convenient for AC drives than other AC machines. Particularly, when these applications involve wide power variation, it has better performance in dynamic behaviour and steady state responses. In fact, this type of AC machine is used in many of industrial control applications such as electric traction; high speed machining, robotics manipulation, watches, automotive or computer peripherals [Krause et al., 2013].

Indeed, the rate of change in rotor speed cannot be accomplished for three – phase synchronous machines, by acting on the frequency of AC power supply. Before the considerable progress in power electronics components, there were no simple ideas and no efficient approach to modify or tuning the power supply frequency. On the other hand, the field of electric traction and the power transmission lines are used either DC or AC single - phase system. Therefore, the three - phase power inverters(DC/AC) provide the possibility to make interconnection between the power grid and AC drives. These inverters have the capability to ensure smooth output voltage through passive or active harmonic filters with frequency variation [Tadger et al., 2014].

As early mentioned, it can be categorized the electric traction motors based on electrical power supply either AC or DC source. DC electric traction is the preferred option for shorter lines, urban systems and tramways. Nevertheless, DC electric traction was also used on several line railway systems. DC series motor is mainly used for the purposes of the motor drives. AC traction system is much more reliable and safer in practical operation according to instructions and orientations of industrial safety. Basically, wound rotor electric machines are used in AC traction systems [see *e.g.* Ehsani et al., 2003].

Essentially, the power system converters provide non-sinusoidal currents; even they are powered by main supply voltages. These converters behave as harmonic currents generators. Because of the short-circuit impedance of the electrical grid, the harmonic currents distort and attenuate the main supply voltages, effectively. Off course, the distortions caused by input currents and main supply voltages will affect on the normal operation, dynamic performances and it entails to damage other household -electric appliances, if the operation conditions are serious. Therefore, with the restriction and limitation of providing an acceptable sinusoidal voltage, energy distributors will support various harmonic mitigation techniques available to solve harmonic problems in power systems. Thus, filtering the harmonic components and presenting the better technical services and good offers for the consumers of electricity are the central concern of the energy distributors in the world during the past decades.

1.1.2 Continuous – time nonlinear state observer design

To apply the state feedback control design to any system, we assumed so far that most of its variables are accessible forever. These measurements will impose additional costs; increase the hardware complexity, and cause wiring interference. Subsequently, that will reflect

Chapter 1: General Introduction

negatively on system control process, effects globally on dynamic performances and reduces the system robustness. These causes are considered the motivations and justifications for scientists facing the problem of sensorless control technique based on input/output injective measurements.

While the scientific contributions dealing with designing of linear observers may have reached a saturation point, whilst research on synthesis of state observers for nonlinear systems is far away from the end. In fact, a unified approach to observer design process of nonlinear systems still seems hard to formulate it globally. In addition, one of the difficulties to achieve in this context is the arbitrary enlargement in stability boundary when discussing the problem of observer stability and convergence analysis. Moreover, the boundary of the attraction region is formed by closed - loop trajectories.

The extended *Kalman* filter (EKF) is widely used in industrial processes. Although, some of design parameters are needed for adjusting process, its synthesis is simple, relatively and it gives some acceptable results for state observation of nonlinear systems. Nevertheless, there is no theoretical justification concerning with its robustness and no formal way for its stability convergence analysis.

The state observer operates in neighbourhood of a certain point, which bounds its dynamic performance under practical stability approach. This approach gives the possibility to study the system characteristics in which the state of state tends to a set rather than equilibrium point. The radius of deviation around the origin could be minimized by selecting satisfactory large enough observer parameter. It is possible to design an observer for a nonlinear system by transforming it into another system for which a class of state observer is known. For this purpose, several uniform approaches had been achieved to convert a nonlinear system into specific classes of general nonlinear systems [see *e.g.* Isidori, 1995; Glumineau et al., 2007] for a class of SISO while for a class of MIMO system, it is highly recommended doing model transformation to a state - affine system and observer design is proposed [see *e.g.* Virgilio et al., 1999]. A class of nonlinear system is transformed into a linear system with an output injection and the ability to synthesis a linear observer so called *Luenberger observer* claimed in(1964).

When this transformation does not applicable, case study dependent, it is recommended to transform the nonlinear system to a linear time varying(LTV) system based on input–output injection for which an exact *Kalman Like Observer* had been synthesized [see *e.g.* Souleiman et al., 2007]. Some of the previous approaches are usually based on linearization and they

Chapter 1: General Introduction

seem attractive due to the simplicity of the state observer design regardless for the complexity of the system. Unfortunately, the drawbacks of the early mentioned approaches ensure local stability of the observation error [Baras et al., 1988].

Some of the applications, state observer design had been done huge revolution in the research preliminaries. It is interested in numerous applications without necessitating to use mechanical or magnetic sensor, which allows saving costs, increase cyclic –maintenance duration, propose a practical solution for real- time measurements and replace unreliable hardware (classical) sensors by on – line (advanced) software sensors, which are relatively low cost, robust to external disturbances and enable to ensure fast clearing for grid faults.

Self – sensing observation techniques and their applications for electric machines had been developed in the previous literatures. Basically, there are two approaches dealing with state observation. One of them is qualified approach without using mathematical model representation. Subsequently, this approach is based on the method of injecting an electrical voltage signal in the stator windings using the property of changing stator inductance value using injection of high frequency voltage signal (HFVS) around 10MHz for rotor position estimation. The drawback of this approach causes harmonics injection in the machine rotor speed [Nussbaumer et al., 2010; Brandstetter et al., 2013]. The benefit of this approach provides information about the rotor position at low rotor speed applications. However, it requires a saliency in the electrical AC machine design for example the PMSMs exhibit the most saliency *i.e.* $(L_q = (2 - 3)) * L_d$ whilst the surface PMSMs exhibit a very small saliency $(L_q \approx L_d)$. In addition, high frequency signal injection is not recommended for high rotor speed applications.

The second approach is based on the electrical AC machine's behaviour using the state observation techniques. The operation of the induced voltage in the stator windings to estimate the rotor position and rotor speed using for example sliding mode state observers, *Kalman* filter or *Luenberger* observer, which are special kinds of the state observers that provides optimal filtering of process and reduce measurements noise [see *e.g.* Qiao et al., 2013; Kailas et al., 2015]. Basically, this approach is desirable for high-speed applications but rather, this approach is not accurate at low rotor speed when the electro - motive force (EMF) is low, relatively.

Nonlinear state observers *e.g.* sliding mode observer design(SMO) had been claimed by many literates, main results and design principles are presented for nonlinear systems[see *e.g.* Spurgeon, 2015; Niaona, et al., 2011]. Design of high - gain observers (HGOs) for on-line

estimation of unmeasured physical system states and parametric uncertainties had been introduced by many scientific contributions[see *e.g.* Abdelhak et al., 2015]. Recently, sampled data nonlinear state observer design is the central concern and an attractive research area for the researchers and scientists during the last decade. For this reason, the next subsection will be presented to give some of importance throughout the present thesis.

1.1.3 Sampled – data nonlinear state observer design

In general, design of sampled – data nonlinear state observers can be carried - out in the literatures through the following three different techniques, which are:

1.1.3.1 Emulation design process

Basically, the state observer design is performed for the closed – loop continuous – time model based on input/output injection measurements. At this step, the sampling effect is completely neglected. In the context of control and communication, sampling means that a continuous – time signal replaced by a sequence of numbers, which represent the values of the signal at certain times. The process of re-converting sequence of numbers into a continuous time signal is called signal reconstruction. The second step of this process is discretized the continuous time – model preparing for digital implementation or interfaced with digital communication networks.

Then, to maintain the observer performances and ensure fast exponential convergence of the observation error, one needs to sample it sufficiently fast; which often exceeds the hardware capability [see *e.g.* Chen et al., 1991]. To achieve the numerical integration, methods such as *Euler*, *Tustin* and other *Runge – Kutta* methods are commonly used for this purpose. This approach usually gives results in the semi-global practical stability of the observation error. Emulation design process is sometimes not adequate in some physical systems. It is important to search about an alternative solution to get better performance so called the direct discrete - time design process [see *e.g.* Arcak et al., 2004].

1.1.3.2 Direct discrete-time design process

It is apparent from the previous design process that the state observer design using emulation process always suffers the deterioration in performance. To minimize the degree of deterioration, it is recommended to use very fast sampling, which may not be efficient because of hardware limitations. In this case, direct discrete – time design process offers an alternative solution, since in this design, sampling effect is considered from starting of the

design process. The state observer is designed in discrete-time mode directly, using one of the discrete-time approximation model of the system (*e.g. Euler approximation model of the plants*) [El Assoudi et al., 2002], whilst this technique disregards the inter-sampled behaviour during the design process.

1.1.3.3 Sampled-data design process

It has been mentioned earlier that direct discrete – time design process has the capability to improve the design process compared with emulation design process. Despite that, inter – sample behaviour is not considered in previous design techniques. This limitation becomes a drawback of this design technique, resides in ripple injection may appear in output response of the system under study. As a matter of fact, careful design and optimal selecting of sampling interval (sampling interval is the time between successive data samples) must be accomplished to ensure better dynamic performance of the closed loop system and ensure fast convergence of the observation errors.

One of the main challenges of network – controlled system is to improve the sampling interval while preserving required in terms of stability and performance properties of the system. Another approach to ameliorate the design process can be achieved through sampled – data design process. In this process, the state observer is designed in discrete-time mode, but using the continuous-time model of the plant including sample and hold devices in the design process (*i.e. ZOH and TR*) [see *e.g. Ahmed-Ali et al., 2009*].

In recent years, a new hybrid observer design based on emulation process has been applied in industrial applications. In fact, inter – sample state prediction coupled with the continuous – time high gain state observer design had been introduced firstly by [Karafyllis et al., 2009]. Once again, the fundamental results proved by formal analysis, provided by [Karafyllis et al., 2008], had been developed in a global form given by the authors in [Karafyllis et al., 2012]. A simple block diagram for sampled - data design is shown in Figure 1.1.

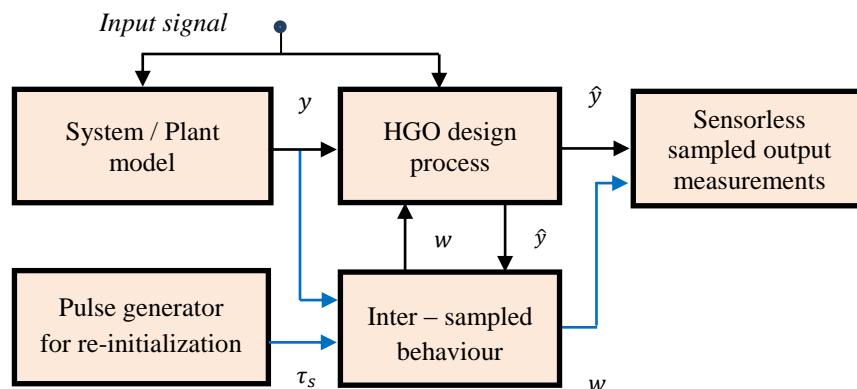


Figure 1.1: A Simple block diagram for sampled - data design process

1.1.4 Electrical power system control techniques

Linear system control techniques using classical regulators for output voltage control had been proposed by many literates [see. e.g. Pan et al., 1993]. The basic idea for most of linear control techniques depend on changing in the modulation index, (modulation index is key parameter, it is necessary to keep the modulation index within limits, $0 < m_o < 1$, to minimize the harmonic distortion), resulting in a slow dynamical response. Subsequently, the linear SFC of output voltage regulation becomes slowly in tracking response and difficult from control point of view. Numerous methods and techniques exist for the analysis and design of nonlinear system control. Full details related with topics about useful fundamentals and control preliminaries are found in several textbooks [see e.g. Khalil, 2002; Najmeijer et al., 2006], and in the control handbook [see e.g. Levine, 1996]. Most of theories and practices focus on closed –loop feedback control. A typical layout of a feedback control system is shown in Figure 1.2. It is obvious from Figure1.2 that sensor element in closed loop may be hardware or software sensor, application dependent. The present thesis will focus on software sensors.

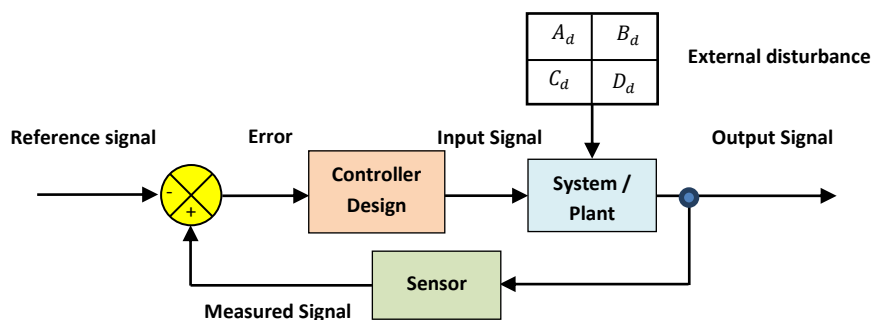


Figure 1.2: A typical layout of a feedback control system

For our knowledge, most of the previous scientific contributions related with control of SM drive systems had been simplified the problem of rotor speed and load torque by omitting the dynamics representation of AC/DC power rectifier and most of the authors focused on the combination DC/AC - machine. The reduced system model had been achieved through different control techniques ranging from simple approach, likes field oriented control (FOC) [see e.g. Kiran et al., 2014]. The FOC consists of controlling the stator currents represented by a vector. This control is based on projections which transform a three- phase system into a ($d - q$ coordinates) time invariant system. These projections lead to a structure like that of a DC machine control. Field orientated controlled machines need two constants as input references, which are torque component (aligned with the q - coordinate) and the flux component (aligned with d - coordinate).

Nonlinear advanced and modern control techniques, such as feedback linearization [e.g. Ramana et al., 2015], direct torque control (DTC) [Hua et al., 2014]. In the DTC scheme, $(d - q)$ axis transformation is not recommended. The electromagnetic torque and the stator flux are estimated and directly controlled by applying the appropriate stator voltage vector. It is possible to estimate the rotor speed, thus eliminating the need for rotor speed encoder.

To solve this problem, many literates propose different method. A comparative study with conventional sliding mode control had been introduced by [Huangfu et al., 2010]. It gives scientific solutions for avoidance chattering phenomenon e.g. pseudo sliding mode uses saturation function instead of *signum* function or higher order sliding mode(HOSM) controller and its application of PMSM [see e.g. Kumari et al., 2015]. Once again, the dynamic performances of a robust speed sensorless nonlinear control of PMSMs had been discussed by several literatures using tools of *Lyapunov* stability theory [see e.g. Fezzani et al., 2014]. Figure 1.3 illustrates the basic scheme for sensorless control of PMSM drives.

A nonlinear control strategy that disregards the presence of AC/DC rectifier has at least two weak - points. First one, the proposed controller design is based on the hypothesis that the DC bus voltage, supplied by the AC/DC power converter, is perfectly regulated to a given reference signal. The second weak - point is completely ignored the PFC requirement. From the control point of view, it is unfairly to consider separately the combination DC/AC – machine drive in one side and the power rectifier (AC/DC), on the other side.

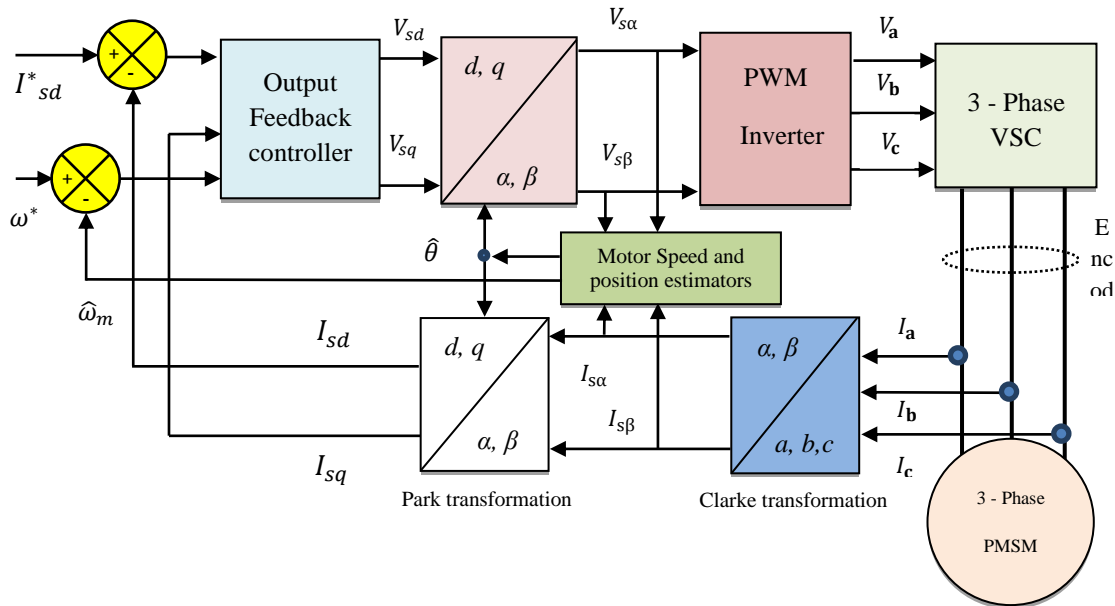


Figure 1.3: Basic scheme for sensorless control of PMSM drive systems

1.1.5 Wind power generation systems

Wind power generation system (WPGS) converts the energy of the moving air into useful electricity. WPGS can be classified either operate at fixed wind speed or variable wind speed. For fixed- speed wind turbines, the generators are directly connected to the electrical networks. Whilst for variable speed operation of wind turbines, the generators are controlled by advanced and modern power electronic components. There are several motivations and justifications for preferring variable speed operation of wind turbines. The possibility to reduce the mechanical stresses, acoustic noise reduction, and achieve active or reactive power regulation as demanded by electrical utility [see *e.g.* Al – Tahir, 2012].

Most of the major wind turbine manufactures are developing, successfully new largescale wind turbines ranging (3 – 5)MW [see *e.g.* Harrison, et al., 2001]. Most of the large- scale wind turbines are based on variable-speed operation with pitch control (VS – VP) using direct- drive PMSG or DFIG. General block diagram of the WPGS is described in Figure 1.4, which illustrates the power flow in WPGS.

Recently, doubly-fed induction generators are commonly used by the wind turbine industry for largescale wind turbines [Lara et al., 2009]. The main benefit of DFIG resides in power electronic components within power converters have the capability to handle (20 - 30%) of the total power system (*i.e.* slip power). Subsequently, the power losses in the power electronic components can be minimized in comparison to power electronic components that had been used for direct-driven PMSG. This technique will reflect the usefulness in cost saving, increasing power system capacity, robust *w.r.t* external disturbances and reducing size of power converters [Al – Tahir, 2011].

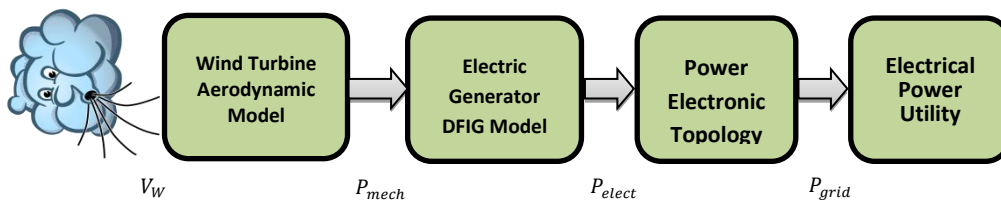


Figure 1.4: General block diagram of the WPGS

1.2 Contribution of the thesis

The first contribution of the present thesis dealt with variable speed PMSM drives involve DC/AC power converter. Basically, the major function of sensorless PMSM drive is draw the

electrical energy from the main source and supplies the required energy to the electric motor. Thus, the desired mechanical output is achieved without resorting to use classical mechanical and magnetic sensors. Also, the second contribution of the present thesis focused on modeling, state observation and stability analysis of DFIGs based VSWT coupled through buck -to- buck boost power converters for grid integration. Whilst the third contribution discussed the problem of adaptive nonlinear output feedback controller of three - phase AC/DC boost power converter for on-line UPS related with critical loads.

Different modes of operation for some of the AC machines have been achieved, which are:

- (i) Permanent magnet synchronous machine under variable speed sensorless drives.
- (ii) Doubly fed induction machine with generating operation mode based VSWT.
- (iii) Adaptive nonlinear output feedback controller of three – phase VSC for on-line emergency power supply. The control signals in third part of present thesis are implemented based on averaged controlled model. Averaging all waveforms over the switching period removes the switching harmonics, while preserving the low-frequency components of the electrical waveforms.

1.3 Objectives and motivations of the thesis

The main objectives and motivations of the present thesis could be summarized as follows:

1. Among the main objectives of the present thesis is synthesis of a sampled output HGO for on-line estimation of rotor position, rotated speed and unknown load torque of PMSM drive without resorting to use traditional mechanical or magnetic sensors. It is apparent, additional mechanical or magnetic sensors will inject DC offsets in measured signals. This may lead to loss the stability of AC system. DC offset is the presence of DC current and/or voltage component in dynamic performance of AC systems. Only the electrical variables are supposed to be accessible (*i.e.* Stator voltages and discrete - time currents).

To realize this target, the present thesis presents in the first phase an observability analysis of PMSM leading to find a sufficient observability condition. In the second phase, it derives an upper bound condition for the maximum allowable sampling period, *i.e.* τ_{MASP} to make sure an exponential convergence of the observation error towards zero and guarantee better tracking response of the closed – loop trajectories. Once again, the stability convergence is formally analysed with elegant and full proof using tools of *Lyapunov* stability theory. To validate the theoretical results described by main theorem and prove the stability convergence of the state observer, the proposed observer is demonstrated

throughout a sample study application to sensorless variable speed PMSM drive in the final phase.

2. One of the scientific directions for the present thesis resides in the electromagnetic torque, T_{em} created by DFIG generator. In effect, T_{em} is considered indirect output injective relation when designing sampled output HGO for on-line estimates of reduced - model. The stator and rotor current vector is considered inaccessible to continuous - time measurements. Only sampled - data output measurements are presently available at each sampling instant. A novel state observer synthesis has been designed and formally stability convergence analysis with assistance of *Lyapunov* stability tools and input - to - state stability (ISS) concept for whatever initial conditions. For systems with external disturbances, ISS had been changed the local concept of total stability with a more useful global concept.
3. One of the huge challenges faced the present thesis resides in complexity of controlling three-phase boost power converter for on-line UPS under parametric uncertainty and strong nonlinearity of system model. The major control objective is twofold, which are:
 - i) Ensuring a satisfactory power factor correction (PFC) at the grid - UPS connection. The total harmonic distortion must be less than 2 %, raised by input grid phase currents.
 - ii) Guaranteeing a tight regulation of the DC output voltage despite of uncertain resistive load and amplitude of grid phase voltage. The DC component of output voltage must be regulated to a given reference level whilst the corresponding AC component must be attenuated with small ripple size.

The considered nonlinear adaptive control problem entails several technical difficulties as:

- The input phase currents are considered inaccessible to ensure on-line measurements, fast fault monitoring and enable rapid protection system.
- The parametric uncertainties related with grid phase voltage and equivalent resistive load across the DC – bus voltage.

1.4 On-line observer design techniques for some of AC machines

The second part of the current thesis involves two chapters (*i.e.* Chapter three and four) focused on sampled – output high gain state observer design and its application to variable speed PMSM drive system and variable wind speed DFIG based WPGS.

1.4.1 Sampled – data observer design for PMSM drive systems

A sampled - output high gain observer design has been proposed recently to get on-line estimates of the rotor speed and the external load torque based on the measurements of stator voltage application to PMSM drive systems. As a matter of fact, detecting the initial rotor position is not necessary when the rotor flux projected on $(\alpha - \beta)$ stationary reference frame is estimated by the state observer. The general structure of the proposed state observer combines the benefits and ideas of HGO structure and inter – sample output predictor. The main principles of the proposed state observer have been inspired entirely by [Karafyllis et al.,2009]. The stability convergence analysis of the proposed observer is formally proved based on *Lyapunov* nonlinear design techniques and ISS concept for a class of MIMO physical systems.

One of the major targets is limiting the observation errors with upper bound and this bound can be made small as possible by selecting sufficient large constant observer parameter and sufficient sampling period to ensure fast exponential convergence of the observation error towards zero with timely progress, taking into consideration heavily interconnection between state observation errors and output - state prediction errors.

Thus, the proposed state observer for sampled output measurements is capable to guarantee an acceptable dynamic response over wide range of operation region. The general scheme for the proposed sampled – output high gain observer design is shown in Figure 1.5.

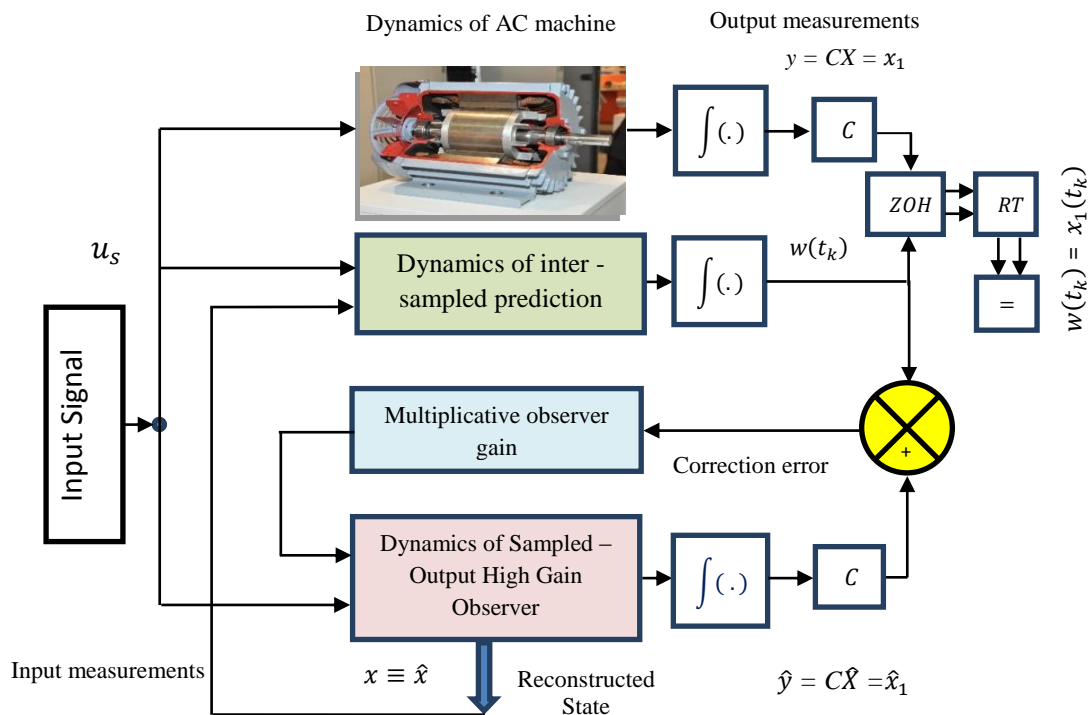


Figure 1.5: The general scheme for sampled – output HGO observer design

1.4.2 DFIG running with non-standard sampled observer

As the PMSG has received a great deal attention based WPGS, the DFIG has acquired much consideration with developing power electronic components. Basically, one of the scientific directions for the present thesis is oriented for observation of variable speed grid connected DFIG based WPGS. Motivated by the fact that the system controlling and state observation of DFIG are very complex and this complexity lies in the availability of multi – state variables, highly nonlinearity property and some of the system state variables are inaccessible. If some of these variables may accessible, but they are impractical and expensive from economical point of view.

One of the major contributions of current thesis will focus on providing main results supported by formal analysis for the proposed theorem. A novel state observer synthesis has been designed and formally stability convergence analysis with the assistance of *Lyapunov* stability tools and ISS concept has been provided through a main result. Also, nonlinear reduced model of DFIG has been analyzed for a class of nonlinear systems, successfully and check its capability for running with reduced – order state observer based on senseless sampled output measurements, without necessitating using traditional mechanical sensors.

Typically, the general structure of the proposed state observer combines the features and ideas of a high – gain structure and an inter – sampled output state prediction based on grid voltage measurements and sampled output measurements using on - injective output relation related to electromagnetic torque. In fact, T_{em} is a linear function with measured stator and rotor current vector. One of the major targets is finding the observation errors with upper bound and this bound can be made small as possible by selecting sufficient large observer gain parameter and small sampling period to ensure fast exponential convergence of observation error towards zero with time progress. These observation errors, caused by technical hypotheses, are relatively acceptable from the physical point of view.

Once again, when one talks about state - observer design for a class of nonlinear systems, this will lead us to discuss the problem of synthesis and stabilization of output - feedback nonlinear control system (for adaptive and non - adaptive versions) with proposal of practical control laws to ensure negative definiteness of *Lyapunov* function candidate using one of the control strategies. So, the next section will discuss the adaptive senseless system.

1.5 Adaptive output feedback control of VSC for UPS system

Recently, modern nonlinear control strategies, combine parameter adaptation with sensorless output-feedback that has been discussed, successfully in the present thesis. The nonlinear adaptive output feedback control scheme can be accomplished in two main steps in response to changing in magnitude of resistive load and grid phase voltage for a class of nonlinear state - affine systems based on input/output injection measurements inspired partly by [Besançon, 2007] and all references therein for more details.

Now, the first step provides inner control loop design to ensure input phase current in phase with grid phase voltage (*i.e.* UPFC) by regulating it to a given reference current. Whilst, the second step deals with outer control loop is built up to achieve DC bus voltage regulation across balanced equivalent resistive load such that the DC component of output voltage must be regulated to a given reference voltage while the AC component of output voltage must be attenuated to small ripple size. These current and voltage regulators are capable to ensure the stability convergence of the closed -loop adaptive control system under acceptable references.

The present work has been supported by a short formal analysis, using the fundamental principles of averaging theory. The power factor correction close to unity is well established with small harmonic distortion less than 2%. Indeed, the present work is unlike of previous literatures, because most of them are considered only resistive load unknown parameter while the present work is considered a resistive load as well as the value of grid phase voltage are uncertain parameters in the designing process of adaptive nonlinear controller. The schematic diagram of the proposed adaptive output feedback controller design for three – phase on-line emergency power supply is shown in Figure 1.6.

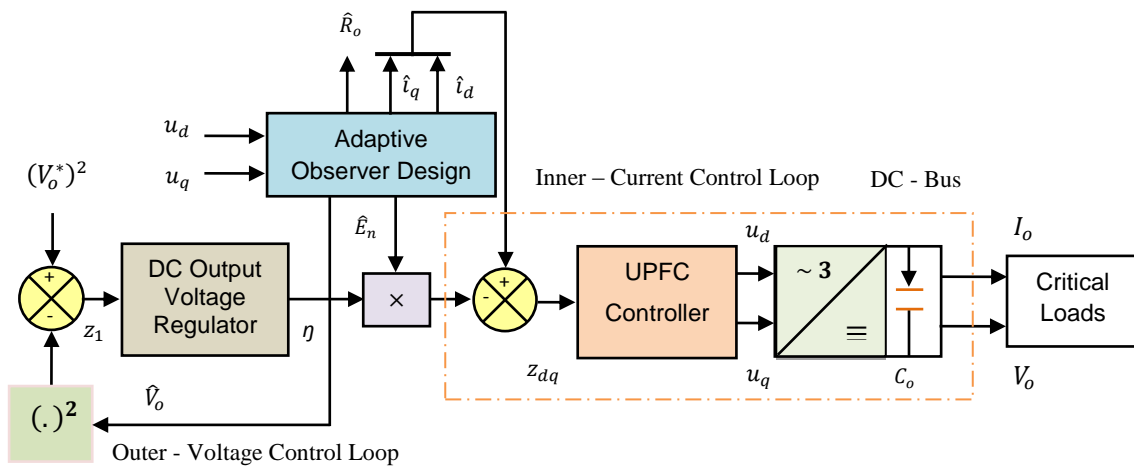


Figure 1.6: The schematic diagram of proposed adaptive output feedback controller design

1.6 Outline of thesis

The present thesis is organized in the following manner to present the layout work, which has been done during my PhD research. For readability in better form, the present thesis is separated in six chapters and classified in three parts, in the following form:

PART I Preliminaries

Chapter 1: General Introduction

This chapter consists of state of the art, contribution of the thesis, objectives and motivations of thesis, general review about state observer design, focused on sampled - output measurement application for some of AC machines based variable speed drives and nonlinear adaptive output feedback controller design for a class of state - affine system.

Chapter 2: Mathematical Models and Control Fundamentals for Online Stabilization

Mathematical models for some of AC machines, advantages and disadvantages of PMSMs, DFIMs have been presented. Also, observability analysis and the control preliminaries for on-line stabilization of MIMO nonlinear systems will be used later in the present thesis. Some of stability tools are well - known *Lyapunov* stability techniques interconnected with ISS concept are just presented for convenience to present work. The basic concepts of backstepping control design technique are also provided in chapter two.

PART I Sampled -Data Nonlinear Observer Design for Some of AC Machines, are

- PMSM in motoring mode of operation.
- DFIG in generating mode of operation.

Chapter 3: Sampled – Data Nonlinear Observer Design for Sensorless Synchronous PMSM

Chapter three is dedicated to my first contribution as published in the article, which involves the mathematical model and dynamic state equations for PMSM are presented. This type of machines is presented in two – phase ($\alpha - \beta$) stationary reference frame. This model is suitable for observer design to provide rotor position without using an additional dynamic equation. The dynamic equations with some coefficients are governing the operation of this electric machine.

On the other hand, the observability analysis of PMSM model is discussed to check simply is it possible synthesis state observer running with PMSM. At the end of this chapter, stability convergence analysis of the proposed sampled output HGO is formally proved through a main

Chapter 1: General Introduction

result using the tools of *Lyapunov* stability theory. In fact, inter – sampled prediction proves to be much more efficient compared to some types of the state predictions given in previous literatures. For nonlinear systems, different forms of predictors had been used, either exact predictors, based on the knowledge of the solution mapping, approximate predictors based on successive approximations or numerical schemes.

Chapter 4: A Novel Observer Design based on Sensorless Sampled Output Measurements: Application to Variable Speed DFIG based WPGS.

This chapter covers a novel exponential convergence nonlinear state observer design of variable speed DFIGs based wind turbines to generate the electrical power and support the electrical networks by clean energy. Also, this chapter focused on modeling and operation of reduced - model grid integration of DFIG based WPGS.

The major feature of the proposed state observer lies in the consistence of sampled-data measurements without necessitating using the traditional mechanical or magnetic sensors. As a matter of fact, rotor position and speed encoders are more costly and may be unreliable or impractical to measurements in most of industrial processes.

PART III Nonlinear Adaptive Output Feedback Controller and Stabilization.

Chapter 5: Output Feedback Nonlinear Adaptive Control Strategy of Three -Phase AC/DC Boost Power Converter for Online UPS Systems.

In Chapter 5, the problem of modeling and controlling of three-phase boost power converter is considered for on-line monitoring of UPS system. Basically, the problem focused on nonlinear adaptive controller that is developed using tools of *Lyapunov stability* theory. The parametric uncertainties are processed by the control laws under backstepping design techniques with a capacity of adaptation to ensure sufficient stability region.

- i. The inner - control loop ensures the PFC objective and involves an adaptive observer for estimating the unmeasured quantities. In fact, the state and parameter estimations are only based on-line measurements of DC output voltage across the equivalent unknown resistive load.
- ii. On the other hand, the outer - control loop regulates the DC output voltage with small ripple size. It is observed in this chapter that the developed algorithm is effective and efficient for improving various power quality features such as unity power factor control requirements, DC - bus voltage regulation and harmonic mitigation in electrical power equipments. An explicit analysis of the closed - loop system composite from regulators,

Chapter 1: General Introduction

an adaptive observer, and the controlled system, is essential to focus on the parameter adjustments necessary for the stability convergence analysis of the whole error system dynamics using tools of *Lyapunov* stability theory.

Chapter6: General Conclusions and Suggestions for Future Works

In chapter six, the summary of the obtained main results in the present thesis and the concluding remarks are highlighted with potential recommendations for future works. The searcher proposes several directions in which results of the present thesis can be further expanded and modified later. The logical sequence of the thesis chapters is shown in Figure 1.7, to facilitate reading and easily understanding the results provided by the present thesis.

1.7 Appendices

To alleviate the presentation, some technical proofs and main fundamentals dealing with the present thesis are appended in the following form:

- A.1. Clarke's transformation converts the (ABC) quantities to the $(\alpha - \beta)$ quantities.
- A.2. Park's transformation converts the $(\alpha - \beta)$ quantities to the $(d - q)$ rotating quantities
- A.3. The PWM generation in the drive systems is briefly described.
- A.4. Derivation of wind power equation. Some mathematical relationships, which are required in chapter 4, are derived in this appendix.
- A.5. *Young's* and *Bellman's* inequalities.

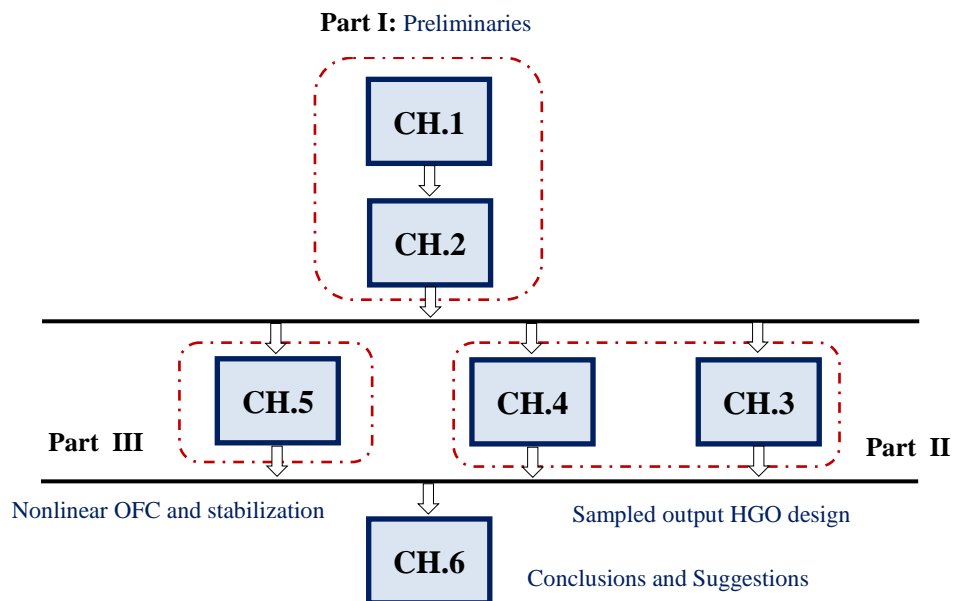


Figure 1.7: Logical sequence of the thesis chapters

Chapter Two

Mathematical Models and Control Fundamentals for On-line Stabilization

Table of Contents	page
2.1 Fundamentals of permanent - magnets electric machine	19
2.1.1 Rotor position sensor elimination	20
2.1.2 PM synchronous machines versus induction machines	21
2.2 Permanent magnet synchronous machine modeling	22
2.2.1 Modeling of PMSM in abc – representations	22
2.2.2 Model of PMSMs in rotating ($d - q$) reference frame	23
2.2.3 Model of PMSMs in ($\alpha - \beta$) representation	25
2.3 Modeling of wind generation power systems	27
2.3.1 Wind turbine mathematical model	28
2.3.2 Doubly fed induction generator model	29
2.4 Wind speed types and operating regions of WPGSs	30
2.4.1 Cut - in wind speed	31
2.4.2 Rated wind speed.....	32
2.4.3 Cut - out wind speed	32
2.5 Wind turbine concepts	32
2.5.1 Fixed speed wind turbines	33
2.5.2 Partial variable speed wind turbine with rotor resistance	33
2.5.3 VSWT with partial-scale converter	33
2.5.4 VSWT with full-scale converter	34
2.6 Observability study for sensorless control design	35
2.7 Backstepping control design techniques	36
2.7.1 Continuous - time backstepping design technique	42
2.8 Introduction for a class of system studied	43
2.9 Fundamental properties for stability convergence analysis	48
2.9.1 Input – to – state stability concept	50
2.9.2 Fundamentals of ISS small - gain condition	50

In this chapter, a short review describing permanent magnet synchronous machine model and doubly fed induction generator based wind power generation system will be presented. More specifically, the related previous studies dealing with system modeling, the state observer design, and the control strategies applied on PMSM drives and DFIG will be presented.

This chapter is organised by nine main sections which are: section 2.1 presents the fundamentals of PMSM meanwhile PMSM modeling concepts focused on section 2.2. Modeling of WPGS is discussed in section 2.3, wind speed types and related operating regions of WPGSs is provided in section 2.4 and wind turbine concepts is described in section 2.5. In section 2.6, observability study of sensorless control design is discussed, briefly. A backstepping control design technique for nonlinear systems is studied in section 2.7. An introduction to a class of system studied is given in section 2.8. Finally, the fundamental properties for stability convergence analysis are achieved in section 2.9.

2.1 Fundamentals of permanent - magnets electric machines

Basically, permanent magnet electric machines are defined as doubly excited electric machines. They have two sources of excitation, namely, armature and the field excitation source. In traditional DFIM (*i.e.* DC commutator machines and synchronous machines), the excitation sources are electric windings connected to an external main power supply. But, in permanent magnet electric machines, the magnetic field is generated by permanent magnets located on the rotor, which eliminating the necessitating using field windings and external main power supply. In contrast to the traditional doubly excited electric machines, the copper loss related with field windings does not exist in PMSMs, which reflects positively in increasing the overall efficiency of the PMSMs.

On the other hand, the use of permanent magnets to generate the field flux allows to design these machines with less weight and compact size compared to the traditional double - excited electric machines. On the other hand, the permanent magnets generate a constant field flux and it cannot be controlled easily as in traditional double - excited electric machines by controlling the field current [Hendershot et al., 2010].

Various rotor topologies exist for PMSMs depending on how the magnets are placed in the rotating part [Gieras, 2009]. Basically, there are two common types, namely, surface – mounted permanent magnet type and interior – mounted permanents magnet type. In surface

magnet type the magnets are mounted on the surface of the rotor core, whereas in interior magnet type the magnets are placed inside the rotor core. Hereinafter the PMSMs with surface magnets rotor configuration are called SPMSMs and PMSMs with interior magnets rotor configuration are called IPMSMs.

2.1.1 Rotor position sensor elimination

Rotor position sensors are usually expensive and they considerably increase the cost of the PMSMs drive systems. Furthermore, a special mechanical arrangement needs to be made for mounting the position sensors and extra signal wires are required for the sensor to the proposed SFC approach [Benchabane et al., 2011; Boussak, 2008].

Some types of position sensors such as *Hall - Effect* based magnetic position sensors, fibre-optic position sensor and optical position sensors are temperature sensitive and their accuracy degrades when the system temperature exceeds the limits. These reasons lead to the elimination of shaft mounted rotor angular position sensor, which is conventionally used for self-synchronization in the control system [see e.g. Lu, 2013; Bobtsov et al., 2015]. The control of PMSMs and DFIGs using the same concepts will discuss later in chapter three and chapter of four for current thesis eliminating rotor angular position sensor, is referred to sensorless control of those machines.

Using this technique for AC machines offers a big advantage of sensorless control. Information about the rotor position can be estimated indirectly from the $(\alpha - \beta)$ representation of rotor flux linkage. The benefits of sensorless machine control can be summarized as:

- Reduced hardware complexity.
- Saving cost.
- Reduced size of AC drives.
- Elimination of the sensor cable and wire.
- Better noise immunity.
- Increased reliability of control systems.
- Less cyclic maintenance.

2.1.2 PM synchronous machines versus induction machines

The PMSMs do not need magnetizing component of the stator current, since the excitation source is induced by permanent magnets, which differ from the induction machines with this idea. Off course, this will reflect positively in a stator copper loss reduction in PMSMs. That is, the copper loss related to rotating parts in induction machines does not exist in PMSMs. This copper loss reduction in stator and rotor significantly improves the electrical efficiency of PMSMs compared to electric induction machines [Doncker et al., 2011].

However, it should be mentioned that during the flux weakening region of operation, the PMSMs require high stator current to weaken the flux linkage [Leonhard, 2001], increasing the stator copper loss. This reduces the efficiency of PMSMs during flux weakening operation region and both PMSMs and induction machines serve with less electrical efficiency in that operation region. This implies that from the efficiency point of view the PMSMs are well convenient over the induction machines in the applications like pumps and fans because there is negligible rotor losses in PMSMs. Nowadays, the growing electrical consumption is one of the major challenges that faces most of the scientist [Mishra et al., 2014].

Another attractive feature of PMSMs over the corresponding electric induction machines are that the possibility of design PMSMs with less weight and volume than induction machines of the same capacity. Then, it is convenient to use PMSM, especially where a space is serious matter. Recently, the IPMSMs were designed with significant reduction of weight and volume over the induction machines. PMSMs have lower inertia when compared with induction machines because of absence of rotor cage. This makes for faster response for a given electric torque. In other words, PMSMs have high electromagnetic torque to moment of inertia (T_{em}/J) ratio. This ratio is highly recommended for applications that require fast dynamic response. Since PMSMs are synchronous machines their control should always be related with self-synchronization concept.

2.2 Permanent magnet synchronous machine modeling

The continuous increase of power system complexity and installation of more and more new equipment in power systems has demanded better methods for power system analysis, planning, and control. At present, analysis of modern power systems is generally based on digital computers. Hence, the establishment of a mathematical model for the analysis of various power system problems, correct and accurate computation for power system analysis

requires a correct mathematical model. Mathematical models employed for steady - state analysis are extremely simple, while the dynamic models for electric systems are not easy to develop. Dynamic modeling is needed for various types of analysis related to system dynamics: stability and control system. Each mathematical model is based on technical hypothesis. The unexpected errors provided by induction hypothesis are practically acceptable. There are three hypotheses used for simplifying the model of PMSM, as:

H₁: The induced electromagnetic force (EMF) is assumed sinusoidal.

H₂: Iron permeability in the machine is assumed tends to infinite. In other word, the magnetic reluctance of the flux linkage path is composed of the air - gap and leakage reluctances. That is, the magnetic characteristics of PMSM are linear and they operated out of weakening region.

H₃: The negative effects of fault currents and the hysteresis losses are insignificant.

2.2.1 Modeling of PMSM in *abc* – representations

The excitation can be induced by permanent – magnets, which provide constant magnetic flux linkage. In current subsection, greater attention is focused on the modeling and analysis of PMSM. One can specify, below, the modifications and simplification used to model the PMSM. This machine has three fixed stator windings, called *a*, *b* and *c*.

By analyzing the electrical equivalent circuit of PMSM, the stator voltages among three – phase windings can be described in the following equation provided by voltage/current *Kirchhoff laws* [El Fadili et al, 2012]:

$$[v_{sabc}] = [R_s][i_{sabc}] + \frac{d}{dt}[\phi_{sabc}] \quad (2.1)$$

where v_{sabc} , i_{sabc} , R_s and ϕ_{sabc} are defined as the stator voltage, current, resistance and stator flux - linkage, respectively. In the rotating part, the permanent magnets provide a constant rotor flux - linkage. However, the expressions of the inductor rotor flux can be specified as:

$$\left\{ \begin{array}{l} \phi_{ra} = \phi_{PM} \cos(n_p \theta_m) \\ \phi_{rb} = \phi_{PM} \cos(n_p \theta_m - 2\pi/3) \\ \phi_{rc} = \phi_{PM} \cos(n_p \theta_m + 2\pi/3) \end{array} \right. \quad \begin{array}{l} (2.2a) \\ (2.2b) \\ (2.2c) \end{array}$$

with ϕ_{PM} is the nominal value of rotor flux - linkage induced by the permanent – magnets and n_p is number of magnetic pole pairs. It should be mentioned that ϕ_{PM} is unaffected with the variation of temperature degree. In such a way, one can write the stator induced flux per

phase by adding the rotor flux induced by the permanent – magnets located on the rotor and the resulting flux linkage by the currents passing through the stator phase windings.

$$[\phi_{sabc}] = [L_{ss}][i_{sabc}] + [\phi_{rabc}] \quad (2.3a)$$

The matrix of self – inductances $[L_{ss}]$ will be defined later in the next subsection equation (2.10).

Now, combining the expression of the rotor flux given in equation (2.2) with equation (2.1) and using the following physical property:

$$\frac{d}{dt}(\cdot) \triangleq \frac{d\theta_r}{dt} \frac{d}{d\theta_r}(\cdot) = \omega_r \frac{d}{d\theta_r}(\cdot) \quad (2.3b)$$

Then, one writes the stator voltages in (abc) representation as:

$$[v_{sabc}] = [R_s][i_{sabc}] + \frac{d}{dt}[L_{ss}][i_{sabc}] + \omega_r \frac{d}{d\theta_r}[\phi_{rabc}] \quad (2.4)$$

The electromagnetic torque provided by PMSMs is presented as follows:

$$T_{em} = \frac{1}{2} [i_{sabc}]^T \left\{ \frac{d}{d\theta_r} [L_{ss}] \right\} [i_{sabc}] + [i_{sabc}]^T \left\{ \frac{d}{d\theta_r} [\phi_{rabc}] \right\} \quad (2.5)$$

For small signal analysis of PMSM, the lumped – mass model (or single – mass model) is used. Now, deriving the state equation of the rotor angular speed, one has the following,

$$\frac{d}{dt} \omega_r = \frac{1}{J} (T_{em} - T_L - f_v \omega_r) \quad (2.6)$$

The mechanical parameters J and f_v are the combined rotor, load inertia, and combined rotor, load viscous friction. Figure 2.1 illustrates coordinate transformation of abc – representation of fixed and rotating reference frame applied on PMSMs.

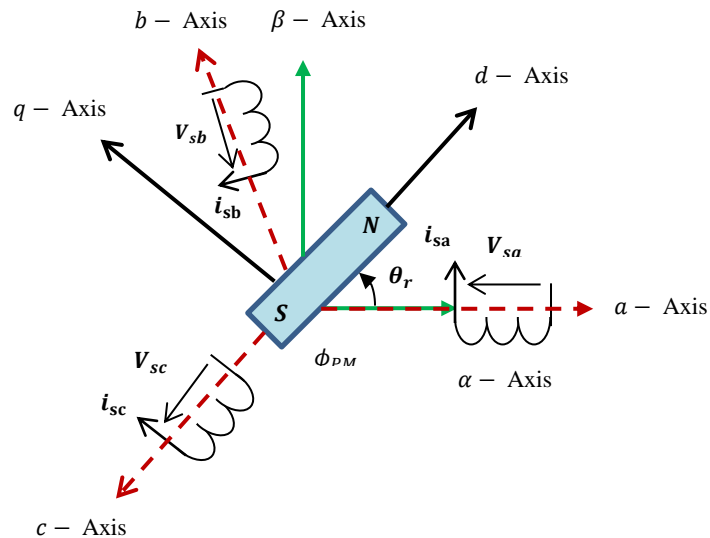


Figure 2.1: Transformation of abc - coordinates to fixed and rotating frame

2.2.2 Model of PMSMs in rotating $(d - q)$ reference frame

- *Electrical equations of PMSMs*

For the control and simulation of a PMSM, a mathematical model in rotating $(d - q)$ reference frame is preferred than others, whilst the $(d - q)$ model of a PMSM is usually used because the stator inductances are treated as constant and independent of rotor position angle. The mathematical model of PMSMs in a rotating reference frame is derived from the abc - representation given by equation (2.4) using *Park's* transformation. The AC machine model had been developed by the scientist *Park* who mathematically transform the fixed frame time - varying stator quantities into time - invariant projected on $(d - q)$ frame. Basically, *Park's* transformation of state variables denoted by $[X_d, X_q]^T$ is described in the following equation:

$$\begin{bmatrix} X_d \\ X_q \end{bmatrix} \triangleq P(\theta_r)^T T_{32}^T \begin{bmatrix} X_a \\ X_b \\ X_c \end{bmatrix} \quad (2.7)$$

where, θ_r is the angular rotor position of the rotating reference frame. $P(\theta_r)$ denotes the *Park's* transformation matrix from the stationary reference frame $(\alpha - \beta)$ to the rotating reference frame $(d - q)$ is given by [Leonhard, 2001]. More details about *Park's* and *Clark's* transformations are found in appendices A.1 and A.2.

$$P(\theta_r) \triangleq \begin{pmatrix} \cos \theta_r & -\sin \theta_r \\ \sin \theta_r & \cos \theta_r \end{pmatrix} \quad (2.8)$$

Using *Park's* transformation defined in (2.7), one deduces that equation (2.4) for machine stator voltages becomes:

$$\begin{aligned} T_{32}P(\theta_r)[v_{sdq}] &= R_s T_{32}P(\theta_r)[i_{sdq}] + \frac{d}{dt} ([L_{ss}]T_{32}P(\theta_r)[i_{sdq}]) \\ &+ \omega_r \frac{d}{d\theta_r} T_{32}P(\theta_r)[\phi_{rdq}] \end{aligned} \quad (2.9)$$

where, the matrix of self - inductances $[L_{ss}]$ is defined as:

$$[L_{ss}] \triangleq L_{sv} \mathbb{I}_3 + \frac{2}{3} L_{sv} T_{32}P(\theta_r)SP(\theta_r)^T T_{32}^T \quad (2.10)$$

Multiplying both sides of equation (2.9) by the term $P(\theta_r)^T T_{32}^T$ and expressing the matrix $[L_{ss}]$ by its definition given in (2.10), one has;

$$\begin{aligned} [v_{sdq}] &= R_s [i_{sdq}] + \omega_r P(\theta_r)^T T_{32}^T \frac{d}{d\theta_r} (T_{32}P(\theta_r)) [\phi_{rdq}] \\ &+ P(\theta_r)^T \frac{d}{dt} \left\{ T_{32}^T \left(L_{sv} \mathbb{I}_2 + \frac{2}{3} L_{sv} T_{32}P(\theta_r)SP(\theta_r)^T T_{32}^T \right) T_{32}P(\theta_r) [i_{sdq}] \right\} \end{aligned} \quad (2.11)$$

$\mathbb{I}_2 \in \mathbb{R}^{2 \times 2}$ is identity matrix. Using the physical property defined in equation (2.3b), gives:

$$\frac{d}{d\theta_m}(P(\theta_r)) = n_p \begin{pmatrix} -\sin \theta_r & -\cos \theta_r \\ \cos \theta_r & -\sin \theta_r \end{pmatrix} \triangleq n_p P(\theta_r) J_2 \quad (2.12a)$$

One can easily verify the following properties as:

$$n_p P(\theta_r) J_2 n_p P(\theta_r)^T = n_p \begin{pmatrix} -\sin \theta_r & -\cos \theta_r \\ \cos \theta_r & -\sin \theta_r \end{pmatrix} \begin{pmatrix} 0 & -1 \\ 1 & 0 \end{pmatrix} n_p \begin{pmatrix} \cos \theta_r & \sin \theta_r \\ -\sin \theta_r & \cos \theta_r \end{pmatrix} = J_2 \quad (2.12b)$$

$$\text{with, } S \triangleq \begin{bmatrix} 1 & 0 \\ 0 & -1 \end{bmatrix}, \quad J_2 \triangleq \begin{bmatrix} 0 & -1 \\ 1 & 0 \end{bmatrix}, \quad L_{sv} \triangleq \frac{3}{4}(L_d - L_q) \quad (2.12c)$$

After simple mathematical manipulation, one has the following expression:

$$\begin{aligned} [v_{sdq}] &= R_s [i_{sdq}] + n_p \omega_r J_2 [\phi_{rdq}] + \left(L_{sv} \mathbb{I}_2 + \frac{2}{3} L_{sv} S \right) \frac{d}{dt} [i_{sdq}] \\ &\quad + n_p \omega_r P(\theta_r)^T \left(L_{sv} P(\theta_r) J_2 + \frac{2}{3} L_{sv} T_{32} P(\theta_r) J_2 S \right) [i_{sdq}] \end{aligned} \quad (2.13)$$

Now, let us define the matrix of self-inductances projected on $(d - q)$ representation as:

$$[L_{dq}] \triangleq \begin{pmatrix} L_d & 0 \\ 0 & L_q \end{pmatrix} = L_{cs} \mathbb{I}_2 + \frac{2}{3} L_{sv} S \quad (2.14)$$

In view of equation (2.14), it gives the definition of self - inductances for PMSM projected on $(d - q)$ coordinates as follows:

$$L_d \triangleq 1.5(L_{so} + L_{sv}), \quad L_q \triangleq 1.5(L_{so} - L_{sv}) \quad (2.15)$$

and cyclic inductance, $L_{cs} \triangleq 1.5 L_{so}$.

where, L_{so}, L_{sv} are nonzero real constants depending on the machine structure.

Lastly, the electric equation in $(d - q)$ model can be re-formulated as follows:

$$\begin{aligned} [v_{sdq}] &= R_s [i_{sdq}] + [L_{dq}] \frac{d}{dt} [i_{sdq}] + n_p \omega_r J_2 [L_{dq}] [i_{sdq}] + \left(L_{sv} \mathbb{I}_3 + \frac{2}{3} L_{sv} S \right) \frac{d}{dt} [i_{sdq}] \\ &\quad + n_p \omega_r J_2 [\phi_{rdq}] \end{aligned} \quad (2.16)$$

• Mechanical equation of PMSMs

According to the previous equation mentioned earlier, the mathematical expression of the electromagnetic torque in $(d - q)$ reference frame is written as:

$$\begin{aligned} T_{em} &= n_p \frac{1}{2} [i_{sdq}]^T P(\theta_r)^T T_{32}^T \frac{2}{3} n_p L_{sv} T_{32} P(\theta_r) (J_2 S + S J_2^T) [i_{sdq}] \\ &\quad + n_p [i_{sdq}]^T P(\theta_r)^T T_{32}^T T_{32} P(\theta_r) J_2 P(\theta_r)^T P(\theta_r) S [\phi_{rdq}] \end{aligned} \quad (2.17)$$

Knowing that, $P(\theta_r)^T T_{32}^T T_{32} P(\theta_r) = \mathbb{I}_2, \quad \forall \mathbb{I}_2 \in \mathbb{R}^{2 \times 2}$

$$\text{Also, } [i_{sdq}]^T J_2 S [i_{sdq}] = 2 i_{sd} i_{sq}, \quad J_2 S = S J_2^T = \mathbb{I}_2$$

After simple computations, equation (2.17) becomes;

$$T_{em} = T_L + f_v \omega_r + J \frac{d\omega_r}{dt} = n_p (L_d - L_q) i_{sd} i_{sq} + \frac{2}{3} L_{sv} [i_{sdq}]^T J_2 [\phi_{rdq}] \quad (2.18)$$

2.2.3 Model of PMSMs in $(\alpha - \beta)$ representation

- **Electrical equations of PMSMs:** The mathematical model of the PMSMs in $(\alpha - \beta)$ representation is getting from (*Park – Concordia*) transformation of equation (2.13). The electric equation of the stationary reference model can be written as:

$$\begin{aligned} [v_{s\alpha\beta}] = R_s [i_{s\alpha\beta}] + P(\theta_r) [L_{dq}] \frac{d}{dt} P(\theta_r)^T [i_{s\alpha\beta}] + n_p \omega_r J_2 [L_{dq}] P(\theta_r)^T [i_{s\alpha\beta}] \\ + n_p \omega_r P(\theta_r) J_2 P(\theta_r)^T [\phi_{r\alpha\beta}] \end{aligned} \quad (2.19)$$

Using the mathematical properties defined in equations (2.3b) and (2.12a-c), one can re-write equation (2.19) in the following form:

$$\begin{aligned} [v_{s\alpha\beta}] = R_s [i_{s\alpha\beta}] + [L_{dq}] \frac{d}{dt} [i_{s\alpha\beta}] + n_p \omega_r P(\theta_r) (J_2 [L_{dq}] + [L_{dq}] J_2^T) P(\theta_r)^T [i_{s\alpha\beta}] \\ + n_p \omega_r J_2 [\phi_{r\alpha\beta}] \end{aligned} \quad (2.20)$$

It can be checked the term, $n_p \omega_r P(\theta_r) (J_2 [L_{dq}] + [L_{dq}] J_2^T) P(\theta_r)^T \triangleq n_p \omega_r (L_d - L_q)$.

Eventually, one can re-write equation (2.20) in the following new form:

$$[v_{s\alpha\beta}] = R_s [i_{s\alpha\beta}] + [L_{dq}] \frac{d}{dt} [i_{s\alpha\beta}] + n_p \omega_r (L_d - L_q) [i_{s\alpha\beta}] + n_p \omega_r J_2 [\phi_{r\alpha\beta}] \quad (2.21)$$

- **Mechanical equation of PMSMs**

Once again, after doing inverse *Park's* transformation for the corresponding equation of electromagnetic torque in $(d - q)$ rotor reference frame defined in (2.18), one has the following, T_{em} projected on $(\alpha - \beta)$ stationary reference frame:

$$T_{em} = \frac{2}{3} n_p L_{sv} [i_{s\alpha\beta}]^T P(\theta_r) J_2 S P(\theta_r)^T [i_{s\alpha\beta}] + n_p [i_{s\alpha\beta}]^T P(\theta_r) J_2 P(\theta_r)^T [\phi_{r\alpha\beta}] \quad (2.22)$$

To simplify the mathematical manipulation, let us define the term mentioned above as,

$$\mathfrak{R}(\theta_r) \triangleq P(\theta_r) J_2 S P(\theta_r)^T$$

The expression of electromagnetic torque projected on $(\alpha - \beta)$ stationary frame is written as:

$$T_{em} = \frac{2}{3} n_p L_{sv} [i_{s\alpha\beta}]^T \mathfrak{R}(\theta_r) + P(\theta_r)^T [i_{s\alpha\beta}] + n_p [i_{s\alpha\beta}]^T J_2 [\phi_{r\alpha\beta}] \quad (2.23a)$$

It is readily checked that, $[i_{s\alpha\beta}]^T J_2 [\phi_{r\alpha\beta}] \triangleq (\phi_{r\alpha} i_{s\beta} - \phi_{r\beta} i_{s\alpha})$

So, the new form of equation (2.23a) becomes:

$$T_{em} = T_L + f_v \omega_r + J \frac{d\omega_r}{dt} = \frac{2}{3} n_p L_{sv} [i_{s\alpha\beta}]^T \mathfrak{R}(\theta_r) [i_{s\alpha\beta}] + n_p (\phi_{r\alpha} i_{s\beta} - \phi_{r\beta} i_{s\alpha}) \quad (2.23b)$$

Now, using *Park - Concordia* transformation, by considering balanced three - phase system (2.2a-c), the dynamic model for rotor flux linkage projected on $(\alpha - \beta)$ stationary reference frame is written as:

$$\left[\begin{array}{l} \frac{d}{dt} \phi_{r\alpha} \triangleq n_p \omega_r \phi_{r\beta} \\ \frac{d}{dt} \phi_{r\beta} \triangleq -n_p \omega_r \phi_{r\alpha} \end{array} \right. \quad (2.24a)$$

$$\quad (2.24b)$$

The mathematical model for permanent magnet synchronous machines projected on $(\alpha - \beta)$ stationary reference frame is written in the following system state equation (2.25):

$$\left[\begin{array}{l} \frac{d}{dt} i_{s\alpha} = -\frac{R_s}{L_s} i_{s\alpha} - \frac{n_p}{L_s} \omega_r \phi_{r\beta} + \frac{1}{L_s} u_{s\alpha} \\ \frac{d}{dt} i_{s\beta} = -\frac{R_s}{L_s} i_{s\beta} + \frac{n_p}{L_s} \omega_r \phi_{r\alpha} + \frac{1}{L_s} u_{s\beta} \end{array} \right. \quad (2.25a)$$

$$\quad (2.25b)$$

$$\left[\begin{array}{l} \frac{d}{dt} \phi_{r\alpha} = n_p \omega_r \phi_{r\beta} \\ \frac{d}{dt} \phi_{r\beta} = -n_p \omega_r \phi_{r\alpha} \end{array} \right. \quad (2.25c)$$

$$\quad (2.25d)$$

$$\left[\begin{array}{l} \frac{d\omega_r}{dt} = 1.5 \frac{n_p}{J} L_{sv} [i_{s\alpha\beta}]^T \Re(\theta_r) [i_{s\alpha\beta}] + \frac{n_p}{J} (\phi_{r\alpha} i_{s\beta} - \phi_{r\beta} i_{s\alpha}) - \frac{1}{J} (f_v \omega_r - T_L) \\ \frac{dT_L}{dt} = 0 \end{array} \right. \quad (2.25e)$$

$$\quad (2.25f)$$

Note that, modeling of surface - mounted permanent - magnets synchronous machine is exactly same as the corresponding saliency interior magnet type PMSM, if the air - gap between stationary part and rotating part is homogeneous (*i.e.*, smooth and constant air - gap thickness for a complete rotation) and subsequently the variable reluctance torque tends to zero. This implies from (2.12c):

$$L_{sv} = \frac{3}{4} (L_d - L_q) = 0, \quad \rightarrow \quad L_d = L_q = L_s$$

In other words, the expression of electromagnetic torque given in (2.18) for $(d - q)$ representation is just the main couple.

$$T_{em} = T_L + f_v \omega_r + J \frac{d}{dt} \omega_r = n_p \sqrt{1.5} \phi_r i_{sq} \quad (2.26a)$$

and the corresponding expression of, T_{em} in equation (2.23b) expressed in $(\alpha - \beta)$ is:

$$T_{em} = T_L + f_v \omega_r + J \frac{d}{dt} \omega_r = n_p (\phi_{r\alpha} i_{s\beta} - \phi_{r\beta} i_{s\alpha}) \quad (2.26b)$$

2.3 Modeling of wind power generation systems

In recent decades, wind power generation system (WPGS) is transformed from the fixed wind speed to the variable wind speed operation technology. Variable speed machines have

various benefits and features, for example, they reduce mechanical stresses, dynamically adjust in case of power or torque pulsations, improve power quality and conversion efficiency, high - power handling capability, good stability performances both at low and high speed operations. Numerous electric generators can be compatible with variable speed operation of wind turbine. However, variable speed operation of wind turbine using DFIG is relatively competitive and powerful because it has many inherent features. These features explain why this type of generator is getting spread in different fields of industry. It has proved to be quite suitable both as a motor in various applications and a generator, especially in wind power generation systems.

Generator rotor speed can be regulated below or above the synchronous speed, ω_s within a specified range $\pm 30\%$, which further depends on the rating of power converters. In DFIG, converters handle only slip power which is just a fraction of the total generated power. This leads to the reduction in power converter rating and hence reduced their costs, from the economic point of view [Simoes et al., 2008; Junyent et al., 2010]. The bidirectional power flow is achieved by using AC/DC/AC pulse width modulated IGBT based voltage source converters with a common DC bus. In grid connected systems, these power converters are referred as rotor side converter, RSC and grid side converter, GSC. While in case of stand-alone systems, the GSC is re-named as a load side converter [Archna et al., 2014].

2.3.1 Wind turbine mathematical model

The aerodynamic power P_a captured by the wind turbine system is given as:

$$\left[\begin{array}{l} P_a = 0.5 \rho \pi R^2 C_p(\lambda_{TSR}, \beta) V_w^3 \\ \lambda_{TSR} = \frac{R\omega_r}{V_w} \end{array} \right. \quad \begin{array}{l} (2.27a) \\ (2.27b) \end{array}$$

where, V_w is the wind speed, ρ is the air density, R is the rotor radius and C_p is the power coefficient. It is defined as the ratio of electricity produced by a wind turbine generator to the total energy available in the wind. For most of the wind turbines, the value of C_p is 48% practically and 60% theoretically. λ_{TSR} is the ratio of turbine blade tip speed to wind speed and β is the blade pitch angle. Wind turbine system, C_p can be represented by nonlinear curve versus tip speed ratio, λ_{TSR} for different pitch angles. The aerodynamic power is also defined based on the fundamental principles of AC machines:

$$\text{Or,} \quad \left[\begin{array}{l} P_a = T_g \omega_r \\ T_g = \frac{P_a}{\omega_r} = \frac{0.5 \rho \pi R^3 C_p(\lambda_{TSR}, \beta) V_w^2}{\lambda_{TSR}} \end{array} \right. \quad \begin{array}{l} (2.27c) \\ (2.27d) \end{array}$$

where, T_g is the aerodynamic torque and ω_r is the WTG rotor speed. It is obvious, changes as small as possible, such as one or two degrees will generate large differences in aerodynamic performances of the turbine since the variation pattern in angle of attack is changed resulting in an altered blade torque pattern around one revolution.

2.3.2 Doubly fed induction generator model

By analysing the electrical equivalent circuit of the DFIG and applying *Kirchhoff* laws, it obtains the dynamic system state equation written in (2.28) after doing *Park's* transformation for the three -phase electrical quantities. The control system is usually synchronized with the $(d - q)$ frame and fixed either with stator voltage or flux linkage, application dependent [El Fadili et al., 2012]. This choice is suitable as it facilitates the control of the active and the reactive power delivered between the electric generator and the super grid. The following simplified model projected on $(d - q)$ frame has been adopted by the following dynamic state equations:

$$\begin{cases} \dot{\phi}_{sd} = -R_s i_{sd} + \omega_s \phi_{sq} + v_{sd} & (2.28a) \\ \dot{\phi}_{sq} = -R_s i_{sq} - \omega_s \phi_{sd} + v_{sq} & (2.28b) \\ \dot{\phi}_{rd} = -\hat{R}_r i_{rd} + (\omega_s - n_p \omega_g) \hat{\phi}_{rq} + \hat{v}_{rd} & (2.28c) \\ \dot{\phi}_{rq} = -\hat{R}_r i_{rq} - (\omega_s - n_p \omega_g) \hat{\phi}_{rd} + \hat{v}_{rq} & (2.28d) \\ \dot{\omega}_g = \frac{1}{J} (T_{em} - T_g - f_v \omega_g) & (2.28e) \end{cases}$$

The flux linkage equations of the stator and rotor sides can be formulated mathematically in terms of their currents projected on $(d - q)$ synchronous rotor reference frame using matrix notation:

$$\begin{bmatrix} \phi_{sd} \\ \phi_{sq} \\ \hat{\phi}_{rd} \\ \hat{\phi}_{rq} \end{bmatrix} = \begin{bmatrix} L_s & 0 & M_{sr} & 0 \\ 0 & L_s & 0 & M_{sr} \\ M_{sr} & 0 & \hat{L}_r & 0 \\ 0 & M_{sr} & 0 & \hat{L}_r \end{bmatrix} \begin{bmatrix} i_{sd} \\ i_{sq} \\ \hat{i}_{rd} \\ \hat{i}_{rq} \end{bmatrix} \quad (2.28f)$$

$$T_{em} \triangleq n_p \frac{M_{sr}}{L_s} (\hat{i}_{rd} \phi_{sq} - \hat{i}_{rq} \phi_{sd}) \quad (2.28g)$$

with, T_{em} denotes the electromagnetic torque in (N.m) created by DFIG. R_s, L_s , are stator side resistance and self - inductance. \hat{R}_r and \hat{L}_r are, respectively the rotor resistance and self - inductance referred to stator side, while M_{sr} is the mutual or coupling inductance between the stator and the rotor windings. $\phi_{sd}, \phi_{sq}, \hat{\phi}_{rd}$, and $\hat{\phi}_{rq}$ denote the stator flux components and rotor flux components referred to stator side, expressed in $(d - q)$ representation.

$(i_{sd}, i_{sq}, i_{rd}, i_{rq})$ and $(v_{sd}, v_{sq}, v_{rd}, v_{rq})$ are the stator components of the current, voltage and the corresponding rotor components referred to stator side, respectively. The symbol n_p designates the number of magnetic poles – pair and ω_s is the constant stator angular speed in (rad/sec). The parameters f_v and J are, respectively the viscous friction coefficient and the total moment of inertia for lumped - mass model (rotor blades, hub, and DFIG generator). Note that, the rotor windings in this type of machine are not short - circuit and the corresponding $(d - q)$ rotor voltages are activated in terms of stator flux ϕ_{sd} , ϕ_{sq} and rotor current i_{rd} , i_{rq} as state variables and under assumption of linear magnetic circuits. If the stator voltage is linked to $(d - axis)$, the new dynamics controlled model of DFIG projected on $(d - q)$ frame is:

$$\left[\begin{array}{l} \frac{d}{dt} \omega_g = \frac{1}{J} (T_{em} - T_g - f_v \omega_g) \quad (2.29a) \\ \frac{d}{dt} \phi_{sd} = -\frac{R_s}{L_s} \phi_{sd} + \omega_s \phi_{sq} + \frac{R_s M_{sr}}{L_s} i_{rd} + v_{sd} \quad (2.29b) \\ \frac{d}{dt} \phi_{sq} = -\frac{R_s}{L_s} \phi_{sq} - \omega_s \phi_{sd} + \frac{R_s M_{sr}}{L_s} i_{rq} \quad (2.29c) \\ \frac{d}{dt} i_{rd} = -\frac{R_s L_s^2 + R_s M_{sr}^2}{\left(1 - \frac{M_{sr}^2}{L_s L_r}\right) L_r L_s^2} i_{rd} + (\omega_s - n_p \omega_g) i_{rq} - n_p \omega_g \frac{M_{sr}}{R_s \left(1 - \frac{M_{sr}^2}{L_s L_r}\right) L_r} \phi_{sq} \\ \quad - \frac{M_{sr}}{\left(1 - \frac{M_{sr}^2}{L_s L_r}\right) L_r L_s} v_{sd} + \frac{1}{L_r \left(1 - \frac{M_{sr}^2}{L_s L_r}\right)} v_{rd} \quad (2.29d) \\ \frac{d}{dt} i_{rq} = -\frac{R_s L_s^2 + R_s M_{sr}^2}{\left(1 - \frac{M_{sr}^2}{L_s L_r}\right) L_r L_s^2} i_{rq} - (\omega_s - n_p \omega_g) i_{rd} + n_p \omega_g \frac{M_{sr}}{R_s \left(1 - \frac{M_{sr}^2}{L_s L_r}\right) L_r} \phi_{sd} \\ \quad + \frac{1}{L_r \left(1 - \frac{M_{sr}^2}{L_s L_r}\right)} v_{rq} \quad (2.29e) \end{array} \right.$$

More details about the reduced model of DFIG based WPGS can be found in chapter four.

2.4 Wind speed types and operating regions of WPGSs

The variable speed wind turbine system always operates with different dynamic characteristics starting from low wind speed up to high wind speed, and the corresponding operating regions of the wind turbine can be clarified by wind turbine power curve. Three different wind velocity and two operation modes are shown in the power curve. It has an abrupt transition from cubic characteristic to constant power operation at a higher wind velocity under stall control. Practically, most of wind turbines do not exhibit like this behaviour (abrupt transition), and the transition is usually smooth under pitch angle control [Jansuya et al, 2013]. The corresponding definitions of wind velocity and operation modes are given below:

2.4.1 Cut - in wind speed

It is the minimum wind speed at which the wind turbine starts to generate usable power. Cut – in wind speed is typically bounded between (3.13 - 4.47) m/sec for most of wind turbines dependent on aerodynamic wind turbine design. At very low wind speeds, there is no sufficient generator torque extracted by the wind prevailing on the wind vane to make them rotate. On the other word, if the wind speed increases far away from cut in - speed, the wind turbine will begin to accelerate and generate useful electricity. It should be mentioned that the starting torque of wind turbine must be greater that aerodynamic frictions.

2.4.2 Rated wind speed

It is the bounded wind speed at which the wind turbine will generate its designated rated power. At wind speeds between the cut-in speed and the rated speed, the wind turbine will operate at the maximum power point tracking (MPPT) mode, and the output power of a wind turbine is proportional with cubic of wind speed (m/s).

As the wind speed rises above the cut-in speed, the level of electrical output power will raise quickly. When, the output power arrives to the expectable limit, this limit to the electrical generator output is called the rated output power corresponding to rated wind speed and there is no further rise in the output electrical power.

2.4.3 Cut - out wind speed

At very high wind speeds, typically bounded between (22 – 45) m/sec, most of the wind turbines terminate output power generation and they are shut down for protection purposes. The wind speed at which shut down operation occurs is called the cut - out speed. As the wind speed increases above the rated wind speed, the affected forces on the wind turbine structure continue to rise and, at some point, there is a risk of damage to the rotor. As a result, a braking system is employed to bring the rotor to a standstill. For large scale - wind turbines, this situation can be avoided by adjusting or tuning the blade pitch angles through nonlinear controller to maintain the output power at the constant level, protect the wind turbine from huge mechanical stresses and ensure continuity in the generation process.

Generally, variable speed wind turbine generator systems have two different control objectives, depending on the wind speed. For low wind speeds, the maximum power point tracking (MPPT) mode is desired so that the output power can be maximized according to the specific wind speed. For high wind speeds, the pitch angle regulation should be achieved to keep the output power at its rated value. In the MPPT operation mode, the speed of the wind

turbine is adjusted in such a way that the wind turbine can capture the maximum power based on the given wind speed. However, this operation has the drawback of generating fluctuated power due to the variations in wind speed. At the rated wind speed point, the controller attempts to maintain the rotor speed at its rated wind speed and the output power at its rated power. This maximum power tracking regulation is mainly achieved by means of the generator side converter control loop [Lalouni, 2015].

In the blade pitch angle control operation mode, if the wind speed exceeds its rated level. It would be harmful for the wind turbine to operate at such high wind speed. Hence, the generator speed must be limited by minimizing the aerodynamic torque. This can be done through regulating the blade pitch angle, so that the aerodynamic conversion efficiency is reduced, and thus less mechanical torque acts on the generator, and lastly the rotor speed can be maintained at a constant level. There is a theoretical limit on the amount of generating power, $C_p = 16/27 \approx 59\%$, that can be extracted by a wind turbine from an airstream. It is called the *Betz limit* and for more details about wind turbine is given in appendix A.4 of the present thesis.

2.5 Wind turbine concepts

Wind power generation system (WPGS) employs either variable or fixed speed wind turbines. They can be classified in four different categories. The main differences between these categories are the approaches used. How the aerodynamic efficiency of the rotor would be limited for different wind speed conditions? These four categories are briefly described as follows [Iov et al., 2008]:

2.5.1 Fixed speed wind turbines

This type of wind turbine uses squirrel - cage induction generator (SCIG) connected to the electrical grid. The so-called fixed speed wind turbine comes from the fact that the rotational speed of the wind turbine cannot be regulated by speed controller and it will only vary directly with the prevailing wind speeds.

2.5.2 Partial VSWT with variable rotor resistance

This type of wind turbine uses a wound rotor induction generator (WRIG) directly connected to the grid. The rotor phase windings of the generator are connected in series with

2.5.4 VSWT with full-scale power converter

This type of wind turbine is usually equipped with permanent magnet synchronous generator and a full-scale power converter. The stator phase windings are connected to the grid through a full-scale power converter. Some of these types of wind turbines adopt with direct driven mechanism. That is a direct driven multi-poles generator is employed without resorting to use a mechanical gearbox (gearless mechanism) [Kramer et al., 2008]. To ensure the wind turbine generator connected to the grid, a buck – to – buck PWM voltage source converters are interfaced between the PMSG and the electrical grid. The grid side PWM inverter allows for controlling of real and reactive power transferred to the grid. The generator side converter is used for electromagnetic torque and rotor speed regulation. The direct – axis current is held to zero to ensure maximum electromagnetic torque with minimum current and attenuate variable reluctance torque [Amirat et al., 2007]. It should be mentioned that, the basic benefits and drawbacks of third wind turbines category coupled with DFIG system are simply summarized as follows [see e.g. Benelghali et al., 2010].

➤ Benefits of the DFIG equipped by WPGSSs

- The DFIG supports rotor speed control, active and reactive power control by regulating the rotor terminal voltages with common DC - bus. Hence, the power factor correction requirements can be carried out in this category.
- DFIG is usually a wound rotor induction generator, which is simpler in construction and lower manufacturing cost compared to PMSG for the same size (rating).
- In a DFIG based WPGSSs, the power rating of three – phase power converters are typically rated $\pm 30\%$ around the total rated power, and this characteristic leads to support several merits, such as, reduce power converter cost, minimize filter size, less switching losses, less harmonic injections into the super grid and thus improving overall system efficiency.

➤ Drawbacks of the DFIG equipped by WPGSSs

- DFIG needs slip-rings and sometimes gearbox, which increases cyclic maintenance.
- It has limited fault ride (FRT) through capability and needs efficient protection schemes. FRT is the capability of electric generator to stay connected for short periods of voltage dip.
- It has a complex control system related with active and reactive power.

Recently, as the PMSG has received much attention in WECS, DFIG is most commonly used in the wind turbine industry for large scale generation systems (*i.e.* $P_g > 1\text{MW}$). Considering these merits of the DFIG based WPGS, the present thesis will focus on modelling and design of novel sampled output high - gain state observer running with a reduced model of DFIG whilst the state observation of PMSG is considered as a future research study with adaptive or non - adaptive version of dynamic models.

2.6 Observability study for sensorless control design

Basically, the observability study is checking the capability to re-construct the closed - loop trajectory of a (linear or nonlinear) system based on the output data (and/or) input measurements. The observability study of a linear system usually needs the output measurements and it does not depend on the input signals applied to the system under study. The approach to achieve this study is dependent on the *Kalman* criterion of the observability. Now, let us study the observability of linear systems described by the dynamic state equation and its output state equation, specifically a time invariant linear system can be applied as [see *e.g.* Glumineau et al., 2015] and all the references therein for more details:

$$\begin{cases} \dot{x} = Ax + Bu \\ y = Cx \end{cases} \quad (2.30)$$

where, $x \in \mathbb{R}^n$ is the state variable, $u \in \mathbb{R}^m$ is the input state and $y \in \mathbb{R}^p$ is the output state while A, B and C are defined state, input and output matrices, respectively. As a result, the observability matrix, \mathcal{O} containing the information that is generated for observability test:

$$\mathcal{O} \triangleq \begin{pmatrix} C \\ CA \\ \vdots \\ CA^{n-1} \end{pmatrix} \quad (2.31a)$$

The system can be verified whatever it is observable, if and only if the observability matrix has full rank almost everywhere. The observability condition is:

$$\text{rank}(\mathcal{O}) \triangleq n \quad (2.31b)$$

where, n is the dimension of the system under study.

Let us consider the following class of nonlinear systems of the form:

$$\begin{cases} \dot{x} = f(x, u_g) \\ y = h(x) \end{cases} \quad (2.32)$$

It is worthy that few observability concepts are introduced by [Vidyasagar et al., 1993]:

Definition 2.1 System in (2.32) is said to satisfy the observability rank condition in x , if $\dim\{d\mathcal{O}(h)\} = n$. Moreover, if the observability rank condition holds $\forall x \in \mathbb{R}^n$, system defined in (2.32) is observable in the rank sense. If the system (2.32) is observable in the rank sense, then it is weakly observable.

Definition 2.2 Two states named, x_0 and x_i are said to be *distinguishable*, if there exists an input function $u(\cdot) \in \mathbb{R}^m$ such that the corresponding output state equations are not equal, *i.e.* $y(\cdot, x_0, u) \neq y(\cdot, x_i, u)$, where $i = 1, 2, 3, \dots$

Definition 2.3 The system is said to be locally observable at, $x_0 \in X$, if there exists a neighbourhood, N of x_0 such that $\forall x \in N$ other than x_0 is distinguishable from x_0 . Hence, the system is said to be locally observable, if it is locally observable at each $x_0 \in X$, $X \in \mathbb{R}^n$.

Definition 2.4 It is possible to define a system to be globally observable if every pair of states $(x_0, x_i) \forall x_0 \neq x_i$, is distinguishable. However, this concept seems much stronger than local observability.

On the other side, the observability of a nonlinear system can be damaged near the singular point, so there are powerful techniques used to provide sufficient conditions such that nonlinear systems are conditionally observable.

Generally, the observability study of the nonlinear systems can be classified into two categories, which are:

- 1) The observability study is independent of the input measurements as in linear systems.
- 2) The observability study is contingent on the input injection.

For the first probability of nonlinear system where the observability concept does not depend on the input measurements, in this case one can check some forms which is useful for synthesis a state observer of nonlinear systems [see *e.g.* [Glumineau et al., 2015](#)].

The second probability, if the observability concept is lost near the singular point when an input is injected into the system under study, consequently the state observer synthesis becomes more complex and the designer must find a suitable solution in this case by designing *e.g.* a robust controller with respect to external disturbances and an improved zero speed estimation to ensure enhanced system monitoring and self-synchronization [[Andrieu et al., 2013](#)].

It should be confirmed that the observability can be relaxed to its detectability. This is natural since the detectability is the observability of the modes, which are not asymptotically stable. Also, the stabilisable is the controllability of the modes, which are not asymptotically stable.

As a matter of fact, it is known in some nonlinear systems, the observability can be lost by a known input, which doesn't occur for linear systems [Vidyasagar et al., 1993]. According to this fact, the authors in [Gauthier et al., 1981] presented the concept of uniform observability, which is applied to whatever input (universal input). In that study, the searchers provided a necessary and sufficient condition for SISO state – affine system that the system is diffeomorphic to system defined in equation (2.30). Unfortunately, there is no such condition for multi – outputs systems. The system proposed in chapter three has been formulated to an interesting class of uniformly observable systems, which can be verified by injecting the time derivatives of the input signals to the system.

In fact, because of the strong nonlinearity nature of the dynamic models, the observability property for some of AC machines depends on the physical operating conditions of each machine supported by sufficient and necessary conditions which are dependent on *Jacobian* state matrix. Hence, the required machine is checked either it is observable or unobservable.

It is worth mentioning that the observability study of AC machines had been discussed successfully by many literates [see e.g. Koteich et al, 2015; Vaclavek et al., 2013].

Specifically, the observability of IMs and IPMSMs had been discussed under uncertain external load torque, i.e., $T_L \leq \delta$, is unknown bounded scalar meanwhile the electrical parameters of the AC machines (e.g. R_s, L_s) are considered known and constant. However, the authors in [Zaltni et al., 2010] presented sufficient and necessary conditions depend on the *Jacobian* state matrix in which the SPMSM is checked either observable or unobservable.

Now, for a state - affine and LTV systems parameterized by initial conditions as soon as the functions u_d and u_q are fixed at certain times. The middle term of LMI given bellow corresponds to the so – called observability *Grammian* [Andrieu et al., 2013].

$$\alpha_1 \mathbb{I} \leq \int_t^{t+T_1} \psi_{u_{dq}}(\tau)^T C^T C \psi_{u_{dq}}(\tau) d\tau \leq \alpha_2 \mathbb{I}, \quad \forall t \geq t_0$$

For some constants $\alpha_1, \alpha_2, T_1 > 0$ and $\psi_{u_{dq}}$, denotes the transition matrix for autonomous part of the system, $\dot{X} = A(u_d, u_q)X$, $y_o = CX$, such that:

$$\begin{cases} d\psi_{u_{dq}}(\tau)/d\tau = A(u_d(\tau), u_q(\tau))\psi_{u_{dq}}(\tau) \\ \psi_{u_{dq}}(t, t) = \mathbb{I}_n \end{cases}$$

Motivated example:

A motivated, practical example for checking the observability of permanent magnet synchronous machine based variable speed WPGS will be discussed as follows [Giri, 2013]:

$$\Sigma \text{ PMSM} \quad \left\{ \begin{array}{l} \frac{d}{dt} i_g = -\frac{R_a}{L_a} i_g - \frac{n_p}{L_a} \omega_r T_2 \psi_r - \frac{1}{L_a} u_g \\ \frac{d}{dt} \psi_r = n_p \omega_r T_2 \psi_r \\ \frac{d}{dt} \omega_r = -1.5 \frac{n_p}{J} i_g^T T_2 \psi_r - \frac{f_v}{J} \omega_r + \frac{1}{J} (T_g) \\ \frac{d}{dt} T_g = 0 \end{array} \right. \quad (2.33)$$

with $i_g \triangleq [i_{g\alpha} \ i_{g\beta}]^T$, $\psi_r \triangleq [\psi_{r\alpha} \ \psi_{r\beta}]^T$, $u_g \triangleq [u_{g\alpha} \ u_{g\beta}]^T$ are, respectively, the stator vector of currents, the rotor fluxes and the generator input command signals. ω_r and T_g denote the rotor speed, generator torque, and dry wind turbulence torque, respectively. T_2 is a square matrix, $T_2 \in \mathbb{R}^{2 \times 2}$, defined as follows: $T_2 \triangleq \begin{bmatrix} 0 & -1 \\ 1 & 0 \end{bmatrix}$; J and f_v are the generator moment of inertia and viscous friction; n_p is the number of pole pairs. The electrical parameters, R_a and L_a are the armature resistor and inductance, respectively. Let us study the observability concept of system (2.33) by considering the stator current measurement in ($\alpha - \beta$) reference frame as an output state vector. For the sake of clarity, one can define the following state vectors:

$$\text{with} \quad \left\{ \begin{array}{l} x \triangleq (x_1 \ x_2 \ x_3)^T \\ x_1 \triangleq (x_{11}, x_{12})^T = (i_{g\alpha}, i_{g\beta})^T \\ x_2 \triangleq (x_{21}, x_{22})^T = (\psi_{r\alpha}, \psi_{r\beta})^T \\ x_3 \triangleq (x_{31}, x_{32})^T = (\omega_r, T_g)^T \end{array} \right. \quad (2.34)$$

As a result, the notation \mathbb{I}_k and 0_k will be used to denote $k \times k$ identity matrix and the $k \times k$ null matrix, respectively. The rectangular ($k \times m$) null matrix will be denoted by $0_{k \times m}$. Then, system model defined in equation (2.32) can be re-written under the following compact form for a class of MIMO nonlinear system disturbed by external load torque:

$$\left\{ \begin{array}{l} \dot{x} = f(x, u_g) + B T_g \\ y = h(x) \end{array} \right. \quad (2.35)$$

where the vector field function, $f(x, u_g)$ is defined as:

$$f(x, u_g) \triangleq \begin{pmatrix} f_1(x, u_g) \\ f_2(x, u_g) \\ f_3(x, u_g) \end{pmatrix} = \begin{pmatrix} -\frac{n_p}{L_a} x_{31} T_2 x_2 - \frac{R_a}{L_a} x_1 - \frac{1}{L_s} u_g \\ n_p x_{31} T_2 x_2 \\ \{-\frac{3 n_p}{2 J} x_1^T T_2 x_2 - \frac{f_v}{J} x_{31} + \frac{1}{J} x_{32}, 0\} \end{pmatrix} \quad (2.36)$$

The nonlinear system input / output matrices are defined as follows:

$$B \triangleq [0_{5 \times 1} \ 1]^T \in \mathbb{R}^{6 \times 1}, \quad C \triangleq [\mathbb{I}_2 \ 0_2 \ 0_2] \in \mathbb{R}^{2 \times 6}$$

As the proposed model is not in normal form of observability, thus it is required to define sufficient and necessary conditions such that the considered state transformation is globally diffeomorphic. The observation objective is to reconstruct the unmeasured mechanical and magnetic state variables using the available measurements on stator currents and voltages.

From the first subsystem model of (2.35) PMSG projected on $(\alpha - \beta)$ frame, one has:

$$\begin{bmatrix} \frac{di_{g\alpha}}{dt} \\ \frac{di_{g\beta}}{dt} \end{bmatrix} = -\frac{R_a}{L_a} \begin{bmatrix} i_{g\alpha} \\ i_{g\beta} \end{bmatrix} + \frac{n_p}{L_a} \omega_r \begin{bmatrix} \psi_{r\beta} \\ -\psi_{r\alpha} \end{bmatrix} - \frac{1}{L_a} \begin{bmatrix} u_{g\alpha} \\ u_{g\beta} \end{bmatrix} \quad (2.37)$$

Let us denote the output function as: $h(x) = [h_1(x), h_2(x)]^T \triangleq [i_{g\alpha}, i_{g\beta}]^T$

The study of observability concept can be evaluated from the stator current measurements and its corresponding derivatives, respectively.

$$f(x, u_g) \triangleq [f_1(x, u_g), f_2(x, u_g), f_3(x, u_g)]^T$$

Definition 2.5 [Glumineau et al., 2015] Let us consider the observation space containing the information that is generated for the observability criterion. The observation space is the smallest subspaces of the functions belong in \mathbb{R}^n whose values belong to the output space, which contains $h_1(x)$, $h_2(x)$, and which closed for *Lie - derivatives* which getting of:

$$\mathcal{O}_{PMSM} h(x) \triangleq \{h_1(x), h_2(x), L_f h_1(x), L_f h_2(x), L_f^2 h_1(x), L_f^2 h_2(x)\}.$$

$L_f^k h$ is called the k 'th order *Lie - derivative* of the output function $h(x)$ along the vector field $f(x, u)$ w.r.t machine states for any input.

Definition 2.6 [Besançon, 2007] An input function, u_g is said to be universal for system (2.35) on the time interval $[0, T]$, if any distinct initial states pair $\{x_0, x'_0\}$ can be distinguished by means of the outputs on the specified time interval. A non - universal input is said to be singular input.

So, $h(x) \stackrel{\text{def}}{=} [L_f^0 h_1(x), L_f^0 h_2(x)]^T = [h_1(x), h_2(x)]^T = [i_{g\alpha}, i_{g\beta}]^T = [y_1, y_2]^T \quad (2.38)$

$$L_f h_1(x) \stackrel{\text{def}}{=} \sum_{i=1}^3 \frac{\partial h_1(x)}{\partial x_i} f_i(x, u_g)$$

$$= \left[\frac{\partial h_1(x)}{\partial x_1} \quad \frac{\partial h_1(x)}{\partial x_2} \quad \frac{\partial h_1(x)}{\partial x_3} \right] [f_1(x, u_g), f_2(x, u_g), f_3(x, u_g)]^T$$

$$= -\frac{R_a}{L_a} x_{11} - \frac{1}{L_a} u_{g\alpha} + \frac{n_p}{L_a} x_{31} x_{22}$$

$$L_f^2 h_1(x) \stackrel{\text{def}}{=} \sum_{i=1}^3 \frac{\partial L_f h_1(x)}{\partial x_i} f_i(x, u_g)$$

$$= \left[-\frac{R_a}{L_a} \quad , \quad \frac{n_p}{L_a} x_{31} \quad , \quad \frac{n_p}{L_a} x_{22} \right] [f_1(x, u_g), f_2(x, u_g), f_3(x, u_g)]^T$$

also, $L_f h_2(x) \stackrel{\text{def}}{=} \sum_{i=1}^3 \frac{\partial h_2(x)}{\partial x_i} f_i(x, u_g)$

$$= -\frac{R_a}{L_a} x_{12} - \frac{1}{L_a} u_g \beta - \frac{n_p}{L_a} x_{31} x_{21}$$

$$\text{and, } L_f^2 h_2(x) \stackrel{\text{def}}{=} \sum_{i=1}^3 \frac{\partial L_f h_2(x)}{\partial x_i} f_i(x, u_g) \\ = \left[-\frac{R_a}{L_a}, -\frac{n_p}{L_a} x_{31}, -\frac{n_p}{L_a} x_{21} \right] [f_1(x, u_g), f_2(x, u_g), f_3(x, u_g)]^T$$

It is readily; that the observability analysis is made by evaluating the *Jacobian* of nonlinear systems, $J_{O_{PMSM}h(x)}$, with respect to machine state variables.

$$J_{O_{PMSM}h(x)} \triangleq \frac{\partial}{\partial x} O_{PMSM} h(x) \quad (2.39)$$

The *Jacobian* state transformation matrix characterizes the observability of the PMSG model in the rank sense. If the $J_{O_{PMSM}h(x)}$ has full rank, this means that, $\dim(J_{O_{PMSM}h(x)}) = 6$, so if the observability rank condition holds $\forall x \in \mathbb{R}^6$, then system defined by (2.35) is observable in the rank sense.

$$\text{rank}(J_{O_{PMSM}h(x)}) = \text{rank} \begin{pmatrix} dh_1(x) \\ dh_2(x) \\ dL_f h_1(x) \\ dL_f h_2(x) \\ dL_f^2 h_1(x) \\ dL_f^2 h_2(x) \end{pmatrix} = n = 6 \quad (2.40)$$

where, d is the usual partial derivative. The associated observability matrix gives observability criterion matrix has dimensions of (6×6), is:

$$J_{O_{PMSM}h(x)} \triangleq \begin{bmatrix} 1 & 0 & 0 & 0 & 0 & 0 \\ 0 & 1 & 0 & 0 & 0 & 0 \\ \frac{\partial L_f h_1(x)}{\partial x_{11}} & \frac{\partial L_f h_1(x)}{\partial x_{12}} & \frac{\partial L_f h_1(x)}{\partial x_{21}} & \frac{\partial L_f h_1(x)}{\partial x_{22}} & \frac{\partial L_f h_1(x)}{\partial x_{31}} & \frac{\partial L_f h_1(x)}{\partial x_{32}} \\ \frac{\partial L_f h_2(x)}{\partial x_{11}} & \frac{\partial L_f h_2(x)}{\partial x_{12}} & \frac{\partial L_f h_2(x)}{\partial x_{21}} & \frac{\partial L_f h_2(x)}{\partial x_{22}} & \frac{\partial L_f h_2(x)}{\partial x_{31}} & \frac{\partial L_f h_2(x)}{\partial x_{32}} \\ \frac{\partial L_f^2 h_1(x)}{\partial x_{11}} & \frac{\partial L_f^2 h_1(x)}{\partial x_{12}} & \frac{\partial L_f^2 h_1(x)}{\partial x_{21}} & \frac{\partial L_f^2 h_1(x)}{\partial x_{22}} & \frac{\partial L_f^2 h_1(x)}{\partial x_{31}} & \frac{\partial L_f^2 h_1(x)}{\partial x_{32}} \\ \frac{\partial L_f^2 h_2(x)}{\partial x_{11}} & \frac{\partial L_f^2 h_2(x)}{\partial x_{12}} & \frac{\partial L_f^2 h_2(x)}{\partial x_{21}} & \frac{\partial L_f^2 h_2(x)}{\partial x_{22}} & \frac{\partial L_f^2 h_2(x)}{\partial x_{31}} & \frac{\partial L_f^2 h_2(x)}{\partial x_{32}} \end{bmatrix} \quad (2.41)$$

It is obvious that the *Jacobian* state transformation matrix has full rank if the square matrix has full rank,

$$J_{O_{PMSM}h(x)} = \begin{bmatrix} \frac{\partial L_f h_2(x)}{\partial x_{21}} & \frac{\partial L_f h_2(x)}{\partial x_{22}} & \frac{\partial L_f h_2(x)}{\partial x_{31}} & \frac{\partial L_f h_2(x)}{\partial x_{32}} \\ \frac{\partial L_f^2 h_1(x)}{\partial x_{21}} & \frac{\partial L_f^2 h_1(x)}{\partial x_{22}} & \frac{\partial L_f^2 h_1(x)}{\partial x_{31}} & \frac{\partial L_f^2 h_1(x)}{\partial x_{32}} \\ \frac{\partial L_f^2 h_2(x)}{\partial x_{21}} & \frac{\partial L_f^2 h_2(x)}{\partial x_{22}} & \frac{\partial L_f^2 h_2(x)}{\partial x_{31}} & \frac{\partial L_f^2 h_2(x)}{\partial x_{32}} \end{bmatrix} \quad (2.42)$$

Now, it can be proved that, $J_{O_{PMSM}}h(x)$ is a regular square matrix, which can be computed the determinant of, $J_{O_{PMSM}}h(x)$ and after simple mathematical manipulation, it gives the observability condition:

$$\det(J_{O_{PMSM}}h(x)) = \frac{n_p^4 R_a}{J L_a^5} (x_{21})^2 (x_{32} - x_{31}) \quad (2.43)$$

The previous equation stated in (2.43) can be re-written using the original state variables as:

$$\det(J_{O_{PMSM}}h(x)) = \frac{n_p^4 R_a}{J L_a^5} (\omega_r)^2 \psi_r \quad (2.44)$$

Once again, one can focus on *Jacobian* state transformation matrix to provide a sufficient and necessary condition such that, $J_{O_{PMSM}}h(x)$, has full rank almost everywhere, consequently the system under study is uniformly observable in the rank sense. Now, after checking the observability of the system model, one can focus on state observer synthesis in next step taken into account the technical limits associated with physical operating points.

This ends the prove of observability of system ■.

Remark 2.1: It is worth mentioning that if, $\det(J_{O_{PMSM}}h(x)) \neq 0$, this implies that PMSM system is observable in the rank sense. Physically, study of observability concept is shrinking (damaged) either the machine at standstill to protect the system from huge mechanical stresses resulted by wind fluctuation (wind gust) or the rotor flux linkage vanish (*i.e.*, There is no electromagnetic field excited in the machine through permanent – magnets located either outside or inside of the machine rotor). As a matter of fact, this case is practically impossible because the norm of the rotor flux linkage (residual flux) induced by permanent magnets is constant and never vanishes since considering the operation with linear magnetic characteristics and acceptable limit for the increasing temperature degree to avoid risk of demagnetization. No additional information for observability criterion is expected, even doing higher order *Lie - derivatives* for stator current measurements along the vector field function *w.r.t* state variables.

2.7 Backstepping control design techniques

In this section, backstepping design is a recursive procedure developed in 1990 by the scientist *Petar V. Kokotovic*. He used it to design a feedback controller to stabilize the origin of the system based *Lyapunov* function. Backstepping is a useful technique for solving stabilization, tracking and robust control problems. This technique is appropriate for wide

range of linear and nonlinear systems. The design process ends when the control law is injected. For that, it is called backstepping design technique.

It should be mentioned that many of physical amounts, such as electrical signals, have an upper bound. When that bound is arrived; the linearity property is damaged at that instant. The differential state equations are handling some of system models, such as thermal, biological systems, are inherently nonlinear. There are several benefits when considering the nonlinearity property in the design process and analyzing feedback controllers for such systems. Many of mechanical systems are subject to nonlinear friction. Also, ferromagnetic cores in most of electrical machines and transformers are usually supported by nonlinear magnetization curves and dynamic equations for system model [Ojha, et al., 2015].

Indeed, *Lyapunov* function is scalar function used to prove the stability of ordinary differential equation. *Lyapunov* function is important for stability analysis and control theory. Actually, there is no general technique for constructing *Lyapunov* functions within ODEs. But in many specific cases, the construction of *Lyapunov* function is known. Basically, *Lyapunov* function takes positive values everywhere except at the equilibrium point, and decreases along the trajectory of the ODE. The main benefit of *Lyapunov* function based stability analysis of ODE resides in the actual solution of the ODE is not needed in many cases.

2.7.1 Continuous - time backstepping design technique

An integrator backstepping technique used to design a SFC to stabilize the origin of the system [Krstic et al., 1995]. Now, let us consider the process described by the following dynamic state equation:

$$\dot{x} = f(x) + g(x)u, \quad \forall f(0) = 0 \quad (2.45)$$

where $x \in \mathbb{R}^n$ is the state variable and $u \in \mathbb{R}^m$ is the control input. There exists a continuously differentiable feedback control law:

$$u \triangleq \alpha(x), \quad \forall \alpha(0) = 0 \quad (2.46)$$

and a smooth, positive definite, radially unbounded function (*i.e.* $W \rightarrow \infty$ as $t \rightarrow \infty$), $W: \mathbb{R}^n \rightarrow \mathbb{R}$ and $x \in \mathbb{R}^n$:

$$\frac{\partial V}{\partial x}(x)[f(x) + g(x)\alpha(x)] \leq -V(x) \leq 0 \quad (2.47)$$

where $V: \mathbb{R}^n \rightarrow \mathbb{R}$ is a positive semidefinite continuous function.

The control law defined in (2.46) ensures the global boundedness of state variables and according to fundamentals of *Lasalle - Yoshizawa theorem*, the regulation of, $V(x)$ satisfies, $\lim_{t \rightarrow \infty} V(x) = 0$.

Obviously, if, $V(x)$ is positive definite function, the control law defined in (2.46) contributes the GAS the origin of (2.45). Now, let us consider a continuous - time plant of the strict feedback form defined in (2.48) below consisting of the system (2.45) increased by a pure integrator seeking for a practical control law stabilizes the system stated below.

$$\begin{cases} \dot{x} = f(x) + g(x) \xi & (2.48a) \\ \dot{\xi} = u & (2.48b) \end{cases}$$

Note that, if ξ was the real control input, it would have been sufficient choosing, $\xi = \alpha(x)$ to stabilize the origin of the system (2.48a). But, $\xi \in \mathbb{R}$, is only a state variable and it is not actual control input. It is usually called *virtual control law*. It would have made the actual control, *i.e.*, $\alpha(x)$ is called *stabilizing function*. The difference between the virtual control law and the stabilizing function is called the tracking error variable.

$$z \triangleq \xi - \alpha(x) \quad (2.49)$$

and differentiation the variables x and z *w.r.t* time index, equation (2.47) are re-written as:

$$\dot{x} = f(x) + g(x) [\alpha(x) + z] \quad (2.50)$$

$$\dot{z} = u - \frac{\partial \alpha}{\partial x}(x) [f(x) + g(x)(\alpha(x) + z)] \quad (2.51)$$

Now, one can define a new *Lyapunov* function expanded by the error variable term:

$$V_o(x, \xi) \triangleq V(x) + \frac{1}{2} [\xi - \alpha(x)]^2 \quad (2.52)$$

The derivative of *Lyapunov* function defined in (2.52) along the closed loop trajectories is expressed as follows with assistance of *Lasalle - Yoshizawa theorem*:

$$\begin{aligned} \dot{V}_o(x, \xi) &= \frac{\partial V}{\partial x}(f + g\alpha + gz) + z \left[u - \frac{\partial \alpha}{\partial x}(f + g(\alpha + z)) \right] \\ \dot{V}_o(x, \xi) &\leq -W(x) + z \left[u - \frac{\partial \alpha}{\partial x}(f + g(\alpha + z)) + \frac{\partial V}{\partial x} g \right] \end{aligned} \quad (2.53)$$

If one imposes the control law, such that the second term in equation (2.53) between two brackets equal to, $-cz$, to ensure negative definiteness of (2.53), yields:

$$u = -cz + \frac{\partial \alpha}{\partial x}[f + g(\alpha + z)] - \frac{\partial V}{\partial x} g \quad (2.54)$$

Or,

$$u = -c(\xi - \alpha(x)) + \frac{\partial \alpha}{\partial x}(x)[f(x) + g(x)\xi] - \frac{\partial V}{\partial x} g(x)$$

where, c is a positive constant design parameter. After substituting (2.54) in (2.53), one gets:

$$\dot{V}_o(x, \xi) \leq -W(x) - cz^2 \triangleq -W_o(x, z) \leq 0 \quad (2.55)$$

It is apparent that $W_o(x, z) \geq 0$, is semi - positive definite function, if $W(x) \geq 0$ is also semi-positive definite. So, the system (2.48) has the same stability properties of the system (2.45). Hence, the system is GAS.

Once again, backstepping control design technique gives great flexibility in selection of feedback control law. Indeed, any command ensures positive definiteness of $W_o(x, z)$ will contribute to an asymptotic stability for the system.

It is worthy emphasized that the backstepping controller achieves global asymptotic stabilization for the continuous-time system. It should be emphasized that backstepping design technique does not only apply to systems in strict feedback form, but also to a more general feedback form or even in a larger class of systems that do not follow any formal feedback structure. The detailed procedure about backstepping design technique is provided by [see e.g. Khalil, 2002; Praly et al., 1991].

Motivated Example: Consider the three - states nonlinear system dynamics:

$$\left\{ \begin{array}{l} \dot{\xi}_1 = \xi_1^2 + \xi_2 \\ \dot{\xi}_2 = \xi_3 \\ \dot{\xi}_3 = u \end{array} \right. \quad (2.56a)$$

$$(2.56b)$$

$$(2.56c)$$

where $\xi \in \mathbb{R}^3$ is the state variable and u is the control input. In order to design a state feedback control law for stabilizing the three - state system dynamics shown above based on principles of backstepping control design technique, one can follow the following three - steps [Krstic et al., 1995].

Step 1:

Let us consider ξ_2 as a controller to stabilize ξ_1 given in (2.56a). Hence, one can re-write equation (2.56a) in the following form:

$$\dot{\xi}_1 = \xi_1^2 + v_1 \quad (2.57)$$

But, v is only a state variable and it is not actual control input. It is usually called *virtual control law*. It would have been considered the actual control law, as *stabilizing function*. Equation (2.57) is a first order system with v_1 is virtual controlling input to stabilize the system (2.57). Let us consider the following candidate *Lyapunov* function in quadratic form:

$$V_1 \triangleq \frac{1}{2} \xi_1^2 \quad (2.58a)$$

Accordingly, the time derivative of the first *Lyapunov* function is:

$$\dot{V}_1 = \xi_1 \dot{\xi}_1 = \xi_1(\xi_1^2 + v_1) \quad (2.58b)$$

To ensure the negative definiteness of, \dot{V}_1 , let us propose the following equation:

$$\xi_1^2 + v_1 \triangleq -\gamma \xi_1 \quad (2.59)$$

with, $\gamma > 0$ is a positive design parameter. The term $(-\gamma \xi_1)$ is chosen to ensure providing the necessary damping to the system. The virtual control law, v_1 can be defined as:

$$v_1 \triangleq -\xi_1^2 - \gamma \xi_1 \quad (2.60)$$

Then, the time derivative of the first *Lyapunov* function, \dot{V}_1 will be,

$$\dot{V}_1 = \xi_1 \dot{\xi}_1 = -\gamma \xi_1^2 < 0, \quad \forall \xi_1 \neq 0 \quad (2.61)$$

This implies that ξ_1 decays exponentially to the origin of the system. To do this state, ξ_2 should act like, v_1 behaviour, therefore; it should be back step by introducing a new variable, z_2 .

$$z_2 \triangleq \xi_2 - v_1$$

Or equivalently combine (2.60) in (2.62), it gives: $z_2 = \xi_2 + \xi_1^2 + \gamma \xi_1$ (2.62)

Now, one differentiates equation (2.62), leads to second error dynamics:

$$\dot{z}_2 = \dot{\xi}_2 + (\xi_2 + \xi_1^2)(2\xi_1 + \gamma) \quad (2.63)$$

From equation (2.62), one can find, ξ_2 w.r.t output variable, z_2 in the following way:

$$\xi_2 = z_2 - \xi_1^2 - \gamma \xi_1 \quad (2.64)$$

In view of equation (2.64), one has the dynamics of the first state:

$$\dot{\xi}_1 = -\gamma \xi_1 + z_2 \quad (2.65)$$

and (2.63) becomes,

$$\dot{z}_2 = \dot{\xi}_2 + (z_2 - \gamma \xi_1)(2\xi_1 + \gamma) \quad (2.66)$$

Step 2:

Now, it is clear that in order to stabilize the system expressed in (2.65), z_2 must be equal to zero (*i.e.* $\xi_2 = v_1$). To achieve this, equation (2.66) will be re-written by setting, ξ_3 as a control input in the following way:

$$\dot{z}_2 = v_2 + (z_2 - \gamma \xi_1)(2\xi_1 + \gamma) \quad (2.67)$$

where, v_2 is another virtual controller to stabilize the system defined by (2.65) and (2.66).

Thus, one can re-write equation (2.67) as follows:

$$\dot{z}_2 = v_2 + \varphi_1(\xi_1, \xi_2) \quad (2.68)$$

where, $\varphi_1(\xi_1, \xi_2) = (z_2 - \gamma \xi_1)(2\xi_1 + \gamma) = 2\xi_1 \xi_2 + 2\xi_1^3 + \gamma \xi_2 + \gamma \xi_1^2$

The next step is writing the expanded *Lyapunov* function by the term of second error as:

$$V_2 \triangleq V_1 + \frac{1}{2}z_2^2$$

Or,
$$V_2 \triangleq \frac{1}{2}\xi_1^2 + \frac{1}{2}z_2^2 \quad (2.69a)$$

Now, the time derivative of the second *Lyapunov* function, V_2 is,

$$\dot{V}_2 = \xi_1 \dot{\xi}_1 + z_2 \dot{z}_2$$

$$\dot{V}_2 = \xi_1(z_2 - \gamma\xi_1) + z_2(v_2 + \varphi_1(\xi_1, \xi_2))$$

From (2.65), it gives:
$$\dot{V}_2 = -\gamma\xi_1^2 + z_2(v_2 + \xi_1 + \varphi_1(\xi_1, \xi_2)) \quad (2.69b)$$

To guarantee the negative definiteness of (2.69b), one can propose the following equation;

$$v_2 + \xi_1 + \varphi_1(\xi_1, \xi_2) = -\alpha_1 z_2 \quad (2.70)$$

with, $\alpha_1 > 0$ and the term $(-\alpha_1 z_2)$ is chosen to guarantee providing the necessary damping to stabilize the system with α_1 is a positive design parameter. The second virtual control law v_2 can be defined as:

$$\begin{aligned} v_2 &\triangleq -\alpha_1 z_2 - \xi_1 - \varphi_1(\xi_1, \xi_2) \\ &= \varphi_2(\xi_1, \xi_2) \end{aligned} \quad (2.71)$$

where, $\varphi_2(\xi_1, \xi_2) = -(1 + \alpha_1\gamma)\xi_1 - (\gamma + \alpha_1)\xi_1^2 - 2\xi_1^3 - (\gamma + \alpha_1)\xi_2 - 2\xi_1\xi_2$

By substituting equation (2.71) in equation (2.68), one has the following form;

$$\dot{z}_2 = -\xi_1 - \alpha_1 z_2 \quad (2.72)$$

Step3:

To achieve the above control objectives, ξ_3 must act like introducing a new variable, which represents a change of variables should act like, v_2 . Thus, one can introduce a new variable error, z_3 as:

$$z_3 \triangleq \xi_3 - v_2$$

Or,
$$z_3 = \xi_3 - \varphi_2(\xi_1, \xi_2) \quad (2.73)$$

Using equation (2.73), to find ξ_3 in terms of z_3 as follows:

$$\xi_3 = z_3 + \varphi_2(\xi_1, \xi_2)$$

Now, differentiating equation (2.73) w.r.t time index, one has third error dynamics;

$$\dot{z}_3 = \dot{\xi}_3 - \frac{d}{dt}\varphi_2(\xi_1, \xi_2) \quad (2.74)$$

The term $\frac{d}{dt}\varphi_2(\xi_1, \xi_2)$ can be computed using the so - called *chain rule* as follows:

$$\begin{aligned} \frac{d}{dt}\varphi_2(\xi_1, \xi_2) &= \frac{\partial\varphi_2}{\partial\xi_1} \frac{\partial\xi_1}{\partial t} + \frac{\partial\varphi_2}{\partial\xi_2} \frac{\partial\xi_2}{\partial t} \\ \frac{d}{dt}\varphi_2(\xi_1, \xi_2) &= [-(1 + \alpha_1\gamma) - 2\xi_2 - [2(\gamma + \alpha_1)\xi_1 + 6\xi_1^2](\xi_1^2 + \xi_2)](\xi_1^2 + \xi_2) \end{aligned}$$

$$- [(\gamma + \alpha_1) + 2\xi_1] \xi_3 \quad (2.75)$$

In view of equation (2.73), one has:

$$\dot{\xi}_2 = z_3 + \varphi_2(\xi_1, \xi_2) \quad (2.76)$$

and,
$$\dot{z}_3 = u - \varphi_3(\xi_1, \xi_2) \quad (2.77)$$

where,
$$\varphi_3(\xi_1, \xi_2) = [-(1 + \alpha_1\gamma) - 2\xi_2 - [2(\gamma + \alpha_1)\xi_1 + 6\xi_1^2](\xi_1^2 + \xi_2)](\xi_1^2 + \xi_2) - [(\gamma + \alpha_1) + 2\xi_1](z_3 + \varphi_2(\xi_1, \xi_2))$$

In order to guarantee ($\xi_3 = v_2$), this can be done by letting the composite *Lyapunov* function:

$$V_3 \triangleq V_2 + \frac{1}{2}z_3^2 \quad (2.78)$$

Differentiating *Lyapunov* function in (2.78) *w.r.t* time index; yields:

$$\dot{V}_3 = -\gamma\xi_1^2 - \alpha_1z_2^2 + z_3(u - \varphi_3(\xi_1, \xi_2)) \quad (2.79)$$

By imposing the following equation to ensure negative definiteness of (2.79):

$$u - \varphi_3(\xi_1, \xi_2) = -\alpha_2z_3, \quad \alpha_2 > 0 \quad (2.80)$$

The term ($-\alpha_2z_3$) used to provide the necessary damping to stabilize the system. The final control law, u used for stabilizing the system dynamics is:

$$u = -\alpha_2z_3 + \varphi_3(\xi_1, \xi_2) \quad (2.81)$$

By substituting equation (2.81) in equation (2.77), one has the following;

$$\dot{z}_3 = -\alpha_2z_3 \quad (2.82)$$

Also, substituting equation (2.81) in (2.79), it gives:

$$\dot{V}_3 = -\gamma\xi_1^2 - \alpha_1z_2^2 - \alpha_2z_3^2 \quad (2.83)$$

with, γ, α_1 and $\alpha_2 > 0$ will guarantee negative definiteness of (2.83) and subsequently backstepping controller achieves global asymptotic stabilization of the system. Backstepping controller for stabilization of three - state nonlinear system is shown in Figure 2.3.

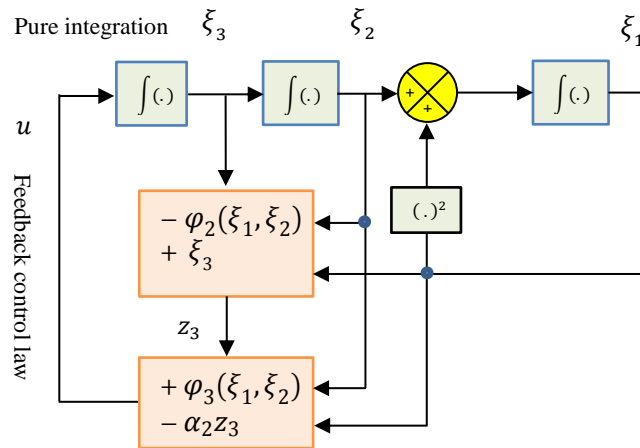


Figure 2.3: Stabilization of three-state continuous – time nonlinear system.

2.8 Introduction for a class of system studied

Let us consider the following general form of continuous-time nonlinear systems [Hann, 2014]:

$$\begin{cases} \dot{\xi}(t) = f(\xi(t), u(t)) \\ y(t) = h(\xi(t)) \end{cases} \quad (2.84)$$

where, $\xi \in \mathbb{R}^n$ represents system state – variable, $y \in \mathbb{R}^p$ is the output of the system and $u \in \mathbb{R}^m$ is the input injection for the system under study.

Let us express the sampling instant at time $t_k, k \in \mathbb{N}$ belong in R_+^0 followed a sequence $\{t_k\}_{k \geq 0}$. At each sampling instant at time, t_k , the system output measurements are sampled and hold through so called zero order hold *ZOH* device: it is a mathematical model used for data reconstruction. Those data can be transmitted for processing depending on the physical case study. This technique is re-initialized impulsively whenever recent output data are available, *i. e.* $y = y_{int}, \forall t = t_k, k \in \mathbb{N}$. To ensure fast exponential convergence of the observation error and prediction error with time progressive, an explicit inequality for upper bound limit of the maximum allowable sampling period between consecutive sampling instants, an upper bound limit of constant design parameter for any input and an upper bound limit for output state prediction error have been proposed, successfully based on state observer design parameter and nonlinearity property of the system.

One of the complexities faced the present work associated with the output - data measurements in continuous - time mode are considered inaccessible. Output measurements are just accessible at sampling instant. Hence, to solve the problem of state estimation, this will lead us to combine the benefits of inter – sampled output state predictor with the proposed high – gain state observer. An approximate predictor for which the prediction is provided by the output of a properly constructed system is introduced by [Ahmed – Ali et al., 2013].

It should be confirmed that unlike of previous scientific contribution dealing with sampled - data observers design, the output state predictor at the last sampling instant has been interred in constructing of the innovation correct term to prove the robustness of the proposed state observer against attenuated sampling interval, achieves self – sensing control techniques and ensures fast tracking time response. From our experience in this field, the transient time response will increase as increasing the sampling time interval. Hence, this will lead to be

careful in design and make a compromise solution when designing such state observer to ensure an acceptable tracking response.

Recently, sampled - data observer proves its capability to be compatible with the advanced power electronic technologies and interfaced with new versions of digital signal processing. Definitely, this will improve the dynamic performances of sensorless control techniques, from a technical viewpoint.

2.9 Fundamental properties for stability convergence analysis

Assumption 2.1: Let us consider the following system dynamic state equation [Khalil, 2002]:

$$\dot{\xi} = f(\xi, u), \quad \forall f(0,0) = 0 \quad (2.85)$$

This system defined in (2.85) is called globally *Lipschitz*, if there exists a positive *Lipschitz* constant, i.e. $L_{global} > 0$, such that the following *Lipschitz* condition must be satisfied:

$$\|f(\xi, u) - f(z, u)\| \leq L_{global} \|\xi - z\|, \quad \text{for all } \xi, z \in \mathbb{R}^n, \forall u \in \mathbb{R}^m \quad (2.86a)$$

Assumption 2.2: $f(\xi, u)$ defined in (2.85) is called locally *Lipschitz* in ξ at a point, $\xi_0 \in D \subset \mathbb{R}^n$, if there exists a neighbourhood:

$$N(\xi_0, r_0) \triangleq \{\xi \in \mathbb{R}^n / |\xi - \xi_0| < r_0\},$$

where the vector field function, $f(\xi, u)$ satisfies the *Lipschitz* condition for all ξ, z in some neighbourhood of ξ_0 and the power energized to the system from external sources, $u \in \mathbb{R}^m$:

$$\|f(\xi, u) - f(z, u)\| \leq L_{loc} \|\xi - z\|, \quad L_{loc} > 0 \text{ and } r_0 > 0 \quad (2.86b)$$

For first order state equation defined in (2.85), $f(\xi, u)$ depends only on ξ such that: $f: \mathbb{R} \rightarrow$

\mathbb{R} ; the *Lipschitz* condition can be written as: $\frac{\|f(\xi, u) - f(z, u)\|}{\|\xi - z\|} \leq L_{loc}$

If one plots the function $f(\xi, u)$ versus ξ , a straight line, connecting any successive two points of $f(\xi, u)$, cannot have a slope whose absolute value is greater than local *Lipschitz* constant.

2.9.1 Input – to – state stability concept

For nonlinear systems injected by disturbances, an input – to – state stability (ISS) concept had been changed the local concept of total stability with a more useful global concept. Indeed, ISS plays a significant role coupled with *Lyapunov* function in the stabilization of adaptive and non-adaptive nonlinear systems. For this reason, this subsection will discuss ISS concept with some of attention. Small gain is a loop gain less than unity. Small gain condition

is one way used to ensure the stability of dynamic systems. It is a combination of gain functions less than identity [Krstic, 1995].

Definition 2.7

The system defined in (2.85) is called *input – to – state stable (ISS)*, if there exists a class K_L function β and a class K function γ such that for any initial state $\xi(0)$ and for any input, $u(t)$, bounded on defined interval $[0, \infty)$, the solution of the system defined in equation (2.85) exists $\forall t \geq 0$ and satisfies the following inequality [Sontag et al., 1996]:

$$|\xi(t)| \leq \beta(|\xi(t_0)|, t - t_0) + \gamma(|u(t)|) , \quad \forall t \in [t_0, t_0 + T), \quad T > 0 \quad (2.87)$$

where, $[t_0, t_0 + T)$ is the definition interval associated with the state variable, $\xi(t)$.

Actually, the equation defined in (2.87) is suitable for a class of nonlinear systems. It considers the effect of the state conditions, $\xi(0)$. Equation (2.87) shows that the, $|\xi(t)|$ depends not only on the input signal $u(t)$, but also involves an exponentially decaying contribution from, $\xi(0)$. More details about the connection between the existences of a *Lyapunov* - like function and the ISS is given by [see e.g. Sontag et al., 1995]. They showed that the ISS concept is equivalent to the existence of an ISS - *Lyapunov* function as:

$$\alpha_1(|\xi|) \leq V(\xi) \leq \alpha_2(|\xi|) \quad (2.88a)$$

such that,
$$\frac{\partial V(\xi, u)}{\partial \xi} f(\xi, u) \leq -\alpha_3(|\xi|) + \sigma(|u|) \quad (2.88b)$$

with, the functions $\alpha_1(\cdot)$, $\alpha_2(\cdot)$ and $\alpha_3(\cdot) \in K_\infty$ and $\sigma(\cdot) \in K$ for any input, $u(t)$.

2.9.2 Fundamentals of ISS small - gain condition

Initially, a small - gain theorem had been well - established by [Hill et al., 1991]. This theorem was extended towards the input - to- state stability framework by [Jiang et al., 1994]. Hence, it was generalized by [Teel, 1996]. For clarification, the combination of an ISS small-gain result for a class of interconnected system described by two subsystems (ξ_1, ξ_2) is:

$$\begin{cases} \dot{\xi}_1 = f_1(\xi_1, \xi_2) \\ \dot{\xi}_2 = f_2(\xi_2, \xi_1) \end{cases} \quad (2.89)$$

In view of system (2.89), if the ξ_1 - subsystem with ξ_2 considered as its input signal has ISS – gain as, $g_1(\cdot)$, and once gain the ξ_2 - subsystem with ξ_1 considered as its input signal has ISS – gain as, $g_2(\cdot)$. Subsequently, the interconnected system from two subsystems (ξ_1, ξ_2) is globally asymptotically stable (GAS) as time index flights to infinity, if the composite ISS – small gain condition is [see e.g. Kokotovic et al., 2001]:

$$g_1 \circ g_2(\epsilon) < \epsilon \quad , \quad \forall \epsilon > 0 \quad (2.89b)$$

In many published results, ϵ is fixed to unity.

Definition 2.8 [Ahmed – Ali et al., 2013]

Let us considered the system defined by the following equations:

$$\begin{cases} \dot{z} = f(z, y, u) \\ \dot{\hat{\xi}} = \psi(z) \end{cases} \quad (2.90)$$

$$z \in \mathbb{R}^l, y \in \mathbb{R}^p, u \in \mathbb{R}^m, \hat{\xi} \in \mathbb{R}^n.$$

where, $F: \mathbb{R}^l \times \mathbb{R}^p \times \mathbb{R}^m \rightarrow \mathbb{R}^l$ and $\psi: \mathbb{R}^l \rightarrow \mathbb{R}^n$.

One can say that the system defined in (2.90) is a global exponential robust observer for the system defined in (2.85), if there is a non-decreasing function $M: \mathbb{R}_+ \rightarrow \mathbb{R}_+$ and the constant $\sigma > 0$, such that for all $(\xi_0, z_0, u) \in \mathbb{R}^n \times \mathbb{R}^l \times \mathbb{R}^m$, the solution of $(\xi, z) \in \mathbb{R}^n \times \mathbb{R}^l$ of system (2.85), (2.90) with the initial conditions ξ_0, z_0 and the corresponding input, $u \in \mathbb{R}^m$ exist, the state observation error satisfies the following mathematical inequality in CTM:

$$\|\hat{\xi} - \xi\| \leq \exp^{-(\sigma t)} M(|z_0|, |\xi_0|) \quad , \quad \forall t \geq 0, \quad (2.91)$$

In fact, *the Lyapunov* algebraic equation is important for system stability and control in many classes of system models. For this reason, one can prove this through Lemma 2.1.

Lemma 2.1[Khalil, 2002]: For a certain fixed gain vector K , there exists a symmetric positive definite (SPD) matrix $P \in \mathbb{R}^{n \times n}$, $P \triangleq P^T > 0, \forall \mu > 0$ positive free constant, $\mathbb{I}_n \in \mathbb{R}^{n \times n}$ is an identity matrix such that the following *Lyapunov* algebraic equation is satisfied:

$$P(A_c - KC_c) + (A_c - KC_c)^T P = -Q = -\mu \mathbb{I}_n \quad (2.92)$$

where, $A_c \in \mathbb{R}^{n \times n}$ is the system matrix and $C_c \in \mathbb{R}^{1 \times n}$ is output vector. This is a useful tool for checking convergence properties and *Lyapunov* stability test.

Proof Sketch: Necessity condition

Suppose: $A' \triangleq A_c - KC_c$ is *Hurwitz* ($Re[\lambda_i(A')] < 0$). $\| \exp^{(A')t} \| \leq \alpha \exp^{-\lambda t}, \exists \alpha, \lambda > 0, t \geq 0$.

Let us define, $\int_0^\infty \exp^{(A')^T t} Q \exp^{(A')t} dt \triangleq P \quad , \quad \forall t \geq 0, \quad P \triangleq P^T > 0 \quad (2.93)$

Let us consider, $\int_0^\infty \frac{d}{dt} \left(\exp^{(A')^T t} Q \right) \exp^{(A')t} dt = -Q, \quad Q \triangleq Q^T > 0, PDM \quad (2.94)$

$$(A')^T \int_0^\infty \left[\exp^{(A')^T t} Q \exp^{(A')t} \right] dt + \int_0^\infty \left[\exp^{(A')^T t} Q \exp^{(A')t} \right] dt (A') = -Q$$

Combine equation (2.93) in (2.94), the algebraic *Lyapunov* equation for LTI system is:

$$PA' + (A')^T P = -Q = -\mu \mathbb{I}_n \quad (2.94)$$

Hence, the system is asymptotically stable. *This ends the proof of Lemma 2.1* ■

The solution of *Lyapunov* equation can be evaluated using MATLAB functions, e.g. $eig(A)$, $P = lyap(A^T, Q)$, $P = dlyap(A^T, Q)$, $K = place(A^T, C^T, desired\ pole)$ or $K = acker(A^T, C^T, pole)$ $crtb(sys)$, $obsv(sys)$, $pole(sys)$ for state - space representation.

Chapter Three

Sampled – Data Nonlinear Observer Design for Sensorless Synchronous PMSM

Table of Contents	page
3.1 Introduction	55
3.1.1 Review of related research	55
3.1.2 Purposes and contributions	55
3.2 Synchronous machine modeling and model transformation	56
3.2.1 Synchronous PMSM model	57
3.2.2 MIMO Model transformation of PMSM	59
3.2.3 Observability analysis of full order variable speed PMSM	61
3.3 Sampled-data observer design and convergence analysis	62
3.3.1 Sampled – data observer structure	63
3.3.2 Some technical hypotheses	63
3.3.3 Comparison with published results	64
3.3.4 Some definition and notation	65
3.3.5 Stability analysis of the proposed observer	66
3.3.6 Discussion the main result	71
3.3.7 Observer equation in the original coordinates	71
3.4 Simulation results and verifications	72
3.4.1 Implementation considerations	72
3.4.2 Observer dynamic tracking performance	75
3.4.3 Sensorless sampled output measurements	75
3.5 Conclusions	80

The problem of designing nonlinear state observers for Permanent Magnet Synchronous Motors drives (PMSMs) has been given a great deal of interest, especially over the last few years. In this respect, various classes of nonlinear observers had been proposed, but most of them have the following features:

1. Continuous-time measurements of the machine output states.
2. Most of state observers are designed based on simplified approximate model (did not take into consideration nonlinear machine dynamics).
3. Many of them are not backed by a formal stability convergence analysis.

A design of sampled-data state observer, for nonlinear models of DC or AC machines and supported by a formal stability convergence analysis using tools of *Lyapunov* stability theory and input - to - state stability concept was highly recommended in the scientific contributions and it has yet needed to be solved by the searchers and scientists.

In this chapter, a solution to measurement problem is covered and developed by combining benefits and ideas from high - gain design approach and inter-sampled predictor. Compared to classic high-gain state observers, the proposed sampled-data observer including inter-sampled predictor allows the following benefits:

- Without resorting to use persistently exciting input signals.
- Playing a vital role in improving and enhancing the observer dynamic performances and ensure fast exponential convergence of the observation errors.
- The output state predictor at the last sampling instant has been interred in constructing of the innovation correct term to prove the robustness of the proposed state observer against attenuated sampling interval.
- Achieving self – sensing control techniques and ensures fast tracking time response.

In many practical applications (*e.g.*, electric traction, water pumps, air conditioner compressors, direct-drive washing machines, refrigerator compressors, computer peripherals and automotive control, etc...), PMSMs prove to be much more suitable than other AC and DC electric drives, including induction motors. Indeed, PMSMs have better features such as low power consumption and accordingly it has better efficiency. In effect, the *Joule* losses in PMSMs are much less significant since they involve no damper windings and no rotor currents as found in conventional DC machines. Despite of the considerable progress made in the power electronics technology and manufactures have made the control objectives of flexible speed variation an achievable feature for most of industrial and commercial applications.

3.1 Introduction

Presently, the focus is made on systems, including a PMSM driven by an inverter. The role of inverter is made the stator phases switching, depending on the rotor position, so that the PMSMs demanding operating with variable rotor speed. The inverters are acted by nonlinear controllers, but those controllers require rotor speed, position and load torque measurements [see *e.g.* et al., 2010; Benchabane et al., 2012].

It is obvious that the mechanical and magnetic sensors based solutions are costly, relatively, insufficiently reliable, etc... Thus, the powerful solution resides in using state observer's synthesis based system model. If appropriately designed, the latter can provide accurate online estimates of the mechanical and magnetic state variables based on input / output electrical injection measurements.

3.1.1 Review of related research

Recently, the problem of designing state observers, for PMSMs, has been given a great deal of interest over the last decade. Several design approaches had been proposed in literatures, including signal injection method had been proposed by [Zatocil, 2008; Ichikawa et al., 2006], making use of the phase inductance variation property by injection of high - frequency signals. This approach provides rotor position information at low rotor speeds and during standstill operation. However, it necessitates a certain amount of saliency characteristic in the machine structure. Also, injecting of high - frequency signal is not recommended at high speed operation. The fundamental excitation method, proposed by [Bolognani et al., 1999], involves the detection of the rotor position from the stator voltages and currents without necessitating using additional test signals.

In [Fakham et al., 2005; Chen et al., 2003; Liu et al., 2011], the back EMF (*i.e.* the voltage induced in stator windings), was used to estimate rotor position by means of a state observer methodology or extended *Kalman* filters for nonlinear systems [Lang et al., 2007; Wang et al., 2012]. This approach works -well at medium and high speed applications, but it is inefficient at low speed operation since the back EMF is low.

3.1.2 Purposes and contributions

In this chapter, the technical main results supported by proving theorem and the scientific contributions can be generalized in the following directions:

- The considered mathematical representation of PMSM model accounts for six state variables, namely two stator currents, rotor flux, variable motor speed and unknown bounded external load torque.
- The system model submits to an observability test to provide sufficient conditions generated by *Jacobian* state transformation matrix, in which all six-state variable so the PMSM can be estimated based on the sampled - current and stator voltage measurements.
- A nonlinear state observer synthesis using a high – gain framework through change of variables is developed for variable speed PMSM drive system.
- Appropriate state sampled - data observers coupled with inter – sampled predictor that provides on-line estimates of the full state model.

The rest of this chapter is organised as follows. In section 3.2, the state - space model of the PMSM will be the basis for the observability analysis. The section 3.3 is devoted to the observer synthesis. It deals with nonlinear state observer synthesis of the designated system. In section 3.4, the convergence property of the proposed nonlinear observer is proved and realized through numerical simulation and verification using MATLAB/SIMULINK environment application to senseless variable speed PMSM drive. Finally, conclusions are given in section 3.5 of this chapter.

3.2 Synchronous machine modelling and model transformation

As in most motors, the synchronous motor has two main parts. The non-moving is called the stationary part and the moving is called the rotating part. Basically, there are two ways to generate a rotor flux. The first way uses rotor windings induced by the stator windings and the other way is excited by permanent magnets located on the rotor which generate a constant rotor flux linkage. PMSM can be classified according to magnets locations as surface – mounted or interior magnet synchronous machines. To obtain the current supply and generate the rotor flux linkage, a motor fitted out with the rotor windings requires brushes. In this case, the contacts are made of rings and do not have any commutator segment. The major drawbacks of machine structure reside in a variety of cyclic maintenance and less reliability of operation. Replacing common rotor field windings with permanent magnets puts the motor under consideration in the category of brushless motors.

It is possible to construct brushless PMSM with even numbers of magnet poles. Motors have been constructed with (2-50) magnet poles. Increasing number of poles create a greater torque for same motor size. Off course, the usage of permanent magnets enables an efficient use of the radial space and replaces the rotor windings. Accordingly, the rotor copper losses are suppressed. Advanced magnetic materials such as Sm_2Co_{17} (Samarium Cobalt magnet) or $NdFeB$ (Neodymium magnet) permit a considerable reduction in motor dimensions, whilst maintaining high power density. In the case of embedded systems, where the space occupied is important, a PMSM is usually preferred than AC synchronous motor has brushes. PMSM can be considered as hybrid structure mixes of a brushless DC motor (*w.r.t* the rotor structure) and an AC induction motor (*w.r.t* stator structure). PMSMs offer better efficiency, high power factor, high torque/weight ratio, faster transient response time, and rugged composition. They are easy to control and less cyclic maintenance [Bose, 2002].

Although, the nonlinear controller scheme contains a state observer methodology, the closed-loop asymptotic stability cannot be ensured. Since the state observer is no longer tends asymptotically to real value in the presence of an unknown external load torque disturbance. The powerful solution to this situation is to expand the mathematical model of the proposed state observer in which it provides on-line estimates of the system state variables as well as the estimation of external load torque disturbance [Zhu et al., 2000]. If the system is not algebraically observable, one can find the non-observable variables by removing columns in observability matrix and calculating the rank of the reduced matrices or separating the basic *Jacobian* state transition matrix into observable and non-observable submatrices.

3.2.1 Synchronous PMSM model

Because of rotor position is practically inaccessible, specifically for high speed applications, the PMSM model is expressed in $(\alpha - \beta)$ stationary reference frame. This model is more suitable for state observer design. Introduced by [Elmagri et al., 2013b; Rashid, 2011], the variable speed PMSM full state model projected on $(\alpha - \beta)$ coordinates is given by:

$$\begin{cases} \frac{di_s}{dt} = -\frac{R_s}{L_s}i_s + \frac{n_p}{L_s}\omega_m J_2 \psi_r + \frac{1}{L_s}u_s \\ \frac{d\psi_r}{dt} = -n_p \omega_m J_2 \psi_r \\ \frac{d\omega_m}{dt} = \frac{n_p}{J}i_s^T J_2 \psi_r - \frac{f}{J}\omega_m - \frac{1}{J}T_L \\ \frac{dT_L}{dt} = \varepsilon(t) \end{cases} \quad (3.1)$$

where, $i_s \triangleq [i_{s\alpha} \ i_{s\beta}]^T$, $\psi_r \triangleq [\psi_{r\alpha} \ \psi_{r\beta}]^T$, $u_s \triangleq [u_\alpha \ u_\beta]^T$ are respectively, the stator currents, the rotor fluxes and the stator voltages projected on $(\alpha - \beta)$ coordinates. ω_m and T_L respectively, denote the rotor speed and the external load torque. $\varepsilon(t)$ is an unknown bounded function; J_2 is the (2×2) matrix defined as:

$$J_2 \triangleq \begin{bmatrix} 0 & -1 \\ 1 & 0 \end{bmatrix}, \in \mathbb{R}^{2 \times 2} \quad (3.2)$$

Notice that, the time derivative of the external load torque is described by an unknown bounded function. The mechanical parameters, J and f are the motor moment of inertia and viscous friction; respectively. For small signal analysis of PMSM in AC drives, the one mass or lumped – mass model is used because the drive behaves as the single equivalent mass model is based on the second law of *Newton*. n_p is the number of magnet pair of poles. The electrical parameters R_s and L_s are the stator resistor and self-inductance, respectively. Figure 3.1 shows an electrical equivalent circuit for PMSM expressed in $(\alpha - \beta)$ stationary reference frame. Angles between stator and rotor electrical frames are described in Figure 3.2 where, S, R are, respectively the stator and rotor part. More the mathematical details about the PMSM model projected on $(\alpha - \beta)$ coordinates are found in chapter two of the present thesis.

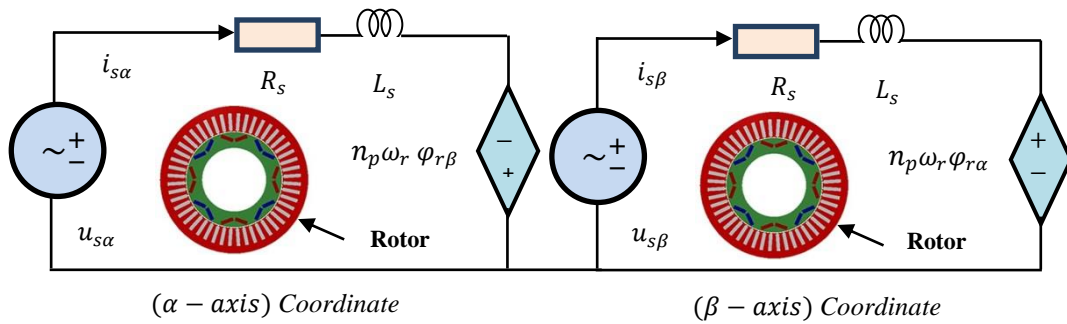


Figure 3.1: Electrical equivalent circuit for PMSM expressed in $(\alpha - \beta)$ frame

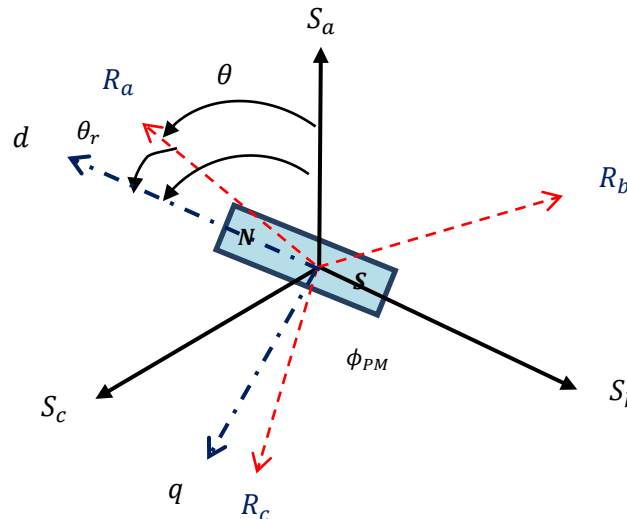


Figure 3.2: Angles between stator and rotor electrical frames

It should be mentioned that the mathematical model defined in equation (3.1) is strongly nonlinear since it involves the product between rotor flux linkage and rotor speed. The major objective is to specify under what conditions that all the state variables of the PMSM can be observed based on MIMO measurements, namely the sampled –data current and voltage measurements. This leads us to study the observability of system stated in (3.1) by considering $y \triangleq i_s$ as an output state vector. For clarity purposes, one introduces the following notations:

$$x \triangleq \begin{pmatrix} x_1 \\ x_2 \\ x_3 \end{pmatrix}, \in \mathbb{R}^6 \quad (3.3a)$$

with

$$\begin{cases} x_1 \stackrel{\text{def}}{=} (x_{11}, x_{12})^T = (i_{s\alpha}, i_{s\beta})^T \\ x_2 \stackrel{\text{def}}{=} (x_{21}, x_{22})^T = (\psi_{r\alpha}, \psi_{r\beta})^T, \in \mathbb{R}^2 \\ x_3 \stackrel{\text{def}}{=} (x_{31}, x_{32})^T = (\omega_m, T_L)^T \end{cases} \quad (3.3b)$$

In the sequel, the notation \mathbb{I}_k and 0_k will be used to denote the $(k \times k)$ well – known identity matrix and the $(k \times k)$ null matrix, respectively. The rectangular $(k \times m)$ null matrix will be denoted by $0_{k \times m}$. Real system model defined in equation (3.1), disturbed by external load torque, can be re-written in the following condensed form:

$$\begin{cases} \dot{x} = f(x, u_s) + B_1 \varepsilon(t) \\ y = Cx = x_1 \end{cases} \quad (3.4)$$

where, $f(x, u_s)$ is vector field function, $f \in \mathbb{R}^n \times \mathbb{R}^m$. It can be defined as follows,

$$f(x, u_s) \triangleq \begin{pmatrix} f_1(x, u_s) \\ f_2(x, u_s) \\ f_3(x, u_s) \end{pmatrix} = \begin{pmatrix} -\frac{n_p}{L_s} x_{31} J_2 x_2 - \frac{R_s}{L_s} x_1 + \frac{1}{L_s} u_s \\ n_p x_{31} J_2 x_2 \\ \left\{ \frac{n_p}{J} x_1^T J_2 x_2 - \frac{f}{J} x_{31} - \frac{1}{J} x_{32}, 0 \right\} \end{pmatrix} \quad (3.5)$$

and, $B_1 = [0_{5 \times 1} \quad 1]^T \in \mathbb{R}^{6 \times 1}$, $C = [\mathbb{I}_2 \quad 0_2 \quad 0_2] \in \mathbb{R}^{2 \times 6}$, $\forall \mathbb{I}_2 \in \mathbb{R}^{2 \times 2}$, $y \in \mathbb{R}^{n_1}$, $n_1 \geq n_2 \geq n_3$.

3.2.2 MIMO Model transformation of PMSM

As the system model given in equations (3.4) and (3.5) is not in normal observability form, one can first transform it into a canonical form. A classical state transformation to get that form can be found in many literates [see *e.g.* Dib, 2012; Ghanes, 2005] and all the references therein for more details. Then, it should define sufficient conditions generated by observability criterion, under which the considered state transformation is a diffeomorphism. Another capability to synthesise a state observer for a nonlinear system is transforming

system under study into another form in which a class of observers becomes known for on-line implementation and state observation.

An analytic proof shall give rise to a sufficient condition in which the *Jacobian* matrix of the considered state transformation has full rank almost everywhere. Now, let us consider the following change of state variables for the full state model.

$$\Phi : \mathbb{R}^6 \rightarrow \mathbb{R}^6, x \rightarrow z = \begin{pmatrix} z_1 \\ z_2 \\ z_3 \end{pmatrix} = \Phi(x) = \begin{pmatrix} \Phi_1(x) \\ \Phi_2(x) \\ \Phi_3(x) \end{pmatrix} \text{ is a diffeomorphism} \quad (3.6)$$

One can illustrate that the above classical state transformation puts the system (3.4) under the following uniformly canonical form:

$$\begin{cases} \dot{z}_1 = z_2 + \varphi_1(z_1, u_s) \\ \dot{z}_2 = z_3 + \varphi_2(z_1, z_2) \\ \dot{z}_3 = \varphi_3(z) + b(z) \varepsilon(t) \\ y = Cz = z_1 \end{cases} \quad (3.7)$$

where, $z \triangleq [z_1 \ z_2 \ z_3]^T$; $z_k \triangleq [z_{k1} \ z_{k2}]^T$ with $(k = 1, 2, 3)$; $\varepsilon(t)$ is specified by a dynamic equation of(3.1) and the nonlinear functions $\varphi_k, b(z)$ and $\varphi_k \in \mathbb{R}^2$ are defined as follows:

$$\begin{cases} z_1 = \Phi_1(x) = x_1 \\ z_2 = \Phi_2(x) = -\frac{n_p}{L_s} x_{31} J_2 x_2 \\ z_3 = \Phi_3(x) = \frac{n_p^2}{L_s} x_{31}^2 x_2 - \left(\frac{n_p^2}{J L_s} x_1^T J_2 x_2 - \frac{n_p}{J L_s} x_{32} \right) J_2 x_2 \end{cases} \quad (3.8)$$

and the other nonlinear functions are defined in the following form,

$$\begin{cases} \varphi_1(z_1, u_s) = -\frac{R_s}{L_s} z_1 + \frac{1}{L_s} u_s \\ \varphi_2(z_1, z_2) = \frac{f}{J} z_2 \\ \varphi_3(z) = \frac{\partial \Phi_3(x)}{\partial x_1} \dot{x}_1 + \frac{\partial \Phi_3(x)}{\partial x_2} \dot{x}_2 + \frac{\partial \Phi_3(x)}{\partial x_{31}} \dot{x}_{31} \\ b(z) \triangleq \frac{\partial \Phi_3(x)}{\partial x_{32}} = \frac{n_p}{J L_s} J_2 x_2 \end{cases} \quad (3.9)$$

with,

$$\begin{cases} \frac{\partial \Phi_3(x)}{\partial x_1} = \frac{n_p^2}{J L_s} (J_2 x_2)^2 \\ \frac{\partial \Phi_3(x)}{\partial x_2} = \frac{n_p^2}{L_s} x_{31}^2 J_2 - \left(\frac{n_p}{J L_s} x_{32} J_2 - \frac{n_p^2}{J L_s} (x_1^T J_2 x_2 + x_1^T x_2 J_2) \right) J_2 \\ \frac{\partial \Phi_3(x)}{\partial x_3} = \left[2 \frac{n_p^2}{L_s} x_{31} x_2, \frac{n_p}{J L_s} J_2 x_2 \right] \end{cases}$$

3.2.3 Observability analysis of full order variable speed PMSM

Indeed, one must find a sufficient condition under which the *Jacobian* matrix of this state transformation has full rank almost everywhere. Now, let us consider $J_{\Phi(x)}$ be the *Jacobian* matrix of, $\Phi(x)$. In view of equation (3.8), one has the following matrix for nonlinear systems *w.r.t* closed - loop trajectories:

$$J_{\Phi(x)} = \begin{bmatrix} \mathbb{I}_2 & \mathbf{0}_2 & \mathbf{0}_2 \\ \mathbf{0}_2 & \frac{\partial \Phi_2(x)}{\partial x_2} & \frac{\partial \Phi_2(x)}{\partial x_3} \\ \frac{\partial \Phi_3(x)}{\partial x_1} & \frac{\partial \Phi_3(x)}{\partial x_2} & \frac{\partial \Phi_3(x)}{\partial x_3} \end{bmatrix} \quad (3.10)$$

Apparently that the *Jacobian* matrix has full rank, if and only if, the following square matrix has full – rank also using *Laplace* expansion method for determinant computation:

$$N_{\Phi(x)} = \begin{pmatrix} \frac{\partial \Phi_2(x)}{\partial x_2} & \frac{\partial \Phi_2(x)}{\partial x_3} \\ \frac{\partial \Phi_3(x)}{\partial x_2} & \frac{\partial \Phi_3(x)}{\partial x_3} \end{pmatrix} \triangleq \begin{pmatrix} N_1(x) & N_2(x) \\ N_3(x) & N_4(x) \end{pmatrix}, \in \mathbb{R}^{4 \times 4} \quad (3.11)$$

Then, one can focus on the matrix $N_{\Phi(x)}$ to find a sufficient condition in which this matrix, or equivalently, $J_{\Phi(x)}$, has full rank almost everywhere. Once again, in view of equation defined in (3.8), one has the following mathematical form:

$$\begin{cases} \frac{\partial \Phi_2(x)}{\partial x_2} \triangleq N_1(x) = -\frac{n_p}{L_s} x_{31} J_2 \\ \frac{\partial \Phi_2(x)}{\partial x_3} \triangleq N_2(x) = \left[-\frac{n_p}{L_s} J_2 x_2, \quad \mathbf{0}_{2 \times 1} \right] \\ \frac{\partial \Phi_3(x)}{\partial x_2} \triangleq N_3(x) = \frac{n_p^2}{L_s} x_{31}^2 \mathbb{I}_2 - \left(\frac{n_p}{J L_s} x_{32} \mathbb{I}_2 - \frac{n_p^2}{J L_s} (x_1^T J_2 x_2 + x_1^T x_2 J_2) \right) J_2 \\ \frac{\partial \Phi_3(x)}{\partial x_3} \triangleq N_4(x) = \left[2 \frac{n_p^2}{L_s} x_{31} x_2, \quad \frac{n_p}{J L_s} J_2 x_2 \right] \end{cases} \quad (3.12)$$

From equation given in (3.12), one can easily demonstrate that: $N_1 N_3 = N_3 N_1$: the multiplication of matrices is reciprocal *i.e.* $N_1 N_3 - N_3 N_1 = 0$. As a result, the determinant of the matrix $N_{\Phi(x)}$ can be written in the following form:

$$\det N_{\Phi(x)} = \det(N_1 N_4 - N_2 N_3)_{(x)} \quad (3.13)$$

According to the mathematical expressions of $N_{\Phi(x)}$ ($i = 1; 2; 3; 4$) given in equation (3.12) and (3.13), after simple computations, it gives:

$$\det N_{\Phi(x)} = \frac{n_p^5}{J L_s} \left(1 + \frac{2n_p}{J} \right) x_{31}^3 x_2^T x_2 \quad (3.14)$$

Or equivalent, $\det N_{\Phi(x)} = D x_{31}^3 x_2^T x_2$,

with, $D \triangleq \frac{n_p^5}{J L_s} \left(1 + \frac{2n_p}{J} \right)$ is a positive real constant.

It consists of mechanical and electrical system parameters.

Then, the considered state transformation has full rank, *i.e.* system (3.1) is observable in the rank sense *w.r.t.* closed - loop trajectories, if the following condition is satisfied as:

$$(x_{31})^3 \|x_2\|^2 \neq 0 \quad (3.15a)$$

The sufficient observability condition defined in equation (3.15a) can be re-expressed using the original motor state variables as follows:

$$\|\psi_r\|^2 (\omega_m)^3 \neq 0 \quad (3.15b)$$

One can deduce that the system defined in equation (3.7) is a uniformly observable system for any input (*i.e.* universal input). Thus, the system model defined in (3.1) will be observable in the rank sense in \mathbb{R}^6 as soon as the state transformation matrix defined in (3.6) exists and it is regular almost everywhere [Hermann et al., 1977].

Remark 3.1: It is known that, for PMS machines, the norm of the rotor flux linkage, generated by permanent magnets, is constant and it does not null at all times. So, from above result given in(3.15b) one can deduce that at non-zero (*i.e.* zero rotor speed is a singular value) rotor speed, the system model defined in (3.1) is uniformly observable system in the rank sense and for any input. In such condition, the major objective of the next section is to design a sampled output HGO for the PMSM drive system after doing model transformation. From all mentioned above, one can summarize the following sufficient condition as follows:

$$\det(\Phi_{(x)}) = \begin{cases} \frac{n_p^5}{JL_s} \left(1 + \frac{2n_p}{J}\right) (x_{31})^3 \|x_2\|^2, & \omega_m \neq 0 & \Rightarrow \text{System is observable} \\ 0, & \omega_m = 0 & \Rightarrow \text{System is unobservable} \end{cases} \quad (3.16)$$

3.3 Sampled-data observer design and convergence analysis

The main purpose of the current section is proposed a state sampled – data observer for nonlinear system defined in (3.1). Such state observer used to provide on-line the demanding estimates of ω_m and T_L including the rotor position based on the measurements of the stator currents at the last sampling instant and stator voltages without using the time derivatives of those measurements. If the on-line estimates of the rotor flux linkage $(\psi_{r\alpha}, \psi_{r\beta})^T$ become available, the mechanical rotor flux position can be estimated using following well - known formula:

$$\begin{cases} \hat{\psi}_{r\alpha} = K_e \cos(\hat{\theta}_e) \\ \hat{\psi}_{r\beta} = K_e \sin(\hat{\theta}_e) \\ \hat{\theta}_r = \frac{1}{n_p} \hat{\theta}_e = \frac{1}{n_p} \tan^{-1} \left(\frac{\hat{\psi}_{r\beta}}{\hat{\psi}_{r\alpha}} \right) \end{cases} \quad (3.17)$$

where, K_e is a power conservation between the two systems of three – phase and two – phase. $\hat{\theta}_r$ and $\hat{\theta}_e$ denote, the mechanical rotor position and electrical position estimate measured in (rad). Apparently from (3.17), rotor position estimation is not a constant *w.r.t* time index.

3.3.1 Sampled – data observer structure

For a suitable situation, the system model defined in (3.7) will present in the following compact structural form. It consists of linear, nonlinear and disturbance terms.

$$\begin{cases} \dot{z} = Az + \varphi(z, u_s) + B_1 b(z) \varepsilon(t) \\ y = Cz = z_1 \end{cases} \quad (3.18)$$

where, the state variable, $z \triangleq (z_1 z_2 z_3)^T \in \mathbb{R}^6$, $b(z) \in \mathbb{R}^{2 \times 2}$ is bounded matrix. It is the function of rotor flux linkage. A is defined as anti-shift block matrix:

$$A = \begin{bmatrix} 0_2 & \mathbb{I}_2 & 0_2 \\ 0_2 & 0_2 & \mathbb{I}_2 \\ 0_2 & 0_2 & 0_2 \end{bmatrix} \in \mathbb{R}^{6 \times 6} \quad (3.19)$$

The function $\varphi(z, u_s)$ has a lower triangular structure, form *w.r.t* z uniformly in u_s , *i.e.* for any input. Finally, the matrices B and C are defined as follows:

$$B_1 \triangleq [0_2 \ 0_2 \ \mathbb{I}_2]^T \in \mathbb{R}^{6 \times 2}, \quad C \triangleq [\mathbb{I}_2 \ 0_2 \ 0_2] \in \mathbb{R}^{2 \times 6} \quad (3.20)$$

Once again, the function $\varphi(z, u_s)$ has a lower triangular structure *w.r.t* z uniformly in u_s , *i.e.*

$$\varphi(z, u_s) \triangleq \begin{pmatrix} \varphi_1(z_1, u_s) \\ \varphi_2(z_1, z_1, u_s) \\ \varphi_3(z, u_s) \end{pmatrix}, \in \mathbb{R}^6$$

3.3.2 Some technical hypotheses

The stability analysis of the proposed high gain state observer approach requires the following technical hypothesis. It is highly recommended to use these hypotheses for stability convergence. Using these hypotheses, the searcher will present some new results on designing state observers for a class of *Lipschitz* nonlinear systems.

H₁: The functions $\varphi_i(z, u_s)$ are globally *Lipschitz w.r.t z* uniformly in u_s *i.e.*, $\exists \xi_1 > 0$, positive *Lipschitz* constant, $\forall (z, \hat{z}) \in \mathbb{R}^6 \times \mathbb{R}^6, \forall u_s \in U$, it could be written in which the following *Lipschitz* condition must be satisfied:

$$\|\varphi_o(\hat{z}, u_s) - \varphi(z, u_s)\| \leq \xi_1 \|\hat{z} - z\|$$

H₂: The function $\varepsilon(t)$ is unknown bounded function and the real, $\delta > 0$ is positive upper bound used in many practical cases to model the external disturbance such that,

$$\delta \geq \sup_{0 \leq t < \infty} \|\varepsilon(t)\|$$

The proposed state observer based on sampled- output measurements combines the benefits and features of high gain structure and inter – sampled output behaviour as illustrated in Figure 3.3. Inter – sampled output behaviour is used to solve the problem of continuous – time output measurements and improve dynamic performances.

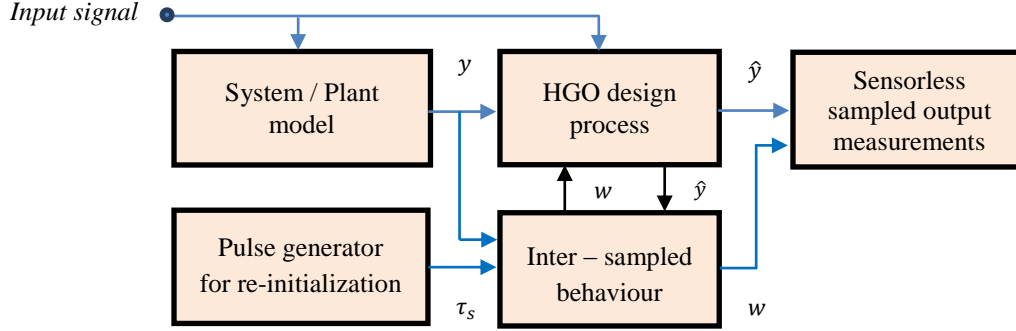


Figure 3.3: Proposed observer combines benefits of high - gain structure and output state predictor

Now, the general structure of the proposed state observer design for variable speed PMSM drive system is written in the following form after doing model transformation:

$$\begin{cases} \dot{\hat{z}} = A \hat{z} + \varphi(\hat{z}, u_s) - \theta \Delta^{-1} K (C \hat{z} - w) \\ \dot{w} = C(A \hat{z} + \varphi(\hat{z}, u_s)) \\ w(t_k) = y(t_k), \quad \forall t \in [t_k, t_{k+1}), k \in \mathbb{N} \end{cases} \quad (3.21)$$

where, $\theta > 1$ is a high – gain observer design parameter and the part of $\theta \Delta^{-1} K$ is called the multiplicative observer gain. The continuous – time signal, w tries to approximate the continuous – time output just sampled - output state vector is accessible at successive sampling instant. The approximation predictor is provided by the output of a properly constructed system. w is re-initialized impulsively through the pulse generator when recent system output measurements are available, $\forall t \in [t_k, t_{k+1}), k \in \mathbb{N}, \mathbb{N} \in \mathbb{R}_0^+$.

3.3.3 Comparison with published results

A simple comparison to similar existing approaches in the previous literatures can be provided to justify the advantages and features of the proposed state observer design. In fact, high gain observers have a long history in scientific research through many literates.

- The main difference compared to a class of nonlinear system claimed by [see e.g. Glumineau et al.,2015] resides in the synthesis of nonlinear state observer disturbed by external torque. The proposed state observer in a current study considered the torque dynamic is unknown function, but bounded by constant scalar, i.e. $\delta \geq$

$\sup_{0 \leq t < \infty} \|\varepsilon(t)\|$, which is useful for many practical cases. Unlike in the corresponding study mentioned above, despite of a new technique for change of coordinates was proposed for nonlinear system in that study.

- It is worthy that the rotor flux linkage and rotor position estimations based PMSMs with relaxed persistency of excitation conditions are proposed by [see *e.g.* Aranovski et al., 2015]. In that study, the stator voltages, currents and angular rotor speed are considered accessible without taking into consideration the advantages and features of high gain design approach in observer synthesis. Some of these benefits are accurately tracking time response with suitable high gain observer parameter and ensure fast exponential convergence of the observation error.
- As a matter of fact, the authors in [see *e.g.* El magri et al., 2013] focused on state - affine system model running with interconnected *Kalman* – like observer injected by persistence excitation inputs and system output state measurements in continuous – time mode. The authors considered the output state vector is accessible without considering the concept of inter - sampled behaviour in the design process for such state observer synthesis.
- Several limitations associated with continuous time output measurements and the necessity of persistently exciting inputs [see *e.g.* Ezzat et al., 2011]. These requirements and limitations make previously some of the state observers not quite suitable for many practical applications. Whilst the present observer enjoys its sampled-data nature and it does not need persistently exciting inputs.

For the knowledge of searcher in this field, most of previous studies related to variable speed PMSM drive systems, the combination of inter – sampled behaviour with high – gain design approach is not discussed, yet. The novel state observer synthesis energized by non-persistence excitation input. The second feature is entering the output state predictor in construction of innovation correct error to ensure the robustness of the proposed observer *w.r.t* disruption of the sampling attenuation. These features will be highlighted deeply in the present scientific contribution.

3.3.4 Some definitions and notations

Before giving the state equations of the candidate sampled - data observer design, one introduces some important definitions and notations, which are highly recommended:

The block diagonal matrix, Δ is defined by the following equation:

$$\Delta \triangleq \text{blockdiag}(\mathbb{I}_2, \frac{1}{\theta}\mathbb{I}_2, \frac{1}{\theta^2}\mathbb{I}_2) \quad (3.22)$$

with, $\theta > 0$, is a constant HGO design parameter and $\mathbb{I}_2 \in \mathbb{R}^{2 \times 2}$.

- The fixed gain matrix corresponding to measurements error $K \in \mathbb{R}^{6 \times 2}$ can be chosen:

$$K^T = [k_1\mathbb{I}_2, k_2\mathbb{I}_2, k_3\mathbb{I}_2] \quad (3.23)$$

with, $k_{i=1,2,3}$ is a real positive scalar so that $(A - KC)$ is Hurwitz and it satisfies the following algebraic Lyapunov equation for solving SPD matrix, i. e. $P = P^T > 0$:

$$P(A - KC) + (A - KC)^T P = -Q \quad (3.24)$$

where, $(P, Q) \in \mathbb{R}^{6 \times 6} \times \mathbb{R}^{6 \times 6}$ is a pair of symmetric positive definite matrices and $(A - KC)^T$ is the transposed matrix for $P(A - KC)$.

The vector \hat{z} is the continuous - time estimate of the system state, z . Figure 3.4 clarifies PMSM drive system running with sampled output high - gain observer design.

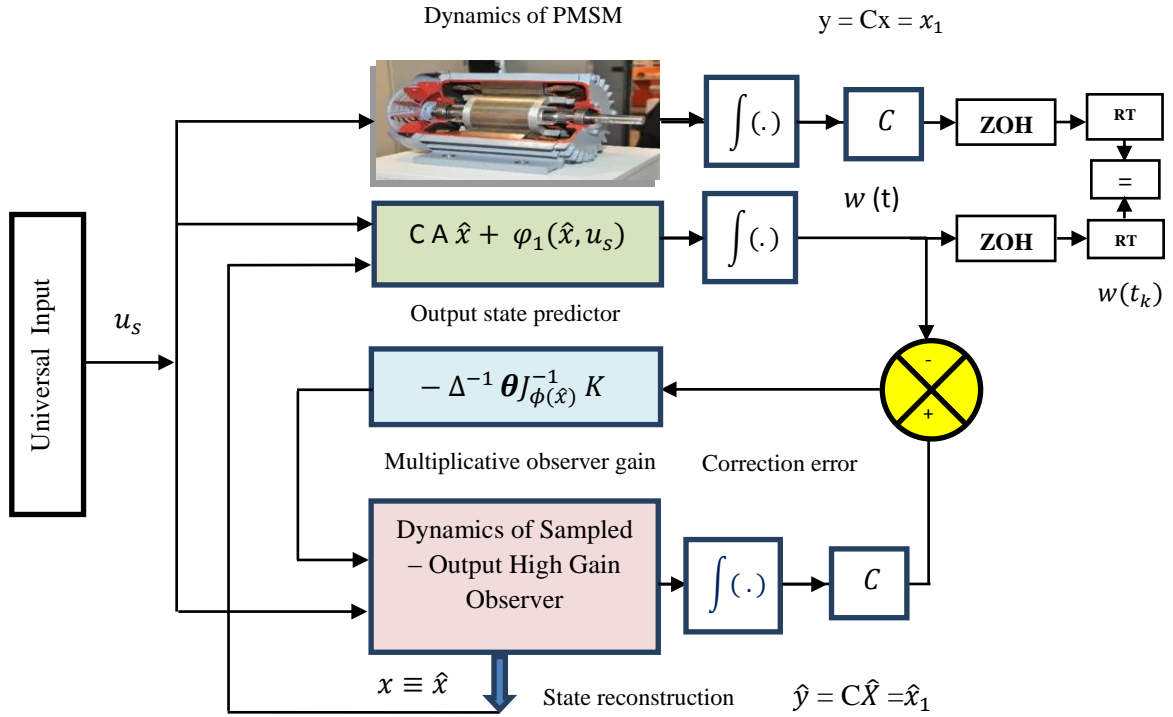


Figure 3.4. PMSM drive system running with sampled - output HGO structure

3.3.5 Stability analysis of the proposed observer

In this subsection, the searcher states the first main result dealing with HGO design based sampled- output measurements. These results are described by the following theorem.

Theorem 3.1 (Main result)

Consider the system defined by equation (3.21) is a sampled output HGO for the real system model stated in equation (3.18) considering the technical hypothesis H_1, H_2 hold. Let us define the following scalar parameter:

$$\theta > \frac{2 \lambda_{PM} \xi_1}{\lambda_{QM}} \quad (3.25)$$

where, $(P, Q) \in \mathbb{R}^{6 \times 6} \times \mathbb{R}^{6 \times 6}$ is a pair of symmetric positive definite matrices, P satisfies the equation (3.24). Then, the system of (3.21) is a sampled-output HGO for system (3.18) for $k_{i=1; 2; 3}$, satisfy the equation (3.24). There exists the state observation error is ultimately bounded and this bound can be made as small as desired by choosing values of, θ satisfactory large enough. Moreover, there exist real positives (non - decreasing parameters) (M_1, M_2, M_3) such that the state observation error $e_z \triangleq \hat{z}(t) - z(t)$ satisfies the following LMI inequality:

$$\|e_z(t)\| \leq M_1 \exp^{-M_2(t-t_k)} + M_3, \forall t \in [t_k, t_{k+1}), k \in \mathbb{N} \quad (3.26)$$

Also, there exists a positive scalar bound; $\tau_{MASP} \forall \tau \in (0, \tau_{MASP}]$, one can deduce the following upper bound of the sampling time interval. It is a sufficient condition to ensure accurate tracking and fast exponential convergence of the observation error with progressive time:

$$\tau_{MASP} = \frac{1}{\theta} \left[\frac{(\lambda_{Km}^2 \lambda_{KM}^2) + (\theta + \xi_1)^2}{\theta \lambda_{QM} - 2 \lambda_{PM} \xi_1} + \frac{1}{c \lambda_{Pm}} \right] \left(\frac{\pi}{2} - 2 \tan^{-1}(\lambda) \right)$$

Proof of theorem 3.1

The searcher will give a formal analysis and elegant full proof of the main theorem using tools of *Lyapunov* stability theory. For writing convenience, the continuous - time index will be cancelled. Let us define the following state observation error vector,

$$e_z \triangleq [e_{z1} \quad e_{z2} \quad e_{z3}]^T = \hat{z} - z$$

Subtracting side by side, one has from state equations defined in (3.21) and (3.18) the system error dynamics:

$$\begin{cases} \dot{e}_z = (A - \theta \Delta^{-1} KC) e_z + (\varphi(\hat{z}, u_s) - \varphi(z, u_s)) + \theta \Delta^{-1} K e_w - B_1 b(z) \varepsilon \\ \dot{e}_w = CA e_z - C(\varphi(\hat{z}, u_s) - \varphi(z, u_s)) \end{cases} \quad (3.27)$$

where, the output - state prediction error vector is: $e_w \triangleq w - y = w - Cz$ (3.28)

Now, one can easily check the following mathematical properties: $\Delta^{-1} A \Delta = A$, $\Delta^{-1} KC = \Delta^{-1} KC \Delta$ and $CA e_z = e_{z2}$. Hence, the dynamic equation given in (3.27), becomes:

$$\begin{cases} \dot{e}_z = \theta \Delta \theta^{-1} (A - KC) \Delta e_z + (\varphi(\hat{z}, u_s) - \varphi(z, u_s)) + \theta \Delta^{-1} K e_w - B_1 b(z) \varepsilon \\ \dot{e}_w = e_{z2} - (\varphi_1(\hat{z}, u_s) - \varphi_1(z, u_s)) \end{cases} \quad (3.29)$$

Let us apply the following change of coordinates, $\epsilon_z \triangleq \Delta e_z$, one obtains the following new error dynamics:

$$\begin{cases} \dot{\epsilon}_z = \theta(A - KC)\epsilon_z + \Delta(\varphi(\hat{z}, u_s) - \varphi(z, u_s)) + \theta K e_w - \Delta B_1 b(z) \varepsilon \\ \dot{e}_w = \theta \epsilon_{z2} + (\varphi_1(\hat{z}, u_s) - \varphi_1(z, u_s)) \end{cases} \quad (3.30)$$

Inspired by the scientific contribution that had been introduced by [Ahmed-Ali, 2012], let us choose the following candidate *Lyapunov* function in quadratic form:

$$V \triangleq \sigma_1 \epsilon_z^T P \epsilon_z + \sigma_2 h(t) \|e_w\|^2 \quad (3.31)$$

where, $\sigma_1 > 0$ and $\sigma_2 > 0$ are two positive constants, which will be computed via the analysis. It should be mentioned that the matrix, P is a symmetric positive definite matrix (and the solution of the algebraic *Lyapunov* equation defined in (3.24)). $h(t)$ is a positive bounded function. It enables to correct the error between the state predictor and the output state vector. It is decreasing between consecutive sampling times and it satisfies that, $h(t_k) = \lambda^{-1}$ and $h(t_{k+1}) = \lambda$, $\forall k \in \mathbb{N}$ where, $\lambda \in (0,1)$ to guarantee that, the second *Lyapunov* function from right less than the same function from the left, i.e. $V_2(t_k) < V_2(t_k^-)$, according to stability concept.

Now, to prove the stability convergence of the proposed observer, it is necessary to find a sufficient condition involving the maximum allowable sampling period, τ_{MASP} , so that the following mathematical inequality hold:

$$\dot{V} < -cV + M\sqrt{V} \quad \forall t \in [t_k, t_{k+1}), k \in \mathbb{N} \quad (3.32)$$

where, c and M are real positives.

Let us decompose the total *Lyapunov* function, V in two sub - functions, which are defined:

$$V_1 \triangleq \sigma_1 \epsilon_z^T P \epsilon_z \text{ and } V_2 \triangleq \sigma_2 h(t) \|e_w\|^2$$

Now, one can compute the time - derivative for first and second *Lyapunov* function, i.e. V_1 and V_2 , doing so, one has the following:

$$\begin{cases} \dot{V}_1 = \sigma_1 \dot{\epsilon}_z^T P \epsilon_z + \sigma_1 \epsilon_z^T P \dot{\epsilon}_z \\ \dot{V}_2 = \sigma_2 \dot{h}(t) \|e_w\|^2 + 2\sigma_2 h(t) \|e_w\| \|\dot{e}_w\| \end{cases} \quad (3.33)$$

Using the dynamic observation and prediction errors defined by (3.29), one can deduce that:

$$\dot{V} \leq \dot{V}_1 + \dot{V}_2$$

$$\begin{aligned} \text{where, } \dot{V}_1 &= \theta \sigma_1 \epsilon_z^T ((A - KC)^T P + P(A - KC)) \epsilon_z + 2 \sigma_1 \epsilon_z^T P \Delta (\varphi(\hat{z}, u_s) - \varphi(z, u_s)) \\ &\quad + 2 \theta \sigma_1 \epsilon_z^T P K e_w - 2 \sigma_1 \epsilon_z^T P \Delta B_1 b(z) \varepsilon \end{aligned} \quad (3.34)$$

One can observe, using the algebraic *Lyapunov* equation given in (3.24):

$$- \epsilon_z^T Q \epsilon_z \triangleq \epsilon_z^T ((A - KC)^T P + P(A - KC)) \epsilon_z$$

Then, the (3.34) has the following form:

$$\begin{aligned} \dot{V}_1 = & -\theta\sigma_1\epsilon_z^T Q\epsilon_z + 2\sigma_1\epsilon_z^T P\Delta(\varphi(\hat{z}, u_s) - \varphi(z, u_s)) \\ & + 2\theta\sigma_1\epsilon_z^T PKe_w - 2\sigma_1\epsilon_z^T P\Delta B_1 b(z)\epsilon \end{aligned} \quad (3.35)$$

Note that, one can easily prove that,

$$(\theta\sigma_1)^2\|e_w\|^2 + (\lambda_{PM}^2 \lambda_{KM}^2)\|\epsilon_z\|^2 \geq 2\theta\sigma_1\epsilon_z^T PKe_w$$

The largest and the smallest positive eigenvalues of the matrix, X (X either Q, P or K), are denoted by λ_{Xm} and λ_{XM} , respectively. Using the hypotheses given in, H_1 and H_2 , it gives: $\Delta\|\varphi(\hat{z}, u_s) - \varphi(z, u_s)\| \leq \xi_1\|\epsilon_z\|$ and $\Delta B_1 b(z)\epsilon \leq \left(\frac{\xi_2}{\theta^2}\right)\delta$, knowing that, ξ_1, ξ_2 and δ are known real positives. Using the fact that, $\lambda_{QM}\|\epsilon_z\|^2 \leq V_1(\epsilon_z) \leq \lambda_{QM}\|\epsilon_z\|^2$, one has the following form after simple mathematical calculations:

$$\dot{V}_1 \leq -\sigma_1 \left(\theta\lambda_{QM} - 2\lambda_{PM}\xi_1 - \frac{(\lambda_{PM}^2\lambda_{KM}^2)}{\sigma_1} \right) \|\epsilon_z\|^2 + 2\sigma_1\lambda_{PM} \left(\frac{\xi_2}{\theta^2} \right) \delta \|\epsilon_z\| + (\sigma_1\theta)^2\|e_w\|^2 \quad (3.37)$$

From second subsystem of error dynamic equation given in (3.29), one can remark that:

$$\|\dot{e}_w\| \leq \theta\|\epsilon_{z2}\| + \|\varphi_1(\hat{z}, u_s) - \varphi_1(z, u_s)\| \leq (\theta + \xi_1)\|\epsilon_z\| \quad (3.38)$$

Using dynamic equations defined by (3.32) and (3.37), and the fact that,

$$2\sigma_2 h(t)(\theta + \xi_1)\|e_w\|\|\epsilon_z\| \leq \sigma_2^2 h(t)^2\|e_w\|^2 + (\theta + \xi_1)^2\|\epsilon_z\|^2$$

Accordingly, one has the following form,

$$\dot{V}_2 \leq (\sigma_2 \dot{h}(t) + \sigma_2^2 h(t)^2)\|e_w\|^2 + (\theta + \xi_1)^2\|\epsilon_z\|^2 \quad (3.39)$$

Therefore, using equations defined by (3.35) and (3.39), and applying superposition theory, one can deduce the following form:

$$\begin{aligned} \dot{V} \leq & -\sigma_1 \left(\theta\lambda_{QM} - 2\lambda_{PM}\xi_1 - \frac{(\lambda_{PM}^2\lambda_{KM}^2) - (\theta + \xi_1)^2}{\sigma_1} \right) \|\epsilon_z\|^2 + 2\sigma_1\lambda_{PM} \left(\frac{\xi_2}{\theta^2} \right) \delta \|\epsilon_z\| + (\sigma_1\theta)^2\|e_w\|^2 \\ & + (\sigma_2 \dot{h}(t) + \sigma_2^2 h(t)^2)\|e_w\|^2 \end{aligned} \quad (3.40)$$

If one chooses, $\dot{h}(t) = -\sigma_2(h(t)^2 + 1)$, $\forall t \in [t_k, t_{k+1})$ and $\tau \in (0, \tau_{MASP}]$ (3.41)

$$\text{and, } \begin{cases} \sigma_1 \triangleq \frac{\theta\lambda_{QM} - 2\lambda_{PM}\xi_1}{(\lambda_{PM}^2\lambda_{KM}^2) + (\theta + \xi_1)^2} + c\lambda_{PM} \\ \sigma_2 \triangleq \sqrt{\sigma_1^2\theta^2 + \rho} \end{cases} \quad (3.42)$$

to guarantee negative definiteness of *Lyapunov* function, where, $c > 0$, $\rho > 0$ are positive constants and the observer design parameter, $\theta > \frac{2\lambda_{PM}\xi_1}{\lambda_{QM}}$.

Using the notation, $M \triangleq 2\sqrt{\frac{\sigma_1}{\lambda_{PM}}}\lambda_{PM} \left(\frac{\xi_2}{\theta^2} \right) \delta$

Thus, the inequality defined by equation (3.40), can be rewritten as follows,

$$\dot{V} \leq -c \sigma_1 \lambda_{pm} \|\epsilon_z\|^2 + M \sqrt{\sigma_1 \lambda_{pm}} \|\epsilon_z\| - \rho \|e_w\|^2 \quad (3.43)$$

From the *Lyapunov* function defined by equation (3.31) and using the mathematical fact that,

$$\|\epsilon_z\| \leq \sqrt{\frac{1}{\sigma_1 \lambda_{pm}}} \sqrt{V}$$

Thus, one can write equation (3.43) in the following new form:

$$\dot{V} < -c V + M \sqrt{V} \quad \text{if, } V > \left(\frac{M}{c}\right)^2 \quad (3.44)$$

to ensure negative definiteness of *Lyapunov* function. This means that, $\forall t \in [t_k, t_{k+1})$, the solution of equation (3.44) is:

$$V(t) \leq V(t_k) \exp^{-M_2(t-t_k)} + \left(\frac{M_3}{c}\right) \quad (3.45)$$

Now, referring to equation defined by (3.31), one has for the discrete – time mode:

$$\sqrt{V(t_k)} \leq \sqrt{\sigma_1 \lambda_{PM}} \|e_z(t_k)\|$$

Using once again the fact that, $\|e_z\| \leq \|\epsilon_z\| \leq \sqrt{\frac{1}{\sigma_1 \lambda_{pm}}} \sqrt{V}$, $\forall t > 0$, and from equations (3.41)

for $\dot{h}(t)$ and (3.44) for \dot{V} , one has the following mathematical inequality:

$$\|e_z(t)\| \leq M_1 \exp^{-M_2(t-t_k)} + M_3, \forall t \geq 0 \quad (3.46)$$

To ensure the validation of the equation given in (3.46), one defines the parameters:

$$\begin{cases} M_1 \triangleq \sqrt{\left(\frac{\lambda_{PM}}{\lambda_{pm}}\right) \|e_z(t_k)\|^2} \\ M_2 \triangleq \frac{c}{2} \\ M_3 \triangleq \frac{2}{c} \left(\frac{\lambda_{PM}}{\lambda_{pm}}\right) \left(\frac{\xi_2}{\theta^2}\right) \delta \end{cases}$$

Sufficient conditions have been given to ensure practical stability of the observation error. The asymptotic stability of the observer is not ensured. This problem can be solved using the practical stability concept. It should be confirmed that the proposed observer is practically stable for whatever initial conditions, $\tilde{X}_0 \in \mathbb{R}^6 \times \mathbb{R}^6$. The observation error vector converges to a compact neighbourhood of the origin with progress time. The size of this compact set can be made sufficiently small by choosing the observer design parameter satisfactory large enough. The selecting value of the maximum allowable sampling time interval, τ_{MASP} can be derived by integrating the equation defined by (3.41) between, t_k , and $t_k + \tau_{MASP}$, with $\rho \rightarrow 0$ (ρ is radius of the compact set) as follows:

$$\begin{aligned} \dot{h}(t) &= -\sigma_2(h(t)^2 + 1) \\ \int_{t_k}^{t_k + \tau_{MASP}} \frac{\dot{h}(t)}{h(t)^2 + 1} dt &= - \int_{t_k}^{t_k + \tau_{MASP}} \sigma_2 dt \end{aligned}$$

The solution based on the definition of $h(t)$ is: $\tan^{-1}(\lambda) - \tan^{-1}(\lambda^{-1}) = -\sigma_2 \tau_{MASP}$,

Let us introduce, $h(t_k) \triangleq \lambda^{-1}$, and $h(t_k + \tau_{MASP}) \triangleq \lambda = h(t_k + 1)$

So,
$$\tau_{MASP} = \lim_{\rho \rightarrow 0} \left(\frac{1}{\sigma_2} [\tan^{-1}(\lambda^{-1}) - \tan^{-1}(\lambda)] \right)$$

Using the mathematical property that, $\tan^{-1}(\lambda^{-1}) + \tan^{-1}(\lambda) = \frac{\pi}{2}$, this leads to compute τ_{MASP} with σ_2 defined by equation (3.42):

$$\tau_{MASP} = \frac{1}{\theta} \left[\frac{(\lambda_{Km}^2 \lambda_{KM}^2) + (\theta + \xi_1)^2}{\theta \lambda_{QM} - 2\lambda_{PM} \xi_1} + \frac{1}{c \lambda_{Pm}} \right] \left(\frac{\pi}{2} - 2 \tan^{-1}(\lambda) \right) \quad (3.47)$$

This ends the proof of theorem, which gives the main result ■

It has been derived an adequate condition for the maximum allowable sampling time interval, τ_{MASP} that ensures an exponential convergence of the observation error towards zero using tools of *Lyapunov* stability theory. It is a sufficient condition to ensure fast exponential convergence of the observation error as $t \rightarrow \infty$.

3.3.6 Discussion the main result

The linear matrix inequality (LMI) stated in (3.47), it defines an upper bound of the sampling time interval. In fact, it is just an adequate condition, but not necessary for the proposed state observer design to make sure globally exponentially convergent (GEC) of the proposed observer. Accordingly, the allowable practical sampling time interval for the numerical simulation environment is probably much higher than the upper bound provided by equation (3.47) that will reflect to increase the transient time response, application dependent. Finally, the error system dynamics are ensured GES of the proposed observer using tools of *Lyapunov* stability theory for closed – loop continuous - time nonlinear systems where \hat{z} is the estimated trajectory given by equation (3.21) for whatever initial conditions $(x_0, \hat{x}_0) \in \mathbb{R}^6 \times \mathbb{R}^6$ and for the satisfactory large enough value of observer design parameter. One expects the possibility to achieve better dynamic performance. This will be confirmed via numerical simulation of a physical model associated with the variable speeds PMSM drive.

3.3.7 Observer equation in the original coordinates

It should be confirmed that if the state observer is synthesized for system model given in (3.18), then its implementation in the original coordinates requires computing the inverse of the *Jacobian* matrix. Note that, from the transformation (or observability) mapping, *i.e.*, $z \triangleq \Phi(x)$, the dynamics of the original state estimate, \hat{x} can be written in terms of inverse *Jacobian* state transformation. Under the condition given in (3.15), $J_{\Phi(x)}$ has full rank. Then, $\Phi(x)$ is a diffeomorphism and so, to any (x, \hat{x}) corresponds a unique (z, \hat{z}) and vice - versa.

According to theorem 3.1, $\forall \theta > \theta_0, \sigma \leq \sigma_0/2$ and $\forall \tau_s \in (0, T_{max}]$, the state estimation error $\hat{z} - z = \Phi(\hat{x}) - \Phi(x)$ is exponentially vanishing for any initial condition, $\Phi(\hat{x}(0)) - \Phi(x(0))$.

$$\hat{\dot{x}} = J_{\Phi(\hat{x})}^{-1}(\hat{z}) \quad (3.48)$$

On the other hand, using equations defined by (3.8) and (3.9), one can see that:

$Az + \varphi(z, u_s) \triangleq J_{\Phi(\hat{x})} f(x, u_s)$. Consequently, from equation (3.21) the following system dynamics is an observer corresponding to the real system model given in equation (3.4).

$$\begin{cases} \hat{\dot{x}} = f(\hat{x}, u_s) - \theta J_{\Phi(\hat{x})}^{-1} \Delta^{-1} K (C(\hat{x}) - w) \\ \dot{w} = C f(\hat{x}, u_s) \\ w(t_k) = y(t_k) \end{cases} \quad \forall t \in [t_k, t_{k+1}), k \in \mathbb{N} \quad (3.49)$$

A flowchart of the proposed approach to PMSM drive system is indicated in Figure 3.5.

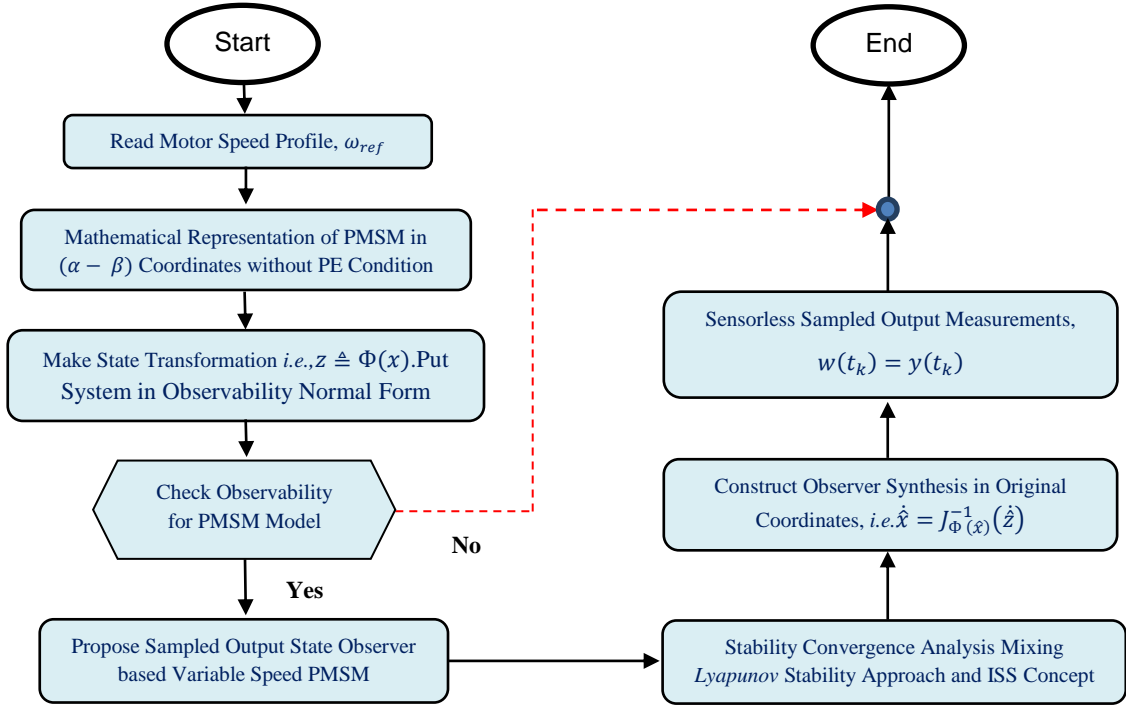


Figure 3.5. A flowchart of the proposed observer applied on variable speed PMSM drive system

3.4 Simulation results and verifications

3.4.1 Implementation considerations

The dynamic performances of the proposed sampled output high - gain observer design are illustrated by numerical simulation in this subsection. To this end, the system is simulated using MATLAB/SIMULINK (version R2015) environment. The tool selected for solving the system state dynamic equations is the MATLAB function called ODE45 (Dormand - Prince) with the relative tolerance error of $(2 \cdot 10^{-5})$ and variable step solver type.

The system sample study is composed of the permanent magnet synchronous machine drive and the DC/AC power converter, including the numerical electrical and mechanical characteristics listed in Table 3.1. The numerical values issued from the technical documentation of PMSM drives. Figure 3.6 describes a block diagram of a motor drive of the system case study running with sampled – output high gain state observer. Basically, the major function of the sensorless PMSM drive system is drawing the electrical energy from the main source and supplies the required energy to the electric motor, such that the desired mechanical output is achieved, successfully without resorting to use classical mechanical and magnetic sensors. Hence, the speed of the motor, load torque, and the rotor position using on-line measurements could be accomplished to provide one of the nonlinear control design techniques. The proposed sampled output HGO is defined by equation (3.21) based nonlinear system model given in equation (3.1) for variable rotor speed. The state observer is also implemented by MATLAB/SIMULINK resources. The observer design parameters are θ, τ_s and, K . They are used to construct the multiplicative observer gain (*i. e.* $\Delta^{-1} \theta K$). Using the try and error principle, it provides the required numerical design values listed in Table 3.2. Now, the dynamic performances of the proposed state observer design given in equation (3.21) have been evaluated in the presence of time-varying rotor speed and external load torque profiles. They are affected by measurement noise with sufficiently large spectrum so as they can be assimilated to white noise with 8 mV peak value for stator voltages, 0.025 rad/sec for mechanical speed and 0.4 N. m for mechanical load torque. They are indicated in Figure 3.7 and Figure 3.8, respectively, for complete one cycle during simulation. Notice that, the reference rotor speed has been chosen such that the PMSM is forced to operate close to the un-observability region bounded between (8 -10) s as in Figure (3.7). It should be emphasized that the fluctuations of the external load torque profile are implicitly accounted by the observer design process. That is, their effects to initial conditions reset is compensated and suppressed dynamically by the proposed observer due to its global convergence nature. The reference motor speed profile for the complete first cycle is forced to operate in various cases as indicated in Figure 3.7 and then repeated once again:

- The reference motor speed is applied at time $t = 0$ s for low rotor speed (30 rad /s), which is fixed from (0 – 2) s at no – load torque operation.
- The reference motor speed is increased gradually up to (100 rad/sec) at time $t = 3$ s.

- The reference motor speed is applied at time $t = 3s$ for high nominal rotor speed (100 rad/s), which is fixed from (3 – 7) s meanwhile the time - varying load torque increases up to nominal torque value (10) N. m at operating time 4s.
- The reference motor speed is decreased once again gradually down to (0 rad/sec) until time $t = 8s$ (near the un-observability region).
- The reference motor speed is applied at time $t = 8s$ for low rotor speed with load torque equals (5) N. m for the rest time of first operating cycle.

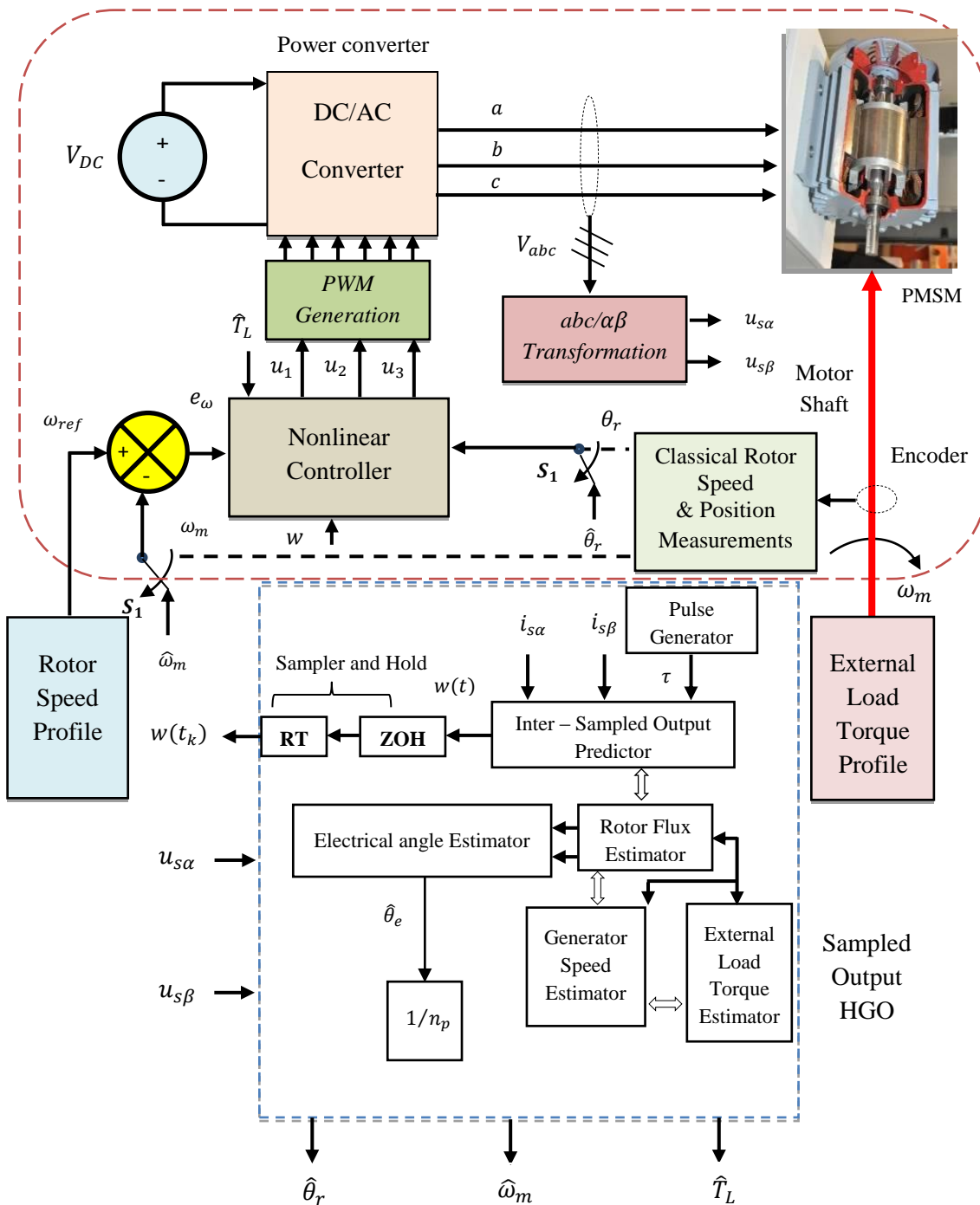


Figure 3.6. Block diagram of a motor drive running with sampled – output HGO

3.4.2 Observer dynamic tracking performances

The observer initial boundaries, $\hat{\psi}_r(0)$, $\hat{\omega}_r(0)$ and $\hat{T}_L(0)$ can be arbitrarily chosen to prove the capability of proposed observer design for whatever initial conditions without resorting to use dynamic equation for rotor position estimation. Hence, it is useful for providing the information about the rotor position for control system before and during the starting - up system model. The resulting observer dynamic performances for complete one operating cycle and zooming around (1) s are illustrated in Figures 3.9, 3.11, 3.13, 3.15 and 3.17. They indicate the waveforms of tracking performance of the proposed state observer are quite satisfactory for variable speed PMSM drive system.

It is apparent from numerical simulation of variable speed PMSM drive system, the sampled - output proposed observer performs - well despite those operating conditions nearing un-observability region bounded between (8 - 10) s. The estimation errors between estimate and actual trajectories are clarified in Figures 3.10, 3.12, 3.14, 2.16 and 3.18. It should be emphasized that it has been used the un-measured of the electrical angle, $\hat{\theta}_e$ in numerical simulation for estimation other un-measured mechanical and magnetic state variables instead of using the actual electrical angle, θ_e to eliminate the necessity of using rotor speed, load torque and rotor position measurements.

The $(\alpha - \beta)$ reference frame represents the electric frame linked with the stator phase windings, *i.e.*, α - axis being aligned with phase - *a* in (abc) model representation. PMSM drive works under nominal operating conditions of the rotor magnetic flux (0.3) Wb during the operating cycle. It is observed that at low value of observer parameter, θ (150), it allows free noise estimates, but these states estimate vary slowly and they are not capable of tracking the actual state variations. On the other side, a very large value of, θ (170) permits a good tracking performance of the missing states variations, but in such case, the observer becomes noise sensitive since the noise level in the provided estimates is significantly high. So, it should be made a compromise solution between both cases by selecting optimum gain design parameter θ (160).

3.4.3 Sensorless sampled - output measurements

It is apparent from observer simulation results shown in Figure 3.19 and Figure 3.20, which indicate the real, estimate and the predict motor currents variation projected on $(\alpha - \beta)$ stationary reference frame correlated with external load torque time variation (compared to Figure 3.8). The prediction errors between output state predictors and actual measured

quantities in $(\alpha - \beta)$ representation are illustrated in Figure 3.21 and Figure 3.22, respectively. Figure 3.23 indicates the evolution of sampling time interval, $\forall t \in [t_k, t_{k+1}), \forall \tau \in (0, \tau_{MASP}]$ with sampling time interval fixed to 1.5 ms. This indicates the robustness of the proposed observer *w.r.t* disturbed sampling schedule although the prediction signal is considered in construction of correction error. Unlike in classical state observers operate with continuous – time output measurements, which considered those measurements, are accessible.

Table 3.1. PMSM nominal mechanical and electrical characteristics

Parameter	Symbol	Value
DC / AC converter	V_{dc}	600 V
Modulation frequency	f_m	10 Hz
Nominal power	P_{nom}	3 kW
Nominal flux	ψ_{nom}	0.3 Wb
Stator resistance	R_s	0.6 Ω
Stator inductance	L_s	0.0094 H
Rotor and load viscous damping coefficient	f	0.003819 N.m/sec
Moment of inertia	J	0.02765 kg.m ²
Number of magnet pole pairs	n_p	2

Table 3.2. Parameters of sampled output HGO

Observer design parameter	Fixed gain vector			Sampling time interval
θ	k_1	k_2	k_3	τ
160	$25 \times \mathbb{I}_2$	$70 \times \mathbb{I}_2$	$90 \times \mathbb{I}_2$	1.5ms

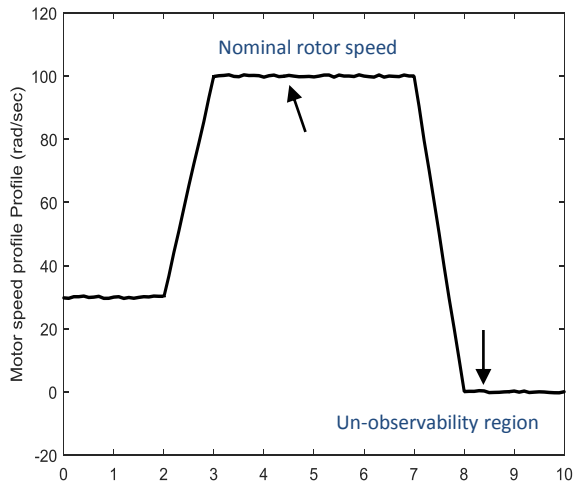


Figure 3.7. Rotor speed profile in (rad/sec)

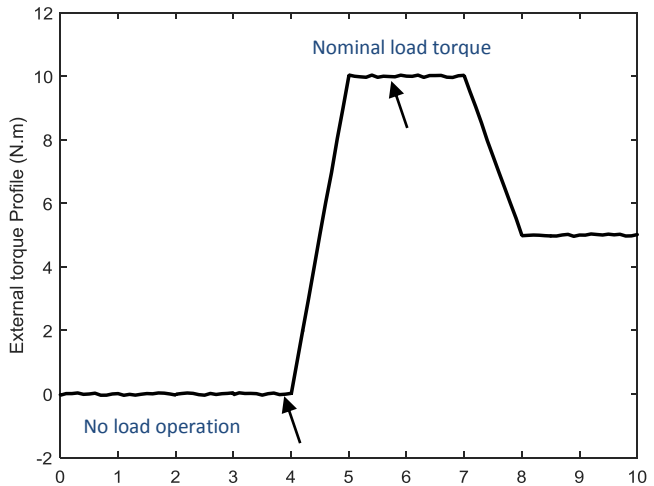


Figure 3.8. External load torque profile in (N. m)

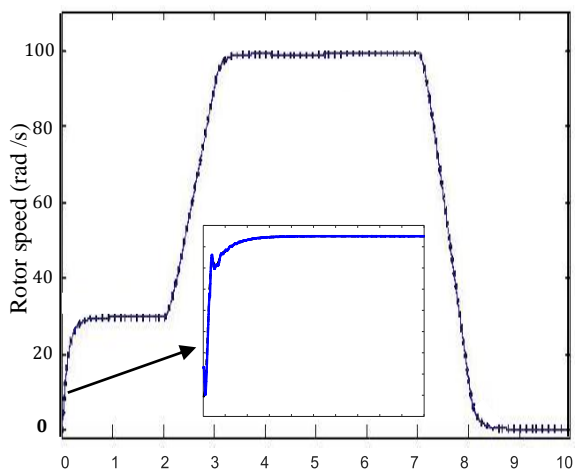


Figure 3.9. Estimated (Blue line) and real (Black dotted) rotor speed (rad/sec)

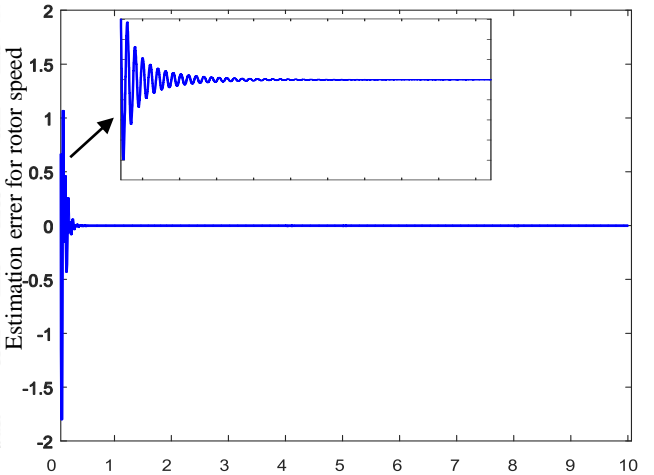


Figure 3.10. Estimation error for rotor speed.

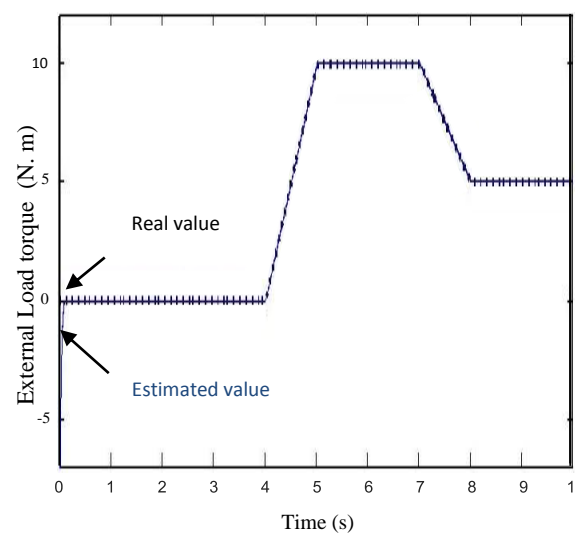


Figure 3.11. Estimated (Blue line) and real (Black dotted) load torque (N. m)

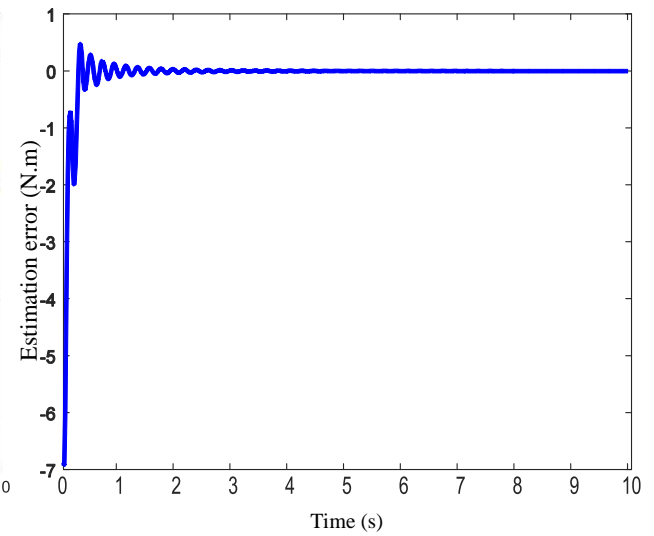


Figure 3.12. Estimation error for load torque

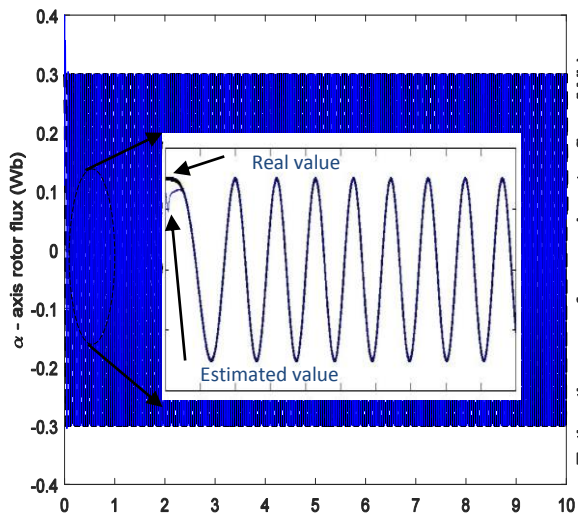


Figure 3.13. Estimated (Blue line) and real (Black dotted) α – axis rotor flux (Wb)

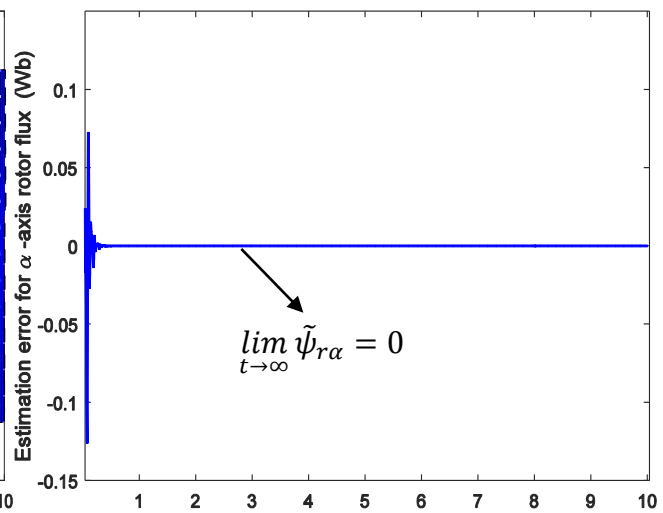


Figure 3.14. Estimation error rotor flux

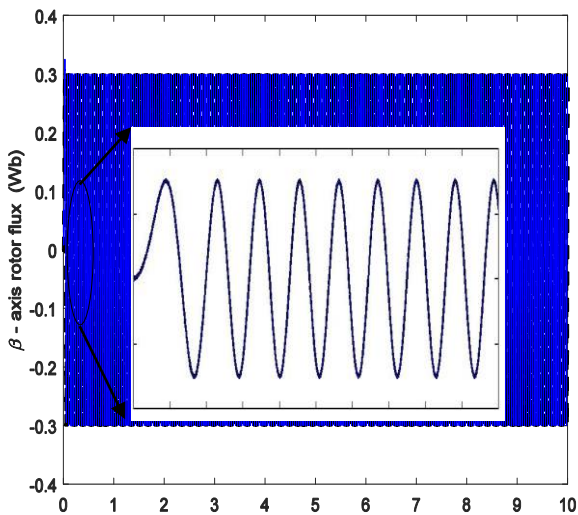


Figure 3.15. Estimated (Blue line) and real (Black-dotted) β – axis rotor flux (Wb)

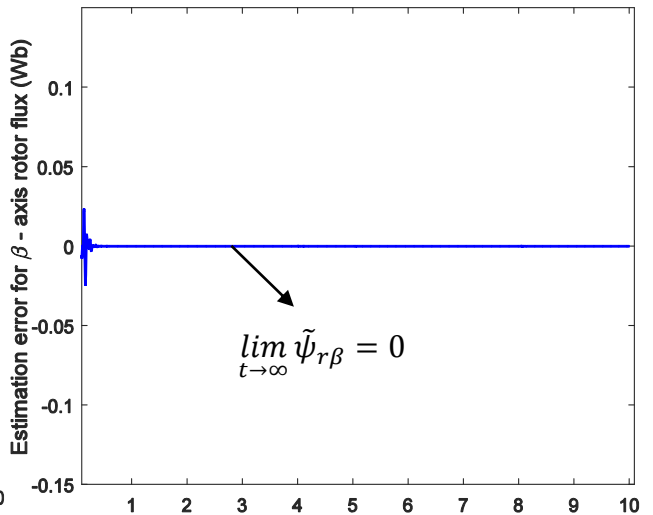


Figure 3.16. Estimation error rotor flux

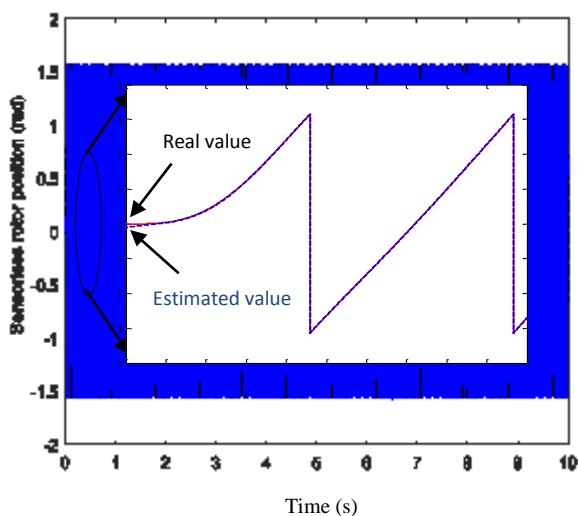


Figure 3.17. Estimated (Blue line) and real (Black dotted) rotor position (rad)

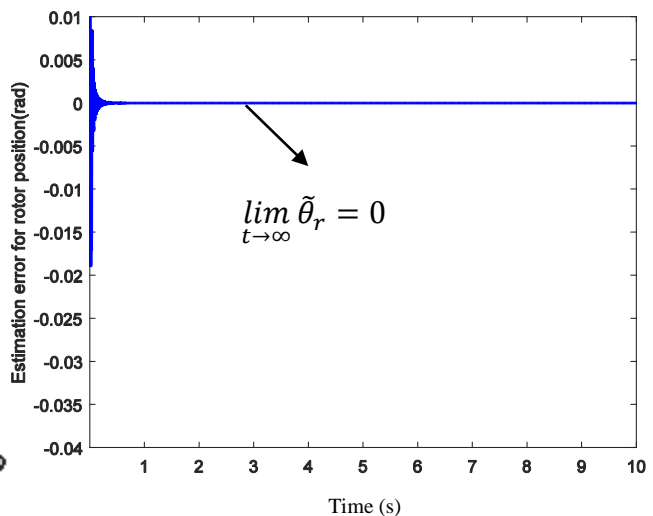


Figure 3.18. Estimation error for rotor position

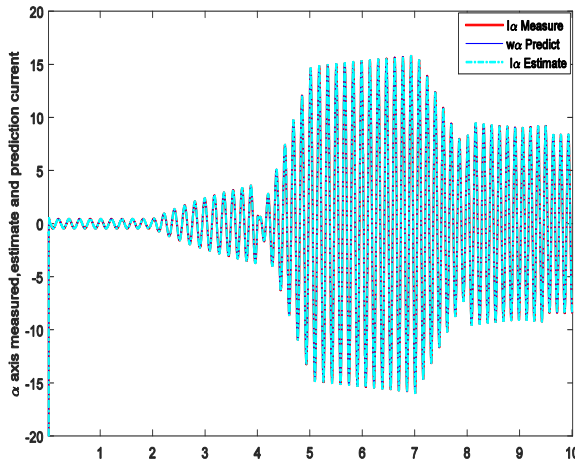


Figure 3.19. Simulated, predicted and estimated α – axis stator current

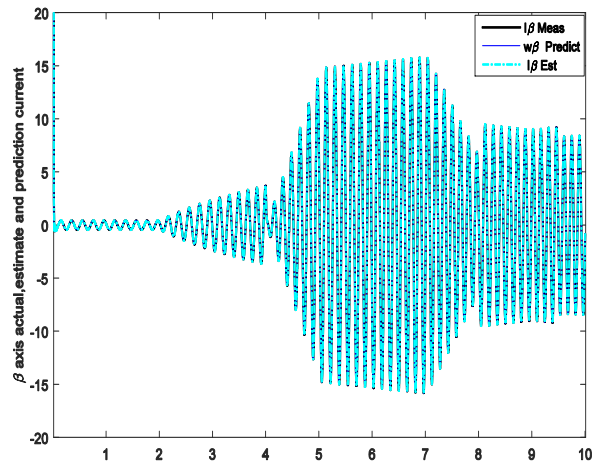


Figure 3.20. Simulated, predicted and estimated β – axis stator current (A)

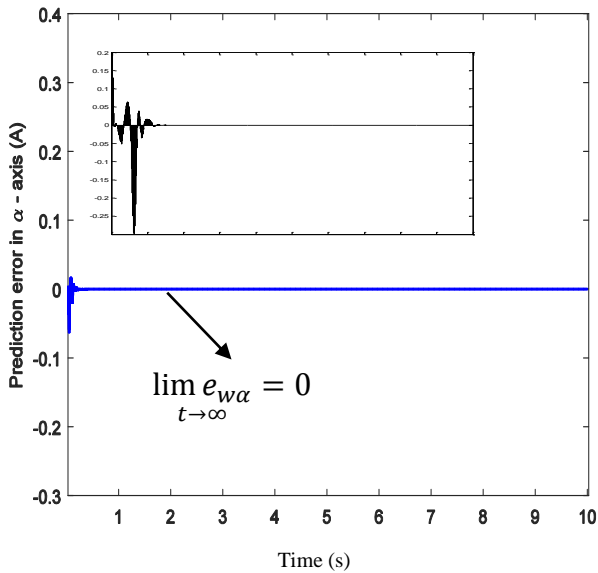


Figure 3.21. Prediction error for α – axis (A)

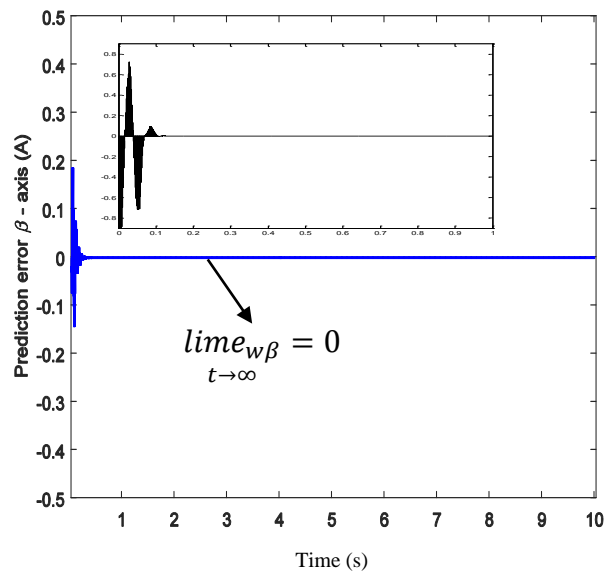


Figure 3.22. Prediction error for β – axis (A)

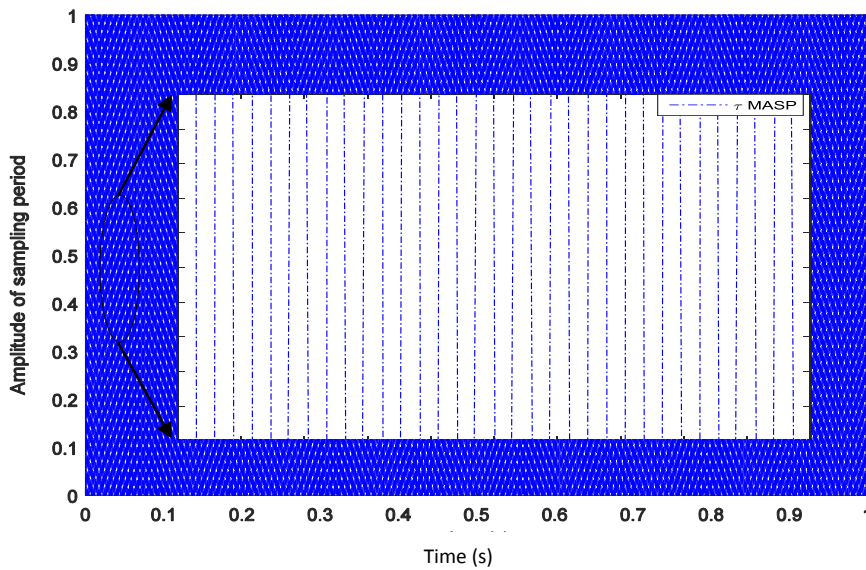


Figure 3.23. Evolution of sampling time interval, $\forall t \in [t_k, t_{k+1})$

3.5 Conclusions

In this section, it has been proposed a state observer for a class of MIMO nonlinear systems based sampled - output measurement. It is uniformly observable system for universal input. The problem of on-line estimation of rotor position, motor speed and external load torque of the PMSM drive has been addressed, successfully. Theoretically, this problem can be coped using existing state observers. However, the previous observers present several limitations associated with necessitating of using outputs measurements in CTM and the necessity of persistently exciting signals. These requirements and limitations make previously some of the state observers not quite suitable for many applications. Whilst the present observer enjoys its sampled-data nature and it does not need persistently exciting inputs. These features are achieved by combining and mixing the HGO approach and inter- sample time predictor. The main benefit of the proposed observer resides in the system state estimates are remained in CTM. It is preferred practically as those data will be injected into nonlinear controller.

It has been derived an adequate condition for the maximum allowable sampling time interval that ensures global exponential convergence of the observation error converges exponentially to a compact neighbourhood of the origin with progress time. The size of this compact set can be made sufficiently small by choosing the observer design parameter satisfactory large enough. The observer simulation results support the presented theorem 3.1 that reflects on attenuating the effect of measurement errors and the improvement *w.r.t* global convergence properties. To prove the robustness of the proposed observer *w.r.t* to attenuation of sampling phenomenon, the innovation corrective term of the proposed observer is a function of the difference between the output estimate and the output predictor at the last sampling instant. It is known that a larger sampling time interval entails a smaller fixed gain vector and increasing transient time response to get a stable state observer. Off course, when the fixed gain vector becomes too small, the inherent nonlinearity nature of the system may prevail in the state observer performance.

It should be mentioned that it has been used the rotor position estimate instead of its actual unmeasured value to provide the nonlinear controller during and after starting - up of the sensorless variable speed PMSM drive.

The presented results are clearly demonstrated the good ability to the proposed sampled-output HGO in providing accurate estimates of the missing states, good external load torque

rejection, although the time variations of external load torque are implicitly accounted by the state observer design, accurate tracking response and robustness of observer performance due to the disturbing effect. Also, it provides slow sensitivity to electrical and mechanical parameter variations; some design gains are easily adjusted compared to *EKF* for nonlinear systems, fast transient time response of observation errors. It has a smooth motion at low speeds and efficient operation at high speeds.

Once again, the searcher expects based on his knowledge in this field, that the present work is the first scientific contribution in the field of AC machine drive systems and particularly for permanent magnet synchronous machine running with sampled – output high gain state observer design. As a matter of fact, the current observer has five basic features. It can be summarized as follows:

- The possibility to achieve sensorless observer control for adaptive or non - adaptive version.
- It has sampled - data output measurements, unlike in many of state observers to solve the problem of output measurements in CTM.
- It has HGO approach coupled with inters – sampled behaviour.
- Eliminate the necessity to use persistence excitation inputs.
- Achieving rotor flux position measurement without resorting to use encoder or fibres instruments, which may degrade their performance when exceeding temperature limit.

Chapter Four

A Novel Observer Design based on Sensorless Sampled Output Measurements: Application to Variable Speed DFIG based Wind Turbine

Table of Contents	page
4.1 Introduction	84
4.1.1 Review of related research	84
4.1.2 Purposes and contributions	87
4.2 Representation of DFIG based wind turbine technology.....	88
4.2.1 Wind turbine modeling	88
4.2.2 Modeling assumptions	90
4.2.3 Full version of DFIG model	90
4.2.4 Power calculation in $(d - q)$ quantities	92
4.2.5 Observability analysis of full version DFIG model	94
4.2.6 Motivations of using reduced model DFIG	97
4.2.7 Reduced version of DFIG model	97
4.3 Position sensorless measurements	100
4.4 Reduced - order state observer design	101
4.4.1 Observer design assumptions	102
4.4.2 Some remarks and notations	103
4.5 Comparison with published results	104
4.6 Sampled - data observer design and convergence analysis	104
4.6.1 Stability analysis of the proposed observer	106
4.6.2 Discussion on the main result	113
4.7 Simulation results and verifications	114
4.7.1 Implementation considerations	114
4.7.2 Observer dynamic tracking performance	116
4.7.3 Sensorless sampled output measurements	117
4.7.4 Sensorless position measurements	118
4.8 Conclusions	122

Chapter 4: A Novel Observer Design based on Sampled Output Measurements

The present chapter covers a novel exponential convergence nonlinear state observer design based sampled - output measurements for DFIG. It is used with VSWT system to generate large amounts of power and support the electric power networks by clean and renewable energy. This chapter also covers the operation of three – phase DFIG used as wound rotor induction machines. The major feature of the proposed observer lies in the consistence of sampled output data measurements and without resorting to use classical mechanical or magnetic sensors such as rotor position or rotor speed encoder. A main component of the state observer, is availability of inter - sampled predictor of the output current vector.

The exponential convergence of the observation error is established and formally analyzed using tools of *Lyapunov* stability theory and fundamentals of small - gain condition to prepare an upper bound of sampling - time interval based on ISS concept. The proposed observer combines features and ideas of HGO structure with inter – sampled output state predictor. The DFIG based wind turbine is one of the most widely used in wind power generation system and this system offers the following advantages:

- Its variable speed operation around the synchronous speed.
- It has completed four – quadrant, active and reactive power control capabilities
- Improving power quality and system efficiency.
- Reduced power converter cost, because converter capacity is typical (25 – 30) % of the wind power generator corresponding to slip power.
- Lower power losses compared to power system based fully fed synchronous generator with full rated power converter.
- DFIG is robust *w.r.t* external disturbances and requires less cyclic maintenance.
- Power factor control (PFC) requirement could be accomplished by saving cost.

The DFIG is capable to control its active and reactive power outputs as desired using system regulators. For the design of proposed state observer, a nonlinear state model of DFIG has been described. The introduction of the present chapter gives a brief history of the topic and the scientific motivations and justifications. The proposed approach using HGO reduced – model design has been addressed in detail supported by MATLAB numerical realization and implementation in the last phase.

4.1 Introduction

As it is well – known, doubly fed electric machines are electric motors or generators. They have three – phase windings distributed on stationary and rotating parts. These windings transfer significant power between shaft and electrical power utility. Typically, the stator windings are directly connected to the electric grid and the corresponding rotor windings are tied to the grid through rotating or static power converters. DFIM are basically used in applications that require varying speed of the machine in a limited range around the synchronous speed, *e.g.*, $\pm 30\%$, because the power converter is partial scale (rating) and the power rating of the frequency converter is varied similarly. Frequency converter converts a basic fixed frequency, fixed sinusoidal voltage waveform with a variable frequency, variable output voltage used to control rotor speed of induction motors. [EL Fadili et al., 2013].

Recently, it is has been recognized that DFIMs become widely applied and one of the main actuators in industrial process. Indeed, as compared to the DC machine, it provides a better power/mass ratio, less maintenance (actually, there are no mechanical commutators), and it is relatively low cost. These machines have promising future perspectives in the industrial process. It is motivated an intensive research activity in DFIM control, especially over the last decade [Giri, 2013].

4.1.1 Review of related research

Recently, DFIMs have entered into common use. There are several contributions focused on studying of DFIG based WECS [Boukhezzar et al., 2009; Poitiers et al., 2009; Song et al., 2012], this in result to the advent and development of wind power technologies for electricity generation. Moreover, the new wind turbine technology integrates with advanced power electronics and different control techniques, making possible to achieve active and reactive power control and provide better power quality and high efficiency [Boldea et al., 2010].

DFIG is one of the most common types of generator used to produce electricity within wind power generation system. DFIGs have numerous attractive advantages compared to other types of electric generators when used based wind turbines. The primary advantage allows the frequency and amplitude of output voltage be maintained at a constant desired level, no matter the velocity of the wind blowing on the wind turbine rotor. DFIG can be directly connected to the AC power network and remain synchronized at all times. Other advantages include the ability to achieve PFC (*e.g.* preserve the power factor close to unity),

while keeping the power electronics components in the field of wind turbine power technology in moderate size [Lajouad et al., 2014].

Measuring mechanical quantities are always a challenge for control systems and visualization of the state variables. In addition, there are at least four common problems caused by traditional mechanical sensors. They are expensive relatively, their associated wiring will reduce the reliability of control systems, some signals are practically complex to measure and these sensors may induce significant errors such as random noise, cyclic errors and DC offset [Bastin et al., 1988]. In fact, the synthesis of an observer running with the controlled system is still beneficial to measure inaccessible quantities or requiring high - end sensors as claimed by [see e.g. Marino et al., 2010; Besançon, 2007]. Exponentially converging observers are exhibited for a large class of MIMO nonlinear systems. Potential applications of these observers had been applied to electromechanical systems as applications in HGO theory [see e.g. Khalil et al., 2013; Deza et al., 1993]. The authors concluded by discussing the use of HGOs in the robustness analysis of feedback controlled systems under joint highly structured perturbations and un-modelled dynamics.

Many research works had been done related to synthesis of observers based DFIM [see e.g. Ozsoy et al., 2016; Barra et al., 2014; Cárdenas et al., 2004], the manuscripts had been proposed a control strategy for control of DFIM running with estimation of unmeasured quantities based on continuous - time measurements of currents and voltages [Gálvez et al., 2011].

In [Lascu et al., 2013], it investigates a family of the stator and rotor flux observers of DFIG. Four stator flux observer topologies are described and compared. All proposed schemes use the voltage and current models connected in parallel or series and no mechanical quantity is estimated. In [Beltran et al., 2011], deals with the sensorless control of DFIG based wind turbine. It combines MPPT control using HGO and second order sliding mode control. The state estimation depends on the time varying of machine parameters. This estimator has the applications where measurement of rotor currents, rotor speed and generator torque are practically inaccessible.

All clearly mentioned design techniques offer continuous - time state observers that need discretization for practical implementation and realization of control laws [see e.g. Laila et al., 2011]. The exact discretization is a highly complex issue due to the strong nonlinearity nature of the state observer. On the other hand, there is no guarantee that approximate discrete-time

versions can maintain the dynamic performances of the original continuous - time adaptive or non-adaptive observers. This interprets why a few studies focused on designing of sampled - data observers that had been applied on nonlinear systems.

In [Deza et al., 1993], discrete - continuous time observers had been designed on the basis of continuous - time system model. The proposed observers included two parts, which are open-loop state predictors operate between successive sampling instants and closed - loop state estimator operates at the sampling times. The output prediction error is ensured exponentially vanishing using technical assumptions.

Another approach had been claimed by [Raff et al., 2008], resides in using a single hybrid continuous - discrete observer with a zero order hold, *ZOH* sampled innovation term. The state observer is applicable to a class of nonlinear *Lipschitz* systems. LMIs are prepared to ensure global stability. It is claimed by [Karafyllis et al., 2009; Kravaris, 2014] a hybrid continuous-discrete observer involving inter - sampled output predictor had been proposed. This technique is re-initialized impulsively; the system state estimate is continuously updated by a general structure observer where the un-available output measurements are replaced by their output predictions. This observer is applied to lower triangular globally *Lipschitz* systems and features exponential convergence of the state observation. A global exponential observer design with sampled data measurements for a class of uniformly observable single output nonlinear systems is proposed by [Nadri et al., 2013]. A special solution of continuous – discrete time *Lyapunov* equation could be used to synthesise uniform observer for adequate large tuning design parameters. Straightforward conditions had been provided to guarantee GEC of the proposed state observer.

The rest of the present chapter is organized in eight sections as follows: The mathematical representation of variable speed DFIG based wind turbine system for full - model and reduced - model of DFIG have been modelled and discussed in section 4.2. In section 4.3, position sensorless measurements have been discussed, successfully. Whilst in section 4.4, it presents non-standard observer of the designated system under the reduced - model. Some remarks and notations related to proposed observer are presented in section 4.5. Simple comparison with published results has been discussed in section 4.6. The main results are described through mathematical theory, meanwhile observer stability convergence has been analysis in section 4.7; all technical results are validated by numerical simulation and

verification through MATLAB/SIMULINK environment, as given in section 4.8. Finally, some conclusions are drawn in section 4.9.

4.1.2 Purposes and contributions

The scientific contribution of the current study presented in this chapter relative to the literature works resides in the challenges and motivations faced this study that is summarized in the following directions:

1. Development of the modeling DFIG based WTGS is carried - out. First, the method of deducing reduced model of the system, the way of transforming the DFIG model from the (abc) frame to different $(d - q)$ reference frames are re-viewed. Moreover, the motivations of using reduced order model instead of the full order model of DFIG.
2. This study tackles the problem of designing non-standard high gain reduced order state observer based on sensorless sampled - output measurements: application of variable speed DFIGs and grid integration.
3. The electromagnetic torque created by DFIG is an indirect output injective relation.
4. The stator and rotor current vector is inaccessible forever and everywhere.
5. Output sampled - data measurements are presently available just at sampling instant.
6. On-line estimation of generator rotor speed, aerodynamic torque, and electromagnetic torque created by the generator.
7. Sensorless rotor and stator position measurements.

The numerical simulation results of the sample study dealing with variable speed DFIG system support the presented main theorem. Through – out these results, they ensure the following features:

- i) Assurance of measurement error convergence to zero with progressive time.
- ii) Improvement *w.r.t* global exponential stability properties and system state estimations.

4.2 Representation of DFIG based wind turbine technology

DFIG is an induction machine has a wound rotor where the rotor and stator are both connected to electrical sources. The rotor has three - phase windings which are energised by currents. These rotor currents establish the rotor magnetic field. It turns out that the rotor magnetic field interacts with the stator magnetic field to develop electromagnetic torque. The

electromagnetic torque created by DFIG depends on the strength of the stator field, the rotor field, and the angular displacement between the two fields.

From the theoretical point of view, the electromagnetic torque is developed by magnetic attraction between magnet poles of opposite polarity where each of the rotor and stator magnetic fields establish a pair of magnet poles. If the stator winding is fed from a three - phase balanced source, the stator flux will have a constant level and it rotates at the synchronous speed [see. *e.g.* Fletcher et al., 2010].

4.2.1 Wind turbine modeling

This sub - section will give the mathematical representation of wind turbine coupled with DFIG system. The output power of a wind turbine is usually given by:

$$P_m = \frac{1}{2} \rho A C_p V_w^3 \quad (4.1)$$

where, C_p is the coefficient of performance also called - power coefficient, $A = \pi r^2$, is the swept area of the turbine blades in (m^2), ρ is the air - density in (kg/m^3) and V_w is the wind velocity in (m/s). The power coefficient C_p is not a constant and it is a nonlinear function as claimed by [see *e.g.* Khajuria et al., 2012]. Actually, it depends on two basic parameters, namely: tip speed ratio, λ_{TSR} and blade pitch angle, β in degree. Depending on this consideration, generator torque is written in the following form:

$$T_g = \frac{P_m}{\omega_r} = \frac{\rho \pi r^3 C_p(\lambda_{TSR}, \beta) V_w^2}{2 \lambda_{TSR}} \quad (4.2)$$

The tip speed ratio, λ_{TSR} is defined as the ratio of the angular rotor speed of the wind turbine to the linear wind velocity at the tip of the blades and could be expressed as follows:

$$\lambda_{TSR} = \frac{\omega_g r}{V_w} \quad (4.3)$$

where, ω_g is the mechanical angular speed of the turbine rotor in (rad/s) and V_w is wind velocity in (m/s). For a variable speed wind turbine (VSWT), the power coefficient is,

$$\lambda_i = \frac{1}{\frac{1}{\lambda_{TSR} + 0.02 \beta} - \frac{0.03}{\beta^3 + 1}} \quad (4.4)$$

where, λ_{TSR} is defined by equation (4.3) and $C_p(\lambda_{TSR}, \beta)$ can be evaluated as follows,

$$C_p(\lambda_{TSR}, \beta) = 0.73 \left[\frac{151}{\lambda_i} - 0.58 \beta - 0.002 \beta^{2.14} - 13.2 \right] \exp \frac{18.4}{\lambda_i} \quad (4.5)$$

It should be mentioned that the maximum theoretical efficiency of wind turbine is 60 % using Betz limit. Turbine's output power versus wind velocity for varying pitch angles is clarified in Figure 4.1 and power coefficient of the wind turbine versus tip speed ratio for varying pitch angles is also shown in Figure 4.2. More details about the fundamentals and principle of operation for a wind power generator system are found in appendix A.4 of the present thesis.

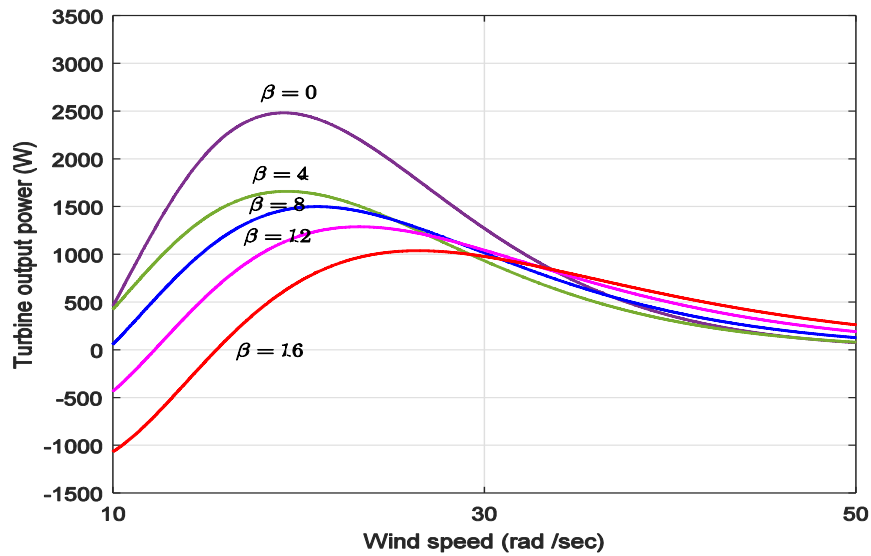


Figure 4.1: Turbine output power versus wind speed for varying β

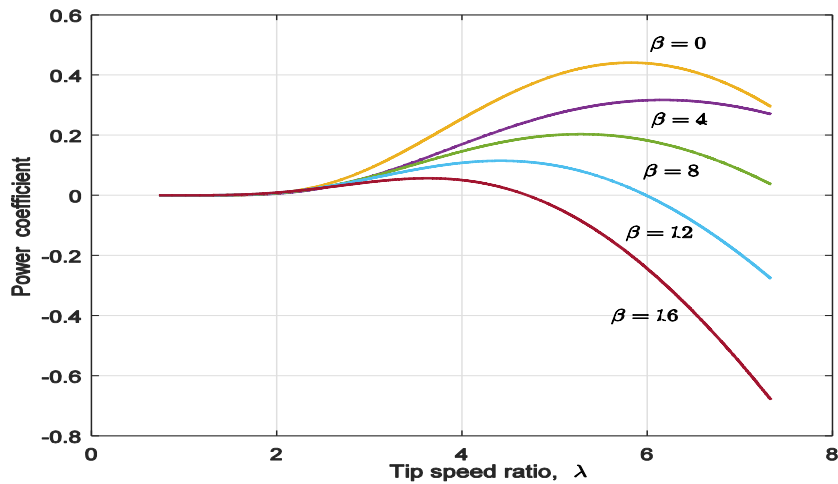


Figure 4.2: C_p of the wind turbine versus λ_{TSR} for varying β

4.2.2 Modeling assumptions

1. All iron losses are neglected via modeling.
2. The electric machine, air – gap length is constant, smooth, and symmetric in space.
3. The stator and the rotor windings present in the symmetrical structure (*i.e.* no saliency) providing DFIG with three - phase electrical equivalent circuit.

4.2.3 Full version of DFIG model

In this sub - section, the dynamic model of DFIG based WTGS is introduced with some important system properties. It is necessary to investigate the actual behaviour and initiate with an appropriate and efficient model of DFIG when designing of realistic nonlinear state observer. Let us choose the stator and rotor windings to be placed sinusoidally and symmetrically in space, the magnetic saturation effects and the mutual capacitance, c_M of the phase windings are null. The mathematical relations between the generator voltages on the phase windings and the corresponding currents at arbitrary generator speed can be used to indicate the mathematical model of (DFIG), projected on $(d - q)$ reference frame after doing *Park's* transformation.

It is suitable for the purposes of modeling and control purposes that all the rotor quantities are referred to the stator side to simplify the mathematical representation and calculations. The system state equation projected on $(d - q)$ reference frame is given as [El Fadili et al., 2012; Novotny et al., 2000]:

$$\left[\begin{array}{l} v_{sd} = R_s i_{sd} + \dot{\phi}_{sd} - \omega_s \phi_{sq} \\ v_{sq} = R_s i_{sq} + \dot{\phi}_{sq} + \omega_s \phi_{sd} \\ \dot{v}_{rd} = \dot{R}_r i_{rd} + \dot{\phi}_{rd} - (\omega_s - n_p \omega_g) \phi_{rq} \\ \dot{v}_{rq} = \dot{R}_r i_{rq} + \dot{\phi}_{rq} + (\omega_s - n_p \omega_g) \phi_{rd} \end{array} \right. \quad \begin{array}{l} (4.6a) \\ (4.6b) \\ (4.6c) \\ (4.6d) \end{array}$$

From equations (4.6a) – (4.6b), it is evident that the dynamic model of DFIG is a nonlinear model because of the strong coupling between the synchronous speed and the stator fluxes. This idea could be generalized for the rotor side. In case of DFIG, the rotor windings are not short – circuit, unlike in PMSG. In the sequel the rotor voltages $\dot{v}_{rd}, \dot{v}_{rq}$ are not omitted. The

stator and rotor flux linkage equations can be formulated in terms of their currents projected on $(d - q)$ synchronous rotor reference frame using the following matrix notation:

$$\begin{bmatrix} \phi_{sd} \\ \phi_{sq} \\ \hat{\phi}_{rd} \\ \hat{\phi}_{rq} \end{bmatrix} = \begin{bmatrix} L_s & 0 & M_{sr} & 0 \\ 0 & L_s & 0 & M_{sr} \\ M_{sr} & 0 & \hat{L}_r & 0 \\ 0 & M_{sr} & 0 & \hat{L}_r \end{bmatrix} \begin{bmatrix} i_{sd} \\ i_{sq} \\ \dot{i}_{rd} \\ \dot{i}_{rq} \end{bmatrix} \quad (4.6e)$$

And the dynamic of rotor speed using the lumped mass model is:

$$\dot{\omega}_g = \frac{1}{J} (T_{em} - T_g - f_v \omega_g) \quad (4.6f)$$

with slip pulsating rotor speed, $\omega_r = \omega_s - n_p \omega_g$. This speed constitutes an image of the generator torque, $\omega_s \triangleq \frac{d\theta_s}{dt} = 2\pi f_s$.

where R_s, L_s , are stator side resistance and self - inductance. \hat{R}_r and \hat{L}_r are, respectively the rotor resistance and self - inductance are referred to stator side, while M_{sr} is the mutual or coupling inductance between the stator and the rotor windings. $\phi_{sd}, \phi_{sq}, \hat{\phi}_{rd}$ and $\hat{\phi}_{rq}$ denote the stator flux components and rotor flux components referred to stator side, which are expressed in $(d - q)$ representation. $(i_{sd}, i_{sq}, \dot{i}_{rd}, \dot{i}_{rq})$ and $(v_{sd}, v_{sq}, \dot{v}_{rd}, \dot{v}_{rq})$ are the stator components of the current, voltage and the corresponding rotor components referred to stator side, respectively. The symbol n_p designates the number of magnetic pole - pairs, ω_s is the constant stator angular speed, ω_g represents the random generator speed. f_v, J and T_g are, respectively the viscous friction coefficient, the total moment of inertia for lumped mass model (rotor blades, hub, and DFIG generator), and generator torque created by the wind turbine system. The equations expressed in (4.6a) - (4.6f) can be re-written in matrix notation as:

$$v = \begin{bmatrix} R_s \mathbb{I}_2 & O_2 \\ O_2 & \hat{R}_r \mathbb{I}_2 \end{bmatrix} i + \frac{d\Phi}{dt} + \begin{bmatrix} \omega_s J_2 & O_2 \\ O_2 & (\omega_s - n_p \omega_g) J_2 \end{bmatrix} \Phi \quad (4.7a)$$

$$\Phi = \begin{bmatrix} L_s \mathbb{I}_2 & M_{sr} \mathbb{I}_2 \\ M_{sr} \mathbb{I}_2 & \hat{L}_r \mathbb{I}_2 \end{bmatrix} i \quad (4.7b)$$

$$\frac{d\omega_g}{dt} = \frac{1}{J} (T_{em} - T_g - f_v \omega_g) \quad (4.8a)$$

where, T_{em} is defined the electromagnetic torque (N.m) created by DFIG. Mathematically, the electromagnetic torque is the vector product of the stator and rotor fields. It can be represented by the following expression:

$$T_{em} \triangleq n_p M_{sr} (\dot{i}_{rd} i_{sq} - \dot{i}_{rq} i_{sd}) = n_p M_{sr} i^T T_0 i \quad (4.8b)$$

with, $i \triangleq [i_{sd} \ i_{sq} \ \dot{i}_{rd} \ \dot{i}_{rq}]^T$, $v \triangleq [v_{sd} \ v_{sq} \ \dot{v}_{rd} \ \dot{v}_{rq}]^T$

and $\Phi \triangleq [\phi_{sd} \ \phi_{sq} \ \dot{\phi}_{rd} \ \dot{\phi}_{rq}]^T$ denote, respectively the system state vector of stator and rotor current, voltage and flux linkage expressed in $(d - q)$ synchronous rotor reference frame, where

$$T_0 \triangleq \begin{bmatrix} O_2 & J_2 \\ O_2 & O_2 \end{bmatrix}, \in \mathbb{R}^{4 \times 4}, \quad J_2 \triangleq \begin{bmatrix} 0 & -1 \\ 1 & 0 \end{bmatrix}, \quad \mathbb{I}_2 \triangleq \begin{bmatrix} 1 & 0 \\ 0 & 1 \end{bmatrix}, \quad O_2 \triangleq \begin{bmatrix} 0 & 0 \\ 0 & 0 \end{bmatrix}, \in \mathbb{R}^{2 \times 2} \quad (4.9)$$

Note that all rotor quantities are now referred to the stator - side. The effect of referring is straight forward as claimed by [Krause, 1995]. It could be defined rotor quantities as:

$$\dot{\phi}_{rd} \triangleq \frac{\phi_{rd}}{s_l}, \quad \dot{v}_{rd} \triangleq \frac{v_{rd}}{s_l}, \quad \dot{\phi}_{rq} \triangleq \frac{\phi_{rq}}{s_l}, \quad \dot{v}_{rq} \triangleq \frac{v_{rq}}{s_l}, \quad \hat{R}_r \triangleq \frac{R_r}{s_l^2}, \quad \hat{L}_r \triangleq \frac{L_r}{s_l^2}, \quad i_{rd} \triangleq s_l i_{rd}, \quad \text{and} \quad i_{rq} \triangleq s_l i_{rq} \quad (4.10)$$

The slip factor is defined as:

$$s_l \triangleq \begin{cases} \frac{\omega_s - \omega_r}{\omega_s} \leq 0 & \text{supersynchronous speed mode} \\ \frac{\omega_s - \omega_r}{\omega_s} > 0 & \text{subsynchronous speed mode} \end{cases}$$

The slip factor is bounded between $[-0.3, 0.3]$ depending on the operation mode of DFIG. The equivalent circuit model of the DFIG based wind turbine system expressed in $(d - q)$ model is shown in Figure 4.3.

4.2.4 Power calculation in d - q quantities

The stator - side active and reactive powers have the following forms, respectively:

$$\text{Stator - side:} \quad \begin{cases} P_s = 1.5 * (v_{sd} i_{sd} + v_{sq} i_{sq}) \\ Q_s = 1.5 * (v_{sq} i_{sd} - v_{sd} i_{sq}) \end{cases} \quad (4.11a)$$

Similarly, the rotor- side power can be calculated in the following form:

$$\text{Rotor - side:} \quad \begin{cases} P_r = 1.5 * (v_{rd} i_{rd} + v_{rq} i_{rq}) \\ Q_r = 1.5 * (v_{rq} i_{rd} - v_{rd} i_{rq}) \end{cases} \quad (4.11b)$$

The mathematical model of DFIG expressed in $(d - q)$ coordinate system can be reformulated in the following state dynamic equations:

$$\begin{cases} \dot{i} = \gamma M_1 v + M_{23} i - n_p \gamma M_4 \omega_g i & (4.12a) \\ \dot{\omega}_g = \frac{1}{J} (n_p M_{sr} i^T T_0 i - T_g - f_v \omega_g) & (4.12b) \\ \dot{T}_g = 0 & (4.12c) \end{cases}$$

It turns out that the model defined in equation (4.12) is clearly nonlinear since the system model involves the product between its output current, i and generator rotor speed, ω_g . Equation (4.12c) is motivated by the fact that, in numerous applications, the generated torque

T_g is assumed bounded, derivable and its time derivative is also bounded. Indeed, the generator torque T_g is infrequent, that is, the input generator torque takes a value with slowly time varying. The remaining parameters are defined as follows, $\triangleq \frac{1}{\varrho L_s \dot{L}_r}$, and ϱ is the leakage - coefficient defined by, $\varrho \triangleq 1 - \frac{M_{sr}^2}{L_s \dot{L}_r}$, while other parameters, M_1, M_2, M_3, M_{23} , and M_4 are constant matrices. They can be written in matrix notation as follows:

$$M_1 \triangleq \begin{pmatrix} L_r \mathbb{I}_2 & -M_{sr} \mathbb{I}_2 \\ -M_{sr} \mathbb{I}_2 & L_s \mathbb{I}_2 \end{pmatrix}, \quad M_2 \triangleq \begin{pmatrix} R_s \dot{L}_r \mathbb{I}_2 & -M_{sr} \dot{R}_r \mathbb{I}_2 \\ -M_{sr} R_s \mathbb{I}_2 & \dot{R}_r L_s \mathbb{I}_2 \end{pmatrix}, \in \mathbb{R}^{4 \times 4} \quad (4.13a)$$

$$M_3 \triangleq \begin{pmatrix} J_2 & O_2 \\ O_2 & J_2 \end{pmatrix}, \quad M_{23} \triangleq -M_3 \omega_s - \gamma M_2, \in \mathbb{R}^{4 \times 4} \quad (4.13b)$$

$$M_4 \triangleq \begin{pmatrix} M_{sr}^2 J_2 & M_{sr} \dot{L}_r J_2 \\ -M_{sr} L_s J_2 & -L_s \dot{L}_r J_2 \end{pmatrix}, \in \mathbb{R}^{4 \times 4} \quad (4.13c)$$

Now, let us introduce the following system variable representation:

$$x_{11} \triangleq i_{sd}, \quad x_{12} \triangleq i_{sq}, \quad x_{13} \triangleq i_{rd}, \quad x_{14} \triangleq i_{rq}, \quad x_2 \triangleq \omega_g, \quad x_3 \triangleq T_g$$

$$\text{Let us define the current vector as: } x_1 \triangleq [x_{11} \ x_{12} \ x_{13} \ x_{14}]^T = [i_{sd} \ i_{sq} \ i_{rd} \ i_{rq}]^T \quad (3.14)$$

Once again, the system model given in equation (4.12) can be re-written in the compact form as follows:

$$\begin{cases} \dot{x} = f(v, x) \\ y = h(x) \end{cases} \quad (4.15)$$

with, $h(x)$ designs a measured output states function of the system given in equation (4.15a), and the vector field function is defined in the following form:

$$\left[\begin{array}{l} f(v, x) \triangleq [f_1, f_2, f_3, f_4, f_5, f_6](v, x), \in \mathbb{R}^{6 \times 6} \\ [f_1, f_2, f_3, f_4]^T(v, x) = \gamma M_1 v + M_{23} x_1 - n_p \gamma M_4 x_2 x_1, \in \mathbb{R}^{4 \times 4} \\ f_5(v, x) = \frac{1}{j} (n_p M_{sr} x_1^T T_0 x_1 - x_3 - f_v x_2) \\ f_6(v, x) = 0 \end{array} \right. \quad (4.16a)$$

$$f_5(v, x) = \frac{1}{j} (n_p M_{sr} x_1^T T_0 x_1 - x_3 - f_v x_2) \quad (4.16b)$$

$$f_6(v, x) = 0 \quad (4.16c)$$

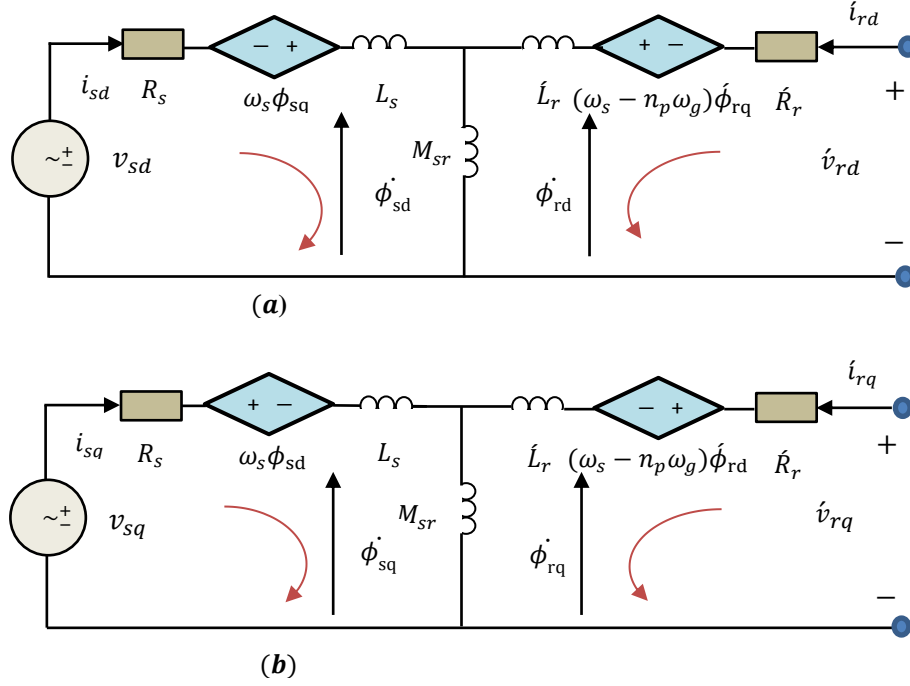


Figure 4.3: Electrical equivalent circuit of the DFIG expressed in $(d - q)$ representation seen from stator side

(a): $d - axis$ circuit

(b): $q - axis$ circuit

4.2.5 Observability analysis of full version DFIG model

The aim of observability analysis is to check is it possible to synthesize high – gain state observer for DFIG model based on system input/output injection measurements. However, readers interested in this topic can refer for this instance to useful references [see *e.g.* Glumineau et al., 2015] and all the references therein for more information. It should be mentioned that one can find an adequate condition in which the *Jacobian* matrix has full rank almost everywhere [see *e.g.* Vaclavek et al., 2013; Khalil et al., 2013].

The observability analysis can be evaluated from the measured output state function and its derivative [see *e.g.* Ibarra-Rojas et al., 2004]. Let us apply the following observation space of the function $\mathcal{O}_{DFIG}(h(x))$ containing the information that generated from the observability criterion knowing that, $L_f^k h$ is called the k 'th order *Lie* - derivative of the function, $h(x)$ w.r.t vector field function along the closed - loop trajectories.

$$\mathcal{O}_{DFIG}(h(x)) \triangleq \{h_1 \ h_2 \ h_3 \ h_4 \ L_f h_1 \ L_f h_2 \ L_f h_3 \ L_f h_4 \ L_f^2 h_1 \ L_f^2 h_2 \ L_f^2 h_3 \ L_f^2 h_4\} \quad (4.17)$$

$$h(x) \triangleq [L_f^0 h_1 \ L_f^0 h_2 \ L_f^0 h_3 \ L_f^0 h_4]^T = [h_1, \ h_2 \ h_3, \ h_4]^T = [i_{sd}, i_{sq}, i_{rd}, i_{rq}]^T$$

In view of the equation given in (4.16a), one has the following direct computations:

$$\begin{aligned}
 L_f h_1(x) &\triangleq f_1(v, x) = \gamma \left[(\dot{L}_r v_{sd} - M_{sr} \dot{v}_{rd}) - (\dot{L}_r \dot{R}_r x_{11} - M_{sr} \dot{R}_r x_{13} - n_p M_{sr}^2 x_{11} x_2 + \right. \\
 &\quad \left. n_p M_{sr} \dot{L}_r x_{14} x_2) \right] + \omega_s x_{12} \\
 L_f h_2(x) &\triangleq f_2(v, x) = \gamma \left[(\dot{L}_r v_{sq} - M_{sr} \dot{v}_{rq}) - (L_s R_s x_{12} - M_{sr} \dot{R}_r x_{14} - n_p M_{sr}^2 x_{12} x_2 - \right. \\
 &\quad \left. n_p M_{sr} L_s x_{13} x_2) \right] - \omega_s x_{11} \\
 L_f h_3(x) &\triangleq f_3(v, x) = \gamma \left[(R_s \dot{L}_r v_{sd} + L_s \dot{v}_{rd}) - (\dot{R}_r L_s x_{13} - M_{sr} \dot{R}_r x_{11} - \right. \\
 &\quad \left. n_p M_{sr} L_s x_{12} x_2 - n_p \dot{L}_r L_s x_{14} x_2) \right] + \omega_s x_{14} \\
 L_f h_4(x) &\triangleq f_4(v, x) = \gamma \left[(R_s \dot{L}_r v_{sq} + L_s \dot{v}_{rq}) - (\dot{R}_r L_s x_{14} - M_{sr} R_s x_{12} + \right. \\
 &\quad \left. n_p M_{sr} L_s x_{11} x_2 + n_p L_s \dot{L}_r x_{13} x_2) \right] - \omega_s x_{13}
 \end{aligned} \tag{4.18}$$

In a similar way for the second *Lie* - derivative of the measured output state function, it gives the general form:

$$L_f^2 h_k(x) \triangleq L_f (L_f h_k(x)), \quad \forall k = 1, 2, 3, 4 \tag{4.19}$$

The DFIG observability matrix is computed from the vectors formed by the *Lie* - derivative terms. It can be written in the following form:

$$\mathcal{O}_{DFIG}(h(x)) \triangleq \begin{pmatrix} [L_f^0 h_1(x) & L_f^0 h_2(x) & L_f^0 h_3(x) & L_f^0 h_4(x)]^T \\ [L_f h_1(x) & L_f h_2(x) & L_f h_3(x) & L_f h_4(x)]^T \\ [L_f^2 h_1(x) & L_f^2 h_2(x) & L_f^2 h_3(x) & L_f^2 h_4(x)]^T \end{pmatrix} \in \mathbb{R}^{12 \times 6} \tag{4.20}$$

Once again, the observability rank condition (ORC) of DFIG is verified by:

$$rank(\mathcal{O}_{DFIG} h(x)) \triangleq rank \begin{pmatrix} dh_k(x) \\ dL_f h_k(x) \\ dL_f^2 h_k(x) \end{pmatrix} = n = 6 \tag{4.21}$$

where, n indicates of full order state - space model. d is usual partial derivative of the measured function. It is readily that the observability analysis is done by evaluating the *Jacobian* matrix of the nonlinear model, along six - state variables.

$$J_{\mathcal{O}_{DFIG}} h(x) \triangleq \frac{\partial}{\partial x} \mathcal{O}_{DFIG}(h(x)) \tag{4.22}$$

It should be confirmed that even taking higher order *Lie* - derivatives of the measured output state function, logically no additional information is given by observability criterion. The *Jacobian* matrix characterizes the observability of DFIG model in the rank sense.

$$J_{O_{DFIG}} h(x) = \begin{bmatrix} 1 & 0 & 0 & 0 & 0 & 0 \\ 0 & 1 & 0 & 0 & 0 & 0 \\ 0 & 0 & 1 & 0 & 0 & 0 \\ 0 & 0 & 0 & 1 & 0 & 0 \\ \frac{\partial L_f^2 h_1}{\partial x_{11}} & \frac{\partial L_f^2 h_1}{\partial x_{12}} & \frac{\partial L_f^2 h_1}{\partial x_{13}} & \frac{\partial L_f^2 h_1}{\partial x_{14}} & \frac{\partial L_f^2 h_1}{\partial x_2} & \frac{\partial L_f^2 h_1}{\partial x_3} \\ \frac{\partial L_f^2 h_2}{\partial x_{11}} & \frac{\partial L_f^2 h_2}{\partial x_{12}} & \frac{\partial L_f^2 h_2}{\partial x_{13}} & \frac{\partial L_f^2 h_2}{\partial x_{14}} & \frac{\partial L_f^2 h_2}{\partial x_2} & \frac{\partial L_f^2 h_2}{\partial x_3} \\ \frac{\partial L_f^2 h_3}{\partial x_{11}} & \frac{\partial L_f^2 h_3}{\partial x_{12}} & \frac{\partial L_f^2 h_3}{\partial x_{13}} & \frac{\partial L_f^2 h_3}{\partial x_{14}} & \frac{\partial L_f^2 h_3}{\partial x_2} & \frac{\partial L_f^2 h_3}{\partial x_3} \\ \frac{\partial L_f^2 h_4}{\partial x_{11}} & \frac{\partial L_f^2 h_4}{\partial x_{12}} & \frac{\partial L_f^2 h_4}{\partial x_{13}} & \frac{\partial L_f^2 h_4}{\partial x_{14}} & \frac{\partial L_f^2 h_4}{\partial x_2} & \frac{\partial L_f^2 h_4}{\partial x_3} \\ \frac{\partial L_f^3 h_1}{\partial x_{11}} & \frac{\partial L_f^3 h_1}{\partial x_{12}} & \frac{\partial L_f^3 h_1}{\partial x_{13}} & \frac{\partial L_f^3 h_1}{\partial x_{14}} & \frac{\partial L_f^3 h_1}{\partial x_2} & \frac{\partial L_f^3 h_1}{\partial x_3} \\ \frac{\partial L_f^3 h_2}{\partial x_{11}} & \frac{\partial L_f^3 h_2}{\partial x_{12}} & \frac{\partial L_f^3 h_2}{\partial x_{13}} & \frac{\partial L_f^3 h_2}{\partial x_{14}} & \frac{\partial L_f^3 h_2}{\partial x_2} & \frac{\partial L_f^3 h_2}{\partial x_3} \\ \frac{\partial L_f^3 h_3}{\partial x_{11}} & \frac{\partial L_f^3 h_3}{\partial x_{12}} & \frac{\partial L_f^3 h_3}{\partial x_{13}} & \frac{\partial L_f^3 h_3}{\partial x_{14}} & \frac{\partial L_f^3 h_3}{\partial x_2} & \frac{\partial L_f^3 h_3}{\partial x_3} \\ \frac{\partial L_f^3 h_4}{\partial x_{11}} & \frac{\partial L_f^3 h_4}{\partial x_{12}} & \frac{\partial L_f^3 h_4}{\partial x_{13}} & \frac{\partial L_f^3 h_4}{\partial x_{14}} & \frac{\partial L_f^3 h_4}{\partial x_2} & \frac{\partial L_f^3 h_4}{\partial x_3} \end{bmatrix}, \in \mathbb{R}^{12 \times 6} \quad (4.23)$$

In fact, there are sixteen probabilities for evaluating the determinant of third submatrix, for each state one calculates the determinant of the resulting matrix size of (6×6). With assistance of symbolic computation methods in MATLAB or using scientific workspace programming tools, one can compute the determinant of the *Jacobian* matrix after simple manipulation as follows:

$$\text{First probability:} \quad \det(J_{O_{DFIG}} h(x)) = n_p^2 R_s M_{sr} (\dot{i}_{rd} \dot{L}_r + i_{sd} M_{sr})^2$$

$$\text{Or equivalent,} \quad \det(J_{O_{DFIG}} h(x)) = n_p^2 R_s M_{sr} (\dot{\phi}_{rd})^2 \quad (4.24)$$

It is worthy that; one can focus on the *Jacobian* matrix in order to introduce an adequate condition such that this matrix has full rank almost everywhere. It is evident from first and second result that the *Jacobian* matrix has full rank (non-singular), if and only if the following quantities are different to zero:

$$\dot{\phi}_{rd} \neq 0 \quad \text{or} \quad \dot{\phi}_{rq} \neq 0 \quad \text{or} \quad n_p^2 R_s L_s^2 \neq 0 \quad (4.25)$$

Remark 4.1: As mentioned above, one can say that if, $\det(J_{DFIG}) \neq 0$, this interprets that DFIG based wind turbine is observable in the rank sense. From the physical viewpoint, the observability concept is lost only at the singular point corresponding to zero rotor flux linkage. The physical interpretation can be summarized in one of the following states:

1. No electromagnetic field in DFIG, if the rotor flux linkage tends to zero. However, the electromagnetic torque vanishes whenever the rotor current pulsation is null. This is called the synchronization principle between stator and rotor part.
2. DFIG does not connect to the electrical network, if the stator or rotor currents converge to zero or in other word, the generator rest in stationary.

4.2.6 Motivations of using reduced model DFIG

The motivations of using a reduced model of DFIG instead of full model when designing the state observers can be summarized as follows:

- Simplifying the mathematical representation and calculations while keeping reasonably accurate transient and steady state process.
- The big weakness of all the control methodologies that we have learned so far they require the full order state model.
- Motivated by the fact that the controlling and observation of DFIG system is very complex and this complexity resides in numerous state variables, the strongly nonlinearity nature of this type of AC machine. Also, some of the system state variables are inaccessible. If some of these variables may be accessible, but their measurements are impractical and they are expensive, relatively in industrial processes.

On the basis of motivations mentioned above, one can present the next subsection dealing with a reduced version of DFIG model.

4.2.7 Reduced version of DFIG model

Now, recall that the electromagnetic torque created by DFIG could be expressed in terms of the generator current vector as follows:

$$T_{em} \triangleq n_p M_{sr} i^T T_0 i \triangleq h(i) \quad (\text{Non injective relation}) \quad (4.26)$$

Using equation defined by (4.4a), it is readily checked that the dynamic of electromagnetic torque undergoes the following equation:

$$\dot{T}_{em} = n_p M_{sr} i^T (T_0 + T_0^T) \frac{di}{dt} \triangleq S_1(i, v) - S_2(i) \omega_g \quad (4.27)$$

$$\text{with} \quad S_1(i, v) \triangleq 2n_p M_{sr} i^T T_0 (\gamma M_1 v + M_{23} i) \quad (4.28a)$$

$$\text{and,} \quad S_2(i) \triangleq n_p^2 \gamma M_{sr} i^T T_0 M_4 i = n_p^2 \gamma M_{sr} L_s i_s^T \sqrt{(\dot{\phi}_{rd})^2 + (\dot{\phi}_{rq})^2} \quad (4.28b)$$

Combining equations (4.12b) and (4.12c) constitute a suitable mathematical state - space representation for the estimation of electromagnetic torque T_{em} , generator rotor speed ω_g and generator torque T_g created by the wind turbine. Obviously from a physical point of view, equations (4.28a) and (4.28a) are measurable as they related to measurable physical quantities for generator voltages and currents.

For writing convenience, the system mathematical representation is re-written in the following new form:

$$\begin{cases} \dot{T}_{em} = S_1(i, v) - S_2(i)\omega_g \\ \dot{\omega}_g = \frac{1}{J}T_{em} - \frac{1}{J}T_g - \frac{f_v}{J}\omega_g \\ \dot{T}_g = 0 \end{cases} \quad (4.29)$$

It turns out that the system model defined by equation (4.29) is clearly still nonlinear nature since the system model involves the coupling product between the continuous – time function of current vector, $S_2(i)$ and generator rotor speed. Throughout this chapter, in order to avoid the mistakes and confusion between the notations of full - order system variables given in subsection 4.2.2 and the corresponding reduced - order variables of DFIG given in this subsection, one can propose the following compact form of the reduced - order with new notations of system variables as:

$$\begin{cases} \dot{\xi} = Y_1(i)\xi + Y_2(i, \xi) \\ y = C \xi \end{cases} \quad (4.30a)$$

$$y = C \xi \quad (4.30b)$$

where, $\xi \triangleq [\xi_1 \ \xi_2 \ \xi_3]^T = [T_{em} \ \omega_g \ T_g]^T, \in \mathbb{R}^3$ (4.31)

The first term of the equation (4.30a) is defined as: $Y_1(i) \triangleq \begin{pmatrix} 0 & -S_2(i) & 0 \\ 0 & 0 & \frac{-1}{J} \\ 0 & 0 & 0 \end{pmatrix}, \in \mathbb{R}^{3 \times 3}$ (4.32a)

The second term of the equation (4.30a) is defined as: $Y_2(i, \xi) \triangleq \begin{pmatrix} S_1(i, v) \\ \frac{\xi_1}{J} - \frac{f_v}{J}\xi_2 \\ 0 \end{pmatrix}, \in \mathbb{R}^3$ (4.32b)

The measured output state vector of reduced model is:

$$C = [1 \ 0 \ 0], \in \mathbb{R}^3 \quad (4.33)$$

For the physical point of view and domain of working principle, it is supposed that most of physical system state variables are bounded in the domain of interest, *i.e.* $\xi \in E \subset \mathbb{R}$. To overcome the blow - up state variables in finite time horizon. Thus, this may reduce the finite escape time of the system and restrict the initial peaking phenomenon, which are practically

reasonable [see *e.g.* Khalil,2002; Khalil et al, 1993] and all references therein for more details and information.

It turns out that the state vector $\xi(t)$ is bounded, $\|\xi(t)\| \leq \rho_\xi, \forall t \geq 0$, for some constant ($0 < \rho_\xi < \infty$) is an upper bound.

Now, the searcher will introduce a state transformation of the observability map, $\Phi \in \mathbb{R}^{3 \times 3}$ to put system given in equation (4.29) under uniformly observable system for any input. Thus, it is required to define an adequate condition such that the considered state transformation is globally diffeomorphic. Let us introduce the following state transformation to put the system model in the observable normal form for any input as follows:

$$\Phi : \mathbb{R}^3 \rightarrow \mathbb{R}^3, \quad \xi \mapsto z \triangleq \Phi(\xi) = [\Phi_1(\xi) \ \Phi_2(\xi) \ \Phi_3(\xi)]^T \quad (4.34)$$

with,

$$z = \Phi(\xi) \triangleq \begin{bmatrix} \xi_1 \\ -S_2(i) \xi_2 \\ \frac{S_2(i)}{J} \xi_3 \end{bmatrix}, \in \mathbb{R}^3 \quad (4.35)$$

The reduced system model given in equation (4.29) satisfies the observability rank condition (ORC),if the *Jacobian* matrix of the vector formed by the *Lie* - derivative terms, $[\xi_1 \ -S_2(i)\xi_2 \ -\frac{S_2(i)}{J}\xi_3]^T$ has full rank all most everywhere. To test the observability condition for the proposed reduced system, the *Jacobian* matrix for transforming system can be presented in the following form:

$$J_{\Phi(\xi)} \triangleq \frac{\partial z}{\partial \xi} = \frac{\partial \Phi(\xi)}{\partial \xi} = \begin{bmatrix} \frac{\partial \xi_1}{\partial \xi_1} & \frac{\partial \xi_1}{\partial \xi_2} & \frac{\partial \xi_1}{\partial \xi_3} \\ -S_2(i) \frac{\partial \xi_2}{\partial \xi_1} & -S_2(i) \frac{\partial \xi_2}{\partial \xi_2} & -S_2(i) \frac{\partial \xi_2}{\partial \xi_3} \\ S_2(i) \frac{\partial \xi_3}{J \partial \xi_1} & S_2(i) \frac{\partial \xi_3}{J \partial \xi_2} & S_2(i) \frac{\partial \xi_3}{J \partial \xi_3} \end{bmatrix}$$

Or equivalent,

$$J_{\Phi(\xi)} = \begin{bmatrix} 1 & 0 & 0 \\ 0 & -S_2(i) & 0 \\ 0 & 0 & \frac{S_2(i)}{J} \end{bmatrix}, \in \mathbb{R}^{3 \times 3} \quad (4.36)$$

where, the generator current vector, $i \triangleq [i_s \ i_r]^T$, $i_s \triangleq [i_{sd} \ i_{sq}]^T$, and $i_r \triangleq [i_{rd} \ i_{rq}]^T$.

The system is uniformly observable for any input if the *Jacobian* matrix is non – singular, *i.e.*, if $\det(J_{\Phi(\xi)}) \neq 0$.

Using the *Laplace* expansion method, one has, $\det(J_{\Phi(\xi)}) = -\frac{S_2^2(i)}{J} \neq 0$ (4.37)

One can easily evaluate this expression after straight forward calculations that will provide the determinant of the *Jacobian* matrix as follows:

$$S_2(i) = n_p^2 \gamma M_{sr} L_s i_s^T \sqrt{(\hat{\phi}_{rd})^2 + (\hat{\phi}_{rq})^2}$$

Or equivalent,

$$S_2(i) = n_p^2 \gamma M_{sr} L_s i_s^T \hat{\phi}_r \quad (4.38)$$

The condition derived from equation (4.37) is forever verified because $S_2^2(i) \neq 0$.

Evidently, from the mathematical condition derived from equation (4.38), this condition will shrink, if one of the following cases is verified:

1. The rotor flux linkage is vanish (*i.e.*, there is no electromagnetic field excited from balanced three – phase source).
2. No stator current (*i.e.*, DFIG does not connect to the electrical power network).
3. The stator or rotor windings may be damaged or deterioration, *i.e.*, $M_{sr} = 0$.

4.3 Position sensorless measurements

Stator position measurement and rotor position are necessary for measurements that will enable us to design output feedback active and reactive power control system without resorting to use mechanical and magnetic sensors only depending on stator voltages and output current measurements. The expressions of the measured stator voltages and estimation of flux linkage are given in equations (4.6a) and (4.6b) and after doing inverse *Park's* transformation, it gives from full – order state observer design [see e.g. Morel et al., 1998]:

$$v_{s\alpha\beta} \triangleq \begin{bmatrix} v_{s\alpha} \\ v_{s\beta} \end{bmatrix} = P_{inv} \begin{bmatrix} v_{sd} \\ v_{sq} \end{bmatrix}, \quad i_{s\alpha\beta} \triangleq \begin{bmatrix} \hat{i}_{s\alpha} \\ \hat{i}_{s\beta} \end{bmatrix} = P_{inv} \begin{bmatrix} \hat{i}_{sd} \\ \hat{i}_{sq} \end{bmatrix}, \quad \hat{\phi}_{s\alpha\beta} \triangleq \begin{bmatrix} \hat{\phi}_{s\alpha} \\ \hat{\phi}_{s\beta} \end{bmatrix} = P_{inv} \begin{bmatrix} \hat{\phi}_{sd} \\ \hat{\phi}_{sq} \end{bmatrix} \quad (4.39)$$

where, P_{inv} stands for inverse *Park's* transformation matrix defined as follows:

$$P_{inv} \triangleq \begin{bmatrix} \cos \hat{\theta}_e & -\sin \hat{\theta}_e \\ \sin \hat{\theta}_e & \cos \hat{\theta}_e \end{bmatrix} \quad (4.40)$$

with, stator flux components $\hat{\phi}_{sd}$, $\hat{\phi}_{sq}$ are estimated from equations (4.6a) and (4.6b) as:

$$\begin{cases} \dot{\hat{\phi}}_{sd} = v_{sd} - R_s \hat{i}_{sd} - \omega_s \hat{\phi}_{sq} - \theta K (\hat{\phi}_{sd} - \phi_{sd}) \\ \dot{\hat{\phi}}_{sq} = v_{sq} - R_s \hat{i}_{sq} + \omega_s \hat{\phi}_{sd} - \theta K (\hat{\phi}_{sq} - \phi_{sq}) \end{cases} \quad (4.41)$$

The estimation of nominal stator flux linkage could be written in the following form:

$$\|\hat{\phi}_s\| = \sqrt{(\hat{\phi}_{s\alpha})^2 + (\hat{\phi}_{s\beta})^2} \quad (4.43a)$$

with stator flux estimation error expressed in ($\alpha - \beta$) stationary reference frame is:

$$e_{\phi_{s\alpha}} \triangleq \hat{\phi}_{s\alpha} - \phi_{s\alpha} \quad \text{and} \quad e_{\phi_{s\beta}} \triangleq \hat{\phi}_{s\beta} - \phi_{s\beta} \quad (4.43b)$$

If the estimation of the stator flux vector $[\hat{\phi}_{s\alpha}, \hat{\phi}_{s\beta}]^T$ in stationary frame is available without needing to use the dynamic equation for estimating stator position [Fletcher et al., 2010]:

$$\hat{\theta}_s \triangleq \frac{1}{n_p} \arctan \left(\frac{\hat{\phi}_{s\beta}}{\hat{\phi}_{s\alpha}} \right) \quad (4.44)$$

As angular rotor position is proportional with electrical angle between stator and rotor variables of the DFIG. The main idea is based on the fact that electromagnetic force, created by three – phase system, could be also created by two - phase system has two windings in quadrature based on *Faraday's* basic law of electromagnetism. The observation of the electromagnetic force in $(\alpha - \beta)$ coordinates could be estimated in the following form:

$$\begin{cases} \hat{e}_\alpha = -\hat{\phi}_{r\beta} \hat{\omega}_g \\ \hat{e}_\beta = \hat{\phi}_{r\alpha} \hat{\omega}_g \end{cases} \quad (4.45)$$

So, from egution given in (4.45), the rotor position could be calculated using well - known mathematical formula without using the dynamic equation for rotor position estimation:

$$\hat{\theta}_r \triangleq \frac{1}{n_p} \arctan \left(\frac{-\hat{e}_\alpha}{\hat{e}_\beta} \right) = \frac{1}{n_p} \arctan \left(\frac{\hat{\phi}_{r\beta}}{\hat{\phi}_{r\alpha}} \right) \quad (4.46)$$

4.4 Reduced – order state observer design

In case of the current vector, $i(t)$ is accessible, $\forall t \geq 0$, the system model given in equation (4.29) almost fits the observable normal form of the standard structure of high - gain state observer claimed by [Gauthier et al., 1994]. As a matter of fact, the system model given in equation (4.29) differs from the standard structure in that the first state variable, denoted by, T_{em} . Actually, it is indirectly measurable. It could be computed using the available current vector, $i(t)$. One of the difficulties is that relation expressed in equation (4.26) is non injective output. Another difficulty faced in the present work is the current vector, $i(t)$ inaccessible, $\forall t \geq 0$. Only, output sampled - data measurements, $i(t_k), (k = 0,1,2 \dots)$ are presently available at sampling instant. Therefore, the following (non-standard) high gain sampled-output state observer is proposed as follows:

$$\left[\begin{array}{l} \dot{\hat{\xi}} = Y_1(\sigma(w))\hat{\xi} + Y_2(\sigma(w), \hat{\xi}) - \theta \Lambda^{-1} K \left(C\hat{\xi} - h(\sigma(w)) \right) \\ \dot{w} = \gamma M_1 v + M_{23} \sigma(w) - n_p \gamma M_4 \hat{\xi}_2 \sigma(w) \\ w(t_k) = i(t_k) \quad \forall t_k \leq t < t_{k+1}, k \in \mathbb{N}, \mathbb{N} \in \mathbb{R}_0^+ \\ \Lambda \triangleq \text{blockdiag} \left[1 \quad \frac{1}{\theta} \quad \frac{1}{\theta^2} \right], \in \mathbb{R}^{3 \times 3} \\ \hat{y} = C \hat{\xi} \end{array} \right. \quad \begin{array}{l} (4.47a) \\ (4.47b) \\ (4.47c) \\ (4.47d) \\ (4.47e) \end{array}$$

4.4.1 Observer design assumptions

Now, suppose that the following inductive assumptions hold, which are useful to exhibit the proposed state observer design in the next sections of this chapter.

A₁: With, $K \in \mathbb{R}^3$, being any fixed gain vector corresponding to measurement errors such that the following inequality holds in which $(\gamma_1(\sigma(w(t))) - KC)$ is *Hurwitz*, for some scalar $\mu > 0$, $\mathbb{I}_3 \in \mathbb{R}^{3 \times 3}$ for time varying system.

$$(\gamma_1(\sigma(w(t))) - KC)^T P(t) + P(t) (\gamma_1(\sigma(w(t))) - KC) \leq -\mu \mathbb{I}_3 \quad (4.48)$$

In which, $(\gamma_1(\sigma(w(t))) - KC)^T$ means the transposed vector of $(\gamma_1(\sigma(w(t))) - KC)$.

As a matter of fact, $P(t)$ is allowed to be time - varying positive definite matrix and it is the solution of equation (4.48). It must be bounded by any upper bound, $\rho_P \geq \sup_{0 \leq t < \infty} \|P(t)\|$, to ensure validation of inequality defined by equation (4.48).

A₂: $\sigma(w(t))$ denotes the saturation function of the signal, $w(t)$. It is bounded by two saturation scalar levels. One can define $\sigma(w(t))$ as given in equation (4.49) and it is described in Figure 4.7.

$$\sigma(w(t)) = \lim_{\substack{w \rightarrow \infty \\ t \rightarrow \infty}} \tanh(w(t)) \min(|w|, i_M) \triangleq \text{sat}(w(t)) \min(|w|, i_M) \quad (4.49)$$

Knowing that, i_M is any upper bound of the generator current vector and it is defined as:

$$i_M \geq \sup_{0 \leq t < \infty} \|i(t)\| \quad (4.50)$$

It should be mentioned that the knowledge of, i_M does not an issue because the maximum generator current vector is a priori known from the practical point of view. $|w|$ is the absolute value of the signal, $w(t)$. Figure 4.4 shows sector bound to saturation function, where $\bar{+} \min(w, i_M)$ denotes its saturation scalar levels.

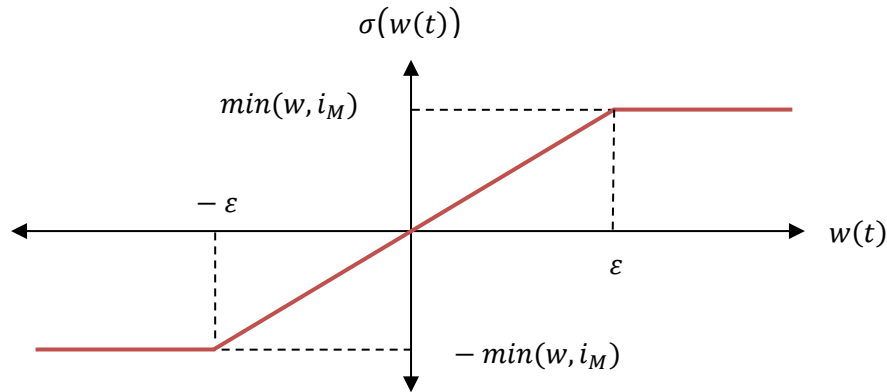


Figure 4.4: Sector bound for saturation function

4.4.2 Some remarks and notations

The proposed nonstandard high – gain state observer design has been developed for DFIG based wind turbine system, which has the following remarks and notations:

a) The existence of fixed gain vector, $K \in \mathbb{R}^3$ is satisfying the algebraic *Lyapunov* equation given in (4.48) and consequence of a technical *Lemma number 4* used for exponential stabilization purposes of systems that are uniformly observable form claimed by [Gauthier et al., 1994; Boizot et al., 2010].

b) Comparing the equations (4.47b) - (4.47c) and (4.12a), it is readily seen that the variable, $w(t)$ undergoes the prediction between two consecutive sampling instants. This equation is a copy of the open loop dynamic equation for the generator current vector.

Furthermore, $w(t)$ is re-initialized at each sampling instant. The signal $w(t)$ is set to the value of the available current vector at those instants. It turns out that, $w(t)$ represents a prediction of the current vector, $i(t)$ over each timing interval, $[t_k, t_{k+1})$. In view of the equation given in equation (4.26), it turns out that $h(w)$ is a prediction of the electromagnetic torque used in innovation correction term. In the present study, the electromagnetic torque is inaccessible as the generator current vector is inaccessible, unlike in most of previous scientific contributions.

c) Notice that, the generator current prediction, $w(t)$ is replaced by its saturated version $\sigma(w(t))$ everywhere on the right - hand side of the state observer defined by equations (4.47a) - (4.47c). Indeed, the introduction of the saturation function in state observer design is a recent practice. Presently, the saturation process has a significant role since the function $Y_2(w, \xi)$ does not *Lipschitz* in w (see equations defined by (4.12a) and (4.32b).

On the other hand, the saturated function of the prediction variable, $\sigma(w(t))$ is closer to the generator current vector, $i(t)$ than a signal of $w(t)$. Thus, the proposed state observer defined by equations (4.47a) - (4.47c) is expected to provide better performance (*i.e.*, it will be faster than the basic version without using a saturation process).

4.5 Comparison with published results

A simple comparison with existing approaches on the literatures could be provided to justify the advantages and benefits of the proposed state observer design.

- It is obvious that, the proposed sampled output reduced – order state observer given in equations (4.47a) - (4.47c) does not involve a zero order hold, *ZOH* device (which is a mathematical model used for data reconstruction at sampling time) within innovation correction term as used in impulsive systems running with continuous – discrete time observers [see *e.g.* Khalil et al., 2013; Dabroom et al., 2001; Raff et al., 2008].
- The present state observer design includes inter - sample predictor inside innovation correction term. This observer differs from the previous studies that proposed sampled – data observers of this type [see *e.g.* Ahmed - Ali et al., 2009]. This resides in the first state variable, *i.e.* T_{em} in the reduced - model given in equation (4.29). It is related to the generator current vector, i via a non-injective relation given in equation (4.26).
- In [Ozsoy et al., 2016], Indeed, the authors discussed the problem of modeling and control of DFIG based wind turbine system. The authors focused on disturbance observer design using a stator voltage oriented approach. Whilst throughout the present chapter, the searcher focused on developing a modified class of high – gain state observer coupled with inter sampled behaviour such that the problem of on-line state estimation for nonlinear systems is addressed in uniform observable system for any input. The searcher expects the capability to achieve better performance, especially when using saturation process of state predictor.

The proposed state observer methodology based sensorless sampled - output measurements, application of variable speed DFIG equipped by wind turbine system is described in Figure 4.5. The system topology comprises from WRIG where the stator windings are directly connected to the electrical grid whilst the rotor windings connected to a three – phase back – to - back power converter [see *e.g.* Bossoufi et al., 2015; Alvi et al., 2016].

4.6 Sampled-data observer design and convergence analysis

In this section, I shall state my second main result associated with a novel proposed state observer design based on sampled - output measurements given in the following theorem.

Theorem 4.1 (Main result):

Given a class of nonlinear system given in equation (4.30) submits to assumptions (A_1 and A_2) related to selection of $\sigma(w)$. Let us use a modified class of high-gain observer coupled with inter-sampled output predictor defined by equation (4.47) such that the evaluation of the observer design parameter is chosen, $\forall 0 < \theta^* < \infty$ be adequately large satisfactory, $\forall \theta > \theta^*$, which is independent on state variables,

$$\theta^* \left(\mu - \frac{\rho_h \|K\| \|P\|}{\zeta} \right) - \|P\| \left(2\rho_G + \frac{1}{\zeta} (\rho_\xi \rho_F + \rho_G) \right) > 0 \quad (4.51)$$

For $k_{i=1;2;3}$, is any fixed gain vector corresponding to measurement errors, $P \triangleq P^T > 0$, is the solution of algebraic *Lyapunov* equation given in equation (4.47) with constant scalar $0 < \rho_h, \rho_\xi, \rho_F, \rho_G < \infty$ exist and the free tracking parameter, ζ be selected such that, $\mu - \frac{\rho_h \|K\| \|P\|}{\zeta} > 0$. The state observation error is ultimately bounded and the corresponding bound can be made as small as possible by choosing, θ high satisfactory value. Moreover, there exist real positives $(M_1; \beta_1; \beta_2)$, such that the closed-loop state observation error, $\bar{\xi}(t) \triangleq \Lambda(\hat{\xi}(t) - \xi(t))$ satisfies the following LMI, $\forall t \in [t_k, t_{k+1})$, $k \in \mathbb{N}$ and α is any scalar such that, $0 < \alpha < \alpha_0/2$,

$$\|\bar{\xi}\| \exp(\alpha t/2) \leq M_1 \frac{1 - \beta_1 \tau_s \exp(\alpha \tau_s/2)}{1 - (\beta_1 + \nu_1 \beta_2) \tau_s \exp(\alpha \tau_s/2)} \quad (4.52a)$$

To ensure fast exponential convergence of the observation error towards zero with progressive time, there exists a real positive bounded, $0 < t - t_k < \tau_s$, with $\tau_s = \sup_{0 \leq k < \infty} (t_k - t_{k-1})$, and a scalar positive τ_{MASP} , $\forall \tau_s \in (0, \tau_{MASP}]$. One can deduce the following upper bound of the sampling time interval, which is a sufficient condition, if the design parameter, $\alpha \rightarrow 0$:

$$\tau_{MASP} \leq \frac{1}{\sqrt{\frac{2\alpha_1}{\alpha_0 \lambda_{\min}(P)}} n_p \gamma \theta \|M_4\| i_M + \|M_{23}\| + \rho_{\xi 2}} \quad (4.52b)$$

In which, the whole nonlinear state observer is GES based on *Lyapunov* stability theory and ISS concept where $\hat{\xi}(t)$ is the estimate trajectory given in equation (4.47a) based input injection measurements and for whatever initial conditions, $(\xi_0, \hat{\xi}_0) \in \mathbb{R}^3 \times \mathbb{R}^3$.

$$e \triangleq \sigma(w) - i, \in \mathbb{R}^4$$

It is readily checked that the proposed high - gain state observer given in (4.47a) - (4.47c) and the system model defined in (4.30), can be re-written in terms of system errors mentioned above in the following form:

$$\left[\begin{array}{l} \dot{\xi} = (\Upsilon_1(\sigma(w)) - \theta \Lambda^{-1} K C) \xi + (\Upsilon_1(\sigma(w)) - \Upsilon_1(i)) \bar{\xi} + \Upsilon_2(\sigma(w), \xi) - \Upsilon_2(i, \xi) - \theta \Lambda^{-1} K (h(i) - h(\sigma(w))) \\ \dot{e} = M_{23}e - n_p \gamma M_4 \xi_2 \sigma(w) + n_p \gamma M_4 \xi_2 i(t) \\ e(t_k) = 0 \quad \forall t_k \leq t < t_{k+1}, k = 0, 1, 2, \dots \end{array} \right. \quad \begin{array}{l} (4.54a) \\ (4.54b) \\ (4.54c) \end{array}$$

Let us consider the following change of coordinates using the block diagonal matrix defined by equation (4.47d) as follows:

$$\bar{\xi} \triangleq \Lambda \xi \quad (4.55)$$

Then, the equation (4.54a) could be rewritten in terms of a new error, $\bar{\xi}$ and using the useful inequalities described below:

$\Lambda \Upsilon_1(i) \Lambda^{-1} = \theta \Upsilon_1(i)$, $\Lambda^{-1} C = C \Lambda = C$, it gives the following error system dynamics:

$$\left[\begin{array}{l} \dot{\bar{\xi}} = \theta (\Upsilon_1(\sigma(w)) - K C) \bar{\xi} + \Lambda (\Upsilon_1(\sigma(w)) - \Upsilon_1(i)) \xi \\ \quad + \Lambda (\Upsilon_2(\sigma(w), \xi) - \Upsilon_2(i, \xi)) - \theta K (h(i) - h(\sigma(w))) \\ \dot{e} = M_{23}e - n_p \gamma M_4 \hat{\xi}_2 \sigma(w) + n_p \gamma M_4 \xi_2 i \\ e(t_k) = 0 \quad \forall t_k \leq t < t_{k+1}, k = 0, 1, 2, \dots \end{array} \right. \quad \begin{array}{l} (4.56) \\ (4.57) \\ (4.58) \end{array}$$

Actually, the error system dynamics defined by equation (4.56), is in one hand, and prediction error dynamics given in equations (4.57) - (4.58), on the other hand. Now, they will be analyzed in two main steps. The searcher will demonstrate that the interconnected (combination) gain functions must be less than unity according to the main principles of small gain condition used for stability analysis of dynamic feedback systems. Basically, small - gain is a loop gain less than unity or identity using matrix notation. It is one way used to ensure stability of dynamic feedback systems. It is a combination of gain functions less than identity using matrix notation [see e.g. Jiang et al., 1994].

Step 1: Output prediction error gives on - line state estimation error. It will be proved as shown below.

Proof the mapping, $e(t) \mapsto \bar{\xi}(t)$, is input - to - state stability, ISS.

Let us define the following direct *Lyapunov* function candidate denoted by, W_{obs} :

$$W_{obs}(\bar{\xi}) \triangleq \bar{\xi}^T P \bar{\xi} \quad (4.59)$$

Differentiating equation (4.59) along the closed – loop trajectories of (4.56) function of $\bar{\xi}$:

$$\dot{W}_{obs}(\bar{\xi}) = \dot{\bar{\xi}}^T P \bar{\xi} + \bar{\xi}^T P \dot{\bar{\xi}} \quad (4.60)$$

For writing convenient and throughout this chapter, let us apply the following definitions,

$$\tilde{Y}_1(\sigma(w), i) \triangleq Y_1(\sigma(w)) - Y_1(i) \quad (4.61a)$$

and,
$$\tilde{Y}_2(\sigma(w), \hat{\xi}, i, \xi) \triangleq Y_2(\sigma(w), \hat{\xi}) - Y_2(i, \xi) \quad (4.61b)$$

$$\bar{Y}_2(\sigma(w), \hat{\xi}, i, \xi) \triangleq \Lambda \left(\tilde{Y}_2(\sigma(w), \hat{\xi}, i, \xi) \right) \quad (4.61c)$$

$$\Lambda \|f(v, \hat{\xi}) - f(v, \xi)\| \leq \rho_\xi \|\bar{\xi}\| \quad (4.61d)$$

Now, substituting the equations defined by (4.56) and (4.48) in equation (4.60), yields after doing the simple mathematical manipulation:

$$\begin{aligned} \dot{W}_{obs}(\bar{\xi}) \leq & -\mu \theta \|\bar{\xi}\|^2 + 2 \rho_\xi \|P\| \|\bar{\xi}\| \|\tilde{Y}_1(\sigma(w), i)\| + 2\|P\| \|\bar{\xi}\| \|\bar{Y}_2(\sigma(w), \hat{\xi}, i, \xi)\| \\ & + 2\theta \|K\| \|P\| \|\bar{\xi}\| \|h(i) - h(\sigma(w))\| \end{aligned} \quad (4.62)$$

On the other hand, as the generated current vector, i and $\sigma(w)$ are both bounded by the known constant scalar, i_M given in equation (4.50) and $S_2(\cdot)$ is a continuous – time function defined by equation (4.28b), it follows from equation in (4.32a) that a constant scalar, $0 < \rho_F < \infty$, is independent on state variables of the reduced – model. The following *Lipschitz* condition is valid such that:

$$\|Y_1(\sigma(w)) - Y_1(i)\| \leq \rho_F \|\sigma(w) - i\| \leq \rho_F \|e\| \quad (4.63)$$

The last equality follows from equation (4.51) and using the fact that, $\sigma(w)$ is closer to generator current vector than, w based on the definition of $\sigma(w)$ and, i_M given in equations (4.49) and (4.50), respectively.

Now, let us prove that there is another constant scalar, $0 < \rho_G < \infty$, is dependent on the state variables of the reduced - model and observer design parameter. It is evident that the *Lipschitz* condition does not valid in w :

$$\|Y_2(\sigma(w), \hat{\xi}) - Y_2(i, \xi)\| \leq \rho_G (\|e\| + \|\bar{\xi}\|) \quad (4.64)$$

Simply, the last inequality given in (4.64) is obtained by combining equations defined by (4.55) and (4.47d). Also, using a similar argument, it is shown from the equation given in

Chapter 4: A Novel Observer Design based on Sampled Output Measurements

(4.26) for $T_{em} \triangleq h(i)$ that a constant scalar, $0 < \rho_h < \infty$, exists such that *Lipschitz* constant is valid:

$$\|h(i) - h(\sigma(w))\| \leq \|i - \sigma(w)\| \leq \rho_h \|e\| \quad (4.65)$$

Using equations defined by (4.63) - (4.65), combined in inequality defined by (4.62), it becomes:

$$\dot{W}_{obs}(\bar{\xi}) \leq (-\mu\theta + 2\rho_G \|P\|) \|\bar{\xi}\|^2 + (2\rho_\xi \rho_F + 2\rho_G + 2\theta\rho_h \|K\|) \|P\| \|\xi\| \|e\| \quad (4.66)$$

In view of the well - known *Young's* inequality specified in appendix A.5 and using free tracking parameter, ζ , one can write equation (4.66) in the following form:

$$\begin{aligned} \dot{W}_{obs}(\bar{\xi}) \leq & -(\theta(\mu - (\rho_h \|K\| \|P\|)/\zeta) - \|P\|(\vartheta)) \|\bar{\xi}\|^2 \\ & + \frac{\zeta}{2} (2\rho_\xi \rho_F + 2\rho_G + 2\theta\rho_h \|K\|) \|P\| \|e\|^2 \end{aligned} \quad (4.67)$$

with, $\vartheta \triangleq 2\rho_G + \frac{1}{\zeta}(\rho_\xi \rho_F + \rho_G)$

Let us introduce a free tracking parameter ζ . One can select, ζ such that it satisfies the following inequality to ensure negative definiteness of *Lyapunov* function:

$$\zeta > \frac{\rho_h \|K\| \|P\|}{\mu} \quad (4.68)$$

Also, let $0 < \theta^* < \infty$ be any scalar such that the first term of the equation (4.66), it becomes:

$$\theta^* \left(\mu - \frac{\rho_h \|K\| \|P\|}{\zeta} \right) - \|P\|(\vartheta) > 0 \quad (3.69)$$

Then, one also has, $\forall \theta > \theta^* > 1$, which is a sufficient condition:

$$\theta \left(\mu - \frac{\rho_h \|K\| \|P\|}{\zeta} \right) - \|P\| \left(2\rho_G + \frac{1}{\zeta}(\rho_\xi \rho_F + \rho_G) \right) > 0 \quad (4.70)$$

To alleviate (make less severe) the forthcoming development, one introduces the notation:

$$\begin{aligned} \alpha_0 &= \frac{1}{\lambda_{max}(P)} \left[\theta \left(\mu - \frac{\rho_h \|K\| \|P\|}{\zeta} \right) - \|P\|(\vartheta) \right] > 0 \\ \alpha_1 &= \frac{\zeta}{2} (2\rho_\xi \rho_F + 2\rho_G + 2\theta\rho_h \|K\|) \|P\| > 0 \end{aligned}$$

where, $\lambda_{max}(P)$ denotes maximum eigenvalue of a positive definite matrix, P . Thus, equation (4.67) could be re-written in the following form:

$$\dot{W}_{obs}(\bar{\xi}) \leq -\alpha_0 \lambda_{max}(P) \|\bar{\xi}\|^2 + \alpha_1 \|e\|^2 \quad (4.71a)$$

Now, combining equation defined by (4.59) in equation (4.71a), and using the fact that:

$$\lambda_{min}(P) \|\bar{\xi}\|^2 \leq W_{obs}(\bar{\xi}) \leq \lambda_{max}(P) \|\bar{\xi}\|^2$$

It gives, $\dot{W}_{obs}(\bar{\xi}) \leq -\alpha_0 W_{obs}(\bar{\xi}) + \alpha_1 \|e\|^2$ (4.71b)

Then, it follows from equation (4.71b) that: $\dot{W}_{obs}(\bar{\xi}) \leq -\alpha_0 W_{obs} + \alpha_1 e^2$

Integrating the above inequality, it gives the general solution taking into consideration the effect of initial condition in stabilization of nonlinear systems, $\forall 0 < t_0 < t$:

$$W_{obs} \leq \exp(-\alpha_0(t-t_0)) W_{obs}(t_0) + \alpha_1 \int_{t_0}^t \exp(-\alpha_0(t-s)) e^2(s) ds \quad (4.72)$$

Given any constant scalar, α such that, $0 < \alpha < \alpha_0/2$, it follows multiplying both sides of the equation (4.72) by the term $\exp^{\alpha t}$, it gives:

$$\exp^{\alpha t} W_{obs} \leq \exp^{-(\alpha_0-\alpha)t} \exp^{\alpha t_0} W_{obs}(t_0) + \alpha_1 \exp^{\alpha t} \int_{t_0}^t \exp^{-\alpha_0(t-s)} e^2(s) ds$$

$$\text{where, } \exp^{\alpha t} W_{obs} \leq M_0 + \alpha_1 \exp^{\alpha t} \int_{t_0}^t \exp^{-\alpha_0(t-s)} e^2(s) ds \quad (4.73)$$

with, $M_0 \triangleq \exp^{\alpha t_0} W_{obs}(t_0)$, using the fact that, $\exp^{-(\alpha_0-\alpha)t} < 1$.

So, the inequality defined by equation (4.73) gives, successively:

$$\begin{aligned} \exp^{\alpha t} W_{obs} &\leq M_0 + \alpha_1 \exp^{\alpha t} \int_{t_0}^t \exp^{-\alpha_0(t-s)} \exp^{-\alpha s} \exp^{\alpha s} e^2(s) ds \\ &\leq M_0 + \frac{2\alpha_1}{\alpha_0} \sup_{t_0 \leq s \leq t} \left(\exp^{\alpha s} e^2(s) \right) \end{aligned} \quad (4.74)$$

By taking the square - root of both sides of the last inequality defined by (4.74), it gives based on the definition of ISS concept that was given in equation (2.87):

$$\exp^{\frac{\alpha t}{2}} \sqrt{W_{obs}} \leq \sqrt{M_0} + \sqrt{\frac{2\alpha_1}{\alpha_0}} \sup_{t_0 \leq s \leq t} \left(\exp^{\frac{\alpha s}{2}} \|e(s)\| \right) \quad (4.75a)$$

On the other hand, it readily follows from the equation given in (4.59):

$$W_{obs} \triangleq \bar{\xi}^T P \bar{\xi} \geq \lambda_{\min}(P) \|\bar{\xi}\|^2 \quad (4.75b)$$

Taking square - root for both sides of inequality given in (4.75b), one obtains, $\sqrt{W_{obs}} = \sqrt{\lambda_{\min}(P)} \|\bar{\xi}\|$ which, combines in equation (4.75a), yields:

$$\|\bar{\xi}\| \exp^{\frac{\alpha t}{2}} \leq \sqrt{\frac{M_0}{\lambda_{\min}(P)}} + \sqrt{\frac{2\alpha_1}{\alpha_0 \lambda_{\min}(P)}} \sup_{t_0 \leq s \leq t} \left(\exp^{\frac{\alpha s}{2}} \|e(s)\| \right) \quad (4.76)$$

It is obvious, that the right hand side RHS of this inequality is monotonically increasing with time index. This will lead us to bound the LHS to ensure validation of this inequality. Then, one has the following form:

$$\sup_{t_0 \leq s \leq t} \left(\|\bar{\xi}(s)\| \exp^{\frac{\alpha s}{2}} \right) \leq M_1 + \nu_1 \sup_{t_0 \leq s \leq t} \left(\exp^{\frac{\alpha s}{2}} \|e(s)\| \right) \quad (4.77)$$

$$\text{with, } M_1 \triangleq \sqrt{\frac{\exp^{\alpha t_0} W_{obs}(t_0)}{\alpha_2}} = \sqrt{\frac{M_0}{\lambda_{\min}(P)}} \quad \text{and} \quad \nu_1 \triangleq \sqrt{\frac{2\alpha_1}{\alpha_0 \lambda_{\min}(P)}} = \sqrt{\frac{2\alpha_1}{\alpha_0 \alpha_2}}$$

Examine $\bar{\xi}(s)$, obviously it is ISS w.r.t $e(s)$.

Which ends the proof of Step 1 ■.

Step 2: On – line state estimation error gives output prediction error. It will be proved as shown below.

Proof that the mapping $\bar{\xi}(t) \rightarrow e(t)$ is input to state stability, ISS. Now, integrating output prediction error dynamics given in equation (4.54b) and from equation (4.55) related to block diagonal matrix, it gives,

$$\bar{\xi}_2 \triangleq \theta \bar{\xi}_2$$

One gets, $\forall k \in \mathbb{N}$ and $t \in [t_k, t_{k+1})$:

$$e = \int_{t_k}^t \left(M_{23}e(s) - n_p\gamma\theta M_4\bar{\xi}_2\sigma(w) + n_p\gamma\theta M_4\xi_2(s)i(s) \right) ds \quad (4.78a)$$

Using the facts that, $\|\bar{\xi}_2\| \leq \rho_{\xi_2}$, $\|\sigma(w(s)) - i(s)\| \leq \|e\|$ and $\|\sigma(w)\| \leq i_M$, $\|i(s)\| \leq i_M$.

The norm of output prediction error could be represented by the following expression:

$$\|e(s)\| \leq \int_{t_k}^t (\beta_1\|e(s)\| + \beta_2\|\bar{\xi}_2(s)\|) ds \quad (4.78b)$$

with, $\beta_1 \triangleq \|M_{23}\| + \rho_{\xi_2}$ and $\beta_2 \triangleq n_p\gamma\theta\|M_4\|i_M$,

Now, multiplying both sides of equation (4.78b) by the term $\exp(\frac{\alpha t}{2})$, $0 < \alpha < \alpha_0/2$, it gives

$$\begin{aligned} \|e(s)\|\exp(\frac{\alpha t}{2}) &\leq \beta_1 \exp(\frac{\alpha t}{2}) \int_{t_k}^t \exp(-\frac{\alpha s}{2}) \exp(\frac{\alpha s}{2}) \|e(s)\| ds \\ &+ \beta_2 \exp(\frac{\alpha t}{2}) \int_{t_k}^t \exp(-\frac{\alpha s}{2}) \exp(\frac{\alpha s}{2}) \|\bar{\xi}_2(s)\| ds \end{aligned} \quad (4.79)$$

From the second term in the right hand side of the inequality (4.79), using the fact that at all times, one has the second state on - line observation error, $\|\bar{\xi}_2\| \leq \|\bar{\xi}\|$.

Using the main principles of *Bellman's* inequality claimed by [Xu,1995], yields:

$$\begin{aligned} \|e(s)\|\exp(\frac{\alpha t}{2}) &\leq \beta_1 \exp(\frac{\alpha t}{2}) \left(\int_{t_k}^t \exp(-\frac{\alpha s}{2}) ds \right) \sup_{t_k < s < t} \left(\exp(\frac{\alpha s}{2}) \|e(s)\| \right) \\ &+ \beta_2 \exp(\frac{\alpha t}{2}) \left(\int_{t_k}^t \exp(-\frac{\alpha s}{2}) ds \right) \sup_{t_k < s < t} \left(\exp(\frac{\alpha s}{2}) \|\bar{\xi}_2(s)\| \right) \end{aligned} \quad (4.80)$$

It is readily checked that, $0 < \int_{t_k}^t \exp(-\frac{\alpha s}{2}) ds \leq \tau_s \exp(-\frac{\alpha t_k}{2})$.

Then, one gets from the equation (4.80), and using the inequalities $0 < t - t_k < \tau_s$, with sufficient small sampling time interval, $\tau_s = \sup_{0 \leq k < \infty} (t_k - t_{k-1})$, it gives the following form:

$$\begin{aligned} \|e(s)\|\exp(\frac{\alpha t}{2}) &\leq \tau_s \exp(\frac{\alpha \tau_s}{2}) \left[\beta_1 \sup_{t_k < s < t} \left(\exp(\frac{\alpha s}{2}) \|e(s)\| \right) \right. \\ &\left. + \beta_2 \sup_{t_k < s < t} \left(\exp(\frac{\alpha s}{2}) \|\bar{\xi}_2(s)\| \right) \right] \end{aligned} \quad (4.81)$$

The right hand side of the inequality (4.81) is an increasing function of time index, t . Thus, it follows the fact that, t_k is an increasing sequence $\forall 0 \leq k \leq \infty$. It is readily seen,

$$\begin{aligned} \sup_{t_k < s < t} \left(\exp\left(\frac{\alpha s}{2}\right) \|e(s)\| \right) &\leq \beta_1 \tau_s \exp\left(\frac{\alpha \tau_s}{2}\right) \sup_{t_k < s < t} \left(\exp\left(\frac{\alpha s}{2}\right) \|e(s)\| \right) \\ &+ \beta_2 \tau_s \exp\left(\frac{\alpha \tau_s}{2}\right) \sup_{t_k < s < t} \left(\exp\left(\frac{\alpha s}{2}\right) \|\bar{\xi}(s)\| \right) \end{aligned} \quad (4.82)$$

Now, by letting, $\beta_1 < 1$ and τ_s be sufficiently small sampling interval according to definition of the small gain condition, it gives the following expression to validate the equation (4.84):

$$\beta_1 \tau_s \exp\left(\frac{\alpha \tau_s}{2}\right) < 1 \quad (4.83)$$

So, one gets from equations defined by (4.83) combined in (4.81) as follows:

$$\sup_{t_k < s < t} \left(\exp\left(\frac{\alpha s}{2}\right) \|e(s)\| \right) \leq \frac{\beta_2 \tau_s \exp\left(\frac{\alpha \tau_s}{2}\right)}{1 - \beta_1 \tau_s \exp\left(\frac{\alpha \tau_s}{2}\right)} \sup_{t_k < s < t} \left(\exp\left(\frac{\alpha s}{2}\right) \|\bar{\xi}(s)\| \right) \quad (4.84)$$

Examine $e(s)$, obviously it is ISS concept *w.r.t* new estimation error, $\bar{\xi}(s)$.

This study introduced an explicit expression of output prediction error between consecutive sampling instants depends on another observer design parameters and system nonlinearity.

Now, substituting the right hand side of equation (4.84) for $\sup_{t_k < s < t} \left(\exp\left(\frac{\alpha s}{2}\right) \|e(s)\| \right)$ in the equation (4.77) at step 1, with assistance of equation (4.83), the following LMI holds:

$$\begin{aligned} \sup_{t_0 \leq s \leq t} \left(\|\bar{\xi}(s)\| \exp\left(\frac{\alpha s}{2}\right) \right) &\leq M_1 + v_1 \frac{\beta_2 \tau_s \exp\left(\frac{\alpha \tau_s}{2}\right)}{1 - \beta_1 \tau_s \exp\left(\frac{\alpha \tau_s}{2}\right)} \sup_{t_k < s < t} \left(\exp\left(\frac{\alpha s}{2}\right) \|\bar{\xi}(s)\| \right) \\ \sup_{t_0 \leq s \leq t} \left(\|\bar{\xi}(s)\| \exp\left(\frac{\alpha s}{2}\right) \right) &\leq \frac{M_1}{1 - \frac{v_1 \beta_2 \tau_s \exp\left(\frac{\alpha \tau_s}{2}\right)}{1 - \beta_1 \tau_s \exp\left(\frac{\alpha \tau_s}{2}\right)}} \text{ if, } \frac{v_1 \beta_2 \tau_s \exp\left(\frac{\alpha \tau_s}{2}\right)}{1 - \beta_1 \tau_s \exp\left(\frac{\alpha \tau_s}{2}\right)} < 1 \end{aligned} \quad (4.85)$$

Now, combining the final result from step 2 given in equation (4.84) with the last result from step 1 given in (4.76), and after simple mathematical manipulation and using the fact that:

$$\|\bar{\xi}\| \exp\left(\frac{\alpha t}{2}\right) \leq \sup_{t_k < s < t} \left(\exp\left(\frac{\alpha s}{2}\right) \|\bar{\xi}(s)\| \right),$$

It gives,
$$\|\bar{\xi}\| \exp\left(\frac{\alpha t}{2}\right) \leq M_1 \frac{1 - \beta_1 \tau_s \exp\left(\frac{\alpha \tau_s}{2}\right)}{1 - (\beta_1 + v_1 \beta_2) \tau_s \exp\left(\frac{\alpha \tau_s}{2}\right)} \quad (4.86)$$

On the other hand, for $\theta > \theta^* > 1$, (sufficient condition) using the:

$$\|\bar{\xi}\| \leq \|\xi\| \leq \Lambda^{-1} \|\bar{\xi}\| \rightarrow \|\bar{\xi}\| \leq \|\xi\| \leq \theta^2 \|\bar{\xi}\| \quad (4.87)$$

Now, combining equation defined by (4.86) in equation (4.87), one gets the following form:

$$\|\bar{\xi}\| \exp\left(\frac{\alpha t}{2}\right) \leq \Lambda^{-1} M_1 \frac{1 - \beta_1 \tau_s \exp\left(\frac{\alpha \tau_s}{2}\right)}{1 - (\beta_1 + v_1 \beta_2) \tau_s \exp\left(\frac{\alpha \tau_s}{2}\right)} \quad (4.88a)$$

Or equivalent,
$$\|\bar{\xi}\| \exp\left(\frac{\alpha t}{2}\right) \leq \theta^2 M_1 \frac{1 - \beta_1 \tau_s \exp\left(\frac{\alpha \tau_s}{2}\right)}{1 - (\beta_1 + v_1 \beta_2) \tau_s \exp\left(\frac{\alpha \tau_s}{2}\right)} \quad (4.88b)$$

It should be confirmed that one can deduce the upper bound of the sampling time interval from the small - gain condition expressed in equation (4.85), which is sufficient condition, ensuring fast exponential convergence of the on-line observation error, $\bar{\xi}(t)$ within high - gain

observer nature. As a special case from equation defined by (4.85), if the design parameter, $\alpha \rightarrow 0$, T_{MASP} becomes:

$$\tau_{MASP} \leq \frac{1}{\beta_1 + v_1 \beta_2}$$

Or equivalent,

$$\tau_{MASP} \leq \frac{1}{\sqrt{\frac{2\alpha_1}{\alpha_0 \lambda_{min}(P)}} n_p \gamma \theta \|M_4\| i_M + \|M_{23}\| + \rho_{\xi 2}} \quad (4.89)$$

It should be emphasized that the upper bound given in equation (4.89) is only sufficient condition and not necessary. It depends on the design parameters of proposed state observer running with variable speed DFIG. Thus, the corresponding on-line observation error if the design parameter, $\alpha \rightarrow 0$, $\bar{\xi}$ becomes:

$$\|\bar{\xi}\| \leq M_1 \frac{1 - \beta_1 \tau_s}{1 - (\beta_1 + v_1 \beta_2) \tau_s} \quad (4.90a)$$

Or equivalent,

$$\|\bar{\xi}\| \leq \theta^2 M_1 \frac{1 - \beta_1 \tau_s}{1 - (\beta_1 + v_1 \beta_2) \tau_s} \quad (4.90b)$$

This ends the proof of the theorem, which gives the second main result ■

4.6.2 Discussion of the main result

The inequality given in equation (4.89), defines an upper bound of the sampling time interval. It is just an adequate condition for the state observer to ensure globally exponentially convergent (GEC). Consequently, the allowed practical sampling time interval, or for the numerical simulation environment, is probably to be much higher than the upper bound defined by equation (4.89). According to stator - side active and reactive powers given in equations (4.11a), (4.11b), respectively, and to prove the robustness of the proposed sampled - output state observer, one can use on-line stator and rotor - side current predictions under saturation process instead of actual generator current vector to ensure better performance as,

$$\text{Stator - side:} \quad \begin{cases} P_s = 1.5 * (v_{sd} \sigma(w_1) + v_{sq} \sigma(w_2)) \\ Q_s = 1.5 * (v_{sq} \sigma(w_1) - v_{sd} \sigma(w_2)) \end{cases} \quad (4.91a)$$

In a simillar way, the rotor power (sometimes rotor power is called slip power) could be evaluated using rotor prediction currents in the following form:

$$\text{Rotor - side:} \quad \begin{cases} P_r = 1.5 * (v_{rd} \sigma(w_3) + v_{rq} \sigma(w_4)) \\ Q_r = 1.5 * (v_{rq} \sigma(w_3) - v_{rd} \sigma(w_4)) \end{cases} \quad (4.91b)$$

Finally, the whole state observer is ensured globally exponentially stable (GES) according to the main principles of ISS stabilization and tools of *Lyapunov* stability theory for dynamic feedback nonlinear systems where $\hat{\xi}$ is the estimate of trajectory given in equation (4.47a)

based on electrical voltage measurements and whatever initial conditions, $(\xi_0, \hat{\xi}_0) \in \mathbb{R}^3 \times \mathbb{R}^3$ and for satisfactory enough values $\forall \theta > \theta^* > 1$. Thus, the searcher expects the possibility to achieve better performance. This will be confirmed through numerical simulation of a physical model dealing with variable speeds DFIG driven by WTS in the next section.

4.7 Simulation results and verifications

4.7.1 Implementation considerations

In this subsection, the dynamic performances of the proposed non-standard high gain state observer design accompanied by an inter-sampled output state predictor has been developed and designated recently, for DFIG system state estimation, which are rotor speed, electromagnetic torque and generator torque with grid integration measurements. DFIG reduced - model has been implemented using MATLAB /Simulink environment (version R2015). The tool selected for solving the dynamic equations is a MATLAB function called ODE 45 with relative tolerance 2×10^{-5} and variable step time.

The satisfying simulation results on the Simulink/MATLAB environment for transforming two - phase DFIG model based grid connected demonstrate good dynamic performance and global exponential stable for the proposed non - standard high gain state observer based sampled - output measurements. To implement of the proposed sampled output high gain observer defined by equations (4.47a) - (4.47d), the corresponding system model given in (4.12) are used with the numerical values listed in Table 4.1. The numerical values are issued from the technical documentation of DFIG. One can implement and realize the simulation using MATLAB / Simulink environment with assistance of the observer gain parameter, fixed gain vector corresponding to measurement error and the sampling time interval are listed in Table 4.2. The virtual model of the WTGS that was built in MATLAB/SIMULINK environment, composite of wind turbine model includes simulation of the direct – drive wind turbine reference torque simulation of DFIG model running with realization of proposed sampled – output state observer design. Wind turbine reference torque is induced by variable wind velocity profile shown in Figures (4.7) and (4.8), respectively. They are affected by measurement noise with sufficiently large spectrum so as it can assimilate to white noise.

Typical DFIG based wind turbine generator system accompanied by non-standard high gain observer design is shown in Figure 4.6. The proposed state observer will estimate rotational speed, generator torque and electromagnetic torque created by DFIG without resorting to use mechanical sensors, such as position encoder which is costly and unreliable, relatively.

To validate the robustness of the proposed observer, the test benchmark includes some limited cases which are:

- Mechanical torque profile is starting from zero when the wind velocity is less than cut-in speed of the direct driven wind turbine generator system.
- The mechanical torque is greater than the nominal torque.
- Slow variation of mechanical torque (which is the usual case).
- Sudden variation of mechanical torque (which is theoretical case).

All simulated figures are presented in solid blue color lines for real measurements whilst the estimation trajectories are displayed in dashed black color lines. Therefore, the reference of the generated torque captured by direct drive wind turbine coupled with DFIG will take the form presented in Figure 4.8 for one complete operating cycle of (20)s. The operating characteristics of variable speed wind turbine are $C_p = 0.478$, $\lambda_{TSR} = 6$, $\beta = 0$, $r = 1.5 m$ to achieve maximum power extraction. Tracking wind velocity entails to adjust rotor (shaft) speed of the DFIG based wind turbine.

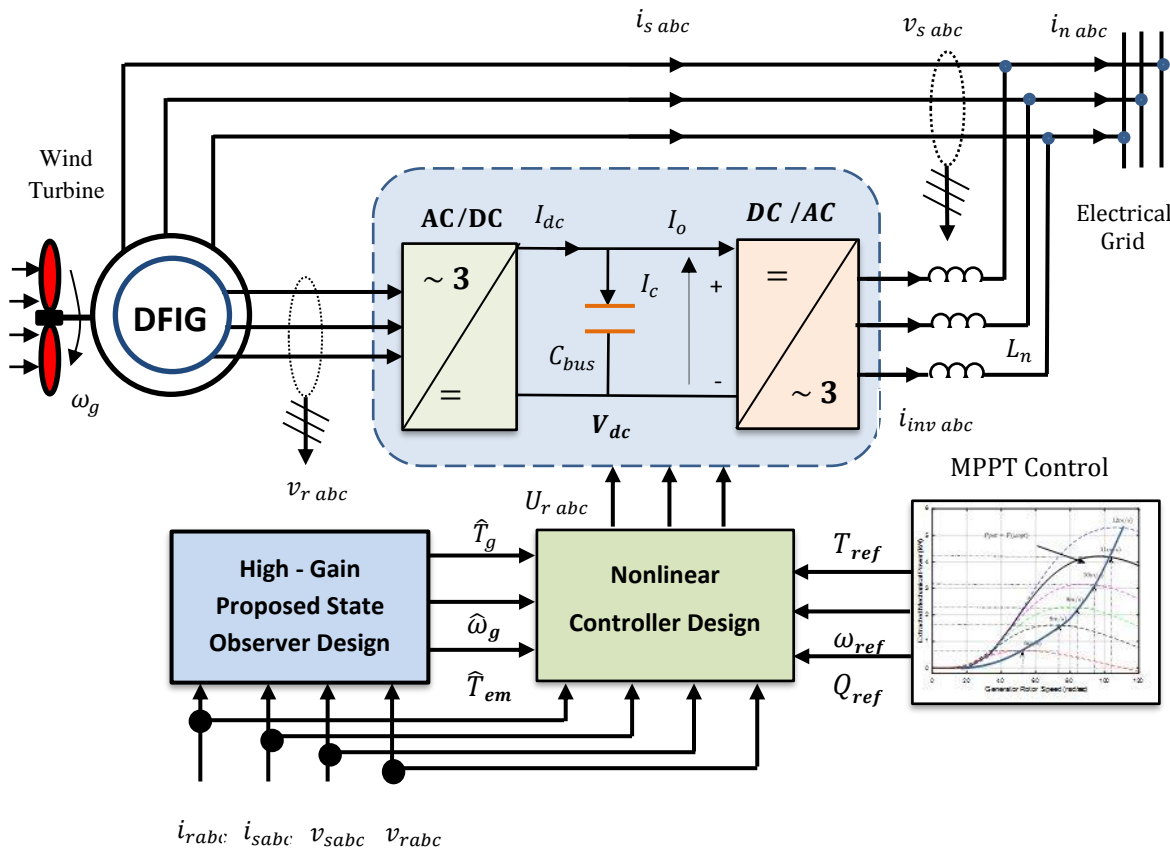


Figure 4.6: Typical DFIG based wind turbine generator running with state observer

Table 4.1. DFIG system nominal features

Characteristics	Symbol	Value	Physical Unit
Doubly Fed Induction Generator			
Nominal power	P_{nom}	5.00	kW
Mutual inductance	M_{sr}	0.103	H
Stator resistor	R_s	0.163	Ω
Stator self inductance	L_s	0.309	H
Rotor resistor	R_r	0.140	Ω
Rotor self inductance	L_r	0.035	H
Leakage coefficient	ϱ	0.01904	-
Number of pole pairs	n_p	2	-
Total moment of inertia	J	2.2	Nm/rd/s ²
Viscous friction coefficient	f_v	0.004	Nm/rd/s
Three - phase electrical network			
Network Voltage	E_n	220/380	V
Network frequency	f_n	50	Hz

Table 4.2. Numerical observer design parameters

	Symbol	Value
High - gain observer design parameter	θ	175
Sampling time interval	τ_s	20 ms
Sampling frequency	f_s	50 Hz
Fixed gain vector	K	$[7 \ 27 \ 30]^T$

4.7.2 Observer dynamic tracking performance

Figure 4.9 illustrates the electromagnetic torque created by DFIG and its estimate, which represents an indirect output injective relation in this study. One notes that the observed electromagnetic torque joined the actual electromagnetic torque, quickly with the assistance of high – gain observer nature. In Figure 4.10 shows generator torque captured by the wind

turbine and its estimate \hat{T}_g with zooming in short time around, $t = 5 \text{ sec}$, the estimated generator torque hooks up the mechanical torque quickly. Typically, wind turbine system has three regions of operation as clarified in chapter two, section four. In Figure 4.11, it is observed that the estimated rotational rotor speed enters the second operation region associated with MPPT control quickly. Figure 4.12 illustrates the dynamic performance of the second term, $S_2(i)$ defined by equation (4.28b). Obviously, it is continuous - time function related to generator current vector. The sudden variations of the mechanical torque (theoretical case) are visible throughout bumps seen in Figure 4.12 and rotor reactive power performance as shown in Figure 4.14.

Figure 4.13 shows the evolution of stator and rotor - side active powers measured in (Watt) generated by DFIG based wind turbine system. The total power injected into an electrical network equals the vector summation of the stator and rotor active powers given in equation (4.91a) and (4.91b) using on - line stator and rotor - side current prediction signals instead of actual generator current vector to ensure robustness of the proposed observer. Figure 4.14 clarifies the evolution of stator and rotor - side reactive powers measured in (VAr). As expected from the fundamental principles related to operation of DFIG, active power generated by the stator - side is normally greater than corresponding power in rotor - side, although the power converter rating in rotor side is partial scale topology and taking the effect of slip power on the performance of DFIG generator.

In the same way, the reactive power exchanged with the electrical network equals the vector summation of the stator and rotor reactive powers with different cases of power factor operation as demanded from grid - side reactive power controller knowing that the reactive power desired reference level in the present chapter equals zero to guarantee unity power factor control that will reflect usefulness on electrical power quality, dynamic performance of three - phase power converter with saving cost. Also, it should be confirmed that unlike in classical WRIG, DFIG can exchange the reactive power with electrical power networks.

4.7.3 Sensorless sampled - output measurements

In this study, inter - sampled output state predictor is re-initialized at each sampling instant whenever a recent generator current vector is available to set new sampled output measurements and it remains continuous between consecutive sampling instants.

It is readily seen from Figures 4.15, 4.16, 4.17, and 4.18 and after doing zoom around $t = 5 \text{ sec}$, the output stator and rotor - side currents in $(d - q)$ reference frame and their output state predictors are decreased and increased, instantaneously with a variation of mechanical torque as shown in Figure 4.8. Figure 4.19 describes the evolution of sampling time interval of 20 ms for sampling - output measurements, $\forall t \in [t_k, t_{k+1})$.

However, as expected associated with sudden variation of mechanical torque captured by wind turbine affect on the estimation and prediction process. This phenomenon is depicted through the appearance of overshoot in Figures 4.9, 4.10, 4.11, 4.12, 4.15, 4.16, 4.17 and 4.18, respectively around $t = 5, 10, 15$ for one complete cycle. There is no error on the initial conditions and the provided estimates still converge to their true closed - loop trajectories.

4.7.4 Sensorless position measurements

The tracking behaviour of measured and estimated stator position is clarified in Figure 4.20 without resorting to use phased locked loop (PLL) for grid integration. As indicated in Figure 4.20, is bounded by the interval $\{0, \pi\}$. The estimated stator position angle almost coincides with the measured position angle, which indicates the good characteristics of the proposed observer for tracking the stator position via VSWT coupled with the electrical grid. The tracking performance of measured and estimated rotor position is shown in Figure 4.21. It is bounded by the interval $\{0, 1.1\}$.

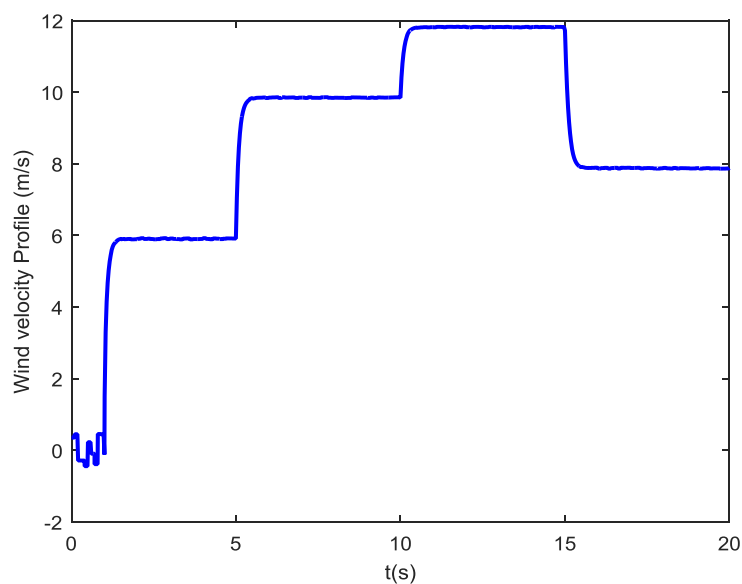


Figure 4.7: Wind velocity profile (m/sec)

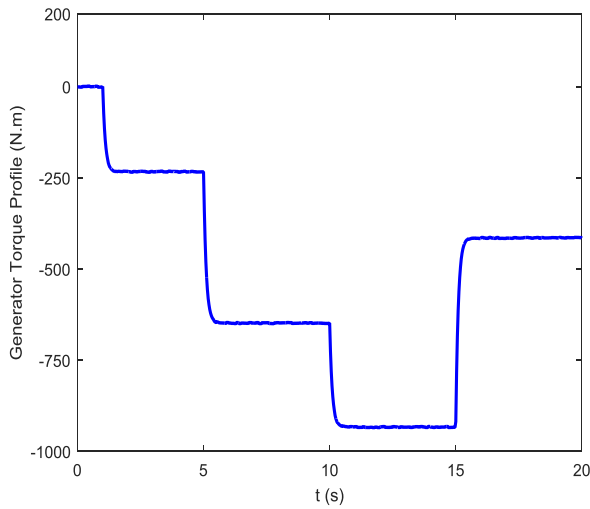


Figure 4.8: DFIG Generator torque profile (N. m)

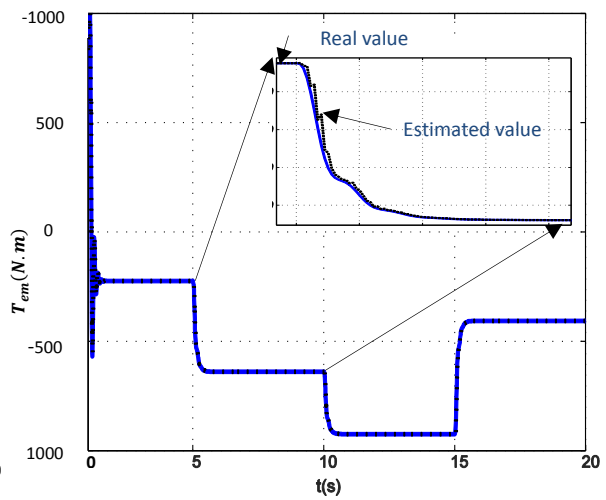


Figure 4.9: DFIG electromagnetic torque and its estimate (N. m)

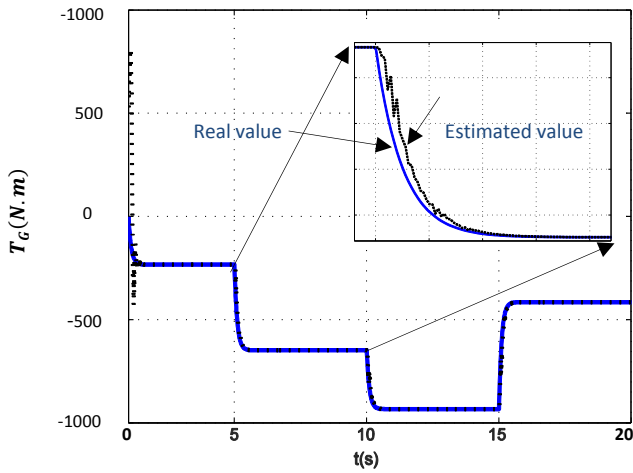


Figure 4.10: DFIG Generator torque and its estimate (N. m)

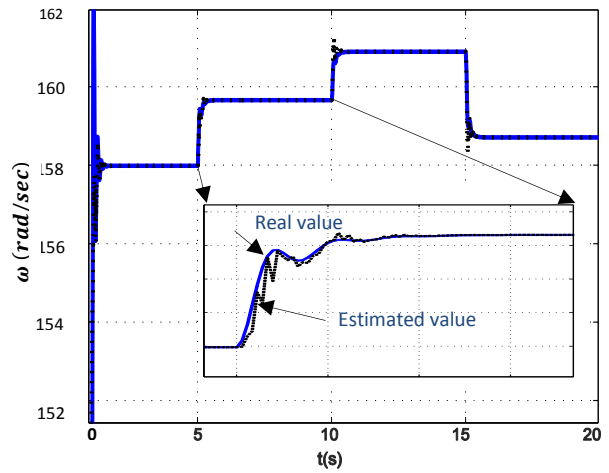


Figure 4.11: DFIG rotational speed and its estimate (rad /sec)

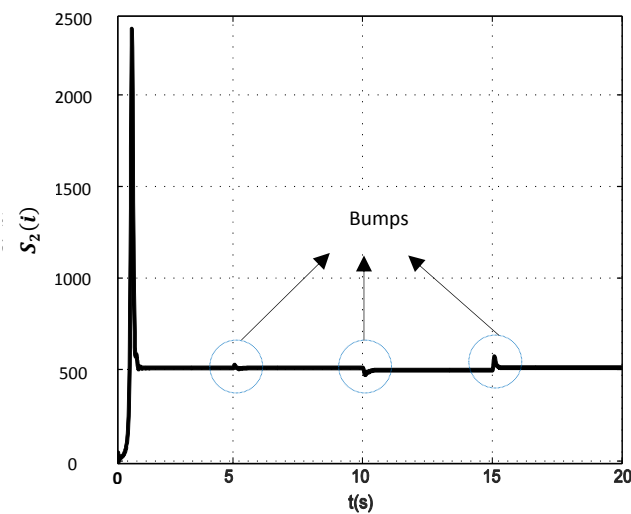


Figure 4.12: Dynamic performance of the term $S_2(i)$

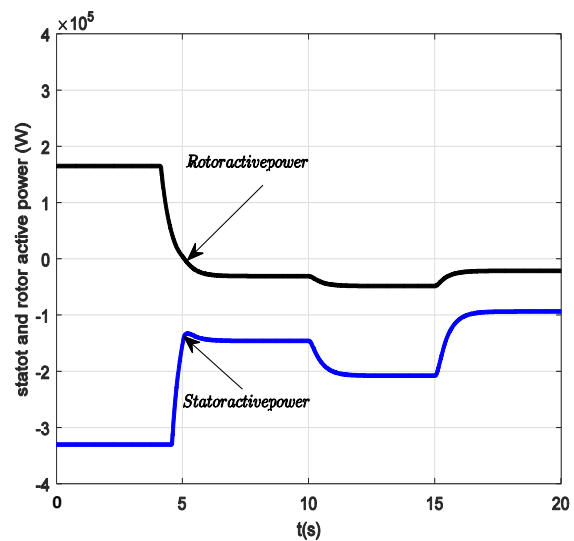


Figure 4.13: Stator and rotor side active power (Watt)

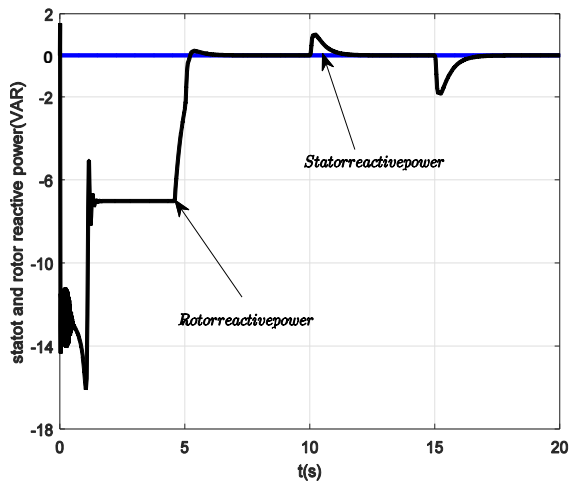


Figure 4.14: Stator and rotor side reactive power (Var)

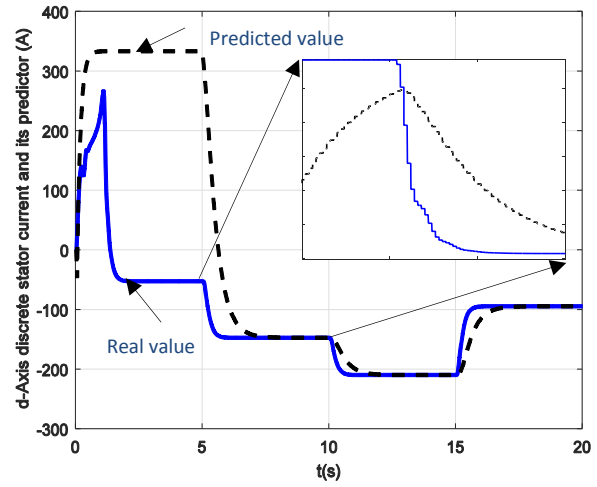


Figure 4.15: d-Axis stator current and its predictor

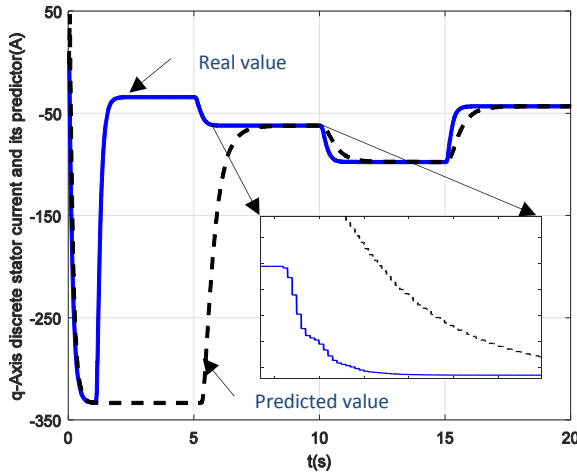


Figure 4.16: q-Axis stator current and its predictor

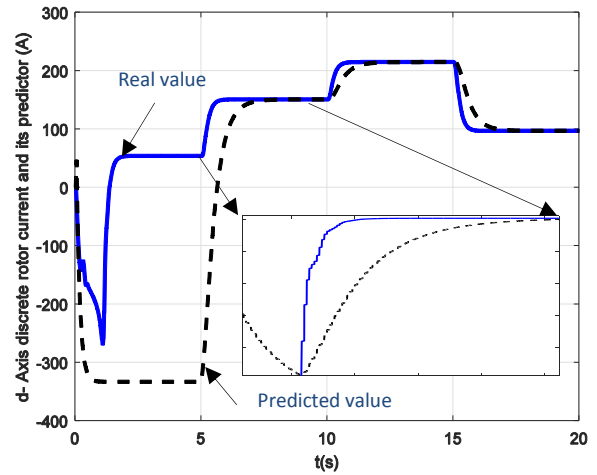


Figure 4.17: d-Axis rotor current and its predictor

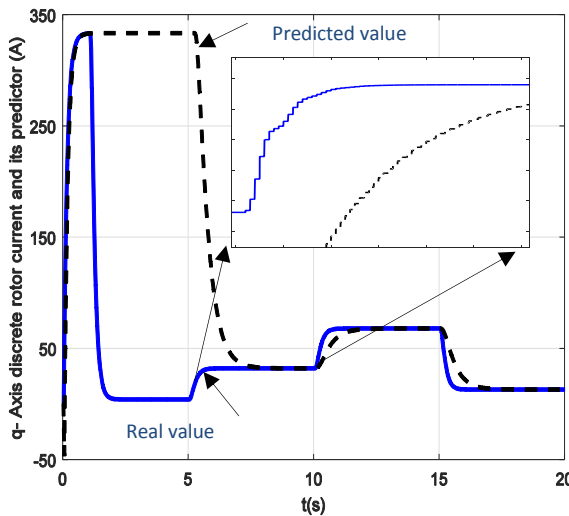


Figure 4.18: q-Axis rotor current and its predictor

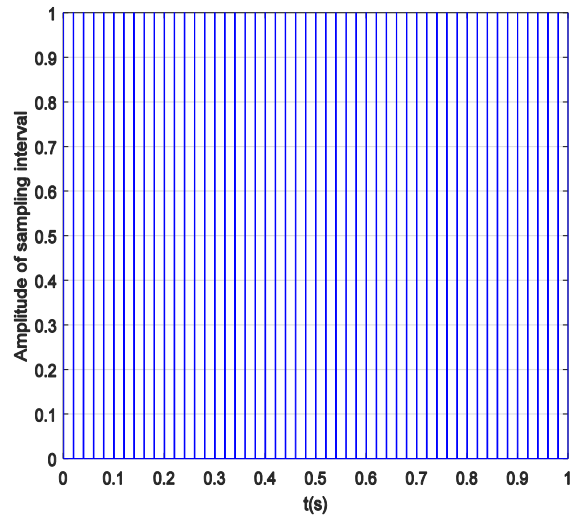


Figure 4.19: Evolution of sampling period, $\forall t \in [t_k, t_{k+1})$

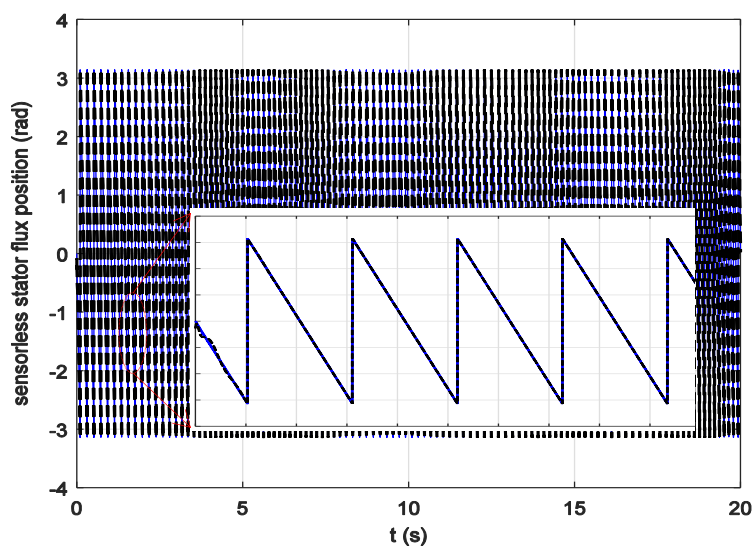


Figure 4.20: Tracking performance of stator position θ_s and its estimate $\hat{\theta}_s$ (rad)

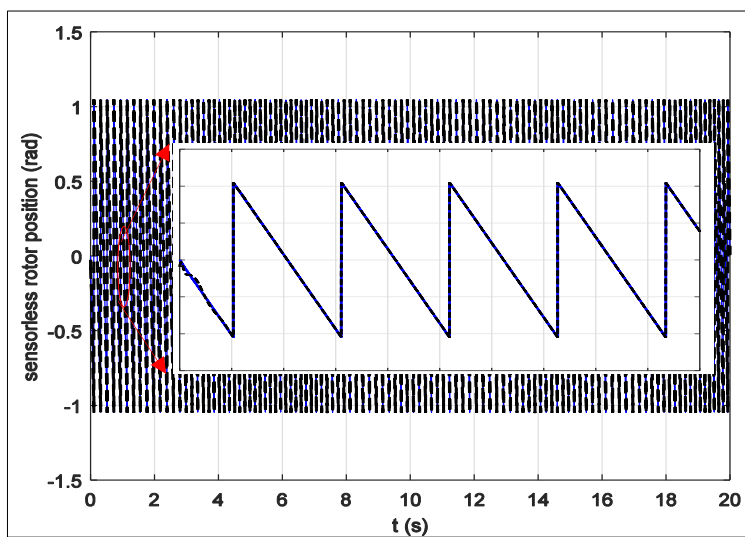


Figure 4.21: Tracking performance of rotor position θ_r and its estimate $\hat{\theta}_r$ (rad)

4.8 Conclusions

The problem of design sampled - output state observer running with DFIG nonlinear model and backed by sound convergence analysis has yet to be solved. In this chapter, the difficulty of solving this problem has been developed by combining the ideas and benefits of HGO structure and inter - sampled output predictor. Hence, this chapter tackles the problem of design non - standard HGO based sensorless sampled output measurements application of DFIG based VSWT. The major benefit of the proposed state observer that all system state estimates are staying in CTM just the generator current vector is measured at sampling instant.

As a matter of fact, the main target of the present chapter is to get on - line estimates of the mechanical and magnetic state variables based on generator voltages (*i.e.* stator and rotor voltages) and sampled - output currents at sampling instant. First once, DFIG generator has been modeled and expressed in $(d - q)$ rotor reference frame. From the control viewpoint, $(d - q)$ representation leads to control flexibility near the setpoint of regulator and provides synchronisation with supply frequency.

The saturation process has a significant role because the mathematical function called, $\gamma_2(w, \xi)$ does not globally *Lipschitz* in w . On the other hand, the saturated value $\sigma(w(t))$ is closer to the generator current vector, $i(t)$ than actual predictor, $w(t)$. That is, the proposed state observer in the reduced - model has better performance. Subsequently the proposed non - standard HGO will be faster than the basic version without involving saturation process.

The observability analysis of full and reduced - model DFIG has been highlighted to check is it possible synthesis a state observer based on input/output injection measurements far away from singular point. The state observation for a class of nonlinear system with indirect output injective under HGO approach accompanied by sampled - output measurements has been discussed, successfully without resorting to use mechanical and magnetic sensors.

A novel state observer synthesis defined by equation (4.47) has been designed and formally analyzed using tools of *Lyapunov* stability theory and ISS concept for whatever initial conditions. It is formally shown that all system estimates converge exponentially to neighbors of their true trajectories. The main results are described by mathematical theorem proved in the present chapter. These results are confirmed by numerical simulation and realization through MATLAB/SIMULINK environment in the last phase.

Chapter 4: A Novel Observer Design based on Sampled Output Measurements

This chapter introduced an explicit inequality for the upper bound of prediction error between consecutive sampling instants depending on observer design parameters and system nonlinearity.

The novelty of the present chapter resides in considering the motivation difficulties faced this work, which are the electromagnetic torque is indirect output injective and generator current vector is inaccessible forever. Just sampled - output data measurements are presently available at sampling instant.

To the readers, the next step of this study probably will focus on global adaptive or non - adaptive output feedback controller design of DFIG based VSWT without resorting to use classical mechanical and magnetic sensors as a natural extention of observer design running with state feedback control of DFIG machine.

Chapter Five

Output Feedback Nonlinear Adaptive Control Strategy of Three - Phase AC/DC Boost Power Converter for Online UPS System

Table of Contents	page
5.1 Introduction	125
5.1.1 Review of related research	126
5.1.2 Purpose and contribution	127
5.2 Uninterruptable power supply topologies	128
5.3 Problem formulation	129
5.3.1 System topology and modeling	129
5.3.2 Main control objectives	132
5.3.3 Comparing with published results	134
5.4 Nonlinear adaptive controller design	135
5.4.1 Observability analysis of on-line UPS system	136
5.4.2 Adaptive observer design	139
5.4.3 Stability convergence analysis	140
5.4.4 Inner control loop design - PFC achievement	142
5.4.5 Outer control loop design - DC output voltage regulation	145
5.4.6 Power factor calculation and estimation	147
5.5 Numerical simulation and verification	151
5.5.1 Implementation considerations.....	151
5.5.2 Tracking performance in presence of constant load	152
5.5.3 Control performance in presence of resistive load uncertainty....	157
5.6 Conclusions	160

In the present chapter, the problem of modeling and controlling of the three-phase boost power converter is addressed in providing on-line uninterruptible power supply (UPS) systems. UPS is a system that allows the electric sensitive loads to keep running, at least for a short time when the primary power source is lost during unexpected power outages. UPS provides protection from power surges using the surge protection device, battery protection and protection against unexpected power outages. The considered sensorless observer control problem entails several difficulties including:

- Numerous state variables that are inaccessible during continuous – time mode.
- The uncertainty prevails on some system parameters.
- Power factor estimation, voltage regulation and harmonic distortion mitigation (supression).
- Dynamic system modelling has strongly nonlinearity property.

The problem is dealt with a cascade nonlinear adaptive controller that is developed using backstepping control design technique. The inner - control loop ensures the PFC objective and involves an adaptive observer used for estimating the grid phase currents without using the traditional current sensors (*i.e.* current transformer for high power applications), the parameters of grid phase voltages and three - phase balanced resistive load. The estimation is based on the on-line measurements of DC output voltage. On the other hand, the outer - control loop regulates the DC bus voltage up to small ripples within permissible range.

A detailed literature survey will be introduced in the next section devoted on output feedback adaptive nonlinear control of three - phase AC/DC boost power converter for on - line UPS systems. Different control schemes for harmonics mitigation which include conventional control and high performance feedback control approaches and techniques.

5.1 Introduction

With the advent (arrival) of distributed DC power sources in the energy sector, boost - type three phase rectifiers are used increasingly in a wide diversity of applications: power supply for microelectronics, household - electric appliances, electronic ballast, DC- motor drives, power conversion, etc... [Mohan et al., 2002] and, especially, battery charger in UPS system which is needed in several industrial fields, *e.g.* power systems involving critical (sensitive) loads such as computer systems, hospitals, and on-line secured transaction systems, etc... [see e.g. Faiz et al., 2006].

Typically, the following are the standard requirements for the output voltage regulation of a UPS inverter [see e.g. Deng et al., 2005; Amir et al., 2016]

1. Constant steady state RMS voltage of 2% permissible variation in any parameter like temperature, load current or battery voltage.
2. Maximum of 10% transient peak voltage deviation is allowed during both loading and unloading of the UPS system.
3. Voltage drop no more than 5% of the rated voltage cannot be tolerated after 2 AC operating cycles.
4. Total harmonic distortion factor (THD) of 4% is allowed for all the load conditions in presence of output filter and 8% without the presence of the output filter.

5.1.1 Review of related research

The power factor correction and DC output voltage regulation have a great importance in PWM AC/DC voltage source converters. To meet these requirements, various control topologies had been proposed, including single-phase and three-phase [see e.g. Rodriguez et al., 2005; Bhattacharya, 2014; Manikandan et al., 2013].

PWM rectifiers are widely used in three-phase AC/DC/AC double conversion on-line UPS systems [Dai et al., 2005]. The problem of controlling three-phase AC/DC converter has been given a great deal of interest, over the last decade. Linear control methods using classical regulators for output voltage control had been given in [see e.g. Pan et al., 1993; Dixon et al., 1988] where a slow change in the modulation index (describes how much the modulated variable of the carrier signal varies around its unmodulated level, $\mu \leq 1$) is resulting in a slow dynamical response. Consequently, the linear feedback control of the rectifier output voltage becomes slow and difficult from the control point of view.

Moreover, due to the strong coupling between the duty-cycle and the conducting states in the AC/DC boost power converter; linear controllers are not able to optimally perform over a wide range of operation conditions. In contrast to linear control, nonlinear approaches can optimize the dynamic performance of the AC/DC boost power converter over a wide range of operating conditions. To remove overall drawbacks resulting from linear control design, different nonlinear control design techniques had been proposed in the literature to achieve power factor correction requirements and tightly DC bus output voltage regulation, such as fuzzy logic control [Cecati et al., 2005], differential Flatness based control [Houari et al., 2012], sliding mode control [Shtessel et al., 2008], a new nonlinear H_∞ feedback control

approach for three-phase voltage source converters introduced by [Rigatos et al., 2016] and continuous – time backstepping control design technique using the tools of *Lyapunov* stability theory [Allag et al., 2007]. This chapter will focus on the last technique mentioned above to achieve output feedback nonlinear adaptive control of voltage source converter for on-line UPS system.

The rest of the present chapter is organized in six main parts as follows: in section 5.2, uninterruptible power supply (UPS) topologies. In section 5.3 problem formulation is presented, meanwhile, the nonlinear adaptive controller has been designed in Section 5.4. The controller performances for the closed - loop model are illustrated through numerical simulation and verification in section 5.5 showing good agreement with theoretical results. Finally, some conclusions and remarks are drawn in section 5.6.

5.1.2 Purposes and contributions

In the present chapter, the problem of controlling three - phase PWM AC/DC boost power converter, operating in the presence of uncertain sensitive or critical loads, will be addressed. One can seek for a suitable control strategy meeting the following simultaneously two control objectives, which are:

- i. Achieving a perfect power factor correction: the grid phase currents and their corresponding voltages must be as close in phase.
- ii. DC output voltage regulation: this voltage must be tightly regulated to a constant reference level with small ripples less than $\pm 4\%$ in presence of the output filter.
- iii. Harmonic mitigation.

This chapter provides a complete framework for the analysis of power quality issues and replaces the conventional PI controller by adaptive output feedback control technique for more accuracy and eliminating the drawbacks of previous linear linear control approaches. To achieve the above control objectives, a cascade adaptive controller is designed using nonlinear control techniques. First, the inner-loop is designed to meet the PFC requirement. The inner controller includes a nonlinear current regulator and a nonlinear adaptive observer. The former is designed on the basis of the observed nonlinear model of the grid-rectifier, using backstepping control design technique. An adaptive observer design for a class of state - affine systems has been inspired partly from [Besançon et al., 2006; Besançon et al., 2003] and all the references therein for more details. It provides on-line estimates of the grid phase currents, unknown parameters of grid phase voltages and load resistance. The outer control -

loop involves a filtered PI regulator, which regulates the DC bus voltage for a given reference level.

5. 2 Uninterruptable power supply (UPS) topologies

Uninterruptible power supply UPS system can be classified depending on the topological configuration as follows [Niroomand et al., 2010]:

- 1) Off - line UPS (stand by) system used for noncritical loads.
- 2) Line - interactive UPS system used for noncritical loads.
- 3) Double conversion on - line UPS system used for sensitive loads.

Off - line and line interactive UPSs provide protection against unexpected power outages in non-critical (or nonsensitive) power computing systems. The off-line UPS is a low cost solution with minimal performance capabilities. The line interactive UPS can be configured to provide power factor enhancement and limited power conditioning. The double conversion UPS provides conditioned and back-up electrical power source to provide critical workstations, servers, networks [Liebert, 2000].

On – line UPS systems consist of a rectifier, charger, battery set, an inverter and a bypass circuit. Double conversion UPS topology uses AC power from the electrical distribution, rectifies the AC power to DC, and converts the DC power back to conditioned AC power. Since the on-line (double conversion) UPS is used for providing the critical and sensitive loads, it will be considered the topic of discussion for the remainder of the present chapter.

For maintenance purposes, a bypass circuit is incorporated. The bypass circuit consists of the static transfer switch and circuit breaker. Static transfer switches are semiconductor switches that could be used in AC power systems and activate them within milliseconds. Circuit breakers are mechanical devices that provide over current protection and automatic switching capabilities to supply different types of critical load. The function of a surge protection device is used to divert transient voltages and currents far away from sensitive equipment, without interruption of the normal circuit operation. A peak current mode control approach could be chosen to regulate the input grid phase currents. This approach is controlled by a peak current passing through a power transistor. There is an inherent overcurrent protection control [Carranza et al., 2010].

5.3 Problem formulation

5.3.1 System topology and modeling

The three-phase voltage source AC/DC full-bridge boost power converter has the structure shown in Figure 5.1. This structure used for high power applications without DC/DC chopper circuit. It is assumed that an equivalent resistive load, R_o is connected to the output of AC/DC boost power converter. The control signals are defined as $\mu \triangleq (\mu_1 \ \mu_2 \ \mu_3)^T$. They take values in the finite discrete set, $\{-1, +1\}$, *i.e.* $\mu_1 = 1$; that corresponds to the conducting state for the upper switching element G_1 and non-conducting state (*i.e.* complement state) for the lower switching element G_4 , operating sequentially through NOT logic gate [Shtessel et al., 2008].

A rectifier should provide an output voltage that should be as smooth as possible. In practice, however, output voltage from the rectifier consists of DC component plus AC component (or AC ripples). The AC component is made up of several dominant harmonics.

Indeed, AC ripples cause more ohmic losses in the circuit leading to reduce the efficiency of the system. This shows that is important to filter out the un-preferred AC component present in the rectifier output. When used on the rectifier output side, these filters are called DC filters. These filters try to make the output voltage as level as possible with small ripple size.

IGBT based fast switching harmonic filters is the solution to supplying reactive power and harmonic mitigation for dynamic loads is the fast switched harmonic filter. These filters are switched very rapidly IN and OUT of the circuit using Isolated Gate Bipolar Transistors (IGBT) instead of contactors. This type of filter is capable of soft switching the capacitors, so as not to create a voltage spike. It can be switched, without discharging the capacitors, at switching rates up to 50 times per second. The main advantages of this filter are the capability to switch without transients and to respond in real time, to dynamically changing load conditions. The performance of the fast switched filter is similar to the performance that can be expected from a typical tuned filter.

The searcher prefers the voltage-source than a current source PWM converter because the voltage source PWM converter is higher in efficiency, lower in cost, and smaller in physical size than the current source PWM converter, particularly in terms of comparison between the DC capacitor and DC inductor.

The mathematical model of the AC/DC boost power converter in (abc) sequence could be obtained through analyzing the electrical circuit based on *Kirchhoff* laws as shown in Figure 5.1 which is introduced firstly by [Pan et al., 1993]:

$$\left\{ \begin{array}{l} \frac{di_a}{dt} = -\frac{r}{L}i_a - \frac{V_0}{6L}(2\mu_1 - \mu_2 - \mu_3) + \frac{1}{L}V_{ga} \\ \frac{di_b}{dt} = -\frac{r}{L}i_b - \frac{V_0}{6L}(2\mu_2 - \mu_1 - \mu_3) + \frac{1}{L}V_{gb} \\ \frac{di_c}{dt} = -\frac{r}{L}i_c - \frac{V_0}{6L}(2\mu_3 - \mu_1 - \mu_2) + \frac{1}{L}V_{gc} \\ \frac{dV_0}{dt} = -\frac{V_0}{R_o C_o} + \frac{1}{2C_o}(i_a\mu_1 + i_b\mu_2 + i_c\mu_3) \end{array} \right. \quad (5.1)$$

System given in (5.1) can also be re-written in matrix notation in the following form,

$$\left\{ \begin{array}{l} \frac{di}{dt} = -\frac{r}{L}i - \frac{V_0}{6L}S_c\mu + \frac{1}{L}V_g \\ \frac{dV_0}{dt} = -\frac{V_0}{R_o C_o} + \frac{1}{2C_o}\mu^T i \end{array} \right. \quad (5.2)$$

with, r , L , R_o and C_o stand for source voltage internal resistance, self inductance, load resistance and output DC - bus capacitance, respectively. The front-end AC/DC power converter has a filter capacitor, C_o used to filter - out the output voltage waveform. Knowing that V_0 is the output voltage, $i \triangleq [i_a \ i_b \ i_c]^T$ are the input phase currents, $V_g \triangleq [V_{g1} \ V_{g2} \ V_{g3}]^T$ are the main source voltages in balanced systems and $\mu \triangleq (\mu_1 \ \mu_2 \ \mu_3)^T$ is the control input vector. They are consistent in matrix gain as follows:

$$S_c \triangleq \begin{bmatrix} 2 & -1 & -1 \\ -1 & 2 & -1 \\ -1 & -1 & 2 \end{bmatrix}, \in \mathbb{R}^{3 \times 3} \quad (5.3)$$

and, the three- phase main source voltage vector is defined as:

$$V_g \triangleq E_n \begin{bmatrix} \sin(\omega_s t) \\ \sin(\omega_s t - 2\pi/3) \\ \sin(\omega_s t + 2\pi/3) \end{bmatrix}, \in \mathbb{R}^3 \quad (5.4)$$

with E_n is defined as the amplitude of the grid source voltages measured in volt.

For modelling and control task, it is suitable to transform three - phase sinusoidal variables from (abc) sequence into (d - q) reference frame. It has the advantage of reducing the current control task into a set - tracking point. According to the grid phase voltage equation of PWM AC/DC converter, it could be written in the following form:

$$V_g = L di/dt + ri + V_{sn}$$

The transformed variables in (d - q) synchronous rotating reference frame are defined as,

$$\mu_{dq} \triangleq \begin{bmatrix} \mu_d \\ \mu_q \end{bmatrix} = P_T \mu, \quad i_{dq} \triangleq \begin{bmatrix} i_d \\ i_q \end{bmatrix} = P_T i, \quad \text{and} \quad V_{gdq} \triangleq \begin{bmatrix} V_{gd} \\ V_{gq} \end{bmatrix} = P_T V_g \quad (5.5)$$

where P_T stands for *Park's* transformation vector defined as follows. More details about *Park's* transformation is found in appendix A.2.

$$P_T \triangleq \frac{2}{3} \begin{bmatrix} \cos(\omega_s t) & \cos(\omega_s t - 2\pi/3) & \cos(\omega_s t + 2\pi/3) \\ -\sin(\omega_s t) & -\sin(\omega_s t - 2\pi/3) & -\sin(\omega_s t + 2\pi/3) \end{bmatrix} \quad (5.6)$$

For balanced system condition, *i.e.*, ($i_a + i_b + i_c = 0$), the dynamical controlled model of the AC/DC boost power converter in ($d - q$) synchronous rotating reference frame [see e.g. Liu et al., 2014], can be expressed (actually $V_{gd} \triangleq 0$ and $V_{gq} \triangleq E_n$) to simplify the control task:

$$\left\{ \begin{array}{l} \frac{di_d}{dt} = -\frac{r}{L} i_d - \frac{V_0}{2L} \mu_d + \omega_s i_q \\ \frac{di_q}{dt} = -\frac{r}{L} i_q - \frac{V_0}{2L} \mu_q + \omega_s i_d + \frac{E_n}{L} \\ \frac{dV_0}{dt} = -\frac{V_0}{R_o C_o} + \frac{3}{4C_o} (i_d \mu_d + i_q \mu_q) \end{array} \right. \quad (5.7)$$

where, ω_s is the constant angular frequency of the grid source voltage measured in (rad/sec). It can be easily shown that DC output current based on *Kirchhoff* current law (*KCL*) is:

$$i_{dc} = C_o \frac{dV_0}{dt} + \frac{V_0}{R_o} = 3/4 (\mu_d i_d + \mu_q i_q)$$

In the transformed state equation given in (5.7), the new state vector is defined as $X \triangleq [x_1 \ x_2 \ x_3]^T = [i_d \ i_q \ V_0]^T$ and the control input vector in ($d - q$) frame, $\mu_{dq} \triangleq [\mu_d \ \mu_q]^T$ are the switching functions in synchronously rotating ($d - q$) frame. From the control point of view, the model of AC/AD boost power converter in ($d - q$) rotary synchronous reference frame has the advantage of reducing the current control task into a set – tracking point [see e.g. Lee, 2003; Kömürçügil et al., 1998].

The model introduced by equation (5.7) is useful for building up an accurate computer simulator for the three-phase AC/DC boost power converter. However, it can not achieve the control task involves binary control inputs, namely μ_d and μ_q .

This difficulty is generally coped with resorting to use averaged models where instantaneous signals are replaced by their corresponding averaged versions. Signal averaging is performed over timing intervals [Abouloifa et al., 2004]. With the notations listed in Table 5.1, the ($d - q$) averaged model expresses as follows, *i.e.* $\mu_d \rightarrow u_d$ and $\mu_q \rightarrow u_q$:

$$\left\{ \begin{array}{l} \frac{dx_d}{dt} = -\frac{r}{L}x_d - \frac{x_0}{2L}u_d + \omega_s x_q \\ \frac{dx_q}{dt} = -\frac{r}{L}x_q - \frac{x_0}{2L}u_q + \omega_s x_d + \frac{1}{L}\theta_1 \\ \frac{dx_0}{dt} = \frac{3}{4C_o}(x_d u_d + x_q u_q) - \frac{x_0}{C_o}\theta_2 \end{array} \right. , \begin{array}{l} \theta_1 = E_n \\ \theta_2 = \frac{1}{R_o} \end{array} \quad (5.8)$$

Nonlinear control systems are those control systems where nonlinearity property plays a significant role, either in the controlled process (*i.e.* plant) or in the controller itself. The averaged model defined by equation (5.8) is strongly nonlinear since the system model involves the product between control input signals, u_d, u_q and the state variables, x_d, x_q, x_0 . These system states – variables are defined in Table 5.1. The basic assumption is made that the system time constants are much longer than the switching time interval, τ_s . One may average the waveforms over a switching time interval which is short compared to the system time constants, without changing or effecting on the system dynamic response.

Particularly, averaging over the switching time interval removes the switching harmonics, while preserving the low-frequency components of the waveforms. In practice, the only work needed for this step is to average the switch dependent state signals. Figure 5.2 shows an exact equivalent circuit of AC/DC boost converter projected on ($d - q$) averaged model.

5.3.2 Main control objectives

The control objectives for the present chapter can be summarized as follows:

- CO1:** PFC requirement: the input phase currents i_a, i_b, i_c should be in phase with corresponding input source voltage V_{g1}, V_{g2}, V_{g3} for getting unity power factor on the grid side.
- CO2:** DC output voltage regulation: the DC component of the output voltage V_o must be regulated to a desired reference voltage, namely V_o^* while its AC component must be attenuated to a given desired level.
- CO3:** Minimizing the harmonic distortion factor to a desired level less than 2% in presence of output filter using one of the harmonic mitigation techniques, specifically PWM technique or IGBT based fast switching harmonic filter.

As mentioned previously, the novelty of the present study resides in taking into account the following difficulties:

- (i) The load resistance, R_o is assumed to be constant, but unknown.

- (ii) The magnitude of grid phase voltages, E_n is considered bounded, but unknown.
- (iii) The input phase currents are considered inaccessible, unlike in most of previous studies for monitoring and security purposes.
- (iv) This difficulty is coped with augmenting nonlinear controller based adaptive observer for providing on-line estimates of the grid phase currents, uncertain of grid phase voltages and load resistance based on the measurement of the DC - bus voltage V_o . It turns out that, numbers of required sensors (measurement appliances) are reduced this implies improving system availability and reliability of operation (reliability is probability of success system and it is a branch of sciences associated with rarities).

Table 5.1: Table 1. State variables and unknown parameters for online UPS

Variables and parameters	Definition	Observation
x_d	Averaged of i_d	Inaccessible to measurements in $d - axis$
x_q	Averaged of i_q	Inaccessible to measurements in $q - axis$
x_o	Averaged of V_o	Accessible to output measurements
θ_1	Uncertain of E_n	Unknown sinusoidally bounded parameter
θ_2	Uncertain of $1/R_o$	Unknown conductance parameter

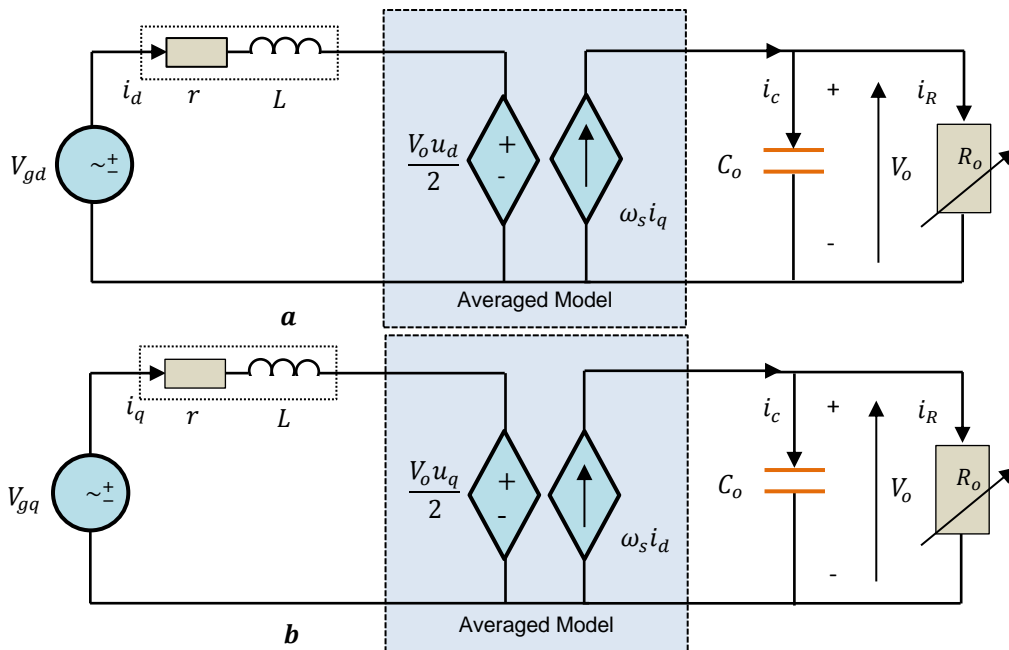


Figure 5.2: Exact equivalent circuit of AC/DC boost converter in $(d - q)$ averaged model
a – direct – axis equivalent circuit **b** – quadrature - axis equivalent circuit

5.3.3 Comparing with published results

A comparison with existing approaches in literatures could be provided to justify the advantages and benefits of the proposed nonlinear adaptive output feedback controller design.

- The input grid phase currents are considered inaccessible, unlike in previous contribution for security, protection purposes and on-line monitoring. Indeed, in most of previous studies [see *e.g.* Liu et al., 2013]; the load resistance and amplitude of grid phase voltages are supposed to be unknown parameter. They used super –twisting sliding mode controller and observer (which is lower harmonic distortion than classical sliding mode observer) to estimate the input phase currents and load resistance based on the measurement of DC - bus voltage and linked current sensors without resorting to use LPF, neglecting the effect of time varying of other system parameters.
- The authors in [Sarinana et al., 2000], compared the numerical results in the article using sliding mode observer (SMO) with the corresponding results using *Kalman* filter like- observer for linear time invariant systems injected by input/output measurements without taking into consideration the effect of parameter uncertainty on system dynamic performances. The practically uncertainty concept is highly recommended in many of physical systems.
- In [Allag et al., 2007], they provided an on-line estimate of load resistance using nonlinear adaptive backstepping control, neglecting the effect of time - varying of other system parameters. Whilst the present chapter focus on the parameter uncertainty when synthesis the adaptive observer for states and some of electrical parameters.
- Many studies are computed the control laws using (input – output) feedback linearization techniques which are based on the exact cancellation of the nonlinearity property, for this reason, most of the linearization techniques are inefficient. However, the drawbacks of the mentioned techniques ensure only the local stability of the observation error. Sometimes, system parameters can be considered uncertain and bounded. In this field, an adaptive controller has been introduced by [see *e.g.* Reddy et al., 2015] for three – phase voltage source converter (VSC) acting as a dynamic compensator to achieve power factor regulation. The authors of that study have proposed an approach based on the approximate nonlinear model of the VSC that accounts the uncertainty of some system parameters. Whilst the system model in the present chapter is strongly nonlinear model.

- It should be confirmed that in most of the previous works [see e.g. Dai et al., 2005] are demanding continuous – time measurements of the AC - voltages, AC - currents, and DC-voltage. It turns out that requires large numbers of voltage and current measurement appliance. Subsequently, this will increase system complexity, cost, and space that will reflect negatively in reducing system availability and reliability of the power system.

Now, the complete nonlinear adaptive control strategy is fully described in the next section of the present chapter. The proof of adaptive observer stability convergence requires that the state vector, X is bounded. Presently, this is not an issue since the grid phase voltages are sinusoidal bounded. Furthermore, the grid power is physically bounded. It turns out that the grid phase currents are also bounded. Knowing that the switching action u_1, u_2 and u_3 are bounded since they take values between -1 and $+1$. Therefore; u_d and u_q are also bound in sample - space with $\|u_d\| \leq 1$ and $\|u_q\| \leq 1$.

5.4 Nonlinear adaptive controller design and analysis

Adaptive control is the control method used by a controller, which must adapt to a controlled system (plant) with parameters are time - varying or are initially unknown. A control law is needed that adapts itself to such changing conditions. Adaptive control is different from robust control in that it does not need a priori information about the bounds on these uncertain or time varying parameters. Robust control ensures that if the changes are within given bounds, the control law need not be changed, while adaptive control is concerned with control law changing them.

A nonlinear adaptive controller design as illustrated in Figure 5.3 will be accomplished in two steps. The inner-loop is designed to ensure the PFC objective. The outer loop is built-up to achieve output voltage regulation of the three - phase AC/DC boost power converter under balanced resistive load. Figure 5.4 clarifies a flowchart of the proposed approach dealing with adaptive output feedback controller design of AC/DC boost power converter topology for on-line UPS systems. Basically, the control structure of a three – phase six switch PWM boost converter consists of an inner current control loop and outer voltage control loop. The current controller senses the input current and compares it with a sinusoidal current reference. To achieve this current reference, the phase information of the utility voltages or current is needed. Normally, this is sensed by employing either a phase – locked loop (PLL) or a

current phase observer design. The present chapter will focus on second one, instead of the traditional control scheme using a PLL.

5.4.1 Observability analysis of on-line UPS system

In order to construct an observer for a system, it is necessary to verify the observability of the system, *i.e.*, there exists the possibility of getting the states of a system based on the input /output injection measurements [Besançon, 2007]. Let us consider the following structure of nonlinear system,

$$\begin{cases} \dot{X} = f(X, u) \\ y = h(X) \end{cases} \quad (5.9)$$

with $X \in \mathbb{R}^n$ is the state vector, and $u \in \mathbb{R}^m$ is bounded input, $y \in \mathbb{R}^p$ is the output state vector and assuming that the vector field function, $f(X, u)$ is smooth function. From system (5.8), it is important to note the nonlinear nature of the three – phase voltage source converter. The observation objective is to reconstruct the grid phase current assuming that they are inaccessible. Notice that, one can find a sufficient condition under which the *Jacobian* matrix has full rank. From the third subsystem model of equation (5.8) projected on $(d - q)$ averaged model, *i.e.*, observing (x_d, x_q) from the measurement of x_o ,

$$\begin{cases} \frac{dx_o}{dt} = -\frac{x_o}{R_o C_o} + \frac{3}{4C_o}(x_d u_d + x_q u_q) \\ h(X) \triangleq x_o = V_o \end{cases} \quad (5.10)$$

Let us denote:

The property of observability can be verified from the measured output state variable and its corresponding derivatives. Let us consider the following observation space involving the information that generated for the observability criterion. $L_f^k h(X)$ is called the *k'th* order *Lie* - derivative of the function $h(X)$ *w.r.t* vector field function along the closed – loop trajectories,

$$f(X, u) \triangleq [f_1(X, u), f_2(X, u), f_3(X, u)]^T, \quad \mathcal{O}_{UPS} h(X) \triangleq \{h_1(X), L_f h_1(X), L_f^2 h_1(X)\} \quad (5.11)$$

Such that,

$$h(X) \triangleq L_f^0 h(X) = x_o$$

and,

$$L_f h(X) \triangleq \sum_{i=1}^3 f_i(X, u) \frac{\partial h(X)}{\partial x_i}$$

$$L_f h = \frac{3u_d}{4C_o} \left(-\frac{r}{L} x_d - \frac{x_o}{2L} u_d + \omega_s x_q \right) + \frac{3u_q}{4C_o} \left(-\frac{r}{L} x_q - \frac{x_o}{2L} u_q + \omega_s x_d + \frac{E}{L} \right) + \frac{x_o}{(R_o C_o)^2} (x_d u_d + x_q u_q) \quad (5.12)$$

and,

$$L_f^2 h(X) \triangleq \sum_{i=1}^3 f_i(x, u) \frac{\partial L_f h(X)}{\partial x_i}$$

$$\begin{aligned} &= -\frac{3}{4C_o} \left(\frac{r}{L} u_d + \omega_s u_q \right) + \frac{1}{(R_o C_o)^2} x_o u_d + \frac{3}{4C_o} \left(-\frac{r}{L} u_q + \omega_s u_d \right) + \frac{1}{(R_o C_o)^2} x_o u_q \\ &\quad - \frac{3}{8LC_o} (u_d^2 + u_q^2) + \frac{1}{(R_o C_o)^2} (x_d u_d + x_q u_q) \end{aligned} \quad (5.13)$$

It is obvious that the observability analysis is accomplished by evaluating the *Jacobian* of nonlinear systems, $J_{\mathcal{O}_{UPS} h(X)}$, *w.r.t* system variables, where $X \in \mathbb{R}^3$.

$$J_{\mathcal{O}_{UPS} h(X)} \triangleq \frac{\partial}{\partial x} \mathcal{O}_{UPS} h(X) \quad (5.14)$$

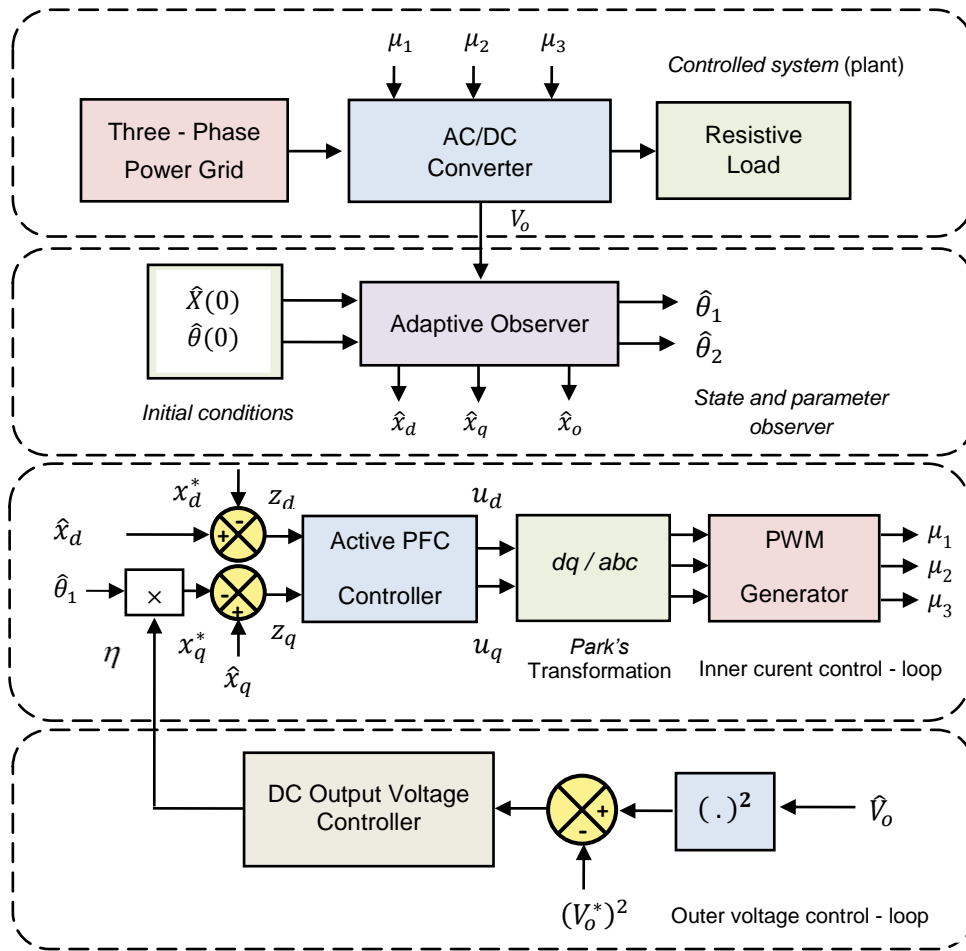


Figure 5.3: Schematic diagram of OFC nonlinear adaptive controller design strategy

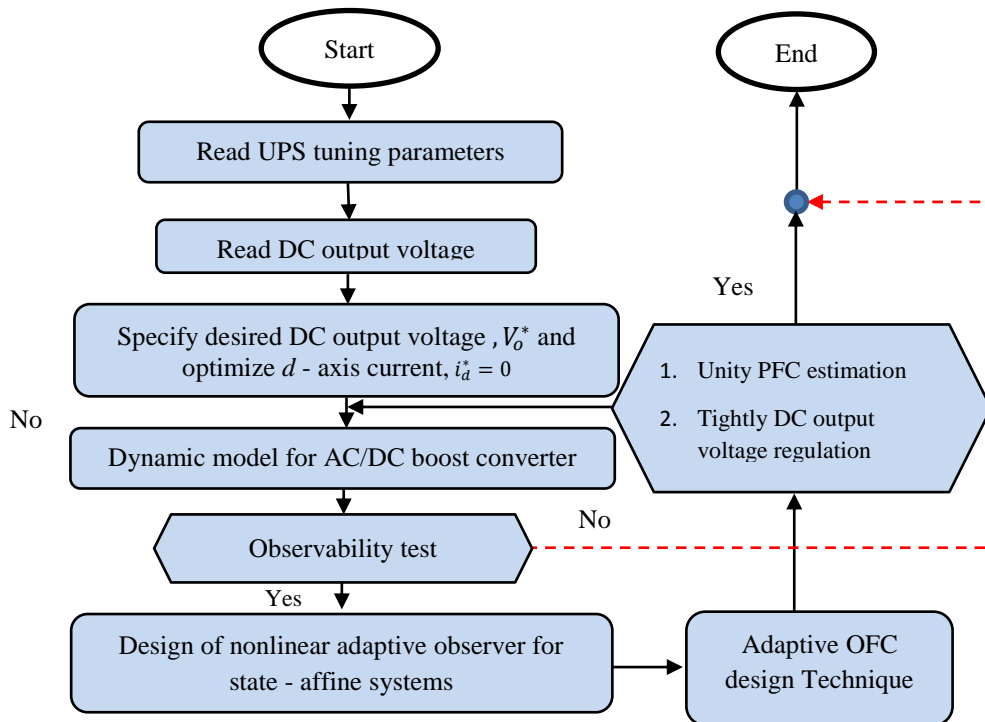


Figure 5.4: A flowchart of the proposed approach

Typically, the *Jacobian* matrix characterizes the observability of the UPS system in the rank sense. If the $J_{\mathcal{O}_{UPS}}h(X)$ has full rank, this means, $\dim(J_{\mathcal{O}_{UPS}}h(X)) = 3$, so if the observability rank condition holds $\forall X \in \mathbb{R}^3$, then system (5.8) is observable in the rank sense [Hermanne et al., 1977].

$$\text{rank}\{J_{\mathcal{O}_{UPS}}h(x)\} = \text{rank}\begin{pmatrix} dh(x) \\ dL_f h(x) \\ dL_f^2 h(x) \end{pmatrix} = n = 3 \quad (5.15)$$

with, d indicates for usual partial derivative along the closed loop trajectories. The associated observability matrix gives observability criteria matrix has dimensions of (3×3) , is:

$$J_{\mathcal{O}_{UPS}}h(X) \triangleq \begin{bmatrix} 0 & 0 & 1 \\ \frac{\partial L_f h(x)}{\partial x_d} & \frac{\partial L_f h(x)}{\partial x_q} & \frac{\partial L_f h(x)}{\partial x_o} \\ \frac{\partial L_f^2 h(x)}{\partial x_d} & \frac{\partial L_f^2 h(x)}{\partial x_q} & \frac{\partial L_f^2 h(x)}{\partial x_o} \end{bmatrix} \in \mathbb{R}^{3 \times 3}$$

$$= \begin{bmatrix} 0 & 0 & 1 \\ \frac{1}{2C_o}u_d & \frac{1}{2C_o}u_q & -1/R_o C_o \\ -[(r/2C_o L) + (1/2R_o C_o^2)]u_q, & \frac{1}{2C_o}\omega_s u_d - [(r/2C_o L) + (1/2R_o C_o^2)]u_q, & -\frac{1}{4LC_o}\|u_{dq}\|^2 + (1/R_o C_o)^2 \end{bmatrix} \quad (5.16)$$

It is apparent that the *Jacobian* matrix, $J_{\mathcal{O}_{UPS}}h(X)$ has full rank if and only if the square matrix of (5.16) has also full rank non-singular,

$$L_{\mathcal{O}_{UPS}}h(X) \triangleq \begin{bmatrix} \frac{\partial L_f h(x)}{\partial x_d} & \frac{\partial L_f h(x)}{\partial x_q} \\ \frac{\partial L_f^2 h(x)}{\partial x_d} & \frac{\partial L_f^2 h(x)}{\partial x_q} \end{bmatrix} \in \mathbb{R}^{2 \times 2} \quad (5.17)$$

Now, it will be proved that, $L_{\mathcal{O}_{UPS}}h(X)$ is a regular square matrix, which can be computed as the determinant of $L_{\mathcal{O}_{UPS}}h(x)$ after simple algebraic calculations, gives us the following condition:

$$\det\{L_{\mathcal{O}_{UPS}}h(X)\} = \frac{\omega_s}{4C_o^2}(u_d^2 + u_q^2) = \frac{\omega_s}{4C_o^2}\|u_{dq}\|^2 = D\|u_{dq}\|^2 \neq 0 \quad (5.18)$$

where, $D > 0$ is a real positive constant. It should be mentioned that one can focus on the matrix $L_{\mathcal{O}_{UPS}}h(X)$ in order to introduce a sufficient condition such that this matrix, or equivalently, $J_{\mathcal{O}_{UPS}}h(X)$ has full rank almost everywhere. Essentially, this means that observability concept is dependent on the control inputs and thus can permit the design of non - uniform observer depending on the control inputs.

This ends the prove of observability ■.

Remark 5.1: Even by taking higher - order derivatives of the measured DC output voltage, no additional information provided by observability criterion.

Remark 5.2: One can say that if, $\det \left(J_{O_{UPS}} h(X) \right) \neq 0$, UPS is observable in the rank sense.

It is possible to estimate all grid phase currents from the output voltage measurement, if the norm of the control inputs $\|u_{dq}\|^2 \neq 0$ at all times. Practically, the observability concept is lost only at the singular point corresponding to singular inputs *i.e.*, $u_d = 0, u_q = 0$. From all above, one can conclude that, $\det \left(J_{O_{UPS}} h(X) \right) \neq 0$ never vanish if and only if the control inputs are cancelled [see *e.g.* Sarinana et al., 2000].

5.4.2 Adaptive observer design

The model described by (5.8) can be re-written in the following compact state - affine form:

$$\begin{cases} \dot{X} = A(u_d, u_q)X + \Phi(y_o)\theta \\ y_o = CX \quad (\text{output}) \end{cases} \quad (5.19)$$

where, the state vector and state transition matrix are defined as follows:

$$X \square \begin{bmatrix} x_d \\ x_q \\ x_o \end{bmatrix}, \quad A \square \begin{bmatrix} -r/L & \omega_s & -u_d/2L \\ -\omega_s & -r/L & -u_q/2L \\ 3u_d/4C_o & 3u_q/4C_o & 0 \end{bmatrix},$$

$$C^T \square \begin{bmatrix} 0 \\ 0 \\ I \end{bmatrix}, \quad \Phi(y_o) \square \begin{bmatrix} 0 & 0 \\ I/L & 0 \\ 0 & -y_o/C_o \end{bmatrix}, \quad \theta = \begin{bmatrix} \theta_1 \\ \theta_2 \end{bmatrix} \square \begin{bmatrix} E_n \\ I \\ R_o \end{bmatrix}$$

Clearly, the system given in equation (5.19) is state - affine in the sense that all unknown quantities (*i.e.*, x_d, x_q and θ) come in linearly. To get on-line estimates of the unmeasured states x_d, x_q and the unknown parameter vector θ , the following adaptive observer for a state – affine system had been proposed by [Besançon et al., 2006]:

$$\left[\begin{array}{l} \dot{\hat{X}} = A(u_d, u_q)\hat{X} + \Phi(y_o)\hat{\theta} + \{ \Lambda S_\theta^{-1} \Lambda^T C^T + S_X^{-1} C^T \} (y_o - C \hat{X}) \quad (5.20a) \\ \dot{\hat{\theta}} = S_\theta^{-1} \Lambda^T C^T (y_o - C \hat{X}) \quad (\text{dynamic adaptive law}) \quad (5.20b) \\ \dot{\Lambda} = \{ A(u_d, u_q) - S_X^{-1} C^T C \} \Lambda + \Phi(y_o) \quad (5.20c) \\ \dot{S}_X = -\rho_X S_X - A(u_d, u_q)^T S_X - S_X A(u_d, u_q) + C^T C \quad (5.20d) \\ \dot{S}_\theta = -\rho_\theta S_\theta + \Lambda^T C^T C \Lambda \quad (5.20e) \\ \hat{y}_o = C \hat{X} = \hat{x}_o \quad (\text{Output}) \quad (6.20f) \end{array} \right.$$

where, $S_x(0) > 0$, $S_\theta(0) > 0$ are any symmetric positive definite matrices and the solution of (5.20d - e), respectively; ρ_x and ρ_θ are any sufficiently, large positive scalars. The matrix S_x is ensured bounded positive definite matrix provided the following regularly persistent excitation condition holds:

$$\alpha_1 \mathbb{I} \leq \int_t^{t+T_1} \psi_{u_{dq}}(\tau)^T C^T C \psi_{u_{dq}}(\tau) d\tau \leq \alpha_2 \mathbb{I}, \quad \forall t \geq t_0 \quad (5.21)$$

For some constants $\alpha_1, \alpha_2, T_1 > 0$ and $\psi_{u_{dq}}$, denotes the transition matrix for autonomous part of the system, $\dot{X} = A(u_d, u_q)X$, $y_o = CX$, such that,

$$\begin{cases} d\psi_{u_{dq}}(\tau)/d\tau = A(u_d(\tau), u_q(\tau))\psi_{u_{dq}}(\tau) \\ \psi_{u_{dq}}(t, t) = \mathbb{I}_n \end{cases}$$

The latter equation given by (5.21) can be seen for a state - affine and a LTV system, parameterized by initial conditions as soon as the functions $u_d(t)$ and $u_q(t)$ are fixed at certain times. The middle term of LMI given in equation (5.21) corresponds to the so - called observability *Grammian*, classically defined for LTV systems, $\forall t \in \mathbb{R}$. Owing to the matrix S_θ is ensured bounded positive definite provided by the following persistent excitation condition holds:

$$\alpha_3 \mathbb{I} \leq \int_t^{t+T_2} \Lambda(\tau)^T C^T C \Lambda(\tau) d\tau \leq \alpha_4 \mathbb{I}, \quad \forall t \geq t_0 \quad (5.22)$$

for some positive constants $\alpha_3, \alpha_4, T_2 > 0$. Figure 5.5. describes the structure of real system / adaptive observer design for a state - affine system based voltage source converter.

5.4.3 Stability convergence analysis

Sketch proof:

The exponential convergence properties of the adaptive observer are analyzed based on the following error system dynamics:

$$\begin{cases} \dot{\tilde{X}} = (A(u_d, u_q) - S_\theta^{-1} \Lambda^T C^T C - S_x^{-1} C^T C) \tilde{X} + \Phi(y_o) \tilde{\theta} \\ \dot{\tilde{\theta}} = -S_\theta^{-1} \Lambda^T C^T C \tilde{X} \end{cases} \quad (5.23)$$

with the errors definitions, $\varepsilon_x \square \tilde{X} - \Lambda \tilde{\theta}$, $\tilde{\theta} \square \hat{\theta} - \theta$, $\tilde{X} \square \hat{X} - X$, it gives [Zhang, 2002]

$$\dot{\varepsilon}_x = (A(u_d, u_q) - S_\theta^{-1} \Lambda^T C^T C - S_x^{-1} C^T C) \varepsilon_x + \Phi(y_o) \tilde{\theta} - \dot{\Lambda} \tilde{\theta} - \dot{\tilde{\theta}} \Lambda$$

Using some matrix manipulation and mathematical computations given in (5.20 b-c), one has:

$$\begin{cases} \dot{\varepsilon}_x = (A(u_d, u_q) - S_x^{-1} C^T C) \varepsilon_x \end{cases} \quad (5.24a)$$

$$\begin{cases} \dot{\tilde{\theta}} = -S_\theta^{-1} \Lambda^T C^T C (\varepsilon_x + \Lambda \tilde{\theta}) \end{cases} \quad (5.24b)$$

To analyze the stability of the system error dynamics given in (5.24 a-b), the following direct *Lyapunov* function candidate is considered in quadratic form as follows:

$$V_{obs}(\varepsilon_x, \tilde{\theta}) = \varepsilon_x^T S_x \varepsilon_x + \tilde{\theta}^T S_\theta \tilde{\theta} \quad (5.25)$$

The time derivative of Lyapunov function, $V_{obs}(\varepsilon_x, \tilde{\theta})$ is given as,

$$\begin{aligned} \dot{V}_{obs}(\varepsilon_x, \tilde{\theta}) &= \varepsilon_x^T \left(A(u_d, u_q) - S_x^{-1} C^T C \right)^T S_x \varepsilon_x + S_x^T \varepsilon_x \left(A(u_d, u_q) - S_x^{-1} C^T C \right) \varepsilon_x \\ &\quad - \left(\varepsilon_x + \Lambda \tilde{\theta} \right)^T \left\{ S_\theta^{-1} \Lambda^T C^T C \right\}^T S_\theta \tilde{\theta} - \tilde{\theta}^T S_\theta \left\{ S_\theta^{-1} \Lambda^T C^T C \right\} \left(\varepsilon_x + \Lambda \tilde{\theta} \right) \\ &\quad + \varepsilon_x^T \dot{S}_x \varepsilon_x + \tilde{\theta}^T \dot{S}_\theta \tilde{\theta} \end{aligned} \quad (5.26)$$

In the same way, after combining of equations (5.20 b-c) in equation (5.26), one gets,

$$\begin{aligned} \dot{V}_{obs}(\varepsilon_x, \tilde{\theta}) &= -\rho_x \varepsilon_x^T S_x \varepsilon_x - \rho_\theta \tilde{\theta}^T S_\theta \tilde{\theta} - \varepsilon_x^T C^T C \varepsilon_x - \varepsilon_x^T C^T C \Lambda \tilde{\theta} \\ &\quad - \tilde{\theta}^T \Lambda^T C^T C \varepsilon_x - \tilde{\theta}^T \Lambda^T C^T C \Lambda \tilde{\theta} \end{aligned} \quad (5.27)$$

Knowing that,

$$\begin{aligned} &-\varepsilon_x^T C^T C \varepsilon_x - \varepsilon_x^T C^T C \Lambda \tilde{\theta} - \tilde{\theta}^T \Lambda^T C^T C \varepsilon_x - \tilde{\theta}^T \Lambda^T C^T C \Lambda \tilde{\theta} \\ &= - \left(\varepsilon_x + \Lambda \tilde{\theta} \right)^T C^T C \left(\varepsilon_x + \Lambda \tilde{\theta} \right) \leq 0 \end{aligned}$$

This implies that, $\dot{V}_{obs}(\varepsilon_x, \tilde{\theta}) \leq -\rho_x \varepsilon_x^T S_x \varepsilon_x - \rho_\theta \tilde{\theta}^T S_\theta \tilde{\theta}$

Actually, the following inequality holds negative definiteness of *Lyapunov* function:

$$\dot{V}_{obs}(\varepsilon_x, \tilde{\theta}) \leq -\rho_{min} V_{obs}(\varepsilon_x, \tilde{\theta}) \quad (5.28)$$

with, $\rho_{min} = \min(\rho_x, \rho_\theta)$, for whatever the initial conditions of $(\varepsilon_x(0), \tilde{\theta}(0))$.

It turns out that the estimation errors ε_x and $\tilde{\theta}$ are exponentially convergence to zero with time progressive. Subsequently, the observation error, $\tilde{X} = \varepsilon_x + \Lambda \tilde{\theta}$ is, also, exponentially vanishes. The convergence rate depends on the selection of system parameters, ρ_{min} and so it can be made fast as desirable by letting the observer gain design parameters ρ_x and ρ_θ satisfactory large enough. Under the conditions given by (5.20) and (5.22), the error system dynamic described by (5.24 a-b) is globally exponentially stable GES along the closed loop trajectories using tools of *Lyapunov* stability theory.

This ends the prove stability convergence analysis ■

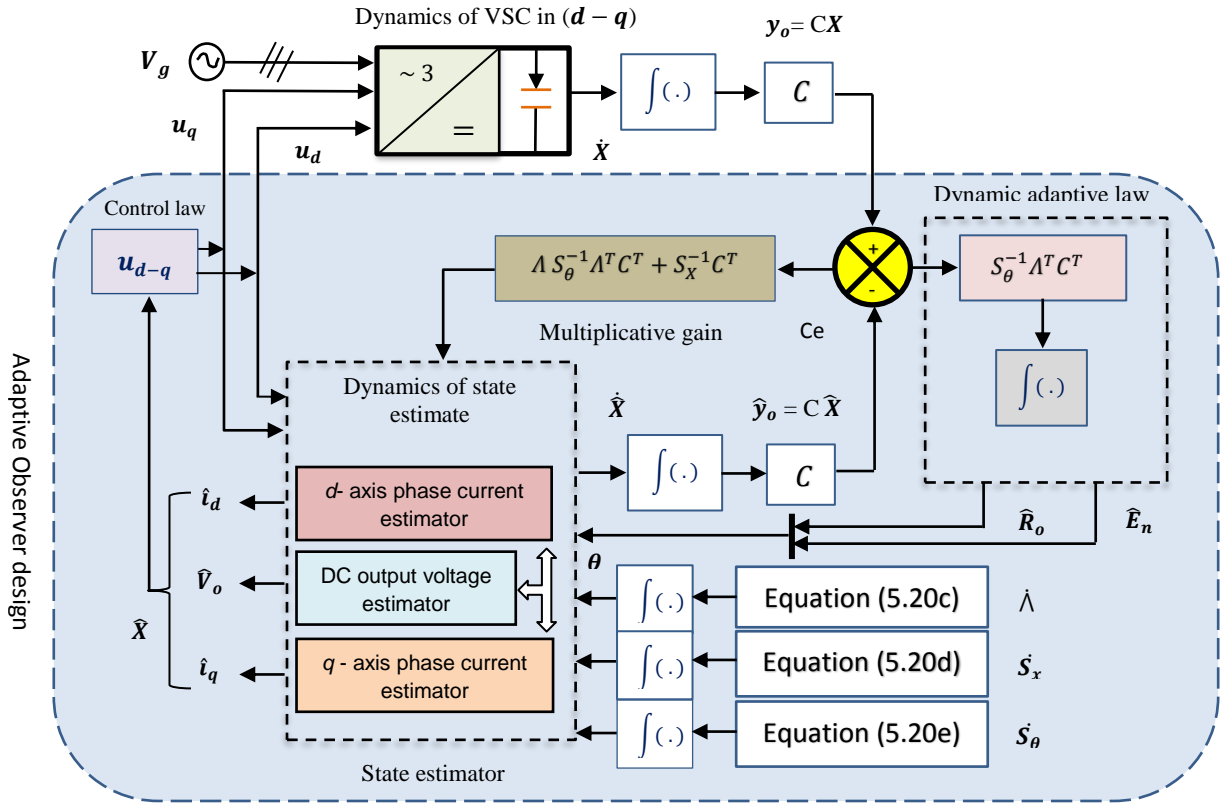


Figure 5.5: Structure of system/adaptive observer synthesis of state - affine system based VSC

Remark 5.3: In the case of singular inputs, (i.e. $u_d = 0, u_q = 0$), a simple solution by setting the multiplicative gains of the adaptive observer for state – affine system equal zero, which gives the following open – loop stable adaptive observer:

$$\begin{bmatrix} \dot{\hat{x}}_d \\ \dot{\hat{x}}_q \\ \dot{\hat{x}}_o \end{bmatrix} = \begin{bmatrix} -r/L & \omega_s & -0/2L \\ -\omega_s & -r/L & -0/2L \\ 0/4C_o & 0/4C_o & 0 \end{bmatrix} \begin{bmatrix} \hat{x}_d \\ \hat{x}_q \\ \hat{x}_o \end{bmatrix} + \begin{bmatrix} 0 & 0 \\ 1/L & 0 \\ 0 & -y_o/C_o \end{bmatrix} \begin{bmatrix} \hat{E}_n \\ 1/\hat{R}_o \end{bmatrix}$$

In the next subsection, backstepping control design technique will be used for forcing the grid phase current projected on $(d - q)$ averaged – model provided by the adaptive observer to track the desired reference level.

5.4.4 Inner control loop design of PFC achievement

The PFC requirement tracks to force the input phase currents denoted by x_d and x_q matching the desired reference level, $x_d^* = 0$ and $x_q^* = \eta \hat{\theta}_l = \eta \hat{E}_n$, with $\eta > 0$ is any positive real signal and E_n denotes the amplitude of the estimate grid phase voltage. As a

matter of fact, η is allowed to be time-varying, but it must converge to a constant value. That is, η stands for an additional control input.

Now, one can design PFC controller using continuous- time backstepping design technique and its stability convergence is analyzed based on tools of *Lyapunov* stability theory, for the system given in (5.19) running with adaptive observer expressed in (5.20 a-f). The tracking error vector for the current control in $(d - q)$ averaged model is defined as:

$$\begin{bmatrix} z_{dq} \end{bmatrix} = \begin{bmatrix} \hat{x}_d - x_d^* \\ \hat{x}_q - x_q^* \end{bmatrix} \quad (5.29)$$

Using equation defined by (5.20a) for adaptive observer, it is readily shown that the tracking error vector for current control, z_{dq} undergoes the following system error dynamics:

$$\begin{bmatrix} \dot{z}_{dq} \end{bmatrix} = \begin{bmatrix} \dot{\hat{x}}_d - \dot{x}_d^* \\ \dot{\hat{x}}_q - \dot{x}_q^* \end{bmatrix} = \begin{bmatrix} -\frac{r}{L} \hat{x}_d + \omega_s \hat{x}_q - \frac{\hat{x}_o}{2L} \hat{u}_d - m_1(t) \tilde{x}_o \\ -\frac{r}{L} \hat{x}_q - \omega_s \hat{x}_d + \frac{1}{L} \hat{\theta}_1 - \frac{\hat{x}_o}{2L} \hat{u}_q - m_2(t) \tilde{x}_o - \dot{\eta} \hat{\theta}_1 - \eta \dot{\hat{\theta}}_1 \end{bmatrix} \quad (5.30)$$

From equation (5.20b), one gets: $\hat{\theta}_1 = n_1(t) \tilde{x}_o$, $\hat{\theta}_2 = n_2(t) \tilde{x}_o$, $\tilde{x}_o = y_o - C x$

where the quantities $m_1(t)$, $m_2(t)$, $m_3(t)$, $n_1(t)$ and $n_2(t)$ are defined as follows:

$$\begin{aligned} [M(t)] &= [m_1(t) \quad m_2(t) \quad m_3(t)]^T = (A S_{\theta}^{-1} A^T C^T + S_x^{-1} C^T) \\ [N(t)] &= [n_1(t) \quad n_2(t)]^T = -S_{\theta}^{-1} A^T C^T \end{aligned} \quad (5.31)$$

Actually, the equation given in (5.30) involves the averaged control inputs, u_d and u_q must be determined so that the z_{dq} - system error is made globally asymptotically stable GAS. To do this, let us consider the following direct *Lyapunov* function candidate:

$$V_{dq} = \frac{1}{2} [z_{dq}]^T [z_{dq}] \quad (5.32)$$

and the time – derivative of the *Lyapunov* function is:

$$\dot{V}_{dq} = \frac{1}{2} \frac{d[z_{dq}]}{dt} [z_{dq}] + \frac{1}{2} [z_{dq}]^T \frac{d[z_{dq}]}{dt} \quad (5.33)$$

It is sufficient to choose the control laws, u_d and u_q such that the system error dynamics given in equation (5.33), holds:

$$\dot{V}_{dq} = -[z_{dq}]^T [c_{dq}] [z_{dq}] \quad (5.34)$$

where the design parameter $[c_{dq}]$ is a symmetric definite matrix, c_{dq} , used to ensure negative definiteness of the *Lyapunov* function.

$$[c_{dq}] = \begin{bmatrix} c_d & 0 \\ 0 & c_q \end{bmatrix}, \in \mathbb{R}^{2 \times 2} \quad (5.35)$$

Using the closed - loop dynamics in equation (5.34), this ensures that:

$$[\dot{z}_{dq}] = - [c_{dq}] [z_{dq}] \quad (5.36)$$

Furthermore, the system error dynamic given in (5.36) is globally asymptotically stable (GAS) *w.r.t* the *Lyapunov* function defined by equation (5.32). Finally, as equation (5.36) is linear nature, the tracking error vector $[z_{dq}]$ tends exponentially fast to zero with progressive time. Comparing the tracking error dynamics given in equations (5.30) and (5.36), one has the following control law vector, $[\hat{u}_d, \hat{u}_q]^T$ based on-line estimation of UPS system quantities.

$$\begin{bmatrix} \hat{u}_d \\ \hat{u}_q \end{bmatrix} = \begin{bmatrix} \frac{2L}{\hat{x}_o} \left(c_d z_q - \frac{r}{L} \hat{x}_d + \omega_s \hat{x}_q - m_1(t) \tilde{x}_o \right) \\ \frac{2L}{\hat{x}_o} \left(c_q z_q - \frac{r}{L} \hat{x}_q - \omega_s \hat{x}_d + \frac{1}{L} \hat{\theta}_1 - \dot{\eta} \hat{\theta}_1 - (\eta n_1(t) + m_2(t)) \tilde{x}_o \right) \end{bmatrix} \quad (5.37)$$

It should be confirmed that the control laws provided in this chapter involve constructing the *Lyapunov* function for the physical system, so that the closed – loop system strictly ensures a sufficient stability region taking into account the uncertain parameters

The above result could be summarized in the following first proposition.

Proposition 5.1. Consider the closed-loop control system, next called inner current control loop, including the state – affine system expressed in (5.19). The adaptive state - affine observer stated in equation (5.20 a-e) and the control laws given in equation (5.37 a-b) based on-line estimation of system quantities. Then, if the additional control input, η and its first time - derivative are available, then the system error dynamics for current control in ($d-q$) averaged model has the following form:

$$[\dot{z}_{dq}] = - [c_{dq}] [z_{dq}] \quad (5.38)$$

where, $[c_{dq}]$ is defined by equation (5.35) to ensure negative definiteness of Lyapunov function. Then, the system error dynamic defined in (5.35) is GAS w.r.t Lyapunov stability theory.

5.4.5 Outer control loop design of DC output voltage regulation

The outer control - loop design is expected to generate the additional control signal, η so that the output DC - bus voltage, x_o is regulated to a given desired level, x_o^* . To this end, the mathematical relation between η and the voltage x_o shown in Figure. 5.3 is firstly established. This will be described via the following second proposition.

Proposition 5.2. Consider the model of three-phase AC/DC boost power converter for on-line UPS systems described by (5.2 a-c) augmented by the adaptive state - affine observer given in (5.20 a-e) and the inner current control laws defined by equation (5.37). Under the same assumptions stated in Proposition 5.1, the desired current in quadrature - axis, i_q^* varies in response to the tuning control input, η and the amplitude of estimated phase voltage to ensure the estimated output voltage tracks the reference desired level, i.e. $\hat{V}_0 \rightarrow V_0^*$.

Proof: One follows third row of the equation matrix given in (5.20a) and substituting the control inputs, u_d and u_q by their corresponding expressions given in (5.37). In such way deriving the output state vector, \hat{x}_o given in (5.20), yields:

$$\frac{d\hat{x}_o}{dt} = \frac{3}{4C_o}(\hat{x}_d u_d + \hat{x}_q u_q) - \frac{x_o}{C_o} \hat{\theta}_2 - m_3(t) \tilde{x}_o \quad (5.39a)$$

On the other hand, one has the tracking error vector expressed in $(d - q)$ averaged model: $z_d = \hat{x}_d - x_d^*$ with $x_d^* = 0$. In same way, $z_q = \hat{x}_q - x_q^*$, $x_q^* = \eta \hat{\theta}_1$, $\hat{x}_o = x_o + \tilde{x}_o$ and putting

$y = \begin{pmatrix} \hat{x}_o \\ x_o \end{pmatrix}^2$, it gives:

$$\dot{y} = 2 \hat{x}_o \dot{\hat{x}_o} - k y + f_1 \begin{pmatrix} \eta \\ \dot{\eta} \end{pmatrix} + f_2 \begin{pmatrix} \dot{\eta} \\ \eta, z_d, z_q, \tilde{x}_o \end{pmatrix} \quad (5.39b)$$

Or,

$$\dot{\hat{x}_o} = \frac{I}{2 \begin{pmatrix} \hat{x}_o \\ x_o - I \end{pmatrix}} \left[-k \begin{pmatrix} \hat{x}_o \\ x_o \end{pmatrix}^2 + f_1 \begin{pmatrix} \eta \\ \dot{\eta} \end{pmatrix} + f_2 \begin{pmatrix} \dot{\eta} \\ \eta, z_d, z_q, \tilde{x}_o \end{pmatrix} \right]$$

with

$$k = 2 \frac{\hat{\theta}_2}{C_o}, \quad f_1 \left(\eta, \dot{\eta} \right) = \frac{3L\eta\hat{\theta}_1}{C_o} \left(\frac{1}{L}\hat{\theta}_1 - \frac{r}{L}\eta\hat{\theta}_1 - \hat{\theta}_1\dot{\eta} \right)$$

$$f_2 \left(\eta, \dot{\eta}, z_d, z_q, \tilde{x}_o \right) = \frac{3L}{C_o} \left(c_d - \frac{r}{L} \right) z_d^2 + \frac{3L}{C_o} \left(c_q - \frac{r}{L} \right) z_q^2$$

and,

$$+ \frac{3L}{C_o} \left((\omega_s - 1)\hat{\theta}_1\eta - m_1(t)\tilde{x}_o \right) z_d - \frac{3L\eta\hat{\theta}_1}{C_o} (m_2(t) + \eta n_1(t)) \tilde{x}_o$$

$$+ \frac{3L}{C_o} \left(\frac{1}{L}\hat{\theta}_1 - \hat{\theta}_1\dot{\eta} + \left(c_q - \frac{2r}{L} \right) \eta\hat{\theta}_1 - (m_1(t)\tilde{x}_o + \eta n_1(t)) \right) z_q$$

$$+ (1 + 2m_3(t)) \tilde{x}_o^2$$

This ends the proof of Proposition 5.2 ■

The additional control input, η stands for a tuning control input given in equation (5.39b).

Now, the problem at hand is a design of tuning control law so that the DC squared output

voltage, $y = \left(\hat{x}_o \right)^2$ tracks a given desired reference level, $y^* = \left(x_o^* \right)^2$ where, x_o^* is a desired

reference signal must be greater than, $2\hat{\theta}_1$, such that to ensure the occurrence elevation feature of the boost power converter. Bearing in your mind the fact that the tuning design input; η and its first time - derivative must be available as stated in (Proposition 5.2). The first order filtered proportional integral (PI) regulator is considered for harmonics reduction and suppression:

$$\eta = \frac{h_3}{h_3 + s} (h_1 z_1 + h_2 z_2) \quad (5.40a)$$

with, $z_1 = y - y^* = C \left(\hat{x}_o^2 - x_o^{*2} \right)$ and $z_2 = \int_0^t z_1 d\tau$

where, s denotes the Laplace variable and $(h_1, h_2, h_3) > 0$ are any positive real constants.

Knowing that the equation defined by (5.40a) implies that the dynamics of tuning control input can be computed using the following equation:

$$\dot{\eta} = h_3 (h_1 z_1 + h_2 z_2 - \eta) \quad (5.40b)$$

Now, throughout this chapter the input phase currents to AC/DC converter for on – line UPS system are considered inaccessible, this will lead us to discuss the problem of power factor estimation in the next subsection. Unlike in most previous studies, the input phase

currents are inaccessible. From this, one expects the possibility to achieve better dynamic performance. This will be confirmed through numerical simulation of a physical model associated with three – phase AC/DC boost power converter for the on-line UPS system.

5.4.6 Power factor calculation and estimation

Power factor is the percentage of electricity that is being used to achieve useful work. It is defined as the ratio of active power used in the circuit denoted by (kW), to the apparent power expressed in (kVA). Power factor is always bounded between zero and unity. For efficient transmission of energy from a main voltage source to an electrical load, it is desired to maximize average power, while minimizing rms currents and voltages. The definition of the power factor, denoted by PF is given by the fundamental formula [Shtessel et al., 2008]:

$$PF \triangleq \frac{P_{av}}{v_{rms} i_{rms}} \quad (5.41)$$

where, the $RMS(\cdot)$ stands for the root-mean-square of physical quantity, which is calculated as:

$$RMS(i(t)) = \sqrt{\frac{1}{T} \int_0^T i^2(\tau) d\tau} = \sqrt{i_1^2 + i_2^2 + i_3^2 \dots + i_n^2} \quad (5.42)$$

where, T is the period of the phase current $i(t)$ waveform, $RMS(i_1(t))$ characterizes the effective value for the fundamental main component of the current $i_1(t)$, $RMS(i(t))$ corresponds to the effective value of the total current and i_n stands for n 'th harmonic component of the input phase current.

It should be mentioned that for case of resistive load non – sinusoidal voltage source, the current harmonics are in phase with and proportional to the voltage harmonics. All harmonics result in the transmission of energy to the critical load, and unity power factor occurs, *i.e.*, $i_n = \frac{v_n}{R_o}$, and the corresponding phase shift angles for n 'th components of voltages and currents in (abc) sequence are $\theta_n^{abc} = \varphi_n^{abc} \rightarrow \cos(\varphi_n^{abc} - \theta_n^{abc}) = 1$.

So, the effective value of input phase voltages and currents are:

$$v_{rms} \triangleq \sqrt{V_{dc}^2 + \sum_{n=1}^{\infty} \frac{v_n^2}{2}} \quad (5.43)$$

$$\text{and, } i_{rms} \triangleq \sqrt{I_{dc}^2 + \sum_{n=1}^{\infty} \frac{i_n^2}{2}} = \sqrt{\frac{V_{dc}^2}{R_o^2} + \sum_{n=1}^{\infty} \frac{v_n^2}{2R_o^2}} = \frac{1}{R_o} v_{rms} \quad (5.44)$$

The average power for three – phase system in (abc) sequence can be defined as follows:

$$P_{av} \triangleq \frac{W_{cycle}}{T} = \frac{3}{T} \int_0^t v(t)i(t)dt \quad (5.45)$$

$$P_{av} = \frac{3}{T} \int_0^t (V_{dc} + \sum_{n=1}^{\infty} v_n \cos(n\omega_s t - \varphi_n)) (I_{dc} + \sum_{n=1}^{\infty} i_n \cos(n\omega_s t - \theta_n)) dt \quad (5.46)$$

Integrals of cross - product terms are zero:

$$\begin{aligned} & \int_0^t \{v_n \cos(n\omega_s t - \varphi_n) i_m \cos(m\omega_s t - \theta_m)\} dt \\ &= \begin{cases} 0 & , \text{if } n \neq m \\ \frac{3v_n i_n}{2} \cos(\varphi_n - \theta_n) & , \text{if } n = m \end{cases} \end{aligned} \quad (5.47)$$

Expression for average power three - phase system in (abc) sequence becomes:

$$P_{av} = 3V_{dc} I_{dc} + \sum_{n=1}^{\infty} 3 \frac{v_n i_n}{2} \cos(\varphi_n^{abc} - \theta_n^{abc}) \quad (5.48)$$

For a particular case of non pure sinusoidal AC voltage source and equivalent resistive load, current harmonics will try to increase the effective current, and hence they decrease the power factor level. The average power for balanced three – phase sinusoidal system could be expressed as follows:

$$P_{av} = \frac{3v_1 i_1}{2} \cos(\varphi_{1a} - \theta_{1a}) \quad (5.49)$$

and, the power factor for phase (a) can be defined as,

$$PF_a = \left(\frac{i_1/\sqrt{2}}{\sqrt{I_{dc}^2 + \sum_{n=1}^{\infty} \frac{i_n^2}{2}}} \right)_a \cos(\varphi_{1a} - \theta_{1a}) \quad \rightarrow \quad PF_a \triangleq PF_{ha} * PF_{da} \quad (5.50)$$

Harmonics are integral multiples of some fundamental frequency that, when added together, result in a distorted waveform. Defined only for sinusoidal voltage source, the harmonic distortion factor can be defined as:

$$PF_{ha} \triangleq \left(\frac{i_1/\sqrt{2}}{\sqrt{I_{dc}^2 + \sum_{n=1}^{\infty} \frac{i_n^2}{2}}} \right)_a = \left(\frac{RMS(i_1)}{RMS(i)} \right)_a * 100\% \quad (\text{for phase a}) \quad (5.51)$$

The displacement factor between a fundamental component of main AC source voltage and input phase current is defined in the following form:

$$PF_{da} \triangleq \cos(\varphi_{1a} - \theta_{1a}) \quad (5.52)$$

The ideal condition of unity power factor corresponds to non - harmonic distortion (*i.e.* phase current has only the fundamental component) and no displacement factor between fundamental input phase current and main source voltage. It is clear from the equation (5.50) that the power factor is determined by harmonic distortion factor and displacement factor. Indeed, a bigger displacement angle $(\varphi_1 - \theta_1)$, leads a huge reactive power compensation. The great harmonic distortion factor, leads a bigger input current harmonics. Subsequently, this will cause input current distortion and hence produces pollution to electric grid, and even

causes damage the electric power equipments, if the operating conditions are serious. The performance of well – known PWM technique is evaluated by total harmonic distortion (THD) factor for the input phase currents. It expresses the reliability of the power system and it can be defined as follows:

$$THD_i \stackrel{\text{def}}{=} \frac{\sqrt{\sum_{n=2}^{\infty} i_n^2}}{i_1} 100\% \rightarrow PF_h = \frac{1}{\sqrt{1+(THD_i)^2}} * 100\% \rightarrow PF = \frac{PF_d}{\sqrt{1+(THD_i)^2}} \quad (5.53)$$

To develop an output voltage regulator with lower harmonic distortion factor for on - line UPS system, a powerful controller is required to achieve outer closed – loop regulation. The PWM technique used for eliminating the harmonics components, which cannot prevent the distortion of output voltage for nonlinear loads. The estimation of power factor is very important for analyzing and verifying the quality and dynamic performances of the proposed nonlinear adaptive output feedback controller. The overall power factor for three-phase AC/DC boost power converter topology in (abc) sequence could be estimated from the estimates of the phase current per wire which will a product of the three single-phase power factor estimation (*i.e.* combined nonlinear characteristics of the AC/DC boost power converter [Liu et al., 2014]):

$$PF_{3-\phi} \square PF_a * PF_b * PF_c$$

$$= \frac{RMS(\hat{i}_{1a}(t))}{RMS(\hat{i}_a(t))} \cos(\hat{\phi}_{1a} - \hat{\theta}_{1a}) * \frac{RMS(\hat{i}_{1b}(t))}{RMS(\hat{i}_b(t))} \cos(\hat{\phi}_{1b} - \hat{\theta}_{1b}) * \frac{RMS(\hat{i}_{1c}(t))}{RMS(\hat{i}_c(t))} \cos(\hat{\phi}_{1c} - \hat{\theta}_{1c}) \quad (5.54)$$

where, $\hat{i}_a, \hat{i}_b, \hat{i}_c$ and $\hat{i}_{a1}, \hat{i}_{b1}, \hat{i}_{c1}$ are the estimates of the input phase currents, and their fundamental components, respectively. $(\hat{\phi}_{1a} - \hat{\theta}_{1a}), (\hat{\phi}_{1b} - \hat{\theta}_{1b}), (\hat{\phi}_{1c} - \hat{\theta}_{1c})$ are the displacement angles in (abc) sequence between the fundamental input currents and main AC source voltages.

The structure of the single-phase power factor estimation in MATLAB/SIMULINK is shown in Figure 5.6, using either fast Fourier transform (FFT) or mean square spectrum method. It includes two important modules first one is *Fourier analysis* and the second one is *Harmonic analysis*. The importance of these modules reside in the first module gives the main-frequency of the input current and corresponding grid source phase voltage, respectively. Whilst, the other module is used to measure the harmonic distortion caused by input phase currents. The dynamic tracking performance of the nonlinear adaptive output feedback control strategy of

three – phase full bridge AC/DC boost power converter for on-line UPS system is summarized in the following proposed theorem.

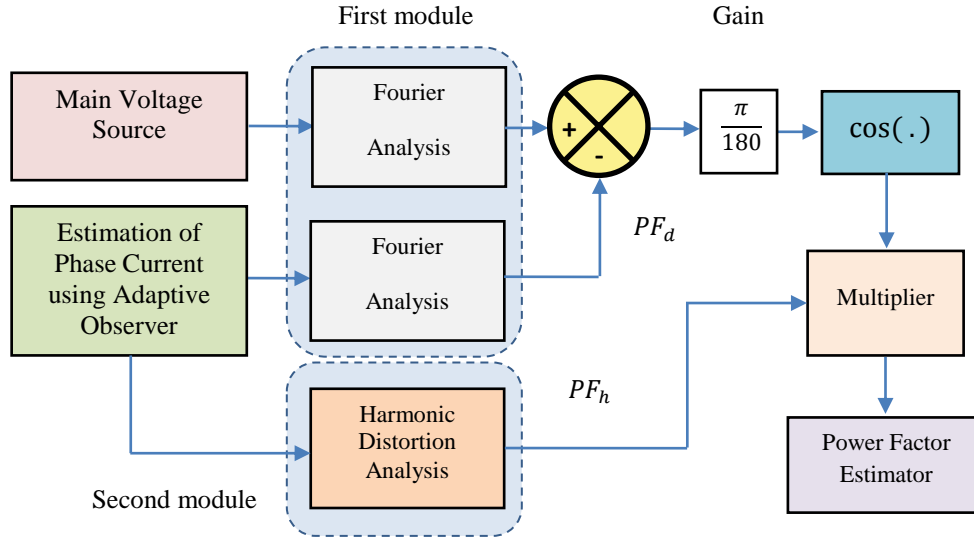


Figure 5.6: Structure of single phase power factor estimation for on-line UPS system

Theorem 5.1 The adaptive observer for state - affine systems given in equation (5.20) combined with backstepping control design defined by equations (5.37), (5.40) and an additional control input are establishing an adaptive nonlinear OFC design of three – phase AC/DC boost VSC for on – line UPS system. It is satisfying the observation errors, parameter estimation errors given in equations (5.24a – b) and the tracking error dynamics described by equation (5.38) and equation (5.40b) are GES to the equilibrium point with progressive time. It should be mentioned that the robustness properties are satisfied so that the complete system is GAS using tools of *Lyapunov* stability theory with satisfactory positive design parameters of $\rho_X, \rho_\theta, c_{dq}, c_1, c_2, c_3 > 0$. It is guaranteed rigorous and robust to parametric uncertainties that will ensure UPF estimation and tight output voltage regulation. Actually the output ripple size is observed insignificant that is interpreted THD less than 2% caused by input grid phase currents.

Remark 5.4: The phase voltage equation of a voltage source converter (VSC) can be written by analyzing the circuit of VSC with assistance of *KVL* as follows:

$$V_g = Ri + L \frac{di}{dt} + v_a \quad (5.55)$$

The $(d - q)$ voltage equations in synchronous reference frame are:

$$\begin{cases} V_{gd} = Ri_d + L \frac{di_d}{dt} - L\omega_s i_q + v_d \end{cases} \quad (5.56a)$$

$$\begin{cases} V_{gq} = Ri_q + L \frac{di_q}{dt} + L\omega_s i_d + v_q \end{cases} \quad (5.56b)$$

The active and reactive power balance equations between the electrical network input and the DC output across the equivalent resistive load are written in the following form:

$$\left[\begin{array}{l} P = \frac{3}{2}(V_{gd}i_d + V_{gq}i_q) = V_{dc}I_{dc} = V_{dc}\frac{V_{dc}}{R_o} \end{array} \right. \quad (5.57a)$$

$$\left[\begin{array}{l} Q = 0 \end{array} \right. \quad (5.57b)$$

applying *KCL*, it gives,
$$\left[\begin{array}{l} i_{dc} = C_o \frac{dV_{dc}}{dt} + \frac{V_{dc}}{R_o} \end{array} \right. \quad (5.57c)$$

From this, one expects the possibility to achieve better dynamic performance. This will be confirmed through numerical simulation of a physical model dealing with three – phase AC/DC boost power converter for on - line UPS system in the next section.

5.5 Numerical simulation and verification

5.5.1 Implementation considerations

The schematic diagram of the proposed nonlinear adaptive output feedback control strategy of three-phase AC/DC boost power converter for on-line UPS systems described in Figure 5.7. This diagram consists of three - phase AC source, PWM rectifier, DC - link capacitor and equivalent resistive load. The system model is simulated using MATLAB/SIMPOWER toolbox (version R2015a). The system model composite from three - phase AC/DC boost power converter supplying three - phase equivalent resistive load, R_o with all numerical values listed in Table 5.2. All involved electrical components are simulated using *SIMPOWER* toolbox which offers a quite accurate representation of power system elements. Actually, the ODE1 (Euler) solver type is selected with a fixed step time of (1) μs . However, for practical implementation, one should further select a data sampling - time and use a digital signal processing DSP Card (*dSPACE*) for doing interfacing with all parts. Selection of sampling-time is performed by taking into account the controlled system dynamics. Actually, the dynamic of inner current loop is more rapid than an outer voltage control loop. So that, the time constant imposes the value of the sampling - time. As listed in Table 5.3, the electrical time constant, τ_e of the inner current control loop (which is faster response than the outer voltage control loop) is $\tau_e \leq 1/c_{max}$, $c_{max} = \max(c_d, c_q)$. Accordingly, the suitable value of the data sampling - time would be $50\mu s$. It should be mentioned that the only voltage sensor is needed in the control scheme of Figure 5.7.

More details about the fundamentals of well – known pulse width modulation PWM generation is found in appendix A.3 of the present thesis. More details about UPFC, DC

output voltage controller and adaptive observer design could be found in Figure (5.3) and Figure (5.5), respectively.

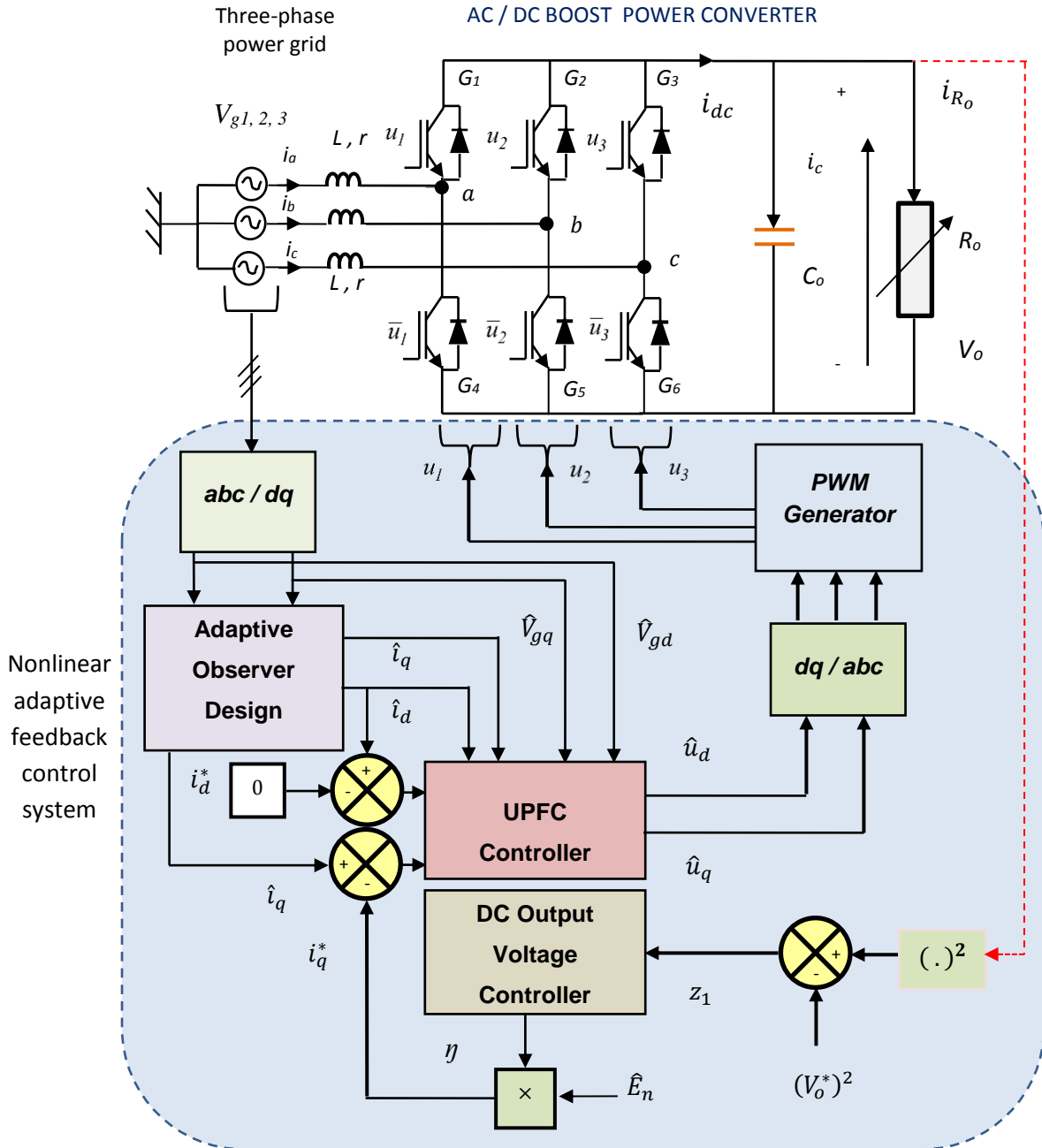


Figure 5.7: Block diagram of PFC tracking design and DC voltage regulator for on-line UPS.

5.5.2 Tracking performance in presence of constant load

The numerical simulation aims for illustrating the proposed controller behaviour in response to step change of the parameter uncertainty dealing with an amplitude of the grid -

phase voltage, θ_l starting from its nominal value, ($E_n = 311.127$ V) down to $0.8 * E_n$ (i.e. 248.902 V) at a time corresponding to 0.2 s and return up to its nominal value at a time corresponding to (0.4s). Meanwhile the equivalent resistive load is kept constant at its nominal value, $R_0 = 100 \Omega$. The criterion for selecting the resistive load must ensure that $1/R_0 C_o \ll \omega_s$, that is $R_0 \gg 1.592 \Omega$. As expected by Proposition 5.1, the dynamic behaviour of the adaptive observer within an inner current control loop is faster than outer voltage control loop which shows that the proposed adaptive controller is robust to external disturbances and critical load variation. Using trial and error approach for the best selection of filter capacitance that gives us a larger capacitance value makes sure the smaller ripple size as listed in Table 5.2.

The control design parameters c_{dq}, c_1, c_2, c_3 and observer design parameter, ρ_θ, ρ_x have been optimized using MATLAB as listed in Table 5.3 must be selected such that the inner current loop controller expressed by the tracking error vector $[z_{dq}]$ is faster than the outer voltage loop controller. In addition to Tables 5.2 and 5.3, the simulation profile of the grid phase voltage has the form shown in Figure 5.8, which step down to 80 % of its nominal value at (0.2) s and return back to its nominal value at (0.4) s. It shows that the estimated value of the grid phase voltage converges rapidly to its true value.

To get better imagination and performance of the proposed controller, it is observed that the estimated value of the equivalent resistive load provided by the adaptive observer converges exponentially to its true value after (0.1) s as specified in Figure 5.9. The numerical results of the proposed controller performances are illustrated in Figures 5.10 - 5.15 in the presence of constant resistive load and bounded uncertain of grid phase voltage. However, the measured and estimated values of output voltage, V_o converge to the desired reference level of (800V) with a good accuracy as shown in Figure 5.10. The output voltage estimate follows its desired reference signal with accuracy depends on the grid supply frequency: accurate output tracking at high frequency.

Furthermore, it is observed that output voltage ripples oscillate at the frequency of $2\omega_s$ (no more than two AC cycles), and their corresponding ripple values are totally small compared to their average values of the voltage signals. Figure 5.11 clarifies the correlation of the current amplitude in $(d - q)$ synchronous reference frame with the variation of input grid phase voltages such that $i_d = 0$. It is obvious from Figure 5.12 and Figure 5.13 that the effect of disturbance due to the uncertain parameter of main voltage source is well dynamically compensated by an adaptive output feedback controller design i.e. $\|u_d\| \leq 1, \|u_q\| \leq 1$

affected by harmonic distortion. Figure 5.14 shows the separate power factor estimation per phase and their product as a combined nonlinear characteristic of the AC/DC boost power converter. The power factor correction requirement is well established with system distortion factor less than 2% as described in Figure 5.15.

In the sequel, the three – phase PWM rectifier linked to the grid source voltage is achieved with power factor correction tends to unity. Off course, this will reflect usefulness on the quality performasnce and robustness of the proposed controller. The effect of electric parameter variation on the active and reactive power was investigated by the adaptive nonlinear controllers. Figure 5.17 shows the dynamic performance for active power in kW and zero convergence reactive power across the sensitive resistive load.

It is apparant from numerical simulation results that the closed – loop system has no stability problem and has satisfactory transient time response despite of system parameteric uncertanties and compared to the classical linear control approaches such as input – output feedback linearization technique. The strategy of the proposed control has been rigorous and robust *w.r.t* uncertain parameters and offers unity power factor and the size of output ripples are actually insignificant caused by input grid phase currents.

Table 5.2. AC/DC converter for UPS system characteristics

<i>Parameters</i>	<i>Symbol</i>	<i>Values</i>
Three phase network	$E_n / f_s / \varphi$	$220\sqrt{2}V / 50Hz / \frac{2\pi}{3}$
AC/DC Converter	L	$1mH$
	r	0.4Ω
	C_o	$2mF$
Nominal load resistance	R_o	100Ω

Table 5.3. Controller design parameters

Parameters	Symbol	Values
PFC Regulateur	c_d	$1 \times 10^4 \text{ s}^{-1}$
	c_q	$1 \times 10^4 \text{ s}^{-1}$
DC Output Voltage Regulator	h_1	$6.75 \times 10^{-7} \text{ V}^{-2} \Omega^{-1}$
	h_2	$3.3 \times 10^{-4} \text{ V}^{-2} \Omega^{-1} \text{ s}^{-1}$
	h_3	$6 \times 10^4 \text{ s}^{-1}$
Adaptive Observer	ρ_x	$5 \times 10^3 \text{ s}^{-1}$
	ρ_θ	$1 \times 10^2 \text{ s}^{-1}$

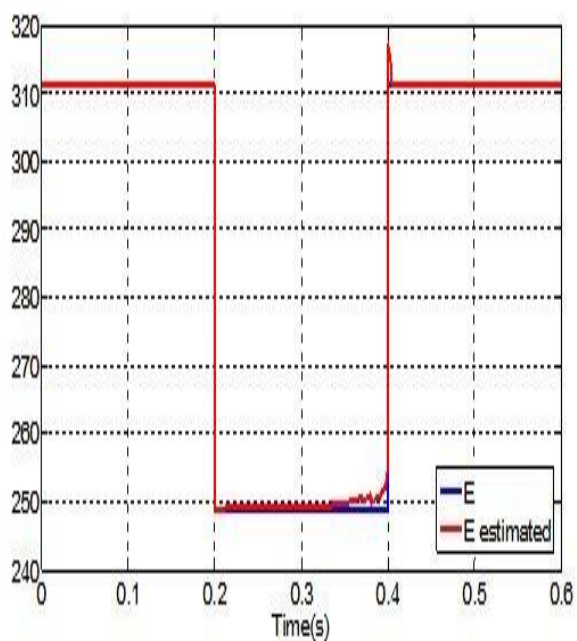


Figure 5.8: Grid voltage and its estimate (V) in presence of uncertain bounded grid phase voltage

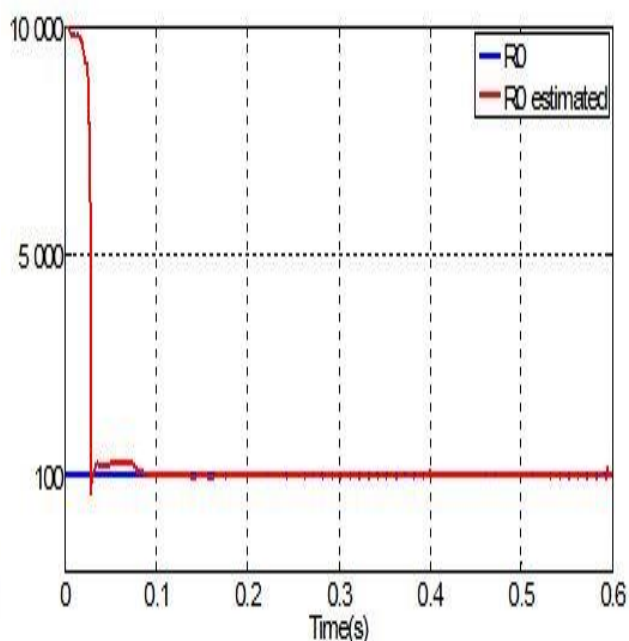


Figure 5.9: Uncertain resistive load and its estimate (Ω) in presence of constant load

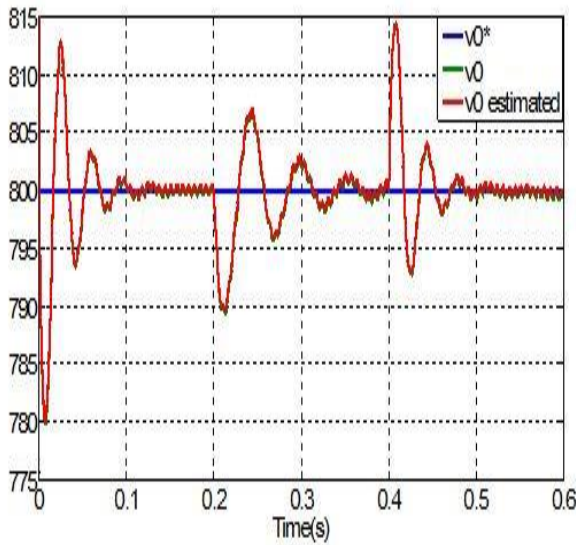


Figure 5.10: DC output voltage; its estimate and desired reference (V)

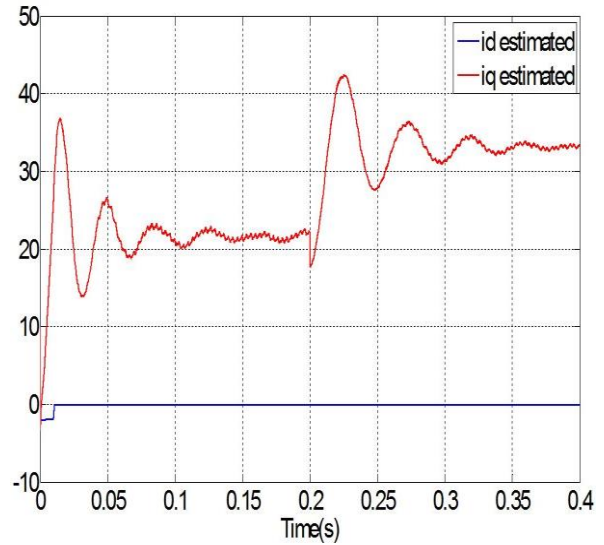


Figure 5.11: Input phase currents in (d - q) rotor frame (A)

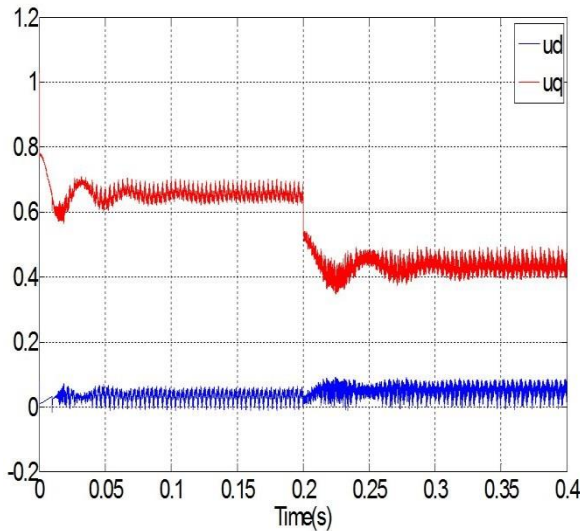


Figure 5.12: Inner control loop signals in (d - q) representation (V)

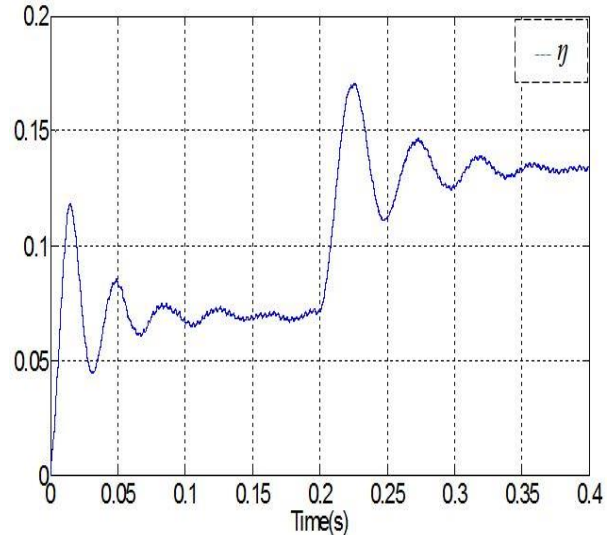


Figure 5.13: Dynamic performance of tuning control signal in response to input phase

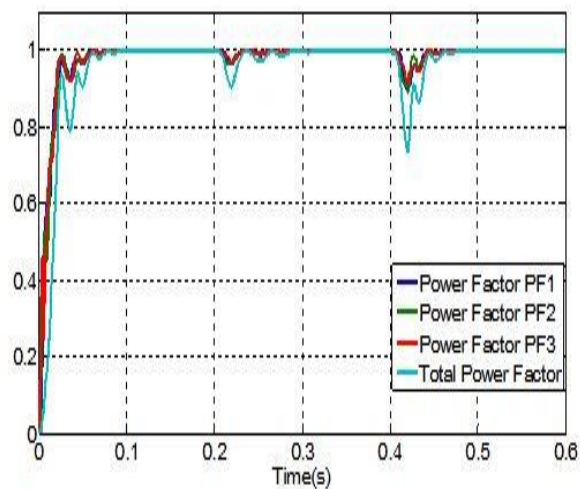


Figure 5.14: Power factor estimation of the three single - phase AC/DC converter

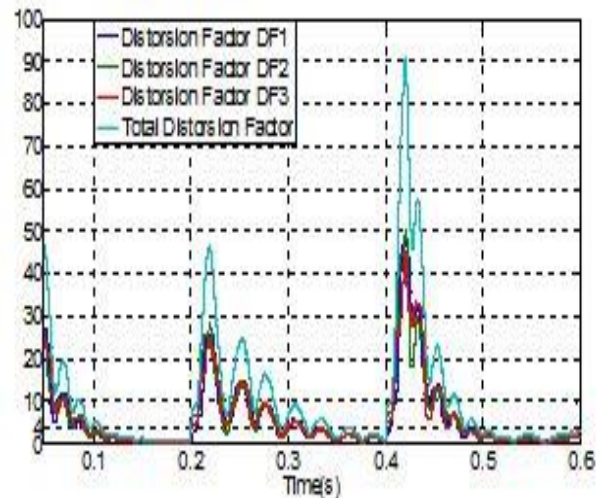


Figure 5.15: Dynamic performance for separate DF and total distortion factor

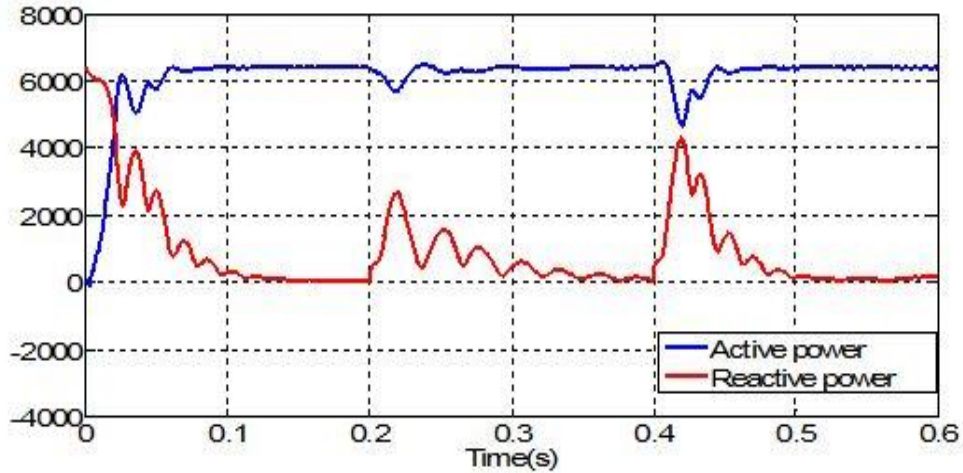


Figure 5.16: Dynamic performance of active and reactive power for first case

5.5.3 Control performance in presence of resistive load uncertainty

The robustness of the proposed nonlinear adaptive controller is tested by considering of unknown load change. Actually, the equivalent resistive load, $R_o = (\theta_2)^{-1}$ changes from its nominal value (100) Ω down to (80) Ω at a time (0.2) s and return to its nominal value at (0.4) s whilst the amplitude of grid phase voltages is kept unchanged at nominal value $E_n = 311.12 V$. The simulated profile of equivalent resistive load is further described by Figure 5.17. It shows the estimated load resistance $(\hat{\theta}_2)^{-1}$ provided by the adaptive observer for the state - affine system, tends exponentially to its true value after short transient time of (0.1) s.

To get a better appreciation of the proposed controller behaviour, it is observed that the estimated value of the grid phase voltage provided by adaptive observer converges exponentially after (0.1)s as illustrated in Figure 5.18. Figure 5.19 clarifies the variation of output voltage converges to its given reference signal with good accuracy whilst the estimated value converges quickly to its true value. Particularly, Figure 5.19 shows that the output voltage regulation is recovered after a short transient time following load change.

Also, Figure 5.20 illustrates the separate active power factor estimation per phase and their product as a combined nonlinear characteristic of the three – phase AC/DC boost power converter. The power factor correction achievement is well carried - out with total distortion factor less than 2% as shown in Figure 5.21. In such a way, the PWM rectifier connection to the grid source voltage is well established with a unity power factor. Figure 5.22 demonstrates

the dynamic performance of active power in (Watt) and zero convergence of reactive power in (Var) across the equivalent resistive load.

It is apparent from the numerical simulation, the second case output feedback controller design, dealing with resistive load uncertainty, achieves faster convergence compared to first one. The availability of function, bounds the unknown parameter, is employed in the designed controller.

The satisfying simulation results using Simulink/MATLAB environment for three - phase AC/DC boost power converter demonstrate the good performance and robust stability of the proposed nonlinear control algorithm *w.r.t* parameter variation, modeling uncertainty, measurement and system distortion factor. It has very good dynamic response to step change amplitude of main voltage and uncertain load resistance. Thus, the quality of the power system could be expressively enhanced and high reliability is provided.

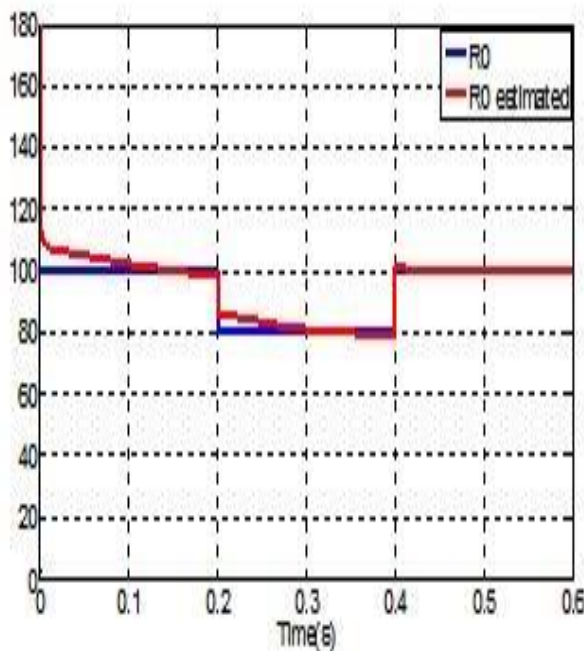


Figure 5.17: Resistive load and its estimate (Ω) in presence of load change

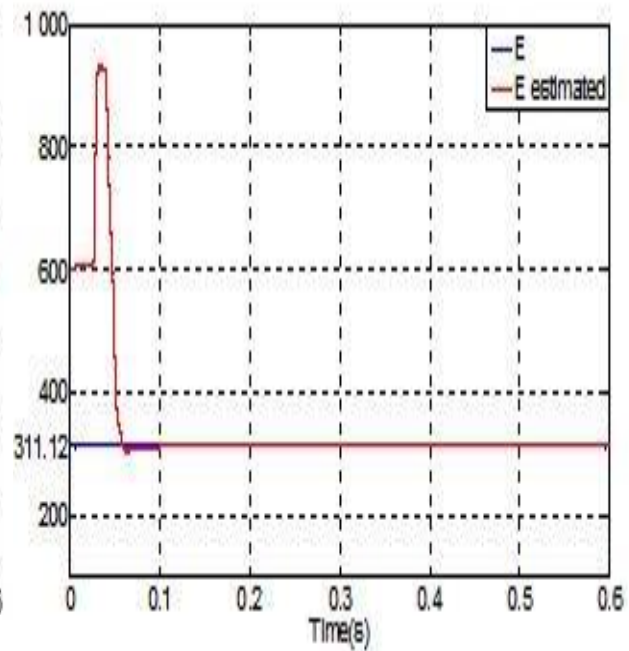


Figure 5.18: Grid phase voltage and its estimate in (V)

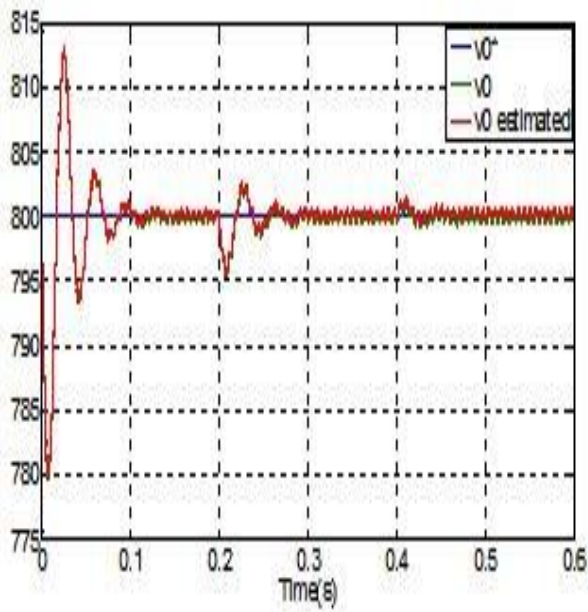


Figure 5.19: DC output voltage, its estimate and desired reference (V)

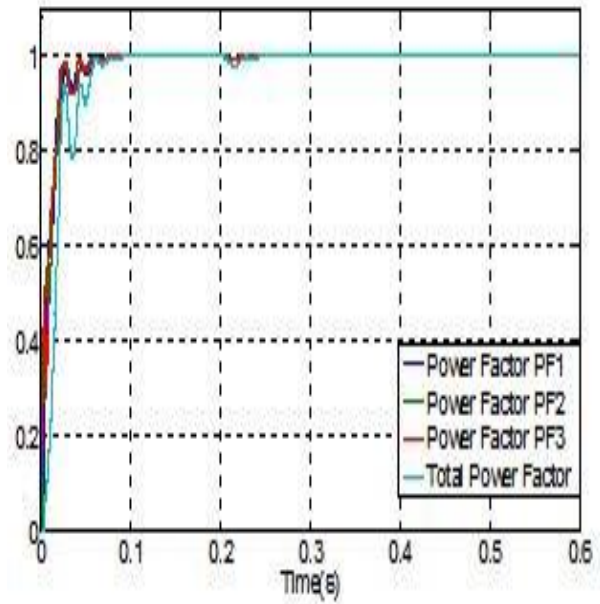


Figure 5.20: Power factor estimation of the three single-phase AC/DC converter

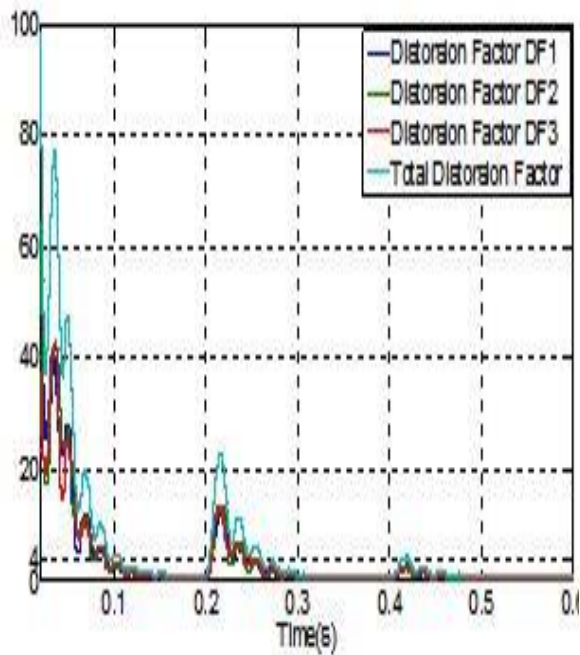


Figure 5.21: Dynamic performance for separate and total distortion factor

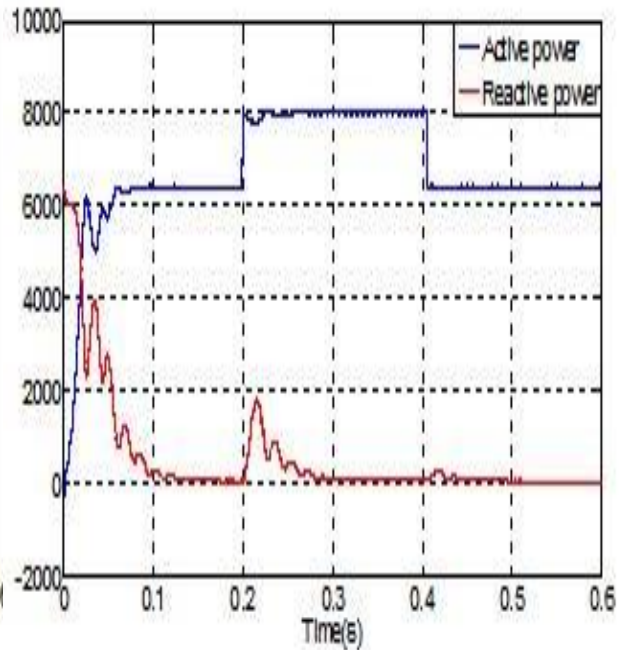


Figure 5.22: Dynamic performance for both active and reactive power for second case

5.6 Conclusions

This chapter covers an adaptive backstepping control design technique using the estimates provided by the adaptive observer to offer nonlinear output feedback controller application of on-line UPS system. The problem of controlling three-phase PWM AC/DC boost power converter has been achieved for on-line UPS system in response to parametric uncertainties. PFC close to unity and regulation of DC-bus voltage to a given reference level will reflect usefulness on converter performance and power quality. The power converter dynamics have been described by the third order nonlinear model projected on $(d-q)$ averaged-model. Based on the averaged-model, a cascade structure controller has been designed. Reference $(d-q)$ frame control strategy has been executed and investigated to minimize the THD raised by input currents, reactive power compensation, and power factor enhancement to ensure power quality at the input and the output terminals of VSC. It is observed throughout the present chapter that the developed algorithm is effective and efficient for improving power quality features such as power factor operation, DC-bus voltage regulation and harmonic mitigation.

The novelty of the present study resides in taking into account the difficulties and control complexities which are the nonlinearity nature of the system model and the uncertainty regarding with the amplitude of the grid phase voltages and equivalent load resistance. The additional feature of the present contribution is summarized by considering the input phase currents are inaccessible. This will lead us to achieve the possibility to reduce the number of appliances or even using soft sensors that will reflect positively on reliability of the power system, on-line monitoring of unmeasured quantities and for security purposes. Definitely, this estimate ensures fast clearing faults in the grid-side during milliseconds by providing command signals for activating the protection system without resorting to use the classical current sensors. These requirements are realized using nonlinear adaptive output feedback control system composed from the adaptive observer for state-affine system defined by equation (5.20), the inner current loop regulator stated in equation (5.37) and the outer voltage loop regulator defined by equation (5.40).

Specifically, it is shown that all control objectives presented in this chapter have been accomplished, successfully via an experimental study achieved by numerical simulation, including the PFC requirement and output voltage regulation. These control objectives are

compatible with technical features, starting from small units up to large units of on-line UPS systems used in some industrial processes .

On the other hand, the observability concept of the three – phase boost power converter has been highlighted. On the basis of some structural properties of three – phase AC/DC boost converter, this chapter shows in the rank sense that is possible design of an adaptive observer for on-line estimates of unmeasured quantities for getting an accurate adaptive output feedback controller even in presence of singular control inputs *i.e.*, $\hat{u}_d = 0, \hat{u}_q = 0$. Thus, the system model expressed by equation (5.8) could be presented by reduced - model according to detectability property.

It is proved, supported by simulation results that the convergence analysis of adaptive observer is GES *w.r.t Lyapunov* function candidate. Also, the dynamic performance of the nonlinear adaptive output feedback controller is GAS with progressive time using the tools of *Lyapunov* stability theory. The additional contribution of this study lies in the Simulink implementation is based on analytical solutions for the system state variables and parameter estimate in terms of switching control inputs (*i.e.* \hat{u}_d, \hat{u}_q and η). The proposed output feedback nonlinear adaptive controller has many interesting features which are good dynamic behavior, good harmonic mitigation, tightly DC output voltage regulation and fast transient time response to sudden changes in the simulation profile of resistive load and amplitude of input supply voltage. These features are very important in such applications.

The searcher expects based on his knowledge in this field that the present study is the first attempt in the field of nonlinear adaptive output feedback control strategy has been accomplished for three - phase AC/DC boost power converter. This resides in consideration the uncertain parameters for amplitude of grid phase voltage and equivalent resistive load at the input and the output terminals of VSC running within on-line UPS system.

Chapter Six

General Conclusion and Perspectives

Table of Contents	page
6.1 General conclusions	162
6.2 Suggestions for future works	165

In present chapter, summary of the obtained main results and the concluding remarks are highlighted with potential recommendations for future works. The searcher propose several directions in which results of the current thesis can be further expanded and modified for achieving better performances.

6.1 General conclusions

Among the major objectives of the current thesis is discovering and developing design techniques for on-line estimations of unmeasured quantities such as rotor speed, rotor position, electromagnetic torque, disturbance torque and parametric uncertainties in some kinds of AC machines and on-line UPS based on electrical injection measurements. Those techniques have been used to replace the data collection about system states provided by classical hardware sensors. Subsequently, software sensors are sometimes called intelligent sensors or smart sensors running with smart systems or smart networks. Basically, those sensors depend on mathematical models for system state equations and using on-line input/output injection measurements to provide real - time estimations of physical quantities. As a result, the state observer synthesis can be used directly for output feedback control systems or employed for faults diagnosis in electrical power systems and many applications. In chapter one, general introduction and brief review for development of synchronous machine drives, continuous – time nonlinear state observers, sampled – data nonlinear state observer design, electrical power system control techniques, and the configuration of WPGS. Mathematical models for some kinds of AC drives and control fundamentals for on-line stabilization of nonlinear systems have been presented in chapter two. PMSM variable speed drive applications are receiving more and more interest because of their better dynamic performances, steady state response and better efficiency compared to other AC and DC drives.

Chapter 6: General Conclusion and Perspectives

The present thesis has been discussed the state observers for a class of MIMO nonlinear system running with some kinds of AC machine drives or equipped with variable speed grid - connected WPGS. Different kinds of constraints linked in particular to nonlinear controlled systems integrated with electrical grid. The major targets of the current thesis can be divided in three contributions.

The first contribution of current thesis is proposed a hybrid observer for a class of MIMO nonlinear globally *Lipschitz* systems based sampled - output measurements and application of variable speed PMSM derive. The problem of on-line estimation of rotor position, motor speed and external load torque of the PMSM has been addressed, successfully. Theoretically, this problem can be coped with existing state observers. However, the latter present several limitations reside in output measurements in CTM and the necessity of persistently exciting signals. These limitations make previously proposed observers not quite suitable for applications in industrial processes. For systems with external disturbances, ISS concept had been changed the local concept of total stability with a more useful global concept. This concept plays a vital role in stabilization of adaptive and non-adaptive version for nonlinear systems. Technical hypotheses are used for analyzing the stability convergence of the proposed observer. Using these hypotheses, the searcher will present some new results on designing state observers for a class of nonlinear systems. Based on these theoretical results, it could be developing a computation algorithm to achieve global stabilization of nonlinear systems. The technical features of the proposed observer are achieved by combining the benefits of high-gain design approach and inter- sample time prediction. The main benefit of the proposed state observer that all system state estimates are remained in CTM just sampled output measurements. It has been derived a sufficient condition for the maximum allowable sampling time interval, τ_{MASP} that ensures fast tracking response and an exponential convergence of the observation error towards zero using tools of *Lyapunov* stability theory. The recent developments of lower cost systems through DSP and advanced power electronic components make wide range applications of the proposed sampled - output HGO design. Fast dynamic response, robustness against external disturbances, accurate tracking response, smooth motion at low speeds and efficient operation at high speeds are considered important criteria of high performance systems.

The second contribution of the present thesis tackled with designing of non – standard sampled - output HGO for a class of non *Lipschitz* reduced - model application of variable

speed DFIG based WPGS. The originality of the current study resides in complexities faced this work, which are output states are considered inaccessible. The additional feature involved with the electromagnetic torque created by DFIG generator is non – injective output relation, unlike in previous contribution dealing with sampled - output observer design.

It is apparent that the sampled output reduced – order state observer does not involve *ZOH* device in construction of innovation correction term. The present observer includes inter - sample prediction signal within innovation correction term. On the other hand, the saturated process $\sigma(w(t))$ is closer to the generator current $i(t)$ than $w(t)$. It is expected that the proposed observer has better performance. The proposed HGO will be faster than the basic version without involving saturation process. Tools of *Lyapunve* stability theory and ISS concept have been used to determine the convergence conditions of the error system dynamics using two steps.

For every compact set of initial conditions, one can design an output feedback controller that stabilizes the origin and includes the given compact set in the ROA. The originality of the third contribution resides in taking into consideration the difficulties and control problem complexity which are the non-linearity of the system dynamics and parametric uncertainties regarding with the magnitude of grid phase voltages sinusoidally bounded and load resistance constant but unknown parameter. The additional feature of the third contribution is summarized by considering the input phase currents are inaccessible. This will lead us to discover the possibility of reducing number of sensors or even using software sensors that will reflect usefulness on reliability of power system and security purposes.

Since, the input phase currents are considered inaccessible, this will lead us to discuss the problem of power factor estimation and total harmonic mitigation. These requirements are realized using nonlinear adaptive output feedback control system composed from adaptive observer for state - affine system. The main parts of control system are inner current loop regulator and the outer voltage loop regulator. Inner regulator is used to ensure unity power factor correction by regulating the actual input phase current to a given specified reference signal. Outer regulator is built up to achieve tightly voltage regulation to a given reference voltage level across the equivalent resistive load.

6.2 Suggestions for future works

The scientific contribution that has been conducted in the present thesis, it can be extended in different directions and selection of the best approach is application - dependent:

- 1- The obtained results for sampled - output measurements can be used in designing of output - feedback controller for large scale WPGS integrated with extra high voltage networks.
- 2- Extend the proposed state observer for a class of cascade interconnected state - affine systems combined with inter – sampled behaviour.
3. Simulation and implementation the present sample study in real - time using a hardware prototype of *DSTATCOM* including (*dSPACE DS1104 R&D* controller having TMS320F240 as slave DSP), that will show the benefits from the practical view point.
4. The power electronics converter can be easily extended to matrix converter application on WPGS allowing the simulation of complex power electronics structures. Also, different converter topologies can be implemented to achieve better control process.
5. Focus on global adaptive or non-adaptive output feedback control design of variable speed DFIG based wind turbine without resorting to use mechanical or magnetic sensors to extract maximum power provided to the electrical grid.
- 6- Investigation of the adaptive observer design for nonlinear continuous-time systems: application to fault diagnosis for on-line UPS system taking into consideration the effect of loading and non-loading of sensitive loads.

Appendices

The *Clarke's* and *Park's* transformations are important for implementing vector control methods. Basically, *Clarke's* transformation converts the (abc) stationary quantities to the $(\alpha - \beta)$ quantities. Whilst *Park's* transformation converts the $(\alpha - \beta)$ quantities to the $(d - q)$ rotating quantities [see *e.g.* Chattopadhyay et al., 2010].

A1. Clarke's transformation

To simplify the modeling of the field oriented control drive system, it is common practice to transform system state variables from the three – phase system (abc) to an orthogonal $(\alpha - \beta)$ representation or $(d - q)$ rotating reference frame with a direct (d) and quadrature (q) axis, where the resultant f denotes either the stator voltage, current or magnetic flux linkage and θ_r is the rotor position angle of the rotating $(d - q)$ reference frame.

$$\begin{bmatrix} f_\alpha \\ f_\beta \end{bmatrix} \triangleq \frac{2}{3} \begin{bmatrix} 1 & -\frac{1}{2} & -\frac{1}{2} \\ 0 & \frac{\sqrt{3}}{2} & -\frac{\sqrt{3}}{2} \end{bmatrix} \begin{bmatrix} f_a \\ f_b \\ f_c \end{bmatrix} \quad (\text{A.1})$$

$$\begin{bmatrix} f_\alpha \\ f_\beta \end{bmatrix} = [\text{Clarke Matrix}] \begin{bmatrix} f_a \\ f_b \\ f_c \end{bmatrix}$$

where,
$$[\text{Clarke Matrix}] \triangleq \frac{2}{3} \begin{bmatrix} 1 & -\frac{1}{2} & -\frac{1}{2} \\ 0 & \frac{\sqrt{3}}{2} & -\frac{\sqrt{3}}{2} \end{bmatrix}$$

It is obvious from Figure A.1, the resultant physical quantity from $(\alpha - \beta)$ representation is:

$$f = \sqrt{f_\alpha^2 + f_\beta^2} \quad (\text{A.2})$$

A2. Park's transformation

The *Park's* transformation has been widely used in the analysis of synchronous and induction machines. The novelty of *Park's* work involves his ability to transform any related machine's equation set from time varying coefficients to another with time invariant coefficients.

$$\begin{bmatrix} f_\alpha \\ f_\beta \end{bmatrix} \triangleq \begin{bmatrix} \cos(\theta_r) & -\sin(\theta_r) \\ \sin(\theta_r) & \cos(\theta_r) \end{bmatrix} \begin{bmatrix} f_d \\ f_q \end{bmatrix} \quad (\text{A.3})$$

Appendices

$$\begin{bmatrix} f_\alpha \\ f_\beta \end{bmatrix} = [\text{Park Matrix}] \begin{bmatrix} f_d \\ f_q \end{bmatrix}$$

where,
$$[\text{Park Matrix}] \triangleq \begin{bmatrix} \cos(\theta_r) & -\sin(\theta_r) \\ \sin(\theta_r) & \cos(\theta_r) \end{bmatrix}$$

From equation A.1 and A.3, one has:

$$\begin{bmatrix} f_d \\ f_q \end{bmatrix} = \frac{2}{3} \begin{bmatrix} \cos(\theta_r) & \cos\left(\theta_r - \frac{2\pi}{3}\right) & \cos\left(\theta_r - \frac{4\pi}{3}\right) \\ -\sin(\theta_r) & -\sin\left(\theta_r - \frac{2\pi}{3}\right) & -\sin\left(\theta_r - \frac{4\pi}{3}\right) \end{bmatrix} \begin{bmatrix} f_a \\ f_b \\ f_c \end{bmatrix} \quad (\text{A.4})$$

with,
$$\frac{2}{3} \begin{bmatrix} \cos(\theta_r) & \cos\left(\theta_r - \frac{2\pi}{3}\right) & \cos\left(\theta_r - \frac{4\pi}{3}\right) \\ -\sin(\theta_r) & -\sin\left(\theta_r - \frac{2\pi}{3}\right) & -\sin\left(\theta_r - \frac{4\pi}{3}\right) \end{bmatrix} = [\text{Park Matrix}][\text{Clarke Matrix}]$$

It is obvious from Figure A.1 that the resultant physical quantity from $(d - q)$ representation is :

$$f = \sqrt{f_d^2 + f_q^2} \quad (\text{A.5})$$

The two phases (α, β) frame representation calculated with the *Clarke's* transform is then fed to a vector rotation block where it is rotated over an angle θ_r to follow the (d, q) reference frame attached to the rotor quantity. The rotation over an angle θ_r is done according to the above formulas. Figure A.1 shows combined vector representation for three – phase systems.

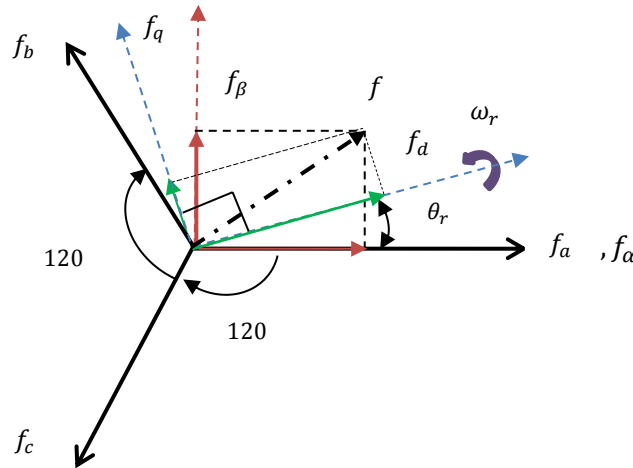


Figure A.1: Combined stationary and rotating frames for three - phase system

A3. Pulse width modulation (PWM) generation

Pulse width modulation (PWM) is a way of delivering energy through a succession train of pulses rather than a continuously varying signal. By increasing or decreasing pulse width, the controller regulates energy flow to the controlled system. Figure A.2 shows circuit diagram for pulse width modulation generator. There are several approaches to generate converter control signals to achieve PWM in field oriented controlled drive systems [Khater et al., 2013].

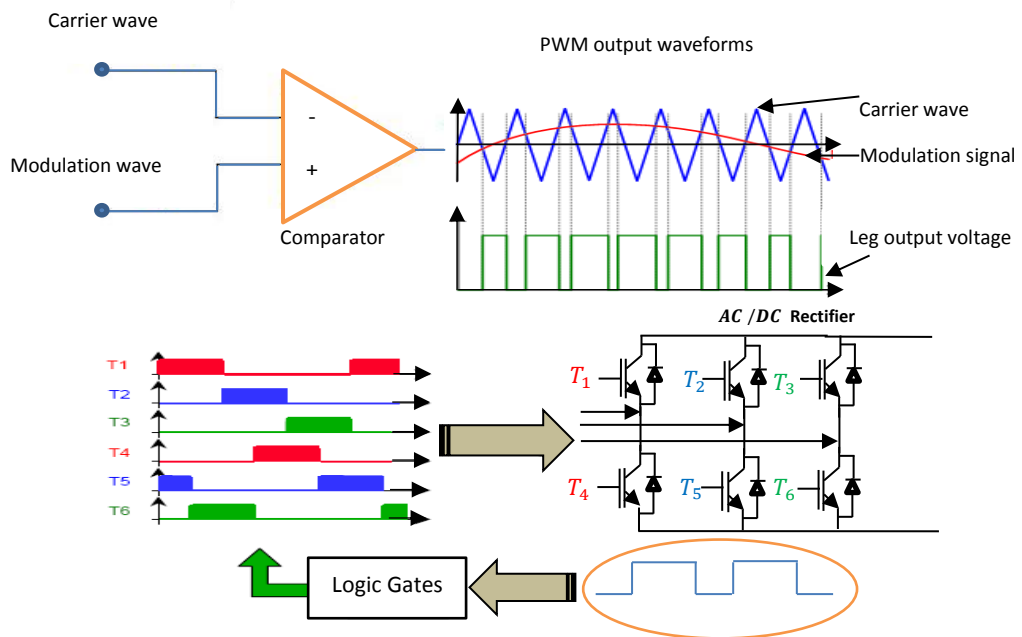


Figure A.2: Circuit diagram for pulse width modulation generator

A4. Derivation of wind power equation

Wind power captured by a VSWT system, can be derived using the well – known wind kinetic energy denoted by E_w as follows [Heir, 2009]:

$$E_w \triangleq \frac{1}{2} m V_w^2 \quad (\text{A.6})$$

where, m is the air - mass in kg , which passes through the blades of a wind turbine, V_w the wind velocity in m/s . By differentiating (A.6) *w.r.t* time index, the wind power is derived as:

$$P_w \triangleq \frac{dE_w}{dt} = \frac{1}{2} \frac{dm}{dt} V_w^2 \quad (\text{A.7})$$

Appendices

Actually, m is computed by multiplying the air - density, ρ in kg/m^3 by the air - volume around the rotor blade. So, the rate of change of air - mass, *w.r.t* time index is:

$$\frac{dm}{dt} \triangleq \rho A_w \frac{dx}{dt} \quad (A.8)$$

where, A_w is the swept area in m^2 around the rotor blades as clarified in Figure A.3 and x is the distance of transferring air - mass, m , through the swept area around the rotor blade.

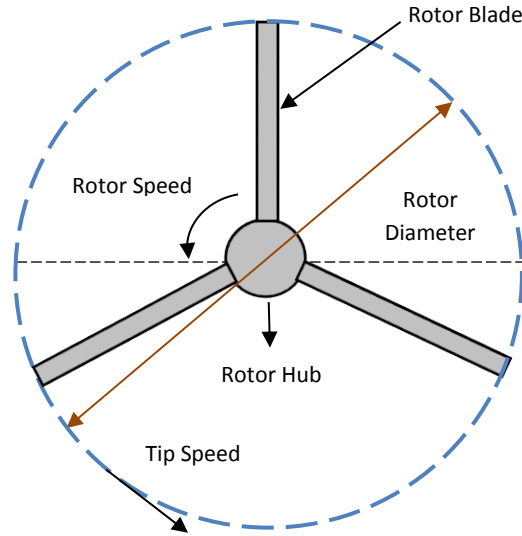


Figure A.3: Schematic diagram of a HAWT for three blades

Combining equation (A.8) in equation (A.7), the wind power, P_w is represented as:

$$P_w = \frac{1}{2} \rho A_w \frac{dx}{dt} V_w^2 \quad (A.9)$$

Replacing, $\frac{dx}{dt}$ with wind velocity, V_w , equation (A.9), becomes.

$$P_w = \frac{1}{2} \rho A_w V_w^3 \quad (A.10)$$

It is readily shown in equation (A.10) that aerodynamic power in (Watt) is proportional to the cubic of wind velocity and the swept area of the rotor blades.

A5. Derivation of wind turbine efficiency

Practically, the actual wind turbine power, P_{wt} , is much less than wind power, *i.e.* $P_{wt} < P_w$ depending on power conversion efficiency, so - called the power coefficient, C_p . So, P_{wt} is given by [see *e.g.* Ochieng et al., 2014]:

$$P_{wt} \triangleq \frac{1}{2} \rho A_w C_p V_w^3 \quad (A.11)$$

Appendices

It should be mentioned that C_p can be computed by applying the momentum theory of wind turbine as shown in Figure A.4, knowing that V_{up} , V_w , and V_{down} are designated the wind velocity on upstream of the wind turbine, at the wind turbine and on downstream of the wind turbine, respectively. A_{up} , A_w , and A_{down} are defined the swept areas on upstream of the wind turbine, at the wind turbine and on downstream of the wind turbine, respectively. Logically, $V_{up} > V_w > V_{down}$ and on the other side, $A_{up} < A_w < A_{down}$. Depending on the continuity theorem of transferring air through a certain pipeline, the multiplication result of the non – uniform area and its corresponding wind velocity as it is at any point in the pipeline, *i.e.*,

$$A_{up} V_{up} = A_w V_w = A_{down} V_{down} \quad (\text{A.12})$$

As shown in Figure A.4, the wind turbine captures part of wind kinetic energy and the corresponding steady – state wind turbine power, P_{wt} can be computed as follows:

$$P_{wt} = \frac{1}{2} \rho A_{up} V_{up}^3 - \frac{1}{2} \rho A_{down} V_{down}^3 \quad (\text{A.13})$$

Rewriting equation (A.13) in the following form:

$$P_{wt} = \frac{1}{2} \rho (A_{up} V_{up}^3 - A_{down} V_{down}^3) \quad (\text{A.14})$$

From equation (A.12), A_{up} and A_{down} can be obtained using equations (A.15) and (A.16), respectively.

$$A_{up} V_{up} = A_w V_w \rightarrow A_{up} = \frac{A_w V_w}{V_{up}} \quad (\text{A.15})$$

$$A_{down} V_{down} = A_w V_w \rightarrow A_{down} = \frac{A_w V_w}{V_{down}} \quad (\text{A.16})$$

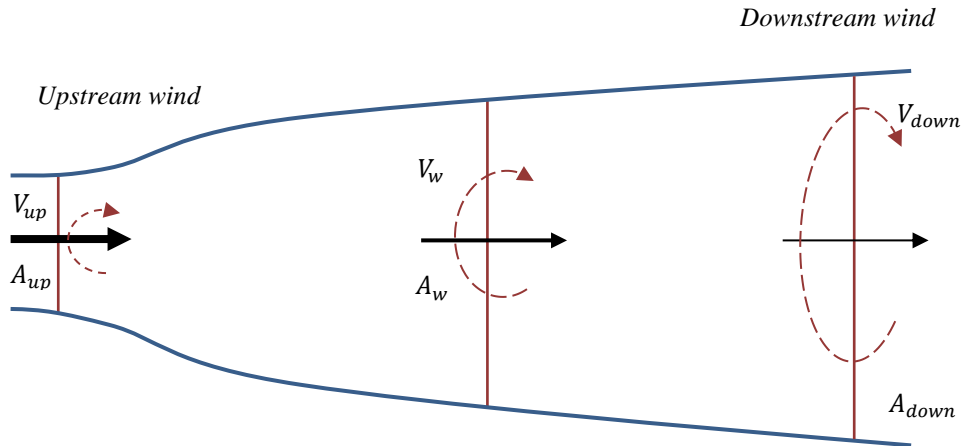


Figure A.4: Distribution of wind around a wind turbine system

Appendices

Perfectly, V_w is proposed by the average value: $V_w \triangleq \frac{V_{up} + V_{down}}{2}$ (A.17)

Substituting equations defined in (A.15) and (A.16) in equation (A.14), gives:

$$P_{wt} = \frac{1}{2} \rho A_w \left[\frac{V_w}{V_{up}} V_{up}^3 - \frac{V_w}{V_{down}} V_{down}^3 \right] \quad (A.18)$$

Once again, combining equation (A.17) in equation (A.18), one has the following:

$$P_{wt} = \frac{1}{4} \rho A_w [V_{up}^3 - V_{up} V_{down}^2 + V_{down} V_{up}^2 - V_{down}^3] \quad (A.19)$$

To obtain the maximum theoretical efficiency of a wind turbine, the first derivative of equation (A.19) *w.r.t* V_{up} must be equal to zero as follows:

$$\frac{dP_{wt-the}}{dV_{up}} = \frac{d}{dV_{up}} \left[\frac{1}{4} \rho A_w (V_{up}^3 - V_{up} V_{down}^2 + V_{down} V_{up}^2 - V_{down}^3) \right] = 0 \quad (A.20)$$

where, P_{wt-the} is the maximum theoretical wind turbine power that be achieved from a wind turbine. Then, equation (A.20) is re-written as:

$$\frac{d}{dV_{up}} [V_{up}^3 - V_{up} V_{down}^2 + V_{down} V_{up}^2 - V_{down}^3] = 0 \quad (A.21)$$

Or equivalently, equation (A.21) becomes:

$$3V_{up}^2 + 2V_{up}V_{down} - V_{down}^2 = 0 \quad (A.21)$$

The mathematical solution of equation (A.21) is given by (A.22).

$$V_{up} = 3V_{down} \quad (A.22)$$

Now, combining equation (A.22) in equation (A.19), the maximum theoretical wind turbine power, P_{wt-the} is:

$$P_{wt-the} = \frac{1}{2} \rho A_w \left(\frac{16}{27} \right) V_w^3 \quad (A.23)$$

where, $\left(\frac{16}{27} \right) \cong 59.3\%$ is the maximum achievable value of wind turbine power efficiency, C_p , which is known as the *Betz limit*. It is accomplished when an interference factor,

$$k_{int} \triangleq \frac{V_{down}}{V_{up}} = \frac{1}{3} \quad (A.24)$$

From the practical view point, the maximum power coefficient is much less than the *Betz limit*. Really, it depends on the blades shape and type of wind turbines, such as HAWT or VAWT. Moreover, power coefficients are not often given as the function of, k_{int} , but as function of, λ_{TSR} , and blade pitch angle, β which is the angle at which the blade surface of a

Appendices

wind turbine contacts winds [Bianchi et al., 2007]. λ_{TSR} is defined as the ratio of a turbine blade tip speed to wind speed:

$$\lambda_{TSR} \triangleq \frac{\omega_r R}{V_w} \quad (\text{A.25})$$

In view of equation stated in (A.11), the power captured by a WPGS is mainly affected by the following factors:

1. Swept area of a wind turbine around the rotor blade, A_w
2. Cubic wind velocity in (m/s), V_w
3. Power conversion efficiency of a wind turbine, C_p

It is readily seen that the only controllable factor is the power coefficient, C_p which can be adjusted at its maximum value by regulating a tip speed ratio, λ_{TSR} or a blade pitch angle, β . The former regulator is designated for controlling WPGS as follows. For each wind velocity, there is an optimal tip speed ratio that keeps the power coefficient at its maximum. To achieve, λ_{opt} , it is required to control rotor speed to track reference rotor speed to guarantee MPPT control strategy.

Bibliography

- [Al – Tahir, 2012] Al – Tahir, A.A. (2012). Modeling and control of hybrid system wind turbine generators, photovoltaic arrays and deep cycle batteries to feed green power. *World Academy of Science, Engineering and Technology*, 64 (2012): 1298 - 1312.
- [Al – Tahir, 2012] Al – Tahir, A.A. (2011). Economic and cost analysis for hybrid wind, photovoltaic power and rechargeable batteries. *1st Scientific Conference of Energy*: 145 -155
- [Ahmed – Ali et al., 2013] Ahmed – Ali, T. Karafyllis, I., Lagarrigue, F.L. (2013). Global exponential sampled – data observer for nonlinear systems with delayed measurements. *Systems and control Letters*, 62(7): 539 – 549.
- [Ahmed-Ali, 2012] Ahmed-Ali, T. (2012). High gain observer design for some networked control systems. *IEEE Transactions on Automatic Control*, 57 (4): 995-1000.
- [Ahmed-Ali et al., 2009] Ahmed-Ali, T. Postoyan, R., Lagarrigue F. L. (2009). Continuous - discrete adaptive observers for state affine systems. *Automatica*, 45(12): 2986 - 2990.
- [Abdelhak et al., 2015] Abdelhak, B., Bachir, B. (2015). A High gain observer based sensorless nonlinear control of induction machine. *International Journal of Power Electronics and Drive System (IJPEDS)*, 5 (3): 305-314.
- [Alvi et al., 2016] Alvi, M., Sharma, R. (2016). Modelling and simulation of DFIG for wind energy generation using stator voltage orientation control. *International Journal of Engineering Research and Applications*, 6 (2): 97-101.
- [Abouloifa et al., 2004] Abouloifa, A., Giri, F., & Lachkar, I. (2004). Voltage regulation of AC-DC PWM rectifier using nonlinear control techniques. *Electromotion - Cluj napoca*: 157-165.
- [Allag et al., 2007] Allag, A., Hammoudi, M., Mimoune, S., Ayad, M., Becherif, M., and Miraoui, A. (2007). Tracking control via adaptive backstepping approach for a three phase PWM AC-DC converter. *IEEE International Symposium on Industrial Electronics, ISIE*: 371 - 376.
- [Amirat et al., 2007] Amirat, Y., Benbouzid, M.E.H, Bensaker, B., Wamkeue, R. (2007). Generators for wind energy conversion systems: state of the art and coming attractions. *Journal of Electrical Systems*, 3(1): 26 – 38.
- [Amir et al., 2016] Aamir, M., Kalwar, K.A., Mekhilef, S. (2016). Review: uninterruptable power supply (UPS) system. *Renewable and sustainable energy reviews*, 58(2016): 1395 – 1410.
- [Andrieu et al., 2013] Andrieu, V., Besancon, G., Serres, U. (2013). Observability necessary conditions for the existence of observers. *52nd IEEE Conference on Decision and Control (CDC)*: 4442 – 4447.

- [Aranovskiy et al., 2015] Aranovskiy, S., Bobtsov, A.A. (2015). Flux and position observer of permanent magnet synchronous motor with relaxed persistency of excitation conditions. *1'st IFAC Conference on Modelling, Identification and Control of Nonlinear Systems*, 48(11): 311 – 316.
- [Arcak et al., 2004] Arcak, M., D. Nešić. (2004). A framework for nonlinear sampled- data observer design via approximate discrete-time models and emulation. *Automatica*, 40 (11):1931–1938.
- [Archna et al., 2014] Archna, A., Mohan, S. L., Bhim, S. (2014). Control strategies for DFIG based grid connected wind energy conversion system. *International Journal of Grid Distribution Computing*, 7 (3): 49-60.
- [Baras et al., 1988] Baras, J., Bensoussan, A., James, M. (1988). Dynamic observers as asymptotic limits of recursive filters: special cases. *SIAM Journal on Applied Mathematics*, 48(5): 1147–1158.
- [Barra et al., 2014] Barra, A., Ouadi, H., (2014). Sensorless speed and reactive power control of a DFIG – wind turbine. *Journal of Theoretical and Applied Information Technology*, 62(2):325 – 334.
- [Baroudi et al., 2007] Baroudi, J. A, Dinavahi, V., Knight, A.M. (2007). A review of power converter topologies for wind generators. *Renewable Energy*, 32 (2007): 2369 – 2385.
- [Bastin et al., 1988] Bastin, G., Gevers M.R (1988). Stable adaptive observers for nonlinear time-varying systems. *IEEE Transactions on Automatic Control*, 33(7):650 - 658.
- [Benchabane et al., 2011] Benchabane, F., Titaouine, A., Bennis, O., Guettaf, A., Yahia, K., Taibi, D. (2011). Robust position and speed estimation algorithms for permanent magnet synchronous drives. *European Journal of Scientific Research*, 57 (1): 6 -14.
- [Benelghali et al., 2010] Benelghali, M., Benbouzid, E.H., Charpentier, J.F. (2010). Comparison of PMSG and DFIG for marine current turbine applications. *XIX International Conference on Electrical Machines*: 1- 6.
- [Benchabane et al., 2012] Benchabane, F., Titaouine, A., Bennis, O., Yahia, K., Yaibi, D., Guettaf, A. (2012). Sensorless direct torque control for salient – pole PMSM based on extended Kalman filter fed by AC/DC/AC converter. *Frontiers in Energy*, 6(3): 247 – 254.
- [Benchabane et al., 2011] Benchabane, F., Titaouine, A., Bennis, O., Guettaf, A., Yahia, K., Taibi, D. (2011). Robust position and speed estimation algorithms for permanent magnet synchronous drives. *European Journal of Scientific Research*, 57 (1): 6 -14.
- [Besançon et al., 2003] Besançon, G., De León-Morales, J., and Huerta-Guevara, O. (2003). On adaptive observers for state affine systems and application to synchronous machines. *42'nd IEEE Conference on Decision and Control CDC Maui, Hawaii USA, December*, 3(2003):2192 - 2197.
- [Besançon, 2007] Besançon, G. (2007). *Nonlinear observers and applications*. ISBN -10 3-540 - 73502-X Springer Berlin Heidelberg New –York.

- [Beltran et al., 2011] Beltran, B. Benbouzid, M.E.H, Ahmed-Ali T. Mangel, H. (2011). DFIG - based wind turbine robust control using high-order sliding modes and a high gain observer. *International Review on Modelling and Simulations*, 4(3):1148 - 1155.
- [Bhattacharya, 2014] Bhattacharya, M. (2014). Improvement power quality using PWM rectifier. *International Journal of Scientific and Research Publications*, 4(7):1 -11.
- [Bianchi et al., 2007] Bianchi, D., Battista, H., Mantz, R.(2007). Wind turbine control systems: principles, modelling and gain scheduling design. *Springer, London*, ISBN 9781846284939.
- [Bobtsov et al., 2015] Bobtsov, A., Pyrkin, A., Ortega, R., Vukosavic, S., Stankovic, A., Panteley, E. (2015). A robust globally convergent position observer for permanent magnet synchronous motor. *Automatica*, 61(2015): 47 – 54.
- [Boussak, 2008] Boussak, M. (2005). Implementation and experimental investigation of sensorless speed control with initial rotor position estimation for interior permanent magnet synchronous motor drive. *IEEE Transactions on Power Electronics*, 20 (6): 1413 – 1422.
- [Bolognani et al., 2003] Bolognani, S., Tubiana, L., Zigliotto, M. (2003). Extended Kalman filter tuning in sensorless PMSM drives, *IEEE Transactions on Industry Applications*. 39 (6):1741–1747.
- [Bose, 2002] Bose, B. K. (2002). Modern power electronics and AC drives: *Prentice Hall*, ISBN-10: 0130167436.
- [Boldea et al., 2010] Boldea,I. and Nasar, S. (2010). *The induction machine handbook*. *CRC Press, Taylor & Francis Group*, ISBN 9780849300042.
- [Bossoufi et al., 2015] Bossoufi, B., Karim, M., Lagrioui, A., Taoussi, M., Derouich, A. (2014). Observer backstepping control of DFIG-Generators for wind turbines variable-speed: FPGA-based implementation. *Renewable Energy*, 81 (2015) 903-917.
- [Boukhezzar et al., 2009] Boukhezzar, B., Siguerdidjane, H. (2009). Nonlinear control with wind estimation of a DFIG variable speed wind turbine for power capture optimization. *Energy Conversion and Management*, 50 (2009): 885-892.
- [Brandstetter et al., 2013] Brandstetter, P., Krecek, T. (2013). Sensorless control of permanent magnet synchronous motor using voltage signal injection. *LEKTRONIKA IR ELEKTROTECHNIKA*, 19 (6): 19 – 24.
- [Bridges et al., 1995] Bridges, M. M., Dowson, D. M., Abdallah, C. T (1995). Control of rigid-link, flexible - joint robots: a survey of backstepping approach. *Journal of Robotic Systems*, 12(3):199 – 216.
- [Cárdenas, et al., 2004] Cárdenas, R., Pena, R., Proboste, J., Asher,G., Clare, J. (2004). Rotor current based MRAS observer for doubly-fed induction machines, *Electronics Letters* , 40 (12): 769 – 770.
- [Carranza et al., 2010] Carranza, O., Garcera, G., Figures, E. Gonzalez, JG,(2010). Peak current mode control of three – phase boost rectifiers in discontinuous conduction mode for small wind power generators. *Applied Energy*, 87(8): 2728 – 2736.

- [Chen et al., 1991] Chen, T., Francis, B. A (1991). Input-output stability of sampled-data systems. *IEEE Transaction on Automatic and Control*, 36 (1):50 -58.
- [Chen, et al., 2003] Chen, Z., Tomita, M., Doki, S., Okuma, S. (2003). An extended electromotive force model for sensorless control of interior permanent-magnet synchronous motors, *IEEE Transactions on Industrial Electronics*, 50 (2): 288 -295.
- [Cecati et al., 2005] Cecati, C., Dell'Aquila, A., Lecci, A., and Liserre, M. (2005). Implementation issues of a fuzzy- logic-based three-phase active rectifier employing only voltage sensors. *IEEE Transactions on Industrial Electronics*, 52(2): 378 - 385.
- [Chattopadhyay et al., 2010] Chattopadhyay, S., Mitra, M., Sengupta, S. (2010). Electric power quality, Ch12. *Springer Dordrecht Heidelberg London*, ISBN 978- 94 -007-0634 -7.
- [Chakir et al., 2015] Chakir, H., Ouadi, H., Giri, H. (2015). Output feedback control of wind energy conversion system with hybrid excitation synchronous generator. *1st IFAC Conference on Modelling, Identification and Control of Nonlinear Systems*: 626 – 631.
- [Dabroom et al., 2001] Dabroom, A.M., Khalil, H.K. (2001). Output feedback sampled-data control of nonlinear systems using high-gain observers. *IEEE Transactions on Automatic Control*, 46(11): 1712 - 1725.
- [Dai et al., 2005] Dai, M., Marwali, M., Jung, J.W., and Keyhani, A. (2005). A PWM rectifier control technique for three-phase double conversion UPS under unbalanced load. *IEEE Applied Power Electronics Conference (APEC'05) Austin, Texas*, 1(2005): 548 - 552.
- [Deza et al., 1993] Deza, F., Bossanne, D., Busvelle, E., Gauthier, J. P., Rakotopara, D. (1993). Exponential observers for nonlinear systems, *IEEE Transactions on Automatic Control*, 38 (3): 482 – 484.
- [Deng et al., 2005] Deng, H., Orugant, R., Srinivasan, D (2005). Modeling and control of single – phase UPS inverters: a survey. *IEEE international conference on power electronics and drives systems PEDS*: 848 – 853.
- [Dib, 2012] Dib. A. (2012). Observation and control of asynchronous machine. PhD thesis, UCBN, France.
- [Doncker et al., 2011] Doncker, D., Pule, D., Veltman, A. (2011). Advanced electrical drives analysis, modelling and control. *Springer Dordrecht Heidelberg*, ISBN 978-94-007-0179- 3.
- [Ehsani et al., 2003] Ehsani, M., Gao, Y., Gay, S. (2003). Characterization of electric motor drives for traction applications. *The 29th Annual Conference of the IEEE, Industrial Electronics Society* , 1 (2003): 891 – 896.
- [El Magri et al., 2013] El Magri, A., Giri, F., El Fadili, A., Dugard, L. (2013). Adaptive nonlinear control of wind energy conversion system with PMS generator. *11th IFAC Workshop on Adaptation and Learning in Control and Signal Processing*: 23 – 26.

Bibliography

- [El Magri et al., 2010] Elmagri, A., Giri, F., Abouloifa, A., and Chaoui, F. (2010). Robust control of synchronous motor through AC/DC/AC converters. *Control Engineering Practice*, 18(5), 540 – 543.
- [El Assoudi et al., 2002] El Assoudi, A., Yaagoubi, E. H., Hammouri, H. (2002). Nonlinear observer based on the Euler discretization, *International Journal of Control*, 75 (11): 784 - 791.
- [El Fadili et al., 2012] El Fadili, A., Giri, F., El Magri, A., Dugard, L., Chaoui, F. Z. (2012). Adaptive nonlinear control of induction motors through AC/DC/AC converters. *Asian Journal of Control*, 14(4):1470 -1483.
- [Ezzat et al., 2011] Ezzat, M., Leonb, J. D., Glumineau, A. (2011). Sensorless speed control of PMSM via adaptive interconnected observer. *International Journal of Control*, 84 (11): 1926 - 1943.
- [Fakham et al., 2005] Fakham, H., Djemai, M., Busawon, K. (2005). Design and practical implementation of a back-EMF sliding-mode observer for a brushless DC motor, *IET Electric Power Applications*, 2(6): 807-813.
- [Faiz et al., 2006] Faiz, J., & Shahgholian, G. (2006). Uninterruptible power supply - A review. *ELECTROMOTION*, 13(4): 276 - 289.
- [Fezzani et al., 2014] Fezzani, A., Drid, S., Makouf, A. (2014). Speed sensorless robust control of permanent magnet synchronous motor based on second – order sliding – mode observer. *Serbian Journal of Electrical Engineering*, 11(3): 419 – 433.
- [Fletcher et al., 2010] Fletcher, J., Yang, J., Nathwani, J., Ng, A. (2010). *Paths to sustainable energy: Introduction to the Doubly-Fed Induction Generator for Wind Power Applications*, selected chapter. *INTECH Europe*, ISBN 978 - 953 - 307 - 401- 6.
- [Gauthier et al., 1981] Gauthier, J.P., Bornard, G. (1981). Observability for any $u(t)$ of a class of nonlinear system. *IEEE Transaction on Automatic Control*, AC – 26 (4): 922 – 926.
- [Gauthier et al., 1994] Gauthier, J. P., Kupka, I. A. (1994). Observability and observers for nonlinear systems. *SIAM Journal on Control and Optimization*, 32(4): 975 - 994.
- [Ghanes, 2005] Ghanes, M. (2005). Observation and mechanical sensorless control of induction machine. PhD thesis, UCBN, France.
- [Gálvez et al., 2011] Gálvez, M, Kinnaert, M. (2011). Sensor fault detection and isolation in doubly-fed induction generators accounting for parameter variations, *Renewable Energy*, 36 (2011): 1447-1457.
- [Giri, 2013] Giri, F. (2013). AC Electric motors control: advanced design techniques and applications. *Wiley & sons*, ISBN 9781118574249.
- [Glumineau et al., 2015] Glumineau, A., Morales, J. (2015). Sensorless AC electric motors control: robust advanced design techniques and applications. *Springer AIC*, ISBN 978 - 3 -319-14585-3.

- [Glumineau et al., 2015] Glumineau, A., Morales, J.L. (2015). Sensorless AC electric motors control: robust advanced design techniques and applications (Advances in Industrial Control). *Published by Springer*, ISBN 978-3-319-14586-0.
- [Gonzalo, et al., 2011] Gonzalo, A., Lopez, J., Rodriguez, M., Marroyo, L., Iwanski, G. (2011). Doubly fed induction machine: modeling and control for wind energy generation. *Wiley, IEEE Press*, ISBN: 9780470768655.
- [Harrison, et al., 2001] Harrison, R., Hau, E., Snel, H. (2001). Large wind turbines: design and economics, 1st edition. *John Wiley & Sons, Ltd*, ISBN - 13: 978 -0471494560.
- [Hann, 2014] Hann, C. (2014). Contribution to the synthesis of observers for nonlinear systems under communication constraints. PhD thesis, University of Caen Lower – Normandy, France.
- [Heir, 2009] Heir, S. (2009). Wind turbine technology: fundamental concepts of wind turbine engineering. *Chichester: Wiley, USA*, ISBN, 0791802604.
- [Hendershot et al., 2010]. Hendershot, R., Miller, T. J. (2010). Design of brushless permanent magnet machines 2nd edition. *Motor Design Books LLC*, ISBN-10: 0198593899.
- [Hill, 1991] Hill, D. (1991). A generalisation of the small - gain theorem for nonlinear feed - back systems. *Automatica*, 27 (6): 1043-1045.
- [Hermann et al., 1977] Hermann, R., Krener, A. (1977). Nonlinear controllability and observability. *IEEE Transactions on Automatic Control*, 22 (5):728 -740.
- [Houari et al., 2012] Houari, A., Renaudineau, H., Martin, J., Pierfederici, S., and Meibody-Tabar, F. (2012). Flatness - based control of three-phase inverter with output filter. *IEEE Transactions on Industrial Electronics*, 59(7): 2890 - 2897.
- [Hua et al., 2014] Hua, X., Yang, J., Wu, H., Liu, J. (2014). Direct torque control of a permanent magnet synchronous generator based on space vector modulation. *17th International Conference on Electrical Machines and Systems (ICEMS)*: 3520 – 3523.
- [Huangfu et al., 2004] Huangfu, Y., Laghrouche, S., Liu, W., Miraoui, A. (2010). A chattering avoidance sliding mode control for PMSM drive. *IEEE International Conference on Control and Automation*: 2082 – 2085.
- [Ibarra-Rojas et al., 2004] Ibarra-Rojas, S., Moreno, J., Espinosa-Perez, J. (2004). Global observability analysis of sensorless induction motos. *Automatica* 40 (2004): 1079 – 1085.
- [Ichikawa et al., 2006] Ichikawa, S., Tomita, M., Doki, S. Okuma, S. (2006). Sensorless control of permanent magnet synchronous motors using online parameter identification based on system identification theory. *IEEE Transactions on Industrial Electronics*, 53 (2): 363-372.
- [Iov et al., 2008] Iov, F., Ciobotaru, M., Blaabjerg, F. (2008). Power electronics control of wind energy in distributed power systems. *11th International Conference OPTIM: XXIX – XLIV*.

Bibliography

- [Isidori, 1995] Isidori, A. (1995). Nonlinear control systems, 3rd edition. *Communications and Control, Engineering Series*. Springer, Berlin, ISBN 9783540199168.
- [Jansuya et al, 2013] Jansuya, P., Kumsuwan, Y. (2013). Gesign of MATLAB / Simulink Modeling of fixed pitch angle wind turbine simulator. *10th Eco – energy and Materials Science and Engineering, Energy Procidia*, 34 (2013): 362 – 370.
- [Jiang et al., 1994] Jiang, Z.P., Teel, A.R, Praly, L. (1994). Small - gain theorem for ISS systems and applications. *Mathematics of Control, Signals, and Systems*, 7(1994): 95-120.
- [Jovanovic, 2002] Jovanovic, M. (2002). Nonlinear control of an electrohydraulic velocity servo system. *26th IEEE American Control Conference*, 1 (CH37301): 588-593.
- [Junyent et al., 2010] Junyent, A., Gomis, O., Sumper, A. Sala, M., Mata M. (2010). Modeling and control of the doubly fed induction generator wind turbine. *Simulation Modelling Practice and Theory*, 18 (2010) 1365 –1381.
- [Kailas et al., 2015] Kailas, B., Sankeshwari S. (2015). Sensorless speed and position estimation of PMSM based on sliding mode observer with tan hyperbolic function. *Journal of Electrical and Electronics Engineering*, 10(4): 42-47.
- [Kalman et al., 1961] Kalman, R. E., Bucy, R. S. (1961). New results in linear filtering and prediction theory. *Journal of Basic Engineering*, 83(3): 95-108.
- [Karafyllis et al., 2008] Karafyllis, I., Kravaris, C. (2008). From continuous – time design to sampled – data design of nonlinear observers. *47th IEEE Conference on Decision and Control (CDC)*: 5408 - 5413.
- [Karafyllis et al., 2009] Karafyllis, I., Kravaris, C. (2009). From continuous – time design to sampled - data design of observers. *IEEE Transaction on Automatic Control*, 54(9): 2169 - 2173.
- [Karafyllis et al., 2012] Karafyllis, I., Kravaris, C. (2012).Global exponential observers for two classes of nonlinear systems. *Systems and Control Letters*, 61(7): 797- 806.
- [Karlsson et al., 2001] Karlsson, N., Teel, A., Hrovat, D. (2001). A backstepping approach to control of active suspensions. *40th IEEE Conference in Decision and Control*, 5 (2001): 4170–4175.
- [Khater et al., 2013] Khater, F., Omar, A. (2013). A review of direct drive PMSG for wind energy systems. *Journal of Energy and Power Engineering*, 7(2013): 1592 – 1603.
- [Khalil et al., 2013] Khalil, H.K., Praly, L. (2013). High-gain observers in nonlinear feedback control. *International Journal of Robust and Nonlinear Control*, 24 (6): 993-1015.
- [Khalil, 2002] Khalil, H. (2002). *Nonlinear systems*. 3rd edition, Prentic – Hall, Inc.
- [Khalil et al., 1993] Khalil, H. K. and Esfandiari, F. (1993). Semiglobal stabilization of a class of nonlinear systems using output feedback. *IEEE Transaction on Automatic and Control*, 38(9):1412 - 1415.
- [Khajuria et al., 2012] Khajuria, S., Kaur, J. 2012. Implementation of pitch control of wind turbine using simulink (MATLAB). *International Journal of Advanced Research in computer Engineering*

Bibliography

- and technology (*IJARCET*), 1 (4):196 - 200.
- [Klempner et al., 2004] Klempner, G., Kerszenbaum, I. (2004). Operation and maintenance of large turbo generators. *John Wiley & Sons, Inc*, ISBN 0 - 471- 61447-5.
- [Krause et al., 2013] Krause, P.C, Wasynczuk, O., Sudhoff, S.D., Pekarek, S. (2013). Analysis of electric machinery and drive systems. *Wiley Interscience - IEEE Press, 3rd edition*, ISBN: 978 - 1-118 - 02429 - 4.
- [Kravaris, 2014] Kravaris, C. (2014). Design of sampled data nonlinear observers, alternative approaches in the context of observer error linearization. *International Journal of Automation and Power Engineering*, 3 (1):14 -17.
- [Krstic et al., 1995] Krstic, M. Kanellakopoulos, I., Kokotovic, P. V. (1995). Nonlinear and adaptive control design, 1st edition. *John Wiley & Sons, Inc*. ISBN: 0471127329.
- [Kramer et al., 2008] Kramer, W., Chakraborty, S., Kroposki, B., Thomas, H. (2008). Advanced power electronic interfaces for distributed energy systems part 1: systems and topologies. *National Renewable Energy Laboratory, Technical Report NREL/TP – 581 - 42672*.
- [Kiran et al., 2014] Kiran, Y. , Puttaswamy, P.S. (2014). Field oriented control of a permanent magnet synchronous motor using a DSP. *International Journal of Advanced Research in Electrical, Electronics and Instrumentation Engineering*, 3 (10):12364 – 12378.
- [Kumari et al., 2015] Kumari, R., Padhan, D. (2015). Sliding mode speed control of permanent magnet synchronous motor. *International Journal of Innovative Research in Electrical, Electronics, Instrumentation and Control Engineering*, 3(10): 16 – 19.
- [Kokotovic et al., 2001] Kokotovic, P., Arcak, M. (2001). Constructive nonlinear control: a historical perspective. *Automatica*, 37 (2001): 637 – 662.
- [Koteich et al, 2015] Koteich, M., Maloum, A., Duc, G., Sandou, G. (2015). Discussion on AC drives observability analysis. *Transaction on Industrial Electronics*, 62 (11): 7224 – 7225.
- [Kömürçügil et al., 1998] Kömürçügil, H., Kükrer, O. (1998). Lyapunov Based Control of Three-Phase PWM AC-DC Voltage-Source Converters, *IEEE Transactions on Power Electronics*, 13(5): 801-813.
- [Lara et al., 2009] Lara, O., Jenkins, N., Ekanayake, K., Cartwright, P., Hughes, M. (2009). Wind energy generation modelling and control, 1st edition. *John Wiley and Sons, Ltd*, ISBN 978-0-470-71433 – 1.
- [Lalouni, 2015] Lalouni, S., Rekioua, D., Idjdarene, K., Tounzi, A. (2015). Maximum power point tracking based hybrid hill-climb search method applied to wind energy conversion system. *Electric Power Components and Systems*, Taylor & Francis, 43(8 -10):1028-1038.
- [Lang et al., 2007] Lang, B. Liu, W., Luo, G. (2007). A new observer of stator flux linkage for permanent magnet synchronous motor based on Kalman filter. *2nd IEEE conference on Industrial Electronics and Applications*. 1813– 1817.

- [Lajouad et al., 2014] Lajouad, R., El Magri, A., El Fadili, A., Chaoui, F.Z., Giri, F. (2015). Adaptive nonlinear control of wind energy conversion system involving induction generator. *Asian Journal of Control*, 17 (4): 1365 - 1376.
- [Lascu et al., 2013] Lascu, C., Boldea, I., Blaabjerg, F., Chen W. (2013). A class of flux observers for doubly-fed induction generators used in small power wind generation systems. *IEEE Energy Conversion Congress and Exposition (ECCE)*:2289 - 2295.
- [Levine, 1996] Levine W.S. (1996). *The Control Handbook*. CRC Press, Florida, ISBN 9780849385704 - 8570.
- [Lee, 2003] Lee, T.S. (2003). Input-Output Linearization and Zero-Dynamics Control of Three-Phase AC/DC Voltage-Source Converters," *IEEE Transactions on Power Electronics*, 18(1):11 - 22.
- [Leonhard, 2001] Leonhard, W. (2001). *Control of electrical drives*, 3rd edition. Springer-Verlag Berlin Heidelberg, ISBN 3-540-41820 -2.
- [Liu et al., 2011] Liu, J., Nondahl, T., Schmidt, P., Royak, S., Harbaugh, M. (2011). Sensorless full - digital PMSM drive with EMF estimation of speed and rotor position. *IEEE Transactions on Industry Applications*, 47 (3): 1310 - 1318.
- [Liebert, 2000] Liebert Corporation (2000). *High-Availability Power Systems, Part 1: UPS Internal Topology*: 1-10.
- [Liu et al., 2014] Liu, J., Laghrouche, S., and Wack, M. (2014). Observer-Based Higher Order Sliding Mode Control of Unity Power Factor in Three-Phase AC/DC Converter for Hybrid Electric Vehicle Applications. *International Journal of Control*, 87(6), 1 - 28.
- [Lu, 2013] Lu, H. (2013). Sensorless position control of SPMLSM based on high – gain observer. *Journal of computers*, 8(3): 661 – 668.
- [Manikandan et al., 2013] Manikandan, P., Umayal, SP. Mariya, A., Chithra, M., Ramachandran, M. (2013). Simulation and hardware analysis of three phase PWM rectifier with power factor correction. *IOSR Journal of Electrical and Electronics Engineering*, 8 (1): 27-33.
- [Marino et al., 2010] Marino, R., Tomei P., Cristiano M. (2010). *Induction motor control design*, Published by Springer, ISBN 978-1-84996-284-1.
- [Mishra et al., 2014] Mishra, S., Tomer, A.S. (2014). Speed control of PMSM drives using neural network controller. *Advances in Electronics and Electric Engineering*, 4 (4): 353 – 359.
- [Morel et al., 1998] Morel, L., Godfroid, H., Mirzaian, A., Kauffmann, J.M. (1998). Double fed induction machine: converter optimisation and field oriented control without position sensor. *IEE Proceedings Electric Power Applications*, 145, (4): 360 – 368.
- [Mohan et al., 2002] N. Mohan, T. Undeland, W. Robbins, (2002). *Power Electronics: Converters Applications and Design*, 3rd edition. Wiley Text Books, ISBN: 0471226939.
- [Najmeijer et al., 2006] Najmeijer, H., van der Schaft, A. J. (2006). *Nonlinear dynamical control systems*. 3rd edition. Springer, New York, ISBN 978-1- 4757-2101-0.

Bibliography

- [Nadri et al., 2012] Nadri, M., Hammouri, H., Grajales, R.M. (2013). Observer design for uniformly observable systems with sampled measurements. *IEEE Transaction on Automatic Control*, 58(3):757 – 762.
- [Niaona, et al., 2011] Niao-na, Z., Guang-lai, Z. (2011). Robust sliding mode observer design for a class of nonlinear uncertain systems based on backstepping. *International Conference on Informatics, Cybernetics, and Computer Engineering*, 112 (2011): 555 - 562.
- [Niroomand et al., 2010] Niroomand, M., Karshenas, H. (2010). Review and comparison of control methods for uninterruptable power supplies. *1st IEEE Power Electronic and Drive Systems and Technologies Conference (PEDSTC)*, 2010:18 – 23.
- [Novotny et al., 2000] Novotny, D.W., Lipo, T.A. (2000). Vector control and dynamics of AC drives. *Oxford University Press: Oxford, UK, ISBN: 978-0198564393*.
- [Nussbaumer et al., 2010] Nussbaumer, P., Wolbank, T. M. (2010). Saliency tracking based sensorless control of ac machines exploiting inverter switching transients. *First Symposium on Sensorless Control for Electrical Drives*: 114 – 119.
- [Ochieng et al., 2014] Ochieng, P.O., Manyonge, A.W. (2014). Mathematical analysis of tip speed ratio of a wind turbine and its effects on power coefficient. *International Journal of Mathematics and Soft Computing*, 4(1): 61 – 66.
- [Ojha, et al., 2015] Ojha, A., Khandelwal, A. (2015). Control of nonlinear system using backstepping. *Journal of Research in Engineering and Technology*, 4 (5): 606 – 610.
- [Ozsoy et al., 2016] Ozsoy , E. E., Golubovic, E., Sabanovic, A., (2016). Modeling and control of doubly fed induction generator with a disturbance observer: a stator voltahe oriented approach. *Journal of Electrical Equipment and Computer Sciences*, 24(2016): 961 – 972.
- [Pan et al., 1993] Pan, C., and Chen, T. (1993). Modelling and analysis of a three - phase PWM AC - DC convertor without current sensor. *IEE Proceedings B: Electric Power Applications, Institute of Electrical and Electronics Engineers*, 140(3): 201 - 208.
- [Poitiers et al., 2009] Poitiers, F., Bouaouiche, T., Machmoum, M. (2009). Advanced control of a doubly-fed induction generator for wind energy conversion. *Electric Power Systems Research*, 79: 1085-1096.
- [Praly et al., 1991] Praly, L., Andrea – Novel, B., Coron, J.M. (1991). *Lyapunov* design of stabilizing controllers for cascade systems. *IEEE Transaction on Automatic Control*, 36 (10): 1177 – 1181.
- [Qiao et al., 2013] Qiao, Z., Shi, T., Wang, Y., Xia, C., He, X. (2013). New sliding-mode observer for position sensorless control of permanent-magnet synchronous motor. *IEEE Transactions on Industrial Electronics*, 60 (2): 710 – 719.
- [Ramana et al., 2015] Ramana, N., Sastry,V. (2015). A Novel speed control strategy for five phases permanent magnet synchronous motor with linear quadratic regulator. *International Journal of Computer and Electrical Engineering*, 7(6):408 – 416.

Bibliography

- [Rashid, 2011] Rashid, M. (2011). Power Electronics Handbook, devices, circuits and applications 3rd Edition, *Elsevier*, ISBN: 978-0-12-382036 - 5.
- [Raff et al., 2008] Raff, T., Kögel, M., & Allgöwer, F. (2008). Observer with sample-and-hold updating for Lipschitz nonlinear systems with non-uniformly sampled measurements. *American Control Conference ACC*: 5254 - 5257.
- [Reddy et al., 2015] Reddy, B., Mohinuddin, S.K, (2015). Adaptive control of a voltage source converter for power factor correction. *International Journal of applied sciences and engineering research, IJASER*, 4(3): 293 – 299.
- [Rigatos et al., 2016] Rigatos, G., Siano, P., Cecati C. (2016). A new non-linear H-infinity feedback control approach for three-phase voltage source converters. *Journal of electric power components and systems*, 44(3): 1- 11.
- [Rodriguez et al., 2005] Rodriguez, J., Dixon, J.W, Espinoza, J.R, Pontt, J., & Lezana, P. (2005). PWM Regenerative Rectifiers: State of the Art. *IEEE Transactions on Industrial Electronic*, 52(1): 5 - 22.
- [Sarinana et al., 2000] Sarinana, A., Bacha, S., and Bornard, G. (2000). On nonlinear observers applied to three - phase voltage source converters. *31st IEEE Annual Power Electronics Specialists Conference PESCO*, 3 (2000):1419 -1424.
- [Shtessel et al., 2008] Shtessel, Y., Baev, S., and Biglari, H. (2008). Unity power factor control in three-phase AC/DC boost converter using sliding modes. *IEEE Transactions on Industrial Electronics*, 55(11):3874 - 3882.
- [Shim et al., 1998] Shim, H., Jin, J., Lee, S., Seo, H. (1998). Output feedback stabilization for completely uniformly observable nonlinear systems. *In Proceeding of IFAC Conference on System Structure and Control*, Nantes, France: 335 – 360.
- [Singh et al., 2007] Singh B., G. Bhuvaneswari, and V. Garg, (2007). An improved quality 30 pulse AC/DC for varying loads. *IEEE Transactions on Power Delivery*, 22 (2):1179 – 1187.
- [Simoes et al., 2008] Simoes, M., Farret, A. (2008). Alternative energy systems: design and analysis with induction generators, 2nd edition. *CRC Press*, ISBN 9781420055320 - 55321.
- [Souleiman et al., 2007] Souleiman, I., Glumineau, A. (2007). Constructive transformation of nonlinear systems into a special state - affine MIMO forms and nonlinear observers. *7th IFAC symposium on nonlinear control systems (NOLCOS)*, 40, (12): 904–909.
- [Sontag et al., 1996] Sontag, E.D, Wang, Y. (1995). New characterizations of input-to-state stability. *IEEE Transactions on Automatic Control*, 41 (9): 1283 – 1294.
- [Sontag et al., 1995] Sontag, E.D., Wang, Y. (1995). On characterizations of the input-to-state - stability property. *Systems and Control Letters*, 24(1995): 351-359.
- [Song et al., 2012] Song, Z., Shi, T., Xia, C., Chen, W. (2012). A novel adaptive control scheme for dynamic performance improvement of DFIG-Based wind turbines. *Energy*, 38 (2012): 104-117.

Bibliography

- [Spurgeon, 2015] Spurgeon, S.K. (2015). Sliding mode observers - historical background and basic introduction. *School of Engineering and Digital Arts University of Kent*, UK.
- [Tadjer et al., 2014] Tadjer, S. A., Chalah, S., Habi, I., Nadji, B. (2014). Influences of pollutant sources on harmonic propagation in a power grid. *International Conference on Control, Engineering & Information Technology (CEIT'14)*:80 0 - 84.
- [Teel, 1996] Teel, A.R. (1996). A nonlinear small - gain theorem for the analysis of control systems with saturation. *IEEE Transactions on Automatic Control*, 41(9): 1256 -1271.
- [Vaclavek et al., 2013] Vaclavek, P., Blaha, P., Herman, I. (2013). AC drives observability analysis. *IEEE Transaction on Industrial Electronics*, 60(8): 3047 – 3059.
- [Virgilio et al., 1997] Virgilio, L., Plestan F, Glumineau, A. (1999). Linearization by generalized input - output injection. *Kybernetika*, 35(6):793–802.
- [Vidyasagar et al., 1993] Vidyasagar, M. (1993). Nonlinear systems analysis, 2'nd edition. *Prentice - Hall.inc* , ISBN 0-13-623463-1.
- [Wang et al., 2012] Wang, Z., Zheng, Y. Zou, Z. Cheng, M. (2012). Position sensorless control of interleaved CSI fed PMSM drive with extended Kalman filter, *IEEE Transactions on Magnetics*. 48 (11): 3688 - 3691.
- [Xu, 1995] Xu, C., (1995).Bellman's inequality. *Linear Algebra and its Applications, Elsevier Science Inc*, 229 (1): 9 - 14.
- [Zaltni et al., 2010] Zaltni, D., Ghanes, M. (2010). Synchronous motor observability study and an improved zero-speed position estimation design. *49'th IEEE Conference on Decision and Control (CDC)*: 5074 – 5079.
- [Zatocil, 2008] Zatocil, H. (2008). Sensorless control of AC machines using high-frequency excitation, *13'th Power Electronics and Motion Control Conference, EPE-PEMC (2008)* 1024 – 1032.
- [Zeitz, 1987] Zeitz, M. (1987). The extended *Luenberger* observer for nonlinear systems. *Systems & Control Letters*, 9 (2):149 –156.
- [Zhu et al., 2000] Zhu, G., Dessaint, A., Akhrif, O., Kaddouri, A. (2000). Speed tracking control of a permanent – magnet synchronous motor with state and load torque observer. *IEEE Transaction on Industrial Electronics*, 47(2): 346 – 355.
- [Zhang, 2002] Zhang, Q. (2002). Adaptive observers for MIMO linear time – varying systems. *IEEE transaction on Automatic Control*, 47 (3): 525 – 529.



Normandie Université

THESIS

Thesis submitted in accordance with the requirements of the Normandie University for the degree of PhD

Specialty (Electrical Engineering)

Prepared in « Normandie University, Ecole doctorale SIMEM »

Synthesis of State Observer and Nonlinear Output Feedback Controller Design of AC Machines

**Presented and defended by
Ali Abdul Razzaq AL TAHIR**

Thesis publicly defended on (December 16, 2016)

in front of the committee consists from:

Mr / Mohamed Benbouzid	Professeur des universités / Université de Bretagne Occidentale, France	Protractor
Mr / Maxime Wack	Maître de Conférences HDR Emérite/ Université de Technologie de Belfort - Montbéliard, France	Protractor
Mr / Fayçal Ikhouane	Professeur des universités / Universitat Politècnica de Catalunya, Spain	Examiner
Mr / Salah Laghrouche	Maître de Conférences HDR/ Université de Technologie de Belfort-Montbéliard, France	Examiner
Mr / F. Giri	Professeur des universités/ Normandie Université, France	Supervisor
Mr / Tarek Ahmed - Ali	Professeur des universités / Normandie Université, France	Supervisor

Laboratoire : Groupe de recherche en informatique, image, automatique et Instrumentation de Caen (GREYC)



Résumé:

Le travail de recherche effectué dans cette thèse a été principalement consacré aux problèmes l'état d'observation et de commande des systèmes électriques sans capteurs. Trois contributions principales ont été faites en utilisant le concept de grand gain et retour de sortie commande adaptative non linéaire pour alimentation électrique de secours en ligne. Cette thèse traite la synthèse d'observateur pour les systèmes non linéaires avec des applications sur la machine synchrones à aimant permanent et machine asynchrone a doublé alimentation. En particulier, nous nous intéressons essentiellement aux contraintes effet d'échantillonnage et d'estimation des variables d'état mécaniques et magnétiques non mesurées. La première contribution est un observateur du type grand gain qui permet de réaliser une estimation relativement précise des variables d'état m' mécaniques et magnétiques des moteurs synchrones à partir des mesures disponibles des courants et tensions statoriques. Nous traitons la synthèse d'observateur à grand gain dynamique pour une classe de systèmes non linéaires globalement *Lipschitz* à sorties échantillonnées. Dans la deuxième contribution, nous avons proposé un roman non standard HGO pour non injective relation de retour de sortie application à vitesse variable en fonction aux aérogénérateurs asynchrones. Pendant ce temps, un modèle de système réduit est analysé, fourni par le test d'observabilité pour vérifier qu'il est possible observateur d'état de synthèse pour le contrôle sensoriels. Dans la dernière contribution, un observateur adaptatif pour les états et l'estimation des paramètres sont désignés pour une classe de l'état - affins des systèmes l'application à la rétroaction de sortie commande adaptative non linéaire de triphasés AC/DC convertisseur de puissance pour alimentation électrique de secours en ligne. Fondamentalement, le problème concentré sur cascade régulatrice adaptative non linéaire qui est développé fait usage *Lyapunov* théorie. Les paramètres incertitudes sont traités par les lois de contrôle pratiques dans backstepping techniques de conception avec une capacité d'adaptation.

Mots-Clés: Observateur à grand gain, Système non linéaire, Echantillonnage, Observateur adaptatif, Moteurs à aimants permanents, Alimentation électrique de secours, observateur d'état, *Liapunov*, Stability de.

Abstract:

The research work developed in this thesis has been mainly devoted to the observation and sensorless control problems of electrical systems. Three major contributions have been carried out using the high - gain concept and output feedback adaptive nonlinear control for online emergency power supply. In this thesis, we dealt with the synthesis of sampled high - gain observers for nonlinear systems application to permanent synchronous generators and doubly - fed induction generator. We particularly focus on two constraints: sampling effect and tracking unmeasured mechanical and magnetic state variables. The first contribution consists in a high gain observer design that performs a relatively accurate estimation of both mechanical and magnetic state variable using the available measurements on stator currents and voltages of PMSM. We propose a global exponential observer having state predictor for a class of nonlinear globally *Lipschitz* system. In a second contribution, we proposed a novel non - standard high gain observer design for non-injective feedback relation application to variable speed DFIGs based wind power generation systems. Meanwhile, a reduced system model is analyzed, provided by observability test to check is it possible synthesis state observer for senseless control. In last contribution, an adaptive observer for states and parameters estimation are designed for a class of state - affine systems application to output feedback adaptive nonlinear control of three-phase AC/DC boost power converter for online emergency power supply systems. Basically, the problem focused on the cascade nonlinear adaptive controller that is developed making use *Lyapunov* theory. The parameter uncertainties are processed by the control laws under backstepping design techniques with a capacity of adaptation.

Keywords: High gain observer, Nonlinear systems, Sampling, Adaptive observers, Permanent magnet synchronous machine, Emergency power supply, State observer, *Lyapunov* stability.

Discipline: Génie Electrique, Ingénierie Electrique.

Laboratoire: Groupe de Recherche en Informatique, Image, Automatique et Instrumentation de Caen - GREYC CNRS UMR 6072, Sciences 3, Campus 2, 6 Bd Maréchal Juin, 14032, Normandie université.